NEUROPHYSIOLOGICAL MECHANISMS OF SENSORIMOTOR RECOVERY FROM STROKE

Maxwell DeWolf Murphy

Submitted to the graduate degree program in Bioengineering and the Graduate Faculty of the University of Kansas in partial fulfillment of the requirements for the degree of Doctor of Philosophy.

Dissertation Committee:

_____

(Chairperson) Randolph J. Nudo, Ph.D.

_____

David J. Guggenmos, Ph.D.

_____

Jonathan S. Brumberg, Ph.D.

_____

Carl W. Luchies, Ph.D.

_____

Victor S. Frost, Ph.D.

Date Defended: Friday, October 9th, 2020

The Dissertation Committee for Maxwell DeWolf Murphy certifies that this is the approved version of the following dissertation:

NEUROPHYSIOLOGICAL MECHANISMS OF SENSORIMOTOR RECOVERY FROM STROKE

_____

Chairperson Randolph J. Nudo, Ph.D.

Date Approved: 2020-12-09

ABSTRACT

Ischemic stroke often results in the devastating loss of nervous tissue in the cerebral cortex, leading to profound motor deficits when motor territory is lost, and ultimately resulting in a substantial reduction in quality of life for the stroke survivor. The International Classification of Functioning, Disability and Health (ICF) was developed in 2002 by the World Health Organization (WHO) and provides a framework for clinically defining impairment after stroke. While the reduction of burdens due to neurological disease is stated as a mission objective of the National Institute of Neurological Disorders and Stroke (NINDS), recent clinical trials have been unsuccessful in translating preclinical research breakthroughs into actionable therapeutic treatment strategies with meaningful progress towards this goal. This means that research expanding another NINDS mission is now more important than ever: improving fundamental knowledge about the brain and nervous system in order to illuminate the way forward.

Past work in the monkey model of ischemic stroke has suggested there may be a relationship between motor improvements after injury and the ability of the animal to reintegrate sensory and motor information during behavior. This relationship may be subserved by sprouting cortical axonal processes that originate in the spared premotor cortex after motor cortical injury in squirrel monkeys. The axons were observed to grow for relatively long distances (millimeters), significantly changing direction so that it appears that they specifically navigate around the injury site and reorient toward the spared sensory cortex. Critically, it remains unknown whether such processes ever form functional synapses, and if they do, whether such synapses perform meaningful calculations or other functions during behavior.

The intent of this dissertation was to study this phenomenon in both intact rats and rats with a focal ischemia in primary motor cortex (M1) contralateral to the preferred forelimb during a pellet retrieval task. As this proved to be a challenging and resource-intensive endeavor, a primary objective of the dissertation became to provide the tools to facilitate such a project to begin with. This includes the creation of software, hardware, and novel training and behavioral paradigms for the rat model. At the same time, analysis of previous experimental data suggested that plasticity in the neural activity of the bilateral motor cortices of rats performing pellet retrievals after focal M1 ischemia may exhibit its most salient changes with respect to functional changes in behavior via mechanisms that were different than initially hypothesized.

Specifically, a major finding of this dissertation is the finding that evidence of plasticity in the unit activity of bilateral motor cortical areas of the reaching rat is much stronger at the level of population features. These features exhibit changes in dynamics that suggest a shift in network fixed points, which may relate to the stability of filtering performed during behavior. It is therefore predicted that in order to define *recovery* by comparison to *restitution*, a specific type of fixed point dynamics must be present in the cortical population state. A final suggestion is that the stability or presence of these dynamics is related to the reintegration of sensory information to the cortex, which may relate to the positive impact of physical therapy during rehabilitation in the postacute window. Although many more rats will be needed to state any of these findings as a definitive fact, this line of inquiry appears to be productive for identifying targets related to sensorimotor integration which may enhance the efficacy of future therapeutic strategies.

ACKNOWLEDGEMENTS

I am deeply indebted to a great number of people whose kind guidance, patience, and friendship have helped me along my PhD journey. From the outset, I must thank my mentor, Dr. Randy Nudo. I have always been so honored to be a part of your lab and to take part in the exciting and important work done here. You fostered my creativity by providing me with the latitude to engage in diverse lines of inquiry while always reminding me not to stray too far into the weeds, and for that I am grateful. I am fortunate to have enjoyed the privilege of something akin to an apprenticeship to Dr. David Guggenmos; any of the works presented herein would have been impossible for me without his tutelage. Thank you as well to the rest of my thesis committee: Dr. John Brumberg, Dr. Victor Frost, and Dr. Carl Luchies. Your valuable advice, instruction, and feedback has served as a source of inspiration throughout my graduate career.

Thank you to Dr. Heather Hudson and Dr. Shawn Frost, without your assistance I would probably always have remained too scared to pick up a rat. Thank you to Dr. Scott Barbay for answering my endless questions with such deep insight while ensuring the lab runs smoothly. Thank you to Page Hayley & Dr. Jordan Borrell for all the great conversations and memories (and for helping me with experiments to boot). Thank you to Dr. Kevin Elliott for coming in on weekends to help me with surgical procedures. Thank you to Dr. Chad Tucheck, your surgical skills are unparalleled. Thank you to Dr. Michela Chiappalone for not only allowing me to visit your wonderful laboratory in IIT but for also allowing me to participate in collaborations with your brilliant students. Thank you to Dr. Alberto Averna, Dr. Stefano Buccelli, & Federico Barban, you guys inspire me to try my best to always become a better engineer. Thank you to Dr. Andrew Roberts for lending me your old textbooks, our conversations about dynamical systems while watching football had a greater impact than you could suspect. Thank you to Dr. Stefano Millighetti for allowing me to collaborate with you on your tDCS experiment in rats. Thank you to Alexis Delgado, Jasmine Deng, Zack Green, Daniel Rittle, and Meg Hollingsworth for your technical assistance with the rats and in scoring videos. Thank you to Andrea Pack for sharing your experiment and collaborating with me on what became the bulk of the empirical data comprising this dissertation. I owe a special thanks to Dr. David Bundy for being such a fantastic role model and friend.

This journey would not have been possible without the support of my beloved friends and family. To my parents, thank you for all your encouragement and love despite the especially trying past months. To my sister, I am so incredibly proud of you and all you have accomplished. Most of all, to my wife Teresa, thank you so much for the unwavering support, for putting up with my rambling and esoteric scientific jargon at dinner, for letting me spend so many hours away from you while I work on weekends and holidays, and for most recently stymying Nigel's relentless attempts to interrupt me during those same work hours. I love you so very much.

-Max

To my *Nana.*
In loving memory of Susan and Jerry Murphy.

TABLE OF CONTENTS

LIST OF TABLES

LIST OF FIGURES

Chapter 2

Chapter 3

Chapter 4

LIST OF ABBREVIATIONS

ADS	.....	Activity Dependent Stimulation
BIBO	.....	Bounded-Input, Bounded-Output
BCI	.....	Brain-Computer Interface
CFA	.....	Caudal Forelimb Area
EEG	.....	Electroencephalography
EMG	.....	Electromyography
FL-S1	.....	Primary forelimb sensory cortex
GLME	.....	Generalized linear mixed-effects
ICMS	.....	Intracortical microstimulation
jPCA	.....	Rotatory principal components analysis
LFADS	.....	Latent factor analysis by dynamical systems
M1	.....	Primary motor cortex

MIMO	……	Multiple inputs, multiple outputs
MLS	……	Multiple least-squares regression
OLS	……	Open-loop stimulation
PCA	……	Principal components analysis
PM	……	Premotor cortex
RFA	……	Rostral Forelimb Area
RNN	……	Recurrent neural network
S1	……	Primary sensory cortex
SPI	……	Serial-parallel interface
TMS	……	Transcranial magnetic stimulation

CHAPTER 1

Introduction

Motivation

Each year, approximately 795,000 people suffer a stroke, contributing to its notoriety as the leading cause of long-term disability in the United States (Mozaffarian et al., 2015). The most prevalent type of stroke is ischemic (Feigin et al., 2009): commonly, ischemia occurs when a blood clot partially or fully dislodges, forming an embolus or thrombus respectively, which blocks the middle cerebral artery. This occludes the supply of nutrients to motor areas of the cerebral cortex, resulting in gradual cell death and diaschisis. The contralateral effectors previously under control by the now dead tissue consequently exhibit paresis (Gowland 1982) and may also become spastic depending on the degree of early paresis as well as the type of connections maintained by the destroyed descending projections (Ward 2012). These deficits functionally inhibit the ability to perform complex motor tasks, particularly those involving fine control of the distal upper extremities. Fortunately, motor impairment due to stroke can be modified in some instances by behavioral rehabilitation after injury (Kleim et al., 2008).

Behavioral experience encourages neuroplasticity that is evident in the temporal encoding and decoding of information in the activity of individual cortical neurons and microcircuits (Mitz et al., 1991; Wise et al., 1998). After brain injury, the sparing of distal forelimb representation near the lesion after intensive behavioral re-training in monkeys suggests that similar processes may relate to the benefits realized by rehabilitation (Nudo et al., 1996). This phenomenon, which is otherwise known as somatotopic map reorganization, likely manifests via simultaneous reorganization of neuronal networks at several levels of the central nervous system. The

reorganized somatotopy may not be specific to motor maps: axonal sprouting in monkeys after brain injury suggests that when possible, *de novo* physical connections arise between spared motor and sensory areas as well (Dancause et al., 2005). While the simplest explanation is that such connections most-likely foster communication between motor and sensory regions of cortex (Hickmott & Steen, 2005), it remains unknown not only to what end, but whether the new projections and the synapses that they form even serve any purpose at all during motor behavior.

The Specific Aims of this thesis are directed toward the considerable technical challenges in answering such a question. The majority of empirical results contained in this work are observational. However, careful consideration of the neural population state during motor behavior predicts that a core mechanism during **Motor Re-optimization**[1] is the assignment of an appropriate sensorimotor synaptic weighting schema.[2] This re-optimization is most especially important after injury, as it is required for the *de novo* axonal processes that sprout and potentially reconnect sensorimotor areas as described in the works of Dancause and colleagues to ever serve as a route of reliable information transfer between the otherwise disconnected

[1] Controversial terms, such as *recovery*, *restitution,* and *compensation* will be avoided if possible. **Motor Optimization** is defined as an optimization process in which the cost function is proportional to the error between the desired motor output (generation of force by any combination of muscles desired to functionally move a peripheral effector through space or to exert force on a foreign body) and the actual motor output. The error magnitude could be specified using a common distance metric, such as the L2-norm. Physiologically, it is likely that some similar calculation occurs, albeit in a highly nonlinear fashion. In this formulation, the error term is non-stationary with respect to time. Intuitively, this relates to the differential likelihood of an error influencing the functional outcome of the behavior during a given phase. **Motor Re-optimization** is different from motor optimization such as occurs during the learning of a motor behavior. The former implies that weightings on error during different phases of the behavior have already converged to a fixed value, while the latter allows that error weightings have yet to converge.

[2] When a motor behavior occurs, motor re-optimization is invoked. Given the perpetual and systemic changes that organisms undergo on the timescales of days, months, and especially years--with causes ranging from growth to disease--the only feature that allows robust and reliable execution of motor tasks is this intrinsic optimization of movement, which is governed at multiple levels of the nervous system. The cerebral cortex is probably not involved when error occurs below a perceptual threshold. However, if the motor error trajectory exceeds a learned threshold, it is perceived (although such a term is controversial in animal research; e.g. Nudo et al. 2000). Subsequent adaptive changes are the purview of the cerebral cortex, and require reassigned weights to motor output on the timescales of seconds, minutes, or hours.

regions[3]. In that light, the main contributions of this work are to provide meaningful hypothesis testing strategies for future experiments that target sensorimotor connections during motor re-optimization after unilateral injury, such as occurs after stroke.

Specific Aims

Before answering the question of whether sensory and motor areas make use of presumptive new connections that form after cortical injury, the first step is to define an assay that is both sensitive to and selective for evidence of said connections. When the evidence must arise from the patterns of neural activity that allow the temporal encoding and decoding of sensory information during movement, it becomes a system identification problem. Because the rat pellet retrieval model is extensively characterized as an animal model of stroke, the system takes the form of the reaching rat as it retrieves pellets[4]. Furthermore, because of the interest in the restoration of connections between sensory and motor areas of cortex, the system measurement must reflect signals from sensory and motor areas of the brain. A final point that is argued in this thesis is that--although cumbersome--the system state[5] must directly correlate with filtering related to the **Motor Phenotype[6]**, rather than to the outcome of the behavior. This is because functional outcomes are abstracted from movement due to the non-monotonicity of the response surface mapping that relates such measurements. The following aims form the basis for defining and implementing the system identification approach. The observational

[3] When motor tasks are complicated (i.e. during skillful behavior; or, after injury), errors are common. The consequent changes in response are predictive. Therefore, the role of the cerebral cortex in **Motor Re-optimization** is to compare sensory feedback measurements from the periphery to the predicted motor (and sensory) state in order to directly modulate motor output weightings associated with the correct phase of a complex movement.

[4] The rat pellet retrieval model is sometimes called “the reaching rat” out of habit.

[5] **Chapter 3** provides definitions of the system state variables and considerations on state architecture.

[6] The **Motor Phenotype** is defined as quantitative measurements describing the series of sub-movements that comprise a compound movement. These measurements may include heuristics such as duration of the movement, or they could be the reconstructed world-coordinate position time-series of markers on the peripheral effectors of interest relative to behavioral landmarks.

results from these experiments provide a basis for future studies elaborating the relevance of connections between presumptive *de novo* connections between sensory and motor cortices after injury:

1. Develop a pipeline to process and extract relevant neurophysiological and kinematic biomarkers from rat pellet retrieval experiments. Rats with a focal vasoconstrictive ischemia contralateral to the preferred forelimb were tested daily on the pellet retrieval task while concurrently acquiring video and neural signals from the behavior.

    a. It was hypothesized that over the first four weeks, plasticity in temporal encoding and decoding related to the motor behavior would exhibit a shift in injured rats, causing activity in premotor cortex of the hemisphere with the injury to more-closely resemble activity in primary motor cortex of uninjured rats.

2. Develop a model to distinguish between motor cortex sensory feedback and motor cortex sensory prediction. Video from multiple stereo-calibrated cameras was synchronized and forelimb markers were extracted using an artificial Deep Neural Network; the markers were then de-noised and reconstructed in an estimate of the 3D world space in which the behavior was performed.

    a. It was hypothesized that integrating kinematic and neural data using a Kalman formulation would allow improved identification of activity related to sensory feedback using a combination of coefficients from the Kalman gain matrix and state-measurement relation matrix, by comparison to the past method of correlating field potentials between the two areas.

Results from experimental data used toward the first aim form the bulk of empirical observation used in predictive models. The surprising discrepancy between observation and the original hypothesis suggests that motor re-optimization after injury is quite different from motor learning,

and that the next experiments clarifying the error modality of the cortical sensorimotor filter could be a critical breakthrough for the future of direct behavioral intervention during physical therapy.

Dissertation Contents

This dissertation contains six chapters, including this road map.

Chapter 2 gives more detailed information regarding stroke and its time course as it relates to upper extremity motor function. The chapter describes progress in acute treatment options as well as long-term therapeutic ones. A section emphasizing the translation of preclinical treatment results to therapeutic brain-computer interface (BCI) options consists primarily of a review article that was accepted for publication in a peer-reviewed journal (Murphy et al., 2016). Since the review was published in 2016, the final section, which discusses strategies for evaluating the efficacy of BCI such as the therapeutic closed-loop microstimulation strategy developed by the cortical plasticity lab, is augmented using newer data. These data include a conference proceedings paper, which implements a strategy for using recurrent neural networks as a variational autoencoder to recover the latent stochastic distribution of Gaussian processes related to the observed spiking time-series[7]. When data are modeled in this manner, it is possible to infer perturbations to an assumed dynamical system that generates the observed population spiking activity (which arise from deviations to the Gaussian prior). The study

[7] In recordings from the extracellular field potentials, action potentials from cells near the recording electrode cause characteristic deflections in the voltage differential between the recording electrode and reference in the range of 300-5,000 Hz. These signals are referred to as “spikes” due to their shape, and so spikes are commonly used interchangeably with “putative action potential” since the latter is cumbersome to say. When the timing of these spikes is treated as a stochastic point-process, the term **Unit Activity** is sometimes invoked to imply the involvement of some unknown number of neurons involved in the generation of the observed spikes. Although tools for spike sorting are provided in **Chapter 3**, with the exception of the conference proceedings paper discussed in Chapter 2 and the comparisons on spike detection performance of the module provided in Chapter 5, spike sorting was **not** applied to data used in neural analyses.

compares the temporal evolution of such perturbations between individual pilot rats receiving (therapeutic) closed-loop and (control) open-loop microstimulation in the primary forelimb sensory cortex (Murphy et al., 2018). An important takeaway is that while such nonlinear methods may sound complex and cutting edge, their ability to yield meaningful insight in this capacity is limited in this context.

Chapter 3 reformulates the problem of studying the motor phenotype with respect to control systems elements. The goal is to align the approaches of the rehabilitation physiologist and control systems engineer. The chapter provides a discussion of tools created for the processing pipeline, as well as preliminary instructions on their use alongside examples. Many of these tools contain documentation that is associated directly with the publicly-available code at the source. Since such documentation continues to evolve, the reader should really check documentation for the relevant tool at the source: the author intends to maintain such tools out of principle and for his own future purposes. However, versions of the tools as of the time of this writing will remain available.

Chapter 4 partially fulfills Aim 1. It describes acquisition system modifications that allow the execution of experiments involving rats performing pellet retrievals while being treated with closed-loop or control microstimulation--a prerequisite step to extracting biomarkers from the rats. The chapter contents were published previously as a manuscript detailing and characterizing the performance of these modifications to the compiled bit-file on the field programmable gate array (FPGA) at the core of the controller's serial-parallel interface (SPI) in a peer-reviewed journal (Murphy et al., 2019). The changes add a programmable state machine module that improves spike detection. The specifications are mostly technical and application-specific, but augment the online spike detection capability of any research done for closed-loop purposes using this equipment while also providing a graphical software interface update to make use of the improved features. Spike detection using this method is low-latency (on the

order of single milliseconds or less) and flexible (it hijacks the 8 DAC channels to allow up to 8 custom inclusion or rejection thresholds on channels of interest). It is suggested that future closed-loop experiments could make use of this capacity to require relatively coincident detection of spikes on multiple channels to trigger a digital event using population features. Furthermore, changing the programmable hardware filter characteristic allows relatively minor changes in the current FPGA code to implement a similar method using the slow features of the local field potential (LFP[8]), which may be particularly useful in the translation of therapeutic closed-loop stimulation techniques.

Chapter 5 contains empirical data collected prior to the arrival of the author at the lab. These data form the basis for the majority of future hypothesis testing suggested in the dissertation, as well as the rationale for formulating the system identification problem as described in **Chapter 6**. This chapter fulfills the rest of Aim 1 using multiple of the preliminary processing pipelines, for which code is also publicly available. A manuscript, which roughly follows the contents of the chapter, is in preparation for submission to Nature Communications (Pack et al. 2020)[9]. A previous version, which pertains to the same data but lacks the descriptions of population dynamics has been archived on a pre-print server (Pack et al. 2020). The results of these data suggest that filtering related to skillful movement that occurs in bilateral motor areas becomes unstable in some rats with focal M1 ischemia. This instability, which most likely arises from sensory errors, is associated with worse functional outcomes, even when only considering stereotyped movements with successful outcomes. In the context of past work (Dancause et al.,

[8] The LFP is an electrical field that is measured using the differential between a measurement electrode and some distant impedance-matched reference electrode attached to the subject. The extracellular field potentials are sometimes referred to generically as the LFP; however, in this thesis the LFP is used specifically with reference to the “slower” signals of the brain. Therefore, further references to the LFP should assume a filter characteristic that is generally a low-order IIR low-pass filter with cutoff frequency of 100-Hz. Due to the frequency content being substantially lower than the acquisition sample rate, when discussed in this thesis, the LFP signal is almost always decimated from either 20 kHz or 30 kHz to 1 kHz after applying a second Chebyshev anti-aliasing filter.

[9] The dissertation author is listed second, but is noted as a co-first-author on this work.

2005; Nudo et al., 2000), the range of postoperative days required before it is possible to accurately regress linearized dynamics of the observed population features suggests that sensory errors are due to inappropriate gain on the synapses forming between *de novo* connections between motor and sensory areas.

Chapter 6 fulfills Aim 2 by providing an example model using the Kalman formulation to model 3D kinematic reconstructions using neural time-series. Code associated with this chapter resides in a public repository with instructions for use, so that the experimenter can tweak different noise parameters or assumptions on time-invariance as dictated by a hypothesized experimental design (such as might be arrived at after considering the results of **Chapter 5**). Preliminary data from an updated version of the pellet retrieval task are described. Data obtained using a peripheral mechanical stimulus in the anesthetized are also provided in order to suggest an activity substrate for filter nonlinearities that might be useful in future experimental design. These data are currently in preparation for submission to a peer-reviewed journal, although the full contents of the manuscript are not included with the chapter as not all of the study is relevant to this final chapter (Hayley et al. 2020).

The end of **Chapter 6** contains a recapitulation of the contents of this dissertation.

Notes to the Reader

Since one of the novelties of this work is its synthesis of approaches from several different disciplines to provide a conceptual framework for future experiments, the first order of business is to make a few clarifications in the hopes of unifying the expectations of a diverse readership.

Should I be reading this?

In all likelihood, if you are reading this work and not a member of the author's thesis committee, then you are a graduate student in the field of rehabilitation medicine. If you are considering performing experiments that relate elements of motor behavior to both injury and patterns of neural activity, then the answer to the section header is: yes. If your experiments involve rats retrieving pellets, then consider this required reading.

The ultimate goals of this work are to:

1) assist you in constructing practical, feasible, and informative future experiments. The work was specifically written for the reader who lacks--but is open to developing--a more technical background. To appreciate the insight that this work offers requires some basic concepts from signal processing, linear algebra, and differential equations. It does not require mastery of any of these areas, although understanding some of the key takeaways benefits greatly from a basic understanding of linear filter design. Some of the more technical sections require a more-detailed understanding of random processes and noise. Concrete parametric values provided in examples are meant to give an engineer without a background in physiology or biology better intuition for forming priors.

How is the motor phenotype studied in this work?

Motor neurophysiologists sometimes use the words "behavior" and "movement" interchangeably. Therefore, in the future contents of this work, "behavior" does not refer to the colloquial definition. Instead, any such reference refers to the building-blocks of behavior:

voluntary movement. In this context, the **Motor Phenotype** is a compound movement that occurs in phases delimited by three (required) landmark events during pellet retrievals in reaching rats:

- *Reach Onset*: the time of the first video frame in which the rat begins lifting and extending its forelimb toward the opening of the box, from inside of the box.
- *Grasp*: the time of the first video frame in which the rat clearly closes its digits. This can occur even if the rat misses the pellet.
- *Complete*: the time of the first video frame in which the rat retracts its supinated paw through the opening in the box and toward the mouth. This can occur even if the rat misses the pellet, although such instances are less common in Intact rats who typically immediately realize the pellet is not present and restart the reach[10].

The two phases allow the definition of three behavioral covariates with distinguishing trends between **Intact** and **Injured**[11] rats:

- *Total Duration***:** The total duration required to complete a trial, which is the time between the *Reach Onset* and *Complete* events.
- *Reach/Advance Duration***:** The duration between the *Reach Onset* and *Grasp* events.
- *Retract Duration***:** The duration between the *Grasp* and *Complete* events.

It should be noted that this description of motor phenotype is necessarily limited to the aspects thought most-likely the purview of the cerebral cortex. The building-blocks of movement (e.g. reflexes, postural control mechanisms, peripheral mechanical deficits), which are better-

[10] This behavior is sometimes referred to as **Flailing**, and is touched on further in **Chapter 5**.
[11] While the only injury model provided in this work is the vasoconstrictive ischemia induced by Endothelin-1 injections (ET-1), the terms **Intact** and **Injured** are used generically to indicate the variety of animal models of cortical injury available to the rehabilitation researcher. **Chapter 5** describes some of these models (as well as the motivation for the use of ET-1).

explained using subcortical or spinal circuits, are either not discussed or their effects are grouped together as process noise terms when relevant to formal models.

A note regarding molecular, cellular, or histological covariates.

The focus of this work is on building an assay to answer complicated and technical questions: are the new synapses on projections connecting spared motor and sensory areas after reorganization involved during movement? If this were the only question, perhaps alternative strategies not requiring the cumbersome relation of neural time-series data to the movement data would suffice. Such strategies could make use of classical tissue stains that relate to fundamental processes related to energy consumption at a cellular and molecular level. However, the refinement on this question suggests its significance to the future of rehabilitation medicine and also why such techniques were not used: can we identify pathological features of presumptive synaptic reorganization that explain why rehabilitation therapies sometimes succeed or fail? The only way to answer this latter question is to relate the neural control system at the level of cortical spiking and LFP patterns to movement measurements. An ideal experiment would also relate these measurements to coincident molecular features or at least make use of anatomical morphological measurements, such as synaptic bouton densities or the presence and orientation of sprouting processes. Unfortunately, all of these assays are more granular than the scope of this work: many cellular and molecular approaches were technically precluded by the mechanical disruption of nervous tissue due to the electrode microwire arrays.

A note regarding descriptions of a lateralized behavior.

A reader with a clinical background should note that the terms *contralateral* and *ipsilateral* are typically used with reference to the preferred reaching forelimb of the rat. Reference to the injury location is denoted as *contralesional* and *ipsilesional* with reference to the corresponding cortical area in both injured and matched intact control rats. Therefore, a description of an area

as *ipsilesional* does not mean that an injury was present, if the rat or group under discussion is the **Intact** group (as non-injured positive control rats shall always be described).

A note regarding mathematical descriptions and notational convention.

Equations appear infrequently as a matter of intent. However, in some cases, mathematical formulations are the clearest option for communication. Therefore, instances requiring mathematical descriptions provide illustrative examples with real values as they might appear in rat experiments. Certain sections, such as the end of **Chapter 2** or the majority of **Chapter 4** require more frequent use of technical language. A reader with a non-technical background should skip these parts. However, the author implores the same reader to work through the equations presented in **Chapter 5** and **Chapter 6**, which is the only way to grasp the significance of this work. Please do not hesitate to contact the author at any point via his personal email address (max.murphy11@gmail.com) with questions regarding clarification or explanation.

Operators used in definitions
Some operators that are not commonly-used[12] for those outside mathematical or technical engineering fields must be defined first to avoid alienating an unfamiliar reader from the outset:

- $\stackrel{\text{def}}{=}$ is read “equals by definition” and appears when defining an expression or formula
- $:=$ is also read “equals by definition” but is reserved for specific values
- $\in$ is read “in” or “element of” and refers to a set that some term belongs to.

Matrix notation

[12] Some notational conventions are different from common convention due to limitations related to the text editing software used in composing a majority of this work.

Upper-case letters denote matrices while lower-case letters denote vectors. Paired subscripts denote matrix row first, and column second[13]:

$$A = \begin{bmatrix} a_{1,1} & \cdots & a_{1,M} \\ \vdots & \ddots & \vdots \\ a_{N,1} & \cdots & a_{N,M} \end{bmatrix}, A \in \mathbb{C}^{NxM}$$

Variable modifiers
An asterisk to the right of a variable denotes a predicted quantity[14]:

$$\boldsymbol{x^*} \stackrel{\text{def}}{=} \text{predicted value of } \boldsymbol{x}$$

A tilde in the superscript to the right of a variable denotes an error quantity[15]:

$$\boldsymbol{x^{\sim}} \stackrel{\text{def}}{=} \boldsymbol{x} - \boldsymbol{x^*}, \text{ which is sometimes called the residual of } \boldsymbol{x}$$

Heuristic for writing means
Angled brackets around a variable denote an averaged quantity:

$$\langle \boldsymbol{x} \rangle \stackrel{\text{def}}{=} \text{average value of } \boldsymbol{x} \text{ (over all } \boldsymbol{x})$$

When a subscript is added to the right of the angled brackets, it indicates that the average was taken for that variable conditionally upon the value of the denoted subscript variable. In practice for the purpose of this text, such a reference is most common with respect to cross-trial

[13] $\mathbf{C}^{NxM}$ refers to the set of all such matrices with N rows and M columns consisting of elements from the set of complex numbers: in most cases, the set of real numbers suffices; however, the regression procedure that is critical to understanding the major findings of **Chapter 5** requires an elementary understanding of linearized dynamical systems.
[14] Often, a hat above a variable is used to the same purpose in other works.
[15] Often, the tilde goes above the variable instead of as a superscript in other works.

averages, where data from different trials aligned to a behavioral event are represented as a function of time relative to that event:

$$\boldsymbol{x}^{i}(t) \stackrel{\text{def}}{=} \text{value of } \boldsymbol{x} \text{ at time } t \text{ in trial } i$$

Where i is an index denoting which trial the function represents. Thus, the cross-trial average for the set of trials described by $i \in K$ is denoted:

$$\langle \boldsymbol{x} \rangle_{K}(t) \stackrel{\text{def}}{=} \text{cross-trial average of value of } \boldsymbol{x}(t) \in \boldsymbol{X}$$

Where $\boldsymbol{X}$ is the ensemble representing all functions $\boldsymbol{x}(t)$. Similarly:

$$\langle \boldsymbol{x} \rangle_{t} \stackrel{\text{def}}{=} \text{time-average for each function } \boldsymbol{x}(t) \in \boldsymbol{X}$$

In practice, such a time-average is used to avoid biases that spuriously decrease the total sum-of-squares during least-squares regression. The time-average is usually computed in epochs of 1-second or less around the motor behavior. Note that multiple subscripts might be used; for example:

$$\langle \boldsymbol{x} \rangle_{K,t} \stackrel{\text{def}}{=} \text{time-average for the cross-trial average function } \langle \boldsymbol{x} \rangle_{K}(t) \in \boldsymbol{X}$$

Conditional Expressions

Outside of notation used for conditional means, in general, if a function is to be realized conditionally upon some parametric value, then a vertical bar delimits the function arguments from the conditional parameter values (note when a function argument takes a specific value it is sometimes denoted in this way rather than supplying only the specific value; in such cases, the notation is a “long-hand” attempt to clarify where terms come from, and so if such notation seems redundant that is because it serves no other purpose than clarification):

$\mathbf{x}(t \mid i \in K) = \boldsymbol{x}^{i}(t)$, where i is an index in the set of L trials denoted by $K = \{i_1, \ldots, i_L\}$

With respect to discrete samples, which are always the form in which data are realized, the distinction between discrete sample functions and their continuous abstractions is signified by brackets:

$\mathbf{x}[t_m \mid m \in \{0,\ldots,M\text{-}1\}] \stackrel{\text{def}}{=}$ the value of the discretely sampled function $\mathbf{x}(t \mid t \in T)$ when $t = t_m$

Here, $T = \{t_0, \ldots, t_{M-1}\}$ denotes the set of M[16] times for which an associated value of $\mathbf{x}(t)$ was saved in the sample record. Such an elaboration of the discrete sample function will not be provided in each case, but here it serves to indicate that the value of time t is continuous, that only the instants denoted by elements of T are members of the set comprising the sample record, and that t_m is the specific value for the m-th sample. Note that $\mathbf{x}[t_m]$ is identical.

Similarly, the conditional operator appears more commonly in association with statements of probability and random variables. In this case, the tilde (~) is used to denote an element drawn from a random distribution[17]. A capital P is used to denote the probability of some expression. While a more detailed discussion of random variables accompanies the relevant parts of the text, a final explanatory example to synthesize the previous parts follows. Here, p is the discrete probability of a sampled function meeting or exceeding some value b:

[16] Note that indexing starts at t_0 (often pronounced "t-naught"). Therefore, a vector containing M samples only takes its final value at t_{M-1}. This semantic point becomes nontrivial when synchronizing time values across different datasets, analytical pipelines, and in general when indexing arrays in code. Realizing that in this formulation t_m is actually the $m\text{-}1$ sample, we will still refer to it as the "*m-th sample*" for convenience.

[17] Most commonly, the random process is hoped to be drawn from a zero-mean, White Gaussian Noise (WGN) process, in which case it is denoted by the normal distribution: $\boldsymbol{N}(\square, \square \mid \square = 0, \square = 1)$, where $\square$ denotes the distribution mean and $\square$ denotes the distribution standard deviation. If the WGN process is thought to have some temporal dependence (and typically, there is a first-order dependence on past values for these data), then $\square$ is used instead of $\square$ to denote the covariance matrix of adjacent samples. Other distributions employed in this work include the related Poisson and Binomial distributions, as well as the Uniform distribution. Each is discussed in the relevant later chapters.

$$p = P[\boldsymbol{x}^{i}[t_m] \geq b \mid \boldsymbol{X}[t_m] \sim \boldsymbol{N}(0,1)]$$

This formula should be read:

> "The value of *p* is equal to the probability that the *m-th* sample of function ***x*** for trial *i* is greater-than-or-equal-to *b*, given that the values of the *m-th* sample for all trial-related functions in the set ***X*** are drawn from a normal distribution with zero-mean and unit standard deviation."

When we restate the formula in english, we see how such a statement could commonly occur: in the case of neural time-series related to behavior, such expressions occur commonly when setting a threshold criterion to define a particular trial of interest.

If you've reached this point of the Introductory chapter, then one of two things has occurred: either you are serious about learning the contents of these works, or you saw equations and skipped to the end. Remember, to appreciate the strategies described herein, the student who lacks a technical background is required to restate each equation from the recommended chapters (specifically, **Chapter 5** and **Chapter 6**) using plain english as is done above. The equations are not conceptually difficult; however, glossing over them precludes the use of the experimental methods they describe.

References

Dancause, Numa, et al. "Extensive cortical rewiring after brain injury." *Journal of Neuroscience* 25.44 (2005): 10167-10179.

Feigin, Valery L., et al. "Worldwide stroke incidence and early case fatality reported in 56 population-based studies: a systematic review." *The Lancet Neurology* 8.4 (2009): 355-369.

Gowland, Carolyn. "Recovery of motor function following stroke: profile and predictors." *Physiotherapy Canada* 34.2 (1982): 77-84.

Hayley, Page, et al. “Modulation and representation of sensory responses in the premotor cortex of the rat following ischemic injury.” *Frontiers in Human Neuroscience*. (In Preparation)

Hickmott, Peter W., and Patricia A. Steen. "Large-scale changes in dendritic structure during reorganization of adult somatosensory cortex." *Nature neuroscience* 8.2 (2005): 140-142.

Kleim, Jeffrey A., and Theresa A. Jones. "Principles of experience-dependent neural plasticity: implications for rehabilitation after brain damage." *Journal of speech, language, and hearing research* (2008).

Mitz, Andrew R., Moshe Godschalk, and Steven P. Wise. "Learning-dependent neuronal activity in the premotor cortex: activity during the acquisition of conditional motor associations." *Journal of Neuroscience* 11.6 (1991): 1855-1872.

Milighetti, Stefano, et al. “Effects of tDCS on Spontaneous Spike Activity in a Healthy Ambulatory Rat Model.” *Brain Stimulation* (2020): In Press.

Mozaffarian, Dariush, et al. "Executive summary: heart disease and stroke statistics—2015 update: a report from the American Heart Association." *Circulation* 131.4 (2015): 434-441.

Murphy, Maxwell D., et al. "Current challenges facing the translation of brain computer interfaces from preclinical trials to use in human patients." *Frontiers in cellular neuroscience* 9 (2016): 497.

Murphy, Maxwell D., et al. "Assessing Perturbations to Neural Spiking Response Dynamics Caused By Electrical Microstimulation." *2018 IEEE International Symposium on Circuits and Systems (ISCAS)*. IEEE, 2018.

Murphy, Maxwell D., et al. "Improving an open-source commercial system to reliably perform activity-dependent stimulation." *Journal of neural engineering* 16.6 (2019): 066022.

Nudo, R.J., Milliken, G.W., Jenkins, W.M., and Merzenich, M.M.: ‘Use-dependent alterations of movement representations in primary motor cortex of adult squirrel monkeys’, J Neurosci, 1996, 16, (2), pp. 785-807

Nudo, Randolph J., Kathleen M. Friel, and Steven W. Delia. "Role of sensory deficits in motor impairments after injury to primary motor cortex." *Neuropharmacology* 39.5 (2000): 733-742.

Pack, Andrea, et al. “Restoration of rodent cortical dynamics after stroke.” *In Preparation* (2020).

Pack, Andrea, et al. "Task Related Neural Activity Following Primary Motor Cortical Ischemic Injury in Rats." *bioRxiv* (2020).

Ramanathan, Dhakshin S., et al. "Low-frequency cortical activity is a neuromodulatory target that tracks recovery after stroke." *Nature medicine* 24.8 (2018): 1257-1267.

Ward, Anthony B. "A literature review of the pathophysiology and onset of post- stroke spasticity." *European journal of neurology* 19.1 (2012): 21-27.

Wise, S. P., et al. "Changes in motor cortical activity during visuomotor adaptation." *Experimental Brain Research* 121.3 (1998): 285-299.

CHAPTER 2

Challenges in relating preclinical results to clinical BCI therapies

Abstract[18]

Current research in brain computer interface (BCI) technology is advancing beyond preclinical studies, with trials beginning in human patients. To date, these trials have been carried out with several different types of recording interfaces. The success of these devices has varied widely, but different factors such as the level of invasiveness, timescale of recorded information, and ability to maintain stable functionality of the device over a long period of time all must be considered in addition to accuracy in decoding intent when assessing the most practical type of device moving forward. Here, we discuss various approaches to BCIs, distinguishing between devices focusing on control of operations extrinsic to the subject (e.g., prosthetic limbs, computer cursors) and those focusing on control of operations intrinsic to the brain (e.g. using stimulation or external feedback), including closed-loop or adaptive devices. In this discussion, we consider the current challenges facing the translation of various types of BCI technology to eventual human application.

[18] The following chapter is mostly quoted from a literature review written by the author of this work and his colleagues (Murphy et al., 2016). Some minor modifications have been made in order to adapt the review to this doctoral thesis. The final section of the chapter includes a method reported by the author of this work and his colleagues in a 2018 conference proceedings paper (Murphy et al., 2018). This method relates to the final section of the review in that it describes a strategy for evaluating trial-by-trial changes in the cortical population spiking responses to microstimulation. It also relates to the subsequent chapters, because the described strategy introduces the consideration of population-level as a dynamical system, a point that is returned to in **Chapter 3**. In this case, the system is approximated using a nonlinear method: a variant of the variational autoencoder that uses a recurrent neural network (RNN) in order to identify the most-likely nonlinear system fit. Once the system has been recovered, it can then be used to estimate system-level perturbations, which may relate to the stimulation treatment regime.

Background

Brain-computer interfaces (BCIs) and their applications for treatment of nervous system damage have shown enormous progress as functional restoration tools in pre-clinical studies. In general, most BCIs are designed to bypass damaged structures and fiber tracts. BCIs range from common devices, such as cochlear implants that use externally recorded sound to directly stimulate auditory nerve fibers, to devices that derive control signals from cortical activity, allowing individuals with paresis to operate a prosthetic device. Other BCIs are designed to aid in acute rehabilitation training sessions. Regardless of the type, the major purpose of BCIs is to improve the quality of life for the patients who use them.

Damage to the nervous system can result in profound sensory, motor, and cognitive deficits that strongly impact day-to-day functioning of afflicted individuals. The type and extent of these deficits are dependent upon the location and extent of the injury. Injuries affecting motor cortex, such as might occur after a focal traumatic brain injury or stroke, can lead to impaired use of digits, limbs, or whole regions of the body due to loss of descending corticospinal neurons or disruption of sensory-motor integration. Spinal cord injury impacts communication of neural signals at the site of injury, leading to motor, sensory and autonomic deficits. For these types of injuries, there are no effective post-acute restorative treatments. Research in stem cell therapy to regenerate damaged neurons that could restore damaged pathways is currently underway (Gavins & Smith 2015, Hosseini et al. 2015, Sharma et al. 2015, Sullivan et al. 2015), but is likely years from fruition. Recovery after central nervous system (CNS) injury is thought to manifest itself through neuroplastic mechanisms, which have been shown to be aided through rehabilitative therapy (Nudo & Friel 1999, Nudo et al. 1996). Dramatic recovery from motor deficits has occurred in some cases (Bajaj et al. 2015, Warnecke et al. 2015), but recovery from neurological injuries rarely results in a full restitution of function. Effectiveness of any therapy is

constrained by the type and extent of injury, efficiency of neuroplastic mechanisms involved, and type of intervention. BCIs offer a pathway, in conjunction with rehabilitative therapy, for promoting restitution of function.

Current technology available for clinical populations ranges from simple devices that stabilize a shaking hand (Grimaldi et al. 2013; Popovic et al. 2011), to devices that augment the ability of a patient with locked-in syndrome to communicate with others (Holz et al. 2015). While these technologies offer promise for recovery from or for relief of symptoms of CNS injury, there are still many challenges in the integration of BCIs into effective prosthetic devices. These challenges include adequate spatiotemporal resolution in interpreting information recorded from the brain for naturalistic control, decoding a sufficient number of degrees of freedom to maintain natural movements, integration of feedback mechanisms, easing the technological support needed for integration of the BCI and reducing the invasiveness of components while maintaining the longevity of signal acquisition. Additionally, a number of recent studies have focused on devices contained entirely within the CNS that create artificial links between related areas. Here, we focus on the advantages and disadvantages of various approaches to interfacing BCI devices with the nervous system, based on results from both pre-clinical and clinical studies. We highlight the challenges associated with the implementation of high fidelity BCI devices to a clinical setting, possible methods for overcoming these challenges, and the distinction between devices that control extrinsic operations and those that control operations intrinsic to the CNS.

BCI operating modes

When considering potential clinical interventions using neural prostheses, a convenient way of classifying devices is based on whether they control extrinsic or intrinsic operations. In this review, BCI devices that operate primarily by detection of electrical signals from the CNS are mainly considered, as techniques for recording other measures of CNS information (i.e. magnetic, metabolic) are typically unwieldy for chronic use or cost prohibitive.

Figure 2.1A

Microelectrode Array

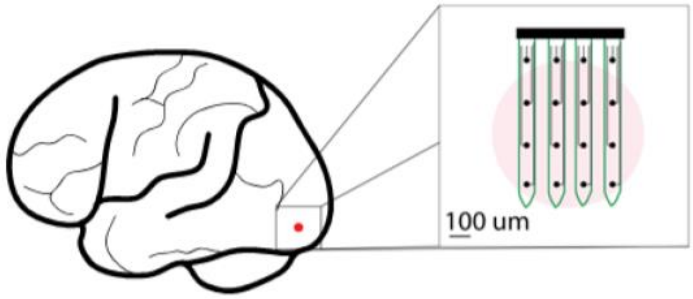

Aflalo et al. (2015)
Decoded recordings posterior parietal cortex.
Perge et al. (2013)
Intra-day instability in recordings from motor cortex.
Collinger et al. (2013)
Recordings from motor cortex allowed tetraplegic individual to move robotic arm with 7 degrees of freedom.
Hochberg et al. (2012)
Recordings from motor cortex allowed two tetraplegic individuals to move a robotic arm.

Figure 2.1B

Electrocorticography

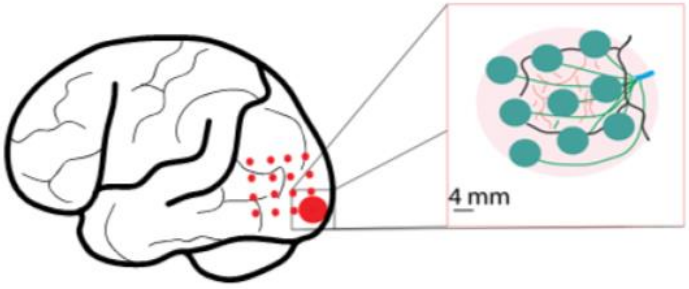

King-Stephens et al. (2015)
Chronic (average 4.7 years) recordings from patients with long-term implants.
Bouchard et al. (2014)
Recordings over speech cortices used to decode vowel acoustic features.
Bleichner et al. (2014)
Recordings over hand knob area decoded hand gestures.
Kellis et al. (2012)
Recordings over motor cortex decoded hand trajectory and controlled a cursor.

Figure 2.1C

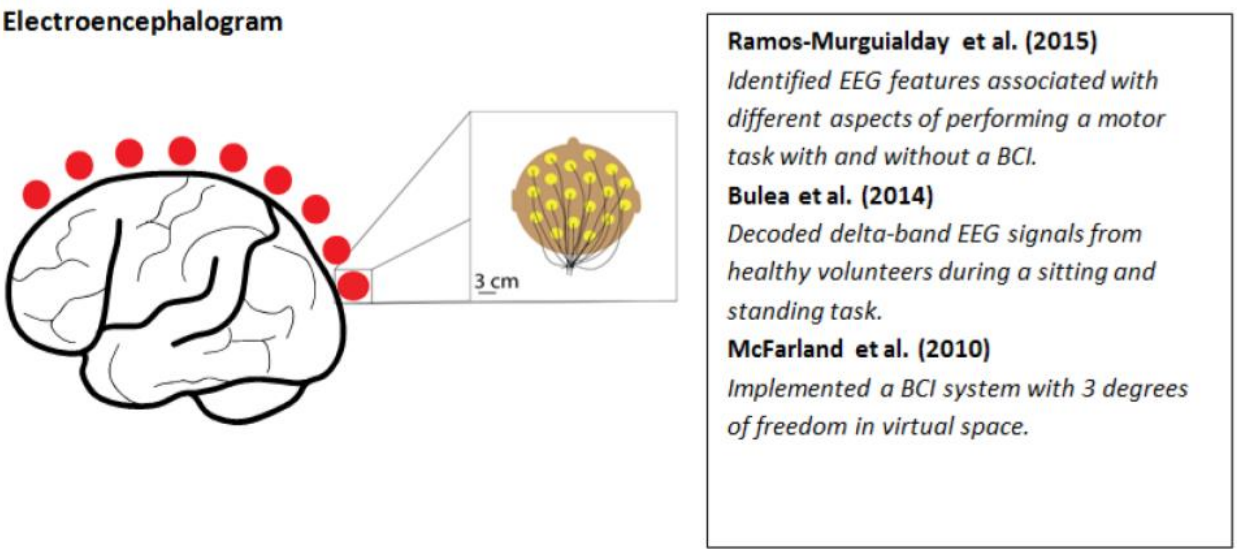

Figure 2.1: Spatial scales of recording types.
The resolution of each type of recording interface, as well as a selection of recent human studies associated with each interface is provided. Red dots represent the relative extent of recording interface placement, while insets demonstrate the scale and possible arrangement of electrodes at that site. **A)** Microelectrode arrays provide the highest spatiotemporal resolution, but must be inserted invasively into the extracellular tissue. **B)** Electrocorticography grids provide better spatiotemporal resolution than noninvasive sensors without compromising nervous tissue. **C)** Electroencephalography is the most readily-deployed in a clinical setting as it is noninvasive; however, the associated spatiotemporal tradeoff in signal fidelity may preclude its use in some applications.

Control of extrinsic operations

Neural prostheses are classified as controlling extrinsic operations when the device contains a decoder that records CNS signals in real-time, modifies those signals via a control algorithm

and outputs the translated and modified signal to a body-external device such as a prosthetic or robotic limb or a computer cursor. In this way the individual gains control over an artificial device that has the possibility to be incorporated into the body schema.

A limitation of devices controlling extrinsic operations is that accuracy in decoding movement intention is typically gained through an increase in the number of recording channels (Carmena et al. 2003); however, increasing recording channels brings the challenge of increasing channel density in a particular location of interest. Depending on the type of information being recorded and the decoding strategy, the increase in computational burden and power required from adding greater numbers of channels may also become nontrivial. Likewise, increasing the invasiveness of the electrodes can lead to increases in decoding accuracy, but at the cost of increased surgical risk and potential immune response (Ward et al. 2009). Additionally, chronic recordings are prone to drift in intent decoding, making repeated calibration necessary. Although these limitations prevent the widespread use of these BCI systems in clinical settings, studies to date are encouraging and represent tangible evidence of the type of functional restoration that can be achieved using BCIs. Here, BCIs controlling extrinsic operations are classified into three different categories based on the electrode interface used for signal acquisition from the CNS (**Figure 2.1**). These include two invasive electrode-CNS interface approaches (microelectrode array recording, electrocorticography) and one non-invasive electrode-CNS interface (electroencephalography).

Microelectrode array recording

Microelectrode array (MEA) recording, used in animal models for decades, represents the most invasive BCI approach, as penetrating microelectrodes are placed within the brain structure itself, typically within the grey matter of the cerebral cortex. Though the technology was initially developed in animal models, a relatively small number of human studies have now been

conducted with implanted MEAs. Microelectrode probes can range from a single-shank electrode to arrays consisting of tens of thousands of recording sites. The specific pattern and distribution of sites allows for dense population recordings throughout a single or multiple regions of interest. MEAs allow the highest spatial and temporal resolution of any type of neurophysiological recording system used in BCIs (Obien et al. 2014), but at the expense of spatial coverage at the site of recording. The use of MEAs allows for detection of the extracellular electric field changes reflecting the membrane potential of the individual neurons closest to the tip of each microelectrode.

While the voltage changes are quite small, neuronal action potentials, or spikes, can be detected within the electrical signal since rapid changes in membrane potential associated with the opening and closing of membrane ion channels have a characteristic temporal pattern. Due to their rapid onset and offset, the resulting detected spikes can be effectively reduced to point processes using voltage thresholding, simplifying the design of decoding algorithms, especially when large MEAs are employed. Further analysis using automated or semi-automated clustering algorithms or manual feature detection allows classification of multiple individual neurons recorded from a given recording site, increasing the accuracy of decoding (Todorova et al. 2014). It should, however, be noted that the process of detecting spikes introduces another source of error, with some techniques sacrificing accuracy for the sake of computational expedience (Rey et al. 2015).Depending on the information that needs to be obtained from spike trains, these errors can have a nontrivial significance (Pazienti & Grun 2006).

Once spikes have been detected and multiple neuronal spikes discriminated (if desired), typically the rate of firing (i.e., spike rate) of the individual neuronal components is calculated. Both accuracy and ease of computational processing are dependent upon the combined choice of a spike rate estimator and a spike rate decoder, with simpler methods allowing computations to be performed on a millisecond time scale and more complex, probabilistic models limiting

computations to seconds or even minutes (Cunningham et al. 2009). Based on these temporal limitations, the practical need for real-time adaptation when implementing a BCI makes some of the simpler methods more attractive (Cunningham et al. 2011). To this end, it has been demonstrated that the use of a closed-loop, adaptive decoder can also lead to increased simultaneous neural adaptation, resulting in improved skill retention (Orsborn et al. 2014).

Preclinical BCI research in animal models has typically utilized implanted MEAs chronically embedded in the cortex for decoding movement intention. The rationale for this approach dates to the 1960s when Evarts found that neurons in the motor cortex of non-human primates (NHPs) altered their firing patterns immediately prior to the onset of movement (Evarts 1966) and was later strengthened when Fetz demonstrated that neuronal firing rate could be volitionally controlled (Fetz 1969). More recent studies in NHPs demonstrate a consistent ability to decode signals to move transiently paralyzed limbs (Ethier et al. 2012), a simulated or robotic limb (Carmena et al. 2003, Velliste et al. 2008, Wessberg et al. 2000, Willett et al. 2013), or a cursor on a screen (Nuyujukian et al. 2014, Taylor et al. 2002, Wu et al. 2004), and even predict hand orientation with extremely high accuracy (Peng et al. 2014).

MEAs have proven resilient in producing reliable signals from a single area over periods of up to a year (Flint et al. 2013). However, longevity of single unit recordings with indwelling electrodes has been one of the major limitations of this approach. For example, studies have shown a decay in signal strength over the course of 100 days (Rousche & Normann 1999), and large performance variability between trials and type of electrode used (Ward et al. 2009). Furthermore, information generated by decoders has been shown to diminish over extended implantations (Nuyujukian et al. 2014). This somewhat variable, and arguably short, lifetime limit for recording robust signals from implanted MEAs still needs to be addressed by future improvements in MEA materials technology. While estimates of the number of neurons needed to decode arm movements off-line range between 150 neurons with serial single unit recordings

and 600 units from MEAs (Georgopoulos et al. 1986), accurate on-line BCI control is possible with far fewer recorded units due to the closed-loop adaptation that occurs when learning BCI skills (Carmena et al. 2003, Taylor et al. 2002). This phenomenon could be a key to improving long-term patency of indwelling MEAs. If it is possible to use only a subset of sites to generate information for decoding, then as those sites slowly lose functionality it may be possible to use redundant sites, allowing for an extended prosthetic lifespan.

Although MEA studies in humans are limited due to their invasive nature, recent results indicate the advantages of using such high-resolution paradigms. Aflalo and colleagues found that the decoding of spike trains associated with motor imagery in a patient chronically implanted with MEAs embedded in the posterior parietal cortex resulted in the smooth movement of a robotic limb with 17 degrees-of-freedom (Aflalo et al., 2015). Two 96-channel MEAs were embedded for 21 months with no signs of adverse effects. The subject was asked to imagine reaching toward a specific goal, and channels that demonstrated preferential firing when the subject imagined achieving the goal were discriminated from neurons tuned to trajectory. When these goal-tuned units were used as tuners for accomplishing a specific task, decoding accuracy was higher for a given number of units. It should be noted, however, that the goal-tuned units changed over time, indicating that an adaptive decoder would be important for this sort of prosthetic device to be implemented in the future for long-term implantations. This problem of varying tuning is also seen in recordings from units in the motor cortex (Perge et al. 2013).

These changes in tuning were most likely due to physiological changes in the neuronal firing patterns as a result of adaptation to the decoder. As the patient learns to operate the BCI, functional reorganization occurs in multiple brain areas, resulting from closed-loop feedback and adaptation to performing the new BCI-related task, and presumably allowing a smaller number of units to function in tuning the device (Carmena et al. 2003, Taylor et al. 2002). The ability to produce a smooth movement based on the decoding of a goal-tuned unit represents a

significant divergence from previous studies involving chronically implanted MEAs in human patients. These studies used motor cortex (Collinger et al. 2013, Hochberg et al. 2006, Hochberg et al. 2012) as an area for control, and were quite successful; however, a noted limitation was that movements produced using these systems were slower and somewhat inflexible (Hochberg et al. 2012) when compared to natural reaching movements. Thus, the ability to use a goal-tuned unit in the posterior parietal cortex as a control source for decoding intent using motor imagery could serve as an informative alternative to decoders focused on the motor cortex.

There are several additional challenges related to using MEAs in BCIs for clinical populations. The insertion of MEAs into cortical tissue is an invasive procedure requiring a craniotomy and resection of the dura. The surgical procedure introduces a possible pathway for infection. MEA implantation can lead to small-scale tissue damage that increases with a greater number of implants. Glial scarring occurs at the insertion site, and is thought to be a major factor reducing the longevity of usable signals that can be recorded in a chronically implanted individual. Another major problem of chronically implanted MEAs is micro-motion, which causes the formation of scar tissue, leading to a decrease in the quality of recordings over time (Ersen et al. 2015, Williams et al. 2007). Current materials research is focusing on changing various properties affecting the stiffness of the microelectrode, in the hope that scar tissue formation caused by micro-motion will be minimized (De Faveri et al. 2014). The different types of MEAs in use as of 2014 is reviewed comprehensively by Obien and colleagues (Obien et al. 2014).

The viability of MEAs in clinical use may ultimately depend upon further advances in materials research (De Faveri et al. 2014, Felix et al. 2013, McCarthy et al. 2011, Tooker et al. 2012).

A potential solution for MEA signal stability would be to implement BCIs that utilize somewhat lower-fidelity neural signals. One signal that can be acquired by MEAs is the local field potential (LFP). The LFP represents the summation of active cellular processes nearest the site of each microelectrode. While the general process of analyzing LFPs is similar to analyzing spike data, the computational stage and filtering is somewhat different (**Figure 2.2**), and some delay is inherent due to the latency with which changes in spectral power occur and can be measured. Despite these limitations of LFPs, the advantages of increased recording stability may outweigh the loss in accuracy.

Figure 2.2

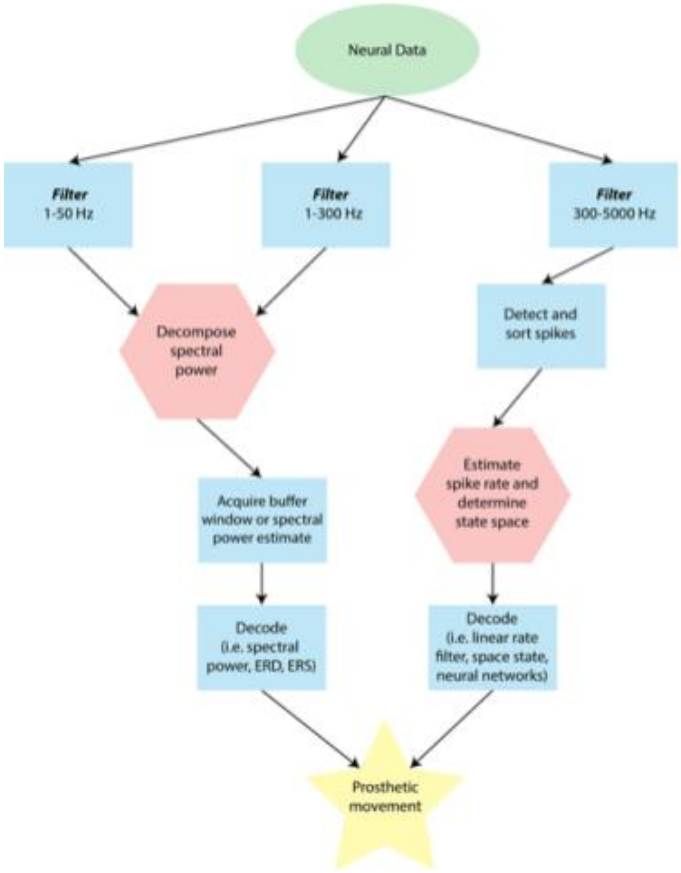

Figure 2.2: Source-dependent BCI schema.

Differences in decoding schema depend upon neural state signal (*left: LFP; right: spikes*). Comparable stages take the same color. The green ellipse represents data as it is recorded and amplified from the neural source. Blue rectangles represents common filtering and processing steps that introduce minimal delay. Red hexagons represent potentially rate-limiting steps in determining the latency of the BCI response to immediate internal changes in patterns of neural activity.

A combination of lower-fidelity LFP recordings and spike recordings might also be desirable. It is possible to generate predictions of the imagined single-joint movements in a tetraplegic individual by decoding the joint trajectory using the LFP frequency signals and multi-unit spike activity similarly to those predicted by decoding single-unit activity (Ajiboye et al. 2012). Hall and colleagues indicate that it is possible to estimate single unit firing rates using the slow potentials from LFPs derived at several cortical locations (Hall et al. 2014). If this method can be applied to estimate the single unit firing rate of a single unit, without the need for first gathering spike data to calibrate the estimation, it could lead to the development of a BCI with sufficient longevity that still offers good spatiotemporal resolution. However, it is important to note that the filters used to perform the necessary calculations to deconvolve the firing rate of a single neuron from the low frequency LFP signals using current methods require prior knowledge of spike train information from multiple neurons. Furthermore, when using single-unit activity decoded from LFPs, there is an additional step of transforming the data during which accuracy could be lost. Despite these limitations, the method described by Hall and colleagues offers the added benefit of allowing accurate single unit firing rate predictions over the course of several weeks, which is an improvement on intra-day instabilities in decoding from single-unit activity itself (Perge et al. 2013). In this way, using LFP decoders in conjunction with single- and multi-unit activity may be a key step in implementing long-term implants.

Electrocorticography grids

Electrocorticography (ECoG) consists of a mesh or grid of electrodes distributed across the cortical surface that can be placed either subdurally or epidurally. This technique can detect the LFPs from the cortical surface at specific locations, but does not have the resolution to detect individual spikes. As less invasive interface approaches are used, the focality of the recorded signal necessarily is degraded. What ECoG lacks in spatiotemporal precision with respect to individual spiking profiles, it makes up for in patency. ECoG has shown resilience in long-term recordings in human patients implanted for up to 7.1 years (King-Stephens et al. 2015). In addition, ECoG has the ability to expand the extent of spatial coverage relative to MEAs. For example, signals can be detected and decoded simultaneously from M1, PMd, and S1. Additionally, using this method, it is possible to detect not only recordings from gyrus, but also from the sulcal wall (Yanagisawa et al. 2009), albeit via a more invasive process.

In humans, most studies investigating the use of ECoG for BCI applications have used clinical electrodes implanted in epilepsy patients for localization of epileptic foci with an electrode size on the order of a few millimeters and an interelectrode distance of approximately 1 cm. In particular, movement-related spectral power changes have been shown to occur not only during overt movements of skeletal musculature, but also during imagined movements (Leuthardt et al. 2004), indicating that these spectral power changes may be useful in motor-impaired patients who are unable to perform overt movements. Furthermore, several studies have demonstrated that functionally motor-intact human patients can modulate the spectral power of ECoG signals to achieve on-line control of a computer cursor (Felton et al. 2007, Leuthardt et al. 2004, Schalk et al. 2008, Wilson et al. 2006).

ECoG has also been used to implement BCI devices in motor-impaired patients. A study in a hemiparetic patient demonstrated that it is possible to use ECoG to control a prosthetic arm using recordings from sensorimotor cortex (Yanagisawa et al. 2011). Additionally, the use of ECoG signals for control of a BCI system with three degrees-of-freedom based upon motor imagery of movements at multiple independent joints has been demonstrated in a quadriplegic patient with good signal quality for durations up to one month (Wang et al. 2013). While on-line BCI control in human patients with ECoG has been limited to short durations, with relatively large electrode sizes, arrays with sub-millimeter electrode sizes have been proposed as a means to obtain signals with increased spatial specificity. These micro-scale arrays have been utilized for online BCI control experiments in NHPs (Leuthardt et al. 2009, Rouse et al. 2013). Importantly, these studies utilized chronic epidural recordings, demonstrating the stability of ECoG signals as well as the potential to implant ECoG BCI systems on the surface of the dura, which would reduce the risks of infection due to isolating the implant from the subdural space.

While closed-loop BCI systems generally have used changes in spectral power associated with imagined movements of a single joint in humans or high gamma power in arbitrary electrodes in NHPs, a more natural control algorithm may be to use signals decoded from natural movements or behaviors. The potential for this type of BCI using ECoG has been demonstrated by studies that have used ECoG signals to decode 2D movement directions in rats (Slutzky et al. 2011) and NHPs (Flint et al. 2012) and to continuously decode movement kinematics of 2D (Flint et al. 2012, Marathe & Taylor 2013) and 3D arm movements in NHPs (Chao et al. 2010). Along with animal models, ECoG recordings from human epilepsy patients have been used to decode information about voluntary movements. ECoG recordings have been used to classify movement directions of arm and hand movements (Chestek et al. 2013, Reddy et al. 2009, Wang et al. 2012). Similarly, it is possible to decode continuous finger flexion/extension (Chestek et al. 2013) and 2D arm and hand trajectories using ECoG with modest accuracy

(Kellis et al. 2012, Pistohl et al. 2008, Sanchez et al. 2008, Schalk et al. 2007), as well as move a cursor to an onscreen target using full neural control with no trajectory decoding (Kellis et al. 2012). Flint and colleagues extended these findings to show that it is possible not only to determine trajectory, but kinetics for use in functional electrical stimulation as well using ECoG (Flint et al. 2014). There are also preliminary indications that ECoG in patients with stroke and epilepsy can be used to predict three degrees-of-freedom in arm trajectory during motor imagery (Nakanishi et al. 2013). Other recent experiments have used high-density ECoG placed over specific areas to yield high accuracy decoding. Placement over the speech cortices yielded accurate prediction of vowel acoustics during speech (Bouchard & Chang 2014), and placement over the hand knob area in sensorimotor cortex resulted in decoding of hand gesturing (Bleichner et al. 2014), with high frequency signals (>65 Hz) showing the most accurate results. In general, it should be noted that the higher frequency signals tend to produce more accurate results, presumably in part because there is a shorter latency between intent and decoding/feedback.

Electroencephalography caps

EEG is the least invasive technique, but also provides signals with the broadest spatiotemporal coverage of the cortex. Similar to ECoG, EEG detects general electric fields that are a sum of the electrical activity for a given region. However, as the EEG signal detection is somewhat distant to the site of interest (e.g. the precentral gyrus) there is an inherent limitation to spatial and spectral resolution during signal acquisition. Because the voltage from a dipole falls off with the inverse of the square of the distance from the dipole, the extra distance between neural sources in the cortex and EEG electrodes causes a summation over a wider range of cortex (Cooper et al. 1965). The spectral resolution limitation is due primarily to the fact that higher frequency signals, which are more focal, tend to be averaged out by the low spatial resolution. In addition, high frequency activity in general is lower in amplitude than low frequency activity,

and can be filtered out from the inherent dampening of the bone and tissue that it must travel through (Cooper et al. 1965, Pfurtscheller & Cooper 1975). Finally, EEG signals are also susceptible to contamination from electromyographical (EMG) artifacts or eye blinks (Cooper et al. 1965, Wolpaw & McFarland 2004). Due to these complications, trajectory predictions using EEG are generally not as accurate as those using MEA recording or ECoG.

Despite these limitations, EEG provides an excellent method for obtaining neural information from patients in a clinical setting without the need for surgery. EEG is also promising for use in acute settings that could be associated with rehabilitation and behavioral recovery, since it is non-invasive in nature. One of the hopes for EEG is that by using proper placement of a sufficient number of leads and a significant amount of prior data in healthy patients, it will be possible to use frequency signatures from different areas to overcome some of the spatiotemporal problems listed previously. As noted previously, EEG has the advantage of broad spatial coverage in recordings. It may be possible to turn this broad spatial coverage into an advantage in resolving the origin of activity in the brain. There is a large body of work in EEG source imaging that focuses on estimating the location of current sources for scalp measurements by solving the so-called static electromagnetic inverse problem. This is done using the collection of scalp measurements as well as a set of reasonable a priori constraints based on the assumed or measured physiology of the brain to determine the most likely origin of the current source or sources. As Michel and colleagues detail in their review of such techniques, such estimates depend on a number of factors, including but not limited to the number and position of electrodes on the scalp, the solution algorithm used to solve the inverse problem, and the integration of MRI data to serve as a prior (Michel et al. 2004). Recent studies demonstrate that it is possible to incorporate such source estimation techniques to EEG recordings for potential use in future BCI applications (Aihara et al. 2012, Yoshimura et al. 2012).

Although a variety of signal analyses have been used for EEG BCI systems (Blankertz et al. 2004), a more traditional approach has been to utilize average features of the frequency spectrum in relation to a motor event. A common strategy is to identify periods of event-related desynchronization (ERD) as a cue for some BCI output. ERD itself is a decrease in a pre-defined spectral frequency band that can have a different physiological interpretation depending on the context of the task. Controlling a BCI system with ERD associated with motor movements has particular relevance to motor-impaired populations. Because ERD has been shown to occur with imagined in addition to overt movements, it is applicable as a BCI control signal in patient populations that are unable to execute motor actions (Pfurtscheller et al. 1997). The application of EEG ERD-based BCI systems has been demonstrated in normal controls and patient populations (Blankertz et al. 2004, McFarland et al. 2010, Pfurtscheller et al. 2003, Wolpaw & McFarland 2004, Wolpaw et al. 1991). While EEG is a powerful tool due to its ease of use and non-invasiveness, its use in BCI system development is hampered by the limitations described above. To date the best performance of an EEG BCI system in control of extrinsic operations is three degrees-of-freedom, which was only achieved after months of intensive training (McFarland et al. 2010).

Although EEG-based BCI that use ERD and event related synchronization (ERS) in various frequency bands are common, recent work has aimed at providing a more comprehensive picture of changes through various power bands through the duration of a variety of tasks. Depending on the task, and thereby, the neural circuits involved, different signal features may be important at different times relative to the event of interest. A recent study identified EEG features in healthy subjects related to several stages of motor activities (Ramos-Murguialday & Birbaumer 2015). Ideally, when using EEG to control a BCI, the different components of a movement would have distinct feature signatures that could be detected. Indeed, in this study it was noted that there were distinct features during active and passive proprioception, active

intention, and passive involvement in motor activity. Importantly, these features were significantly different when performing a BCI task as compared to other motor tasks, indicating that decoder design must take into account changes in EEG features depending on the type of activity involved.

Other less time-sensitive applications than fine motor movement may lend themselves to BCIs that utilize even lower frequency signals, sometimes referred to as slow cortical potentials (SCPs) or movement-related cortical potentials (MRPs). T In these cases accuracy can be added by including pre-processing steps using a variety of methods to reject false positive signals. A recent study has demonstrated that it may even be possible to decode movement intent from delta-band (0.1-4 Hz) features, showing high accuracy in movement classification during a sitting-to-standing task in healthy volunteers (Bulea et al. 2014). In fact, BCIs using slow signals have applications even beyond motor tasks, such as allowing communication via a spelling device for patients with locked-in syndrome (Birbaumer et al. 1999) or even allowing web-browsing for paralyzed patients (Bensch et al. 2007). Another recent direction for improving accuracy is seen in the development of the brain/neuronal computer interface (BNCI). The recent distinction between BNCI and BCI devices draws on the fact that the BNCI makes use of other signals or current sources recorded from the body that are not located directly in the brain. Soekadar and colleagues demonstrated that it is possible to use electrooculography (EOG) in conjunction with EEG to improve use of a grasping hand exoskeleton (Soekadar et al. 2015a).

Control of intrinsic operations

Some implantable devices operate by modifying the flow of information or causing modifications in the functional neural networks of the brain. These devices control what can be considered intrinsic operations in the brain: operations that require internal transformations on information

related to its encoding (e.g. internal model construction or memory formation) or decoding (e.g. prediction or modulation of peripheral motor or sensory effectors). Devices in this category fall into two sets: open-loop and closed-loop stimulators. In open-loop stimulation, some form of stimulation is applied to a region of the brain with a frequency that is often determined using physiological parameters, but not necessarily correlated to the immediate activity of the brain. Such open-loop devices deliver a constant stream of current to the site of interest, as is predominant in deep brain stimulation (DBS), although recent studies have used closed-loop DBS for treatment of Parkinson's Disease (PD), epilepsy, and intention tremors, as will be noted. There is also interest in the application of open-loop stimulation in conjunction with BCI therapy; however, only closed-loop devices will be considered further in this review.

Closed-loop control of intrinsic operations

By nature of their application in primarily remedying some sort of functional deficit to patients, most BCIs could be broadly considered as closed-loop devices by virtue of the feedback a patient receives, typically visually, from the device when using it. In this review, we will be more precise with the definition of closed-loop strategies, and break "closed-loop" into two subcategories. The first subcategory of closed-loop strategies incorporates the ongoing activity patterns of individual neurons or ensembles of neurons to determine when an electrical stimulus will be applied in another location. Therefore, a broad category of such device is any BCI designed to facilitate the flow of information from one region of the brain to another (**Figure 2.3**). These strategies are not driven by patient recognition of some extrinsic goal, but rather form a completely internal closed-loop, which may relate indirectly to a goal-motivated behavior but does not need to be perceived as such. For example, using this definition, a BCI with an extrinsic goal might be an upper extremity BCI prosthesis that reaches to retrieve an object: the target of the reach provides an overt goal that is perceived by the subject. On the other hand, a closed-loop BCI targeting an intrinsic operation would likely not be perceived directly in

combination with a goal; for example, a stimulator designed to provide sensory feedback by restoring cortical interactions between motor and sensory areas may provide sensory stimuli, assisting the subject achieve some movement-related objective, but the actual operation of such a BCI is not immediately related to the perceived goal of the subject performing the task.

Figure 2.3

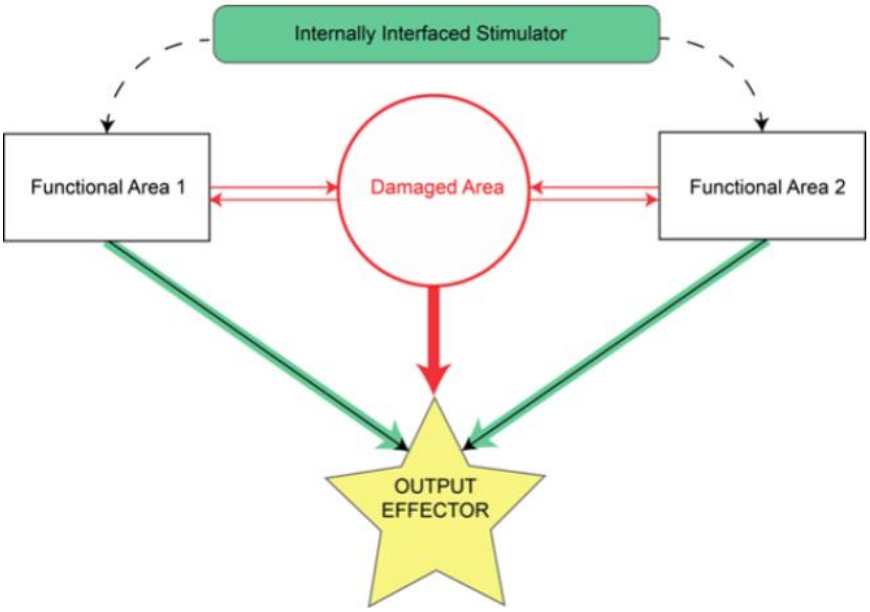

Figure 2.3: Schematic for internally-interfaced BCI

Schematic for intrinsic operation of a stimulation device to restore function lost due to missing or damaged tissue. Prior to injury, the damaged area (red circle) issues output commands to some effector (yellow star). After injury, connections to and from the damaged area are lost (red elements). The stimulator (green) interfaces disconnected elements, strengthening functionally-related output (green arrows).

In general, feedback from an applied stimulus that controls intrinsic operations is less overt, as electrical stimulation is generally at subthreshold levels when generating sensation or

movement, and measures of functional outcome are harder to ascertain on a trial-by-trial basis. In contrast, such feedback results in gradual changes in network connectivity, cognitive function or memory. This feature of intrinsic control provides an additional challenge since the network changes are thought to rely on Hebbian learning mechanisms, as are discussed below. While it is true that at the synapse such a circuit would comprise a feed-forward system, it is generally the case that reciprocal anatomical projections exist between cortical areas (Donoghue & Parham 1983, Zhang & Deschenes 1998), leading to bi-directional information flow and thus closing the loop. Stimulation in this paradigm requires not only a high-fidelity signal to detect and decode trigger events, but a highly focal, transient stimulus delivery. This is relatively simple when using MEAs to deliver the stimulus, but becomes more challenging when using less focal types of stimulation such as epidural stimulators or transcranial magnetic stimulation that stimulate relatively large volumes of tissue.

In PD, it is thought that DBS can improve motor functioning by disrupting abnormal activity. To improve upon existing, open-loop DBS methods, one study in 8 PD patients used frequency characteristics of LFPs recorded from the subthalamic nucleus (STN) to determine when to stimulate. Since beta frequencies (13-30 Hz) are thought to correlate with impairment in PD, stimulating the STN only during periods of high beta activity provides an adaptive, or closed-loop, approach to DBS (Little et al. 2013). This adaptive DBS caused a significant increase in subjects' neurological scores compared with continuous or random DBS. A closed-loop BCI to control intrinsic operations has also been used in epilepsy patients. In a randomized multicenter double-blinded controlled trial of 191 subjects, ECoG electrodes were used to detect epileptiform activity in the recorded signal (Heck et al. 2014). Following detection of epileptiform activity, brief pulses of electrical stimulation were applied to the seizure focus, an approach known as responsive focal cortical stimulation (RNS). Subjects receiving RNS showed a significant reduction in partial-onset seizures after two years in the study. In treatment of

intention tremors, surface electrodes recording EMG activity have been used to create a sort of closed-loop on-demand control system for DBS that may reduce patient resistance to treatment by stimulation (Yamamoto et al. 2013).

Aborting pathological activity using feedback-controlled electrical stimulation is just one application for closed-loop control of intrinsic operations. Another application is to facilitate synaptic efficacy of specific neural connections, using the natural timing of neuronal firing between groups of neurons. This approach derives its rationale from Hebbian plasticity theory, which posits that neuronal connections are strengthened when presynaptic activity is temporally linked with post-synaptic activity. Because synaptic efficacy changes rely on precise millisecond by millisecond timing relationships, approaches to investigate closed-loop control in this context necessarily require the highest temporal resolution possible. To date, this has been achieved only with MEAs recording individual neuronal spikes. In 2006, Jackson, Mavoori, and Fetz showed that it is possible to modulate activity of neurons within the motor cortex based on a spike-dependent stimulation paradigm (Jackson et al. 2006). In this model, monkeys with chronically implanted microelectrodes in two nearby populations of neurons in the motor cortex were trained on a torque-tracking task. The two populations were tuned to different trajectories. However, when one of the microelectrodes was stimulated based on the spikes recorded from the other microelectrode, the trajectory tuning became similar between the two populations. This study suggested that it is possible to alter existing cortical connections by “linking” two areas together using closed-loop stimulation. Of added interest is the fact that these changes persisted even after the closed-loop period ended, indicating that it was possible to induce long-term changes in synaptic efficacy using this paradigm.

Extending this idea to a traumatic brain injury model, Guggenmos et al. (2013) showed that it is possible to restore a reaching function in rats following damage to motor cortex by linking the premotor and somatosensory areas using activity-dependent stimulation (ADS; Guggenmos et

al. 2013). In this study, a focal impact was made over the rat's caudal forelimb area in the motor cortex, abolishing its ability to perform the reaching task effectively, largely due to the disruption in somatosensory motor integration. A recording microelectrode was implanted in the spared rostral forelimb area (RFA), which is somewhat analogous to the primate premotor area. A stimulating electrode, which was triggered by a wireless, battery-operated, head-mounted chip, was implanted in the primary somatosensory (S1) forelimb area. In the ADS paradigm, which ran continuously 24 hours a day for up to 28 days, spikes detected in RFA were used to trigger stimulation in S1 after a brief delay (7.5 ms). Remarkably, rats in the ADS protocol demonstrated a significant recovery of functional reaching behavior within a few weeks of ADS treatment. In conjunction with behavioral improvement, synaptic potentiation between S1 and RFA increased as well. Recently, a version of this paradigm has been applied to the rat cervical spinal cord as well, demonstrating a possible treatment mechanism for spinal cord injury, although the trigger signal was EMG activity and not primary CNS activity (McPherson et al. 2015).

There are still a number of unanswered questions regarding the effects of ADS in the context of neuronal pathologies. For example, it is not yet known how long the effects last, or the duration of the therapeutic window. Nevertheless, such a strategy of changing synaptic efficacy is an attractive option for use in a temporary implant because it raises the possibility of a removable or degradable device that only needs to function transiently. Thus, the simplicity of use of the device would mean a one-time surgical operation for patients, with the possibility of having a degradable or removable device that could then either be left in situ or explanted after treatment. In addition, aside from setting the thresholds for spike detection, there are a minimum of decoding algorithms that must be customized for individual patients, increasing the feasibility of such an approach in a clinical setting.

Other devices that control intrinsic operations have utilized a different approach. These devices restore cognitive function by replacing circuitry of the brain that is missing or malfunctioning (Berger et al. 2011, Berger et al. 2012, Bonifazi et al. 2013, Hampson et al. 2012, Opris et al. 2012). Berger's group demonstrated that it is possible to improve rat memory scores in a delayed non-match-to-sample task by implanting a device to translate spike trains detected in CA3 into stimulus trains in CA1 (Berger et al. 2012). Presumably, this closed-loop stimulation acts as a proxy for lost hippocampal function, modifying the spatiotemporal coding of the neural spike information in a similar way to the intact brain.

A major remaining challenge for these types of devices is that in order to increase the degree of complexity of information transmitted, it is necessary to increase the number of inputs. This problem presents a similar challenge as in the externally operating device case in that there is a density limit to the number of electrode sites that can record from a given area at a particular time. As the number of inputs increases, the computational difficulty increases as well. Put in context, a 2004 study by Izhikevich that modeled 100,000 neurons with 8.5 million connections between them took roughly 60 seconds of computation time for every 1 second of simulation time (Izhikevich et al. 2004). While technology has improved substantially since 2004, it is easy to imagine that as the number of neurons increases the computational difficulty will increase quickly, too. Thus, the complexity of the cognitive task being recovered will most likely determine the feasibility of employing such techniques.

As mentioned previously, a second strategy exists when incorporating closed-loop strategies for control of intrinsic operations. These types of devices are commonly classified as "restorative" BCI, as they are primarily used in rehabilitation treatments as a means to train patients to overcome some form of impairment. While they technically do affect some element extrinsic to the patient, the goal is to cause lasting intrinsic plastic changes that remedy deficits and eventually allow the patient to no longer need the use of the BCI; thus they are classified here

with the other intrinsic devices. For example, a BCI designed to reward desynchronization of particular oscillatory rhythms in stroke patients with corresponding proprioceptive feedback by movement of an orthosis demonstrated a clinically meaningful change in assessment scores of patients receiving the orthotic treatment against controls (Ramos-Murguialday et al. 2013). This type of training BCI has been the subject of much interest in the field. One direction is the adjunctive use of non-invasive electrical stimulation with training BCI to enhance learning by amplifying the ERD signal using anodal transcranial direct current stimulation (Kasashima-Shindo et al. 2015, Soekadar et al. 2015b, Soekadar et al. 2014). Another avenue is the use of graded velocity feedback in response to the relative strength of the ERD signal to improve learning by providing improved visual and proprioceptive feedback during BCI-triggered orthotic movement (Soekadar et al. 2011). In this study, even stroke patients demonstrated improved modulation of ipsilesional activity; a similar study demonstrated evidence that this paradigm could lead to new voluntary EMG activity in hemiparetic patients (Shindo et al. 2011). There are a few case studies involving BCI for modulating intrinsic operations as well. One study used visual feedback for the control of excessive levels of beta band activity detected by EEG, providing some evidence that this paradigm could cause voluntary changes in pathological brain activity and improve handwriting for a patient suffering chronic writer's cramps (Hashimoto et al. 2014). A within-subject withdrawal design in functional EEG BCI-driven neuromuscular electrical stimulation showed some restoration of voluntary EMG activity in a paretic patient where previous rehabilitation treatments had failed (Mukaino et al. 2014). Methods of non-invasive stimulation that could tentatively be used with some of the aforementioned strategies have been proposed, but are still in preliminary stages (Soekadar et al. 2013, Wilde et al. 2015, Zrenner et al. 2015).

Optimization criteria for closed-loop BCI that control intrinsic operations

While many of the restorative closed-loop BCI devices have demonstrated substantial clinical efficacy, one common theme among closed-loop devices that do not fall under this category is that they are still farther from clinical application when compared to their externally interfaced counterparts. This may be, in part, because the underlying mechanisms of some of the internally interfaced devices are still not well understood. For example, in a device attempting to recreate the firing patterns connecting one region to another, what sort of simulated pattern would be important to use? Or in the stimulation-dependent closed-loop system, how does the "linkage" between the two areas occur? Before the translation of these devices to a clinical setting, there remains a large amount of investigation to understand the mechanistic means by which these devices work. Even in those devices that are closer to widespread clinical implementation, the neuronal substrates for improved control and use of BCIs are not entirely understood (Soekadar et al. 2015b).

A large remaining area of study is to demonstrate specific features of how these internally interfaced devices affect changes in network connectivity. For example, a method to measure the putative changes in anatomical connectivity between two artificially linked areas would be to look at the number of projections from one area to the other in animals with and without the device post mortem; this provides a statistical means for comparison between groups, but is limited in the description of functional connectivity that may take place. Alternatively, means of visualizing connections in the brain such as diffusion tensor imaging has been used in rats *in vivo* (Laitinen et al. 2015), and could be employed for such a within-subject comparison study; however, it can be cumbersome to use such methods to map animals pre- and post-implantation. Additionally, implanted devices can obscure the accuracy of such data collection methods.

Rather than tracking changes in anatomical connectivity, it may be easier to track changes in effective connectivity directly using electrophysiological means. It is common practice to use methods such as finding the cross correlation over a sliding window to determine the average cross correlation for spike train firing in two areas in *in-vitro* studies (Perkel et al. 1967). This method has also been used *in-vivo* (Murphy et al. 1985), and has recently been used in conjunction with delayed mutual information to provide insight to the direction of connections as well as the specific patterns of connectivity of individual neurons (Endo et al. 2015; Taghva et al. 2012). Using statistical analyses such as cross correlation and time delayed mutual information may allow for the quantification of these effective changes over time in BCI models.

Eventually, these methods could pinpoint the time scale over which permanent changes take place, or help to identify other parameters necessary for the optimization of such devices. For example, for the closed-loop system used by Guggenmos and colleagues to be generalized to multiple areas of the brain, it will be necessary to test whether the delay between trigger and stimulation is a general property of ADS, or if other factors such as distance and intrinsic connectivity between areas plays a role as well. In order to test different delay times and how well they change the effective connectivity between areas, having a good metric to describe and compare changes will be critical.

In the section that follows, a nonlinear method used to recover the time-course of assumed perturbations caused to a fitted dynamical system is presented. The method was tested to see if it would be sensitive to changes differentiating the closed-loop method described by Guggenmos and colleagues from an open-loop random stimulation control in Intact, pilot rats.

A New Optimization Criterion for Closed-Loop BCI

This section was presented at the 2018 International Symposium on Circuits and Systems in Florence, Italy. The conference proceedings paper was peer-reviewed (Murphy et al. 2018). Some notation has been changed slightly from the original manuscript.

Abstract

This study assesses the feasibility of latent factor analysis via dynamical systems (LFADS) for evaluating differences in the observed spiking response dynamics imposed by two electrical microstimulation regimes in awake rats. LFADS is a recently-developed deep learning method that uses stimulus-aligned neural spiking data to determine the initial neural state of each trial, as well as infer a set of time-dependent perturbations to the learned neural dynamics within trials. We show that time-dependent perturbations inferred by an LFADS model trained on spikes from trials on a single session can distinguish between different stimulation conditions. Furthermore, we use these data to exemplify how LFADS inferences track the evolution of stimulus-related spiking responses during chronic microstimulation experiments.

Electrical stimulation has been used to drive neuronal activity and assess intrinsic neural connections since the beginning of neuroscience as a discipline (Leyton & Sherrington 1917, Penfield & Jasper 1954). Coupled with neuroanatomical studies, it enables manipulations that can inform us of how information propagates through the nervous system. Stimulation-evoked responses are typically measured by peri-stimulus time histograms (PSTHs), which are essentially coherent averages of neural spiking events made possible by the stationarity of the neural response to electrical stimuli (Gerstein & Kiang 1960). A major assumption in using the PSTH as an experimental endpoint is that the neural response to electrical stimulation will remain relatively stable over time and is not impacted by the activity of other neurons (Evarts 1968, Hubel & Wiesel 1962, Cheney & Fetz 1985). New technology that allows measurement of

spiking from hundreds of neurons simultaneously has led to increased interest in ways to better characterize the potentially high-order, nonlinear interactions that may underlie computation integration and outputs of large cortical networks (Shimazaki et al 2012). Recently, quantifying neocortical network interactions has been achieved by assuming that a relatively low-dimensional latent population code captures most of the variance in the high-dimensional spatiotemporal spike train data (Churchland et al 2012, Benjamin et al 2013). Even this more sophisticated approach is confounded by the fact that the nervous system is plastic, constantly undergoing reorganization of the connections between neurons, which poses problems for dimensionality reduction methods that assume linear underlying processes. Cortical plasticity can be manipulated by certain applications of electrical stimulation (i.e. Nudo et al 1990, Jackson et al 2006), further complicating the extraction of meaningful longitudinal information from spiking neural populations in studies that employ it.

Many clinical and pre-clinical neurostimulation techniques to treat neurological disorders are based on this idea that the stimulation will alter the output properties of neurons, or that the population of neurons will adapt and alter their firing characteristics in response to input from the stimulation, as described in the previous sections. Theories of neuroplasticity are largely based on classical Hebbian mechanisms of synaptic potentiation, in which synaptic strength is increased when pre- and postsynaptic events occur closely in time. Along with our colleagues, we developed a microdevice that couples the intrinsic activity of one neuron with the intracortical microstimulation to induce activity in other neurons. By triggering electrical stimulation in one brain region in response to detected neural activity in a distant region we can effectively bridge damaged neural pathways (Azin et al 2011a, Azin et al 2011b). Application of this approach has shown behavioral efficacy in a rodent model of traumatic brain injury (Guggenmos et al 2013). The promising preclinical functional outcomes suggest that understanding how stimulation alters the patterns of recorded activity over time is critical for refining this type of

treatment strategy (McPherson et al 2015, Capogrosso et al 2016). Given the expectation of shifting activity patterns, typical linear measurements and dimensionality reduction techniques are limited.

An ideal analytical model needs to have the flexibility to allow and detect perturbations to the estimated dynamics in some subset of the experimental trials (i.e. longitudinal plasticity in the population response to stimulation). We implemented the recently-developed latent factor analysis by dynamical systems (LFADS) approach detailed in (Pandarinath et al 2018) to demonstrate the feasibility of recovering perturbations to the recovered population dynamics around microstimulation. The trained LFADS model is able to track a shift in per-trial perturbation inferences around electrical stimuli that differs between two different stimulation conditions.

Inference Model

Overview of LFADS model

LFADS is a deep learning method that infers the latent dynamics of processes in the brain under the assumption that the observed set of trial-aligned, binned spike counts are noisy reflections of underlying neural process dynamics. These processes are likely similar due to the imposed experimental conditions. In the following notation, let upper-case denote a random process, and lower-case denote a realization of that process. If $\boldsymbol{X_{1:T}}$ represents the full dataset of m trials,

$$[\boldsymbol{x_1}, \ldots, \boldsymbol{x_m}],$$

each of which consists of spike trains recorded from N units simultaneously counted over bins in T time steps, it is assumed that differences in data observed between trials $\boldsymbol{x_i}$ and $\boldsymbol{x_k}$ are due to 1) observation noise, 2) changes in trial initial conditions ($\boldsymbol{g_0^i}$), and/or 3) time-dependent external perturbation(s) present in $\boldsymbol{x_i}$, but not in $\boldsymbol{x_k}$, ($\boldsymbol{u^i(t)}$). LFADS is an implementation of the variational autoencoder (VAE) framework, which learns and makes inferences about a set of latent

stochastic variables, ***Z***, that represent the observed data, ***X***, by simultaneously training an encoder mapping from $X \rightarrow Z^*$, and a generator that maps a reconstruction of the observations, $Z^* \rightarrow X^*$. Ultimately, this framework should allow recovery of the compressed latent representation in a form that is as simple as possible, while still minimizing the error of the reconstruction mapping.

Figure 2.4

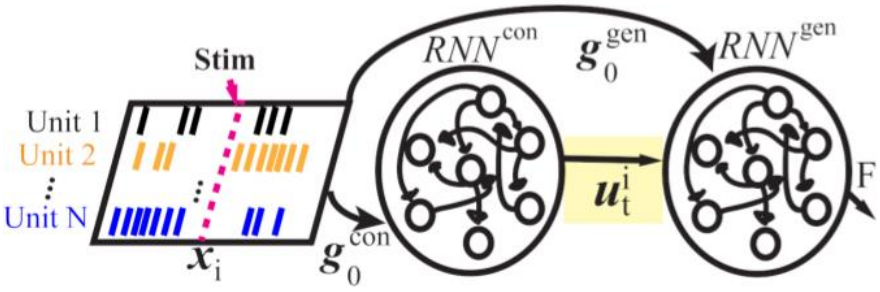

Figure 2.4: LFADS inference model.

Figure 2.4: Schematic of latent factor analysis by dynamical systems (LFADS) model for inferring perturbations. We are interested in the time-dependent output from RNN^{con}, $u^i(t)$ (yellow box). Observed data, X_i, are encoded to the latent stochastic representation, from which samples are drawn and averaged to generate a de-noised observation estimate represented by the dynamical factors, F.

In the LFADS model, the stochastic latent variables correspond to assumptions 2 and 3, such that $\boldsymbol{Z} \stackrel{\text{def}}{=} \{\boldsymbol{G_0}, \boldsymbol{U}(t)\}$. The model approximates a latent representation of $\boldsymbol{x_i}$ as $\boldsymbol{z^*_i}$ by learning the approximate posterior distribution, $Q(\boldsymbol{Z}|\boldsymbol{X})$. At the same time, it attempts to maximize the reconstruction likelihood, $P(\boldsymbol{X^*}|\boldsymbol{X}, \boldsymbol{Z^*})$, by using two recurrent neural networks (RNNs) to generatively produce samples marginalized on batches of samples drawn from and , and estimating the log-likelihood based on the observed data . Both networks use the gated recurrent unit in order to capture sequential dependencies in the data (Chung et al 2014). The generator network, RNN^{gen}, generates the reconstructed observations, while the controller network, RNN^{con}, infers time-dependent perturbations for each trial ($\boldsymbol{u}^i(t)$) that are fed to RNN^{gen} at each time step as it generates samples. The read-out matrix from RNN^{gen} can be adjusted so that LFADS may be applied as a dimensionality reduction technique to extract a set of dynamic factors, $\boldsymbol{F}$, from the high-dimensional spike train data. However, here we primarily consider the controller inferences, $\boldsymbol{u}^i(t)$ (**Figure 2.4**, yellow box). The inferences are intrinsically regularized by the pre-specified low-dimensional output of RNN^{con}, and also by a penalty term in the model loss function that increases with the Kullback-Leibler divergence of from an uninformative learned autoregressive prior. This loss function is designed to discourage "spiky" inferred perturbations unless they help fit the data substantially in ways that cannot be accounted for elsewhere in the model. Large deviations in $\boldsymbol{u}^i(t)$ may represent perturbations to the state of RNN^{gen} during substantially "different" trials. A more thorough discussion of the complete LFADS model is given in (Pandarinath et al 2018), and the most relevant model hyper-parameters used in our study are summarized in **Table 2.1**. Most hyper-parameters were selected to be similar to hyper-parameters in (Pandarinath et al 2018), which were used to recover perturbations to neural dynamics during a monkey cursor movement task.

Table 2.1: LFADS Model Hyper-Parameters

Parameter description	Value	Parameter description	Value
N units RNN^{gen}	128	N units RNN^{con}	128
Dim(F)	50 factors	Dim($U(t)$)	6 control outputs
RNN^{gen} L2 penalty scalar	25 (a.u.)	RNN^{con} L2 penalty scalar	25 (a.u.)
Spike bin size	1 ms	P(dropout)	0.04

Application of LFADS to Stimulation Trials

In this application of LFADS, inferences generated by the model do not necessarily correspond to perturbations of the underlying neural state, since a fixed portion of the observed noisy outputs (spikes) are necessarily obscured in each trial due to the stimulus artifact. Therefore, the LFADS inferences here should not be considered as relating to a set of purely physiological processes underlying the observed data as there is a period during the stimulus artifact when spiking cannot be ascertained. If every sampled trial included in training the model contained only the stimulation artifact at the onset alignment, the apparent suppression of activity across all observed spiking channels should not correspond to an inferred perturbation but rather an expected state of the response that would be learned by the generator network.

To allow LFADS to learn to infer changes in observed spiking around the stimulus artifact, we included a subset of trials that contained stimulus pulses in addition to the alignment pulse. Therefore, although LFADS does not capture neural dynamics due to erroneous information from the stimulus artifact, it should still be able to infer changes in spiking activity around the artifact. This makes it a convenient tool to evaluate the timescale on which plasticity phenomena might be expected to occur over the time-course of a single stimulation session. If electrical stimulation

does not alter intrinsic neural pathways, there should be a relatively consistent evoked spiking response, allowing the model to fit dynamics without large inferred perturbations. Therefore, the LFADS model endpoints of interest are significant deviations in $\boldsymbol{u}^i(t)$ during epochs surrounding the stimulus pulses.

Methods

Experimental overview

All data used for analysis was previously acquired in a separate study that was approved through the Institutional Animal Care and Use Committee at the University of Kansas Medical Center. Rats were implanted with 16-channel polymer microelectrode arrays (NeuroNexus) unilaterally in premotor (PM) and somatosensory (S1) cortex (**Figure 2.5a, 2.5b**). Electrode locations were determined prior to implantation using intracortical microstimulation and sensory recording techniques, identical to that described in (Guggenmos et al 2013).

Figure 2.5A

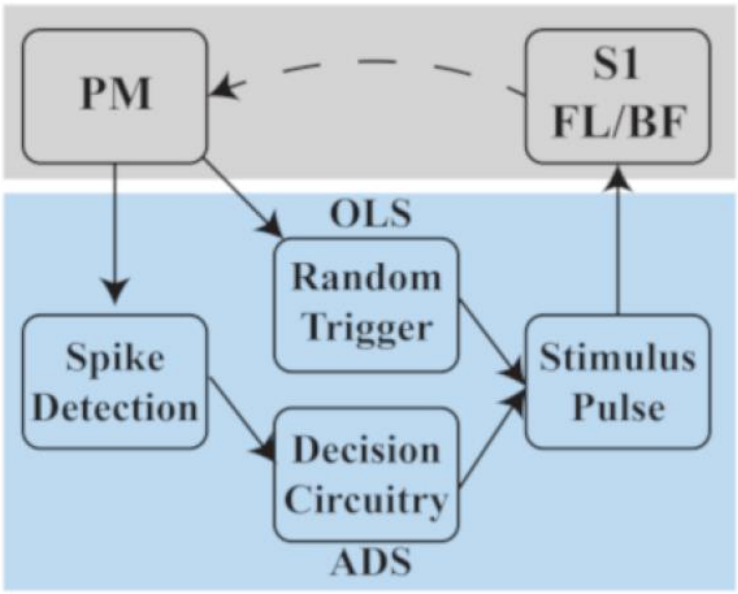

Figure 2.5B

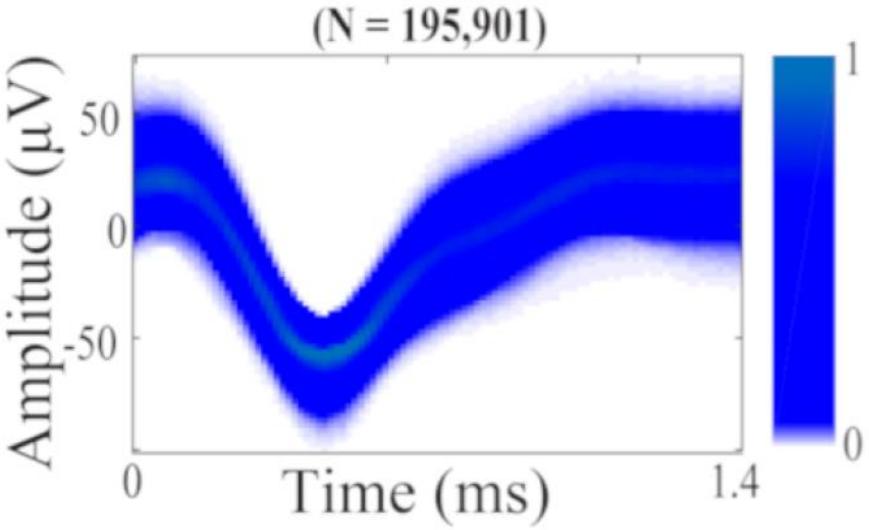

Figure 2.5C

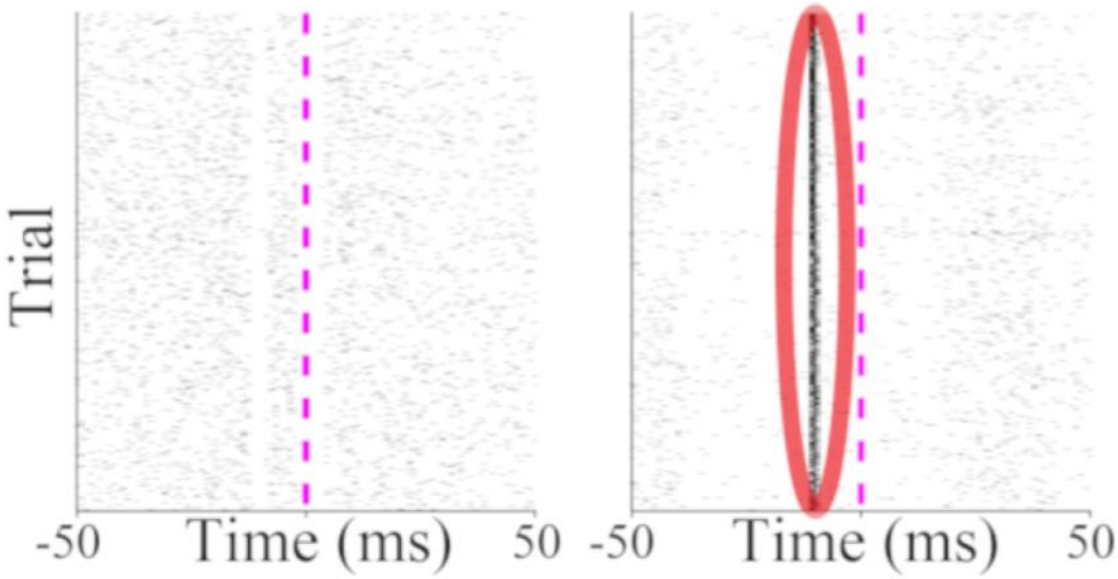

Figure 2.5D

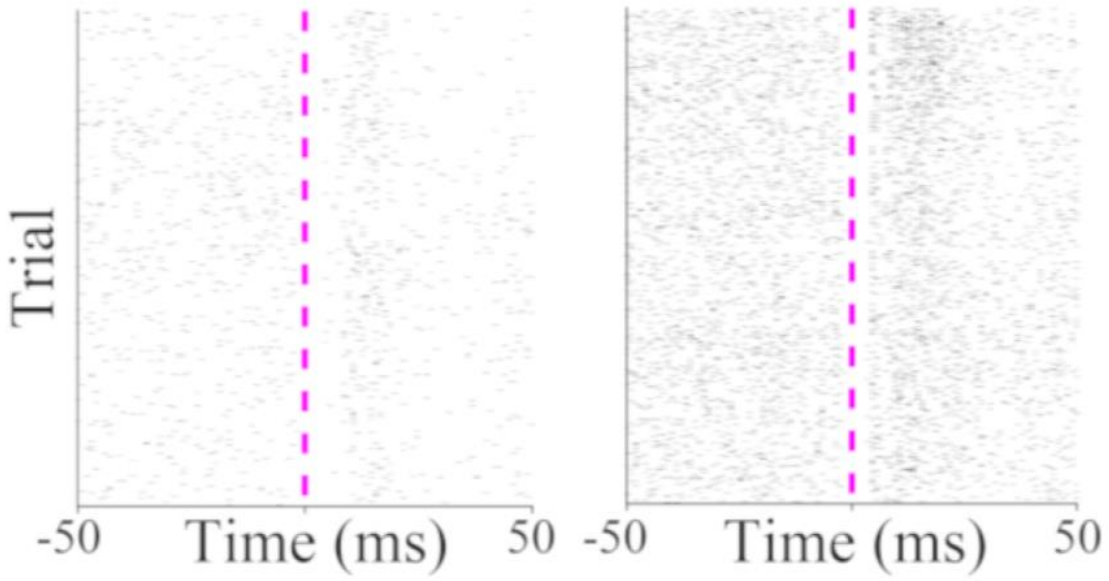

Figure 2.5: LFADS to infer ADS perturbations

A) Experimental design. In the ADS regimen, detected spikes in PM trigger stimulation of S1. **B)** Trigger spikes are shown in blue, with a color bar to indicate the proportion of spikes with characteristic amplitude at each time sample. **C)** Raster plots for ADS experiment, black tick marks indicate observed spiking events. Spikes triggering stimulation during ADS are highlighted by red ellipse (right). The left raster shows a typical raster for a non "trigger" channel that has some evoked activity relative to the stimulus (dashed magenta line). **D)** Raster plots for OLS experiment. There is no relation of pre-stimulus activity to the stimulus, although per-channel activity is variable (differences in density of spiking between left and right rasters).

In vivo stimulation and recording

Recording of PM activity consisted of 160-minute sessions including a 20-minute basal epoch followed by an 80-minute stimulation period and 60-minutes of post-stimulation baseline activity while the animal was tethered, but freely moving within a recording chamber. The PM electrode was connected to a recording preamplifier and S1 electrode was connected to a constant-current stimulus isolator (Tucker-Davis Technologies). Extracellular field recordings were obtained from all 16 sites in PM at a sampling rate of 24 kHz, and bandpass to provide a frequency range from 300 to 3000 Hz. Spikes were discriminated from the filtered unit activity using a fixed amplitude threshold, and sorted online using PCA template matching. For activity-dependent stimulation (ADS), spikes from a single channel that demonstrated moderate spike activity were selected to trigger a stimulus pulse in a single channel within S1 after a delay of 10 ms. A blanking period of 18 ms following the stimulation pulse was employed to limit stimulation based feedback loops, based on values used in past experiments (Jackson et al 2006, Guggenmos et al 2013). In open-loop stimulation (OLS), stimulation was delivered randomly as an approximately Poisson process with an average rate of 7.5 Hz, a value consistent with previous experiments and similar to that of the ADS group (4.1 Hz). All stimulus pulses were single 60 μA biphasic square waves that lasted 100 μs per phase. The timestamp of each stimulus pulse was recorded simultaneously with the raw extracellular waveforms. Data were processed offline to detect and cluster spikes on all recording channels using a combination of automated and supervised classification procedures.

Training LFADS model for inferences

Trials consisting of 1 ms binned spike counts over ±50 ms centered on a stimulus pulse were drawn from the stimulation session of two rats, one ADS and one OLS. A random subset of 2000 trials across the 80-minute stimulation session was used for each rat. Of those trials, 1000 contained only a single stimulus (the trial alignment stimulus), while the other 1000 were evenly

divided between trials demonstrating a second stimulus either before or after the alignment pulse. 25% of the trials were used for validation during training. The model was run in Python using the ADAM optimizer and learning hyper-parameters as specified in (Pandarinath et al 2018). A number of sweeps of the model with the number of controller outputs ranging from 4 to 10 and number of factors ranging between 20 and 50 were relatively robust in demonstrating significant perturbations on a single controller output.

Comparisons using LFADS inferences

After training the model, the inferences $\boldsymbol{u^i(t)}$ for each trial $\boldsymbol{x_i}$ were obtained by averaging 128 sample runs marginalized on the stochastic latent representation $\boldsymbol{z_i}$*. To assess the relationship between model inferences and the actual stimulation times, $\boldsymbol{s_i}$, the cross correlation coefficient, □, between the stimulation times and the controller output ensemble average $\boldsymbol{\langle u_i \rangle}$ was computed up to a maximum lag □ of 28 ms (the minimum inter-stimulus interval), as

$$□_i(□) = \boldsymbol{R}_{su}(□)/(□_u□_s)$$

Where $\boldsymbol{R_{su}(□)}$ is the value of the cross-covariance function for $\boldsymbol{\langle u_i \rangle}$ and $\boldsymbol{s_i}$ computed for lag □, and □ corresponds to the standard deviations of $\boldsymbol{\langle u_i \rangle}$ and $\boldsymbol{s_i}$. The ensemble average is used to intrinsically penalize a spuriously high controller output dimension hyper-parameterization, since unused controller outputs typically appeared to fluctuate around some set noise variance. The average cross correlation, **<□>**, was obtained separately for trials with single or multiple stimuli, as LFADS was not expected to infer perturbations due to stimulation on single-stimulus trials. To estimate the contribution of trial structure to **<□>**, shuffled cross correlations of $\boldsymbol{s_i}$ with $\boldsymbol{\langle u_k \rangle}$, for each $\boldsymbol{i \neq k}$, of matching type (single vs. multiple stimuli) were used to compute $\boldsymbol{\langle □_{rand} \rangle}$. Based on the latency and sign of peaks in **<□>** (**Figure 2.5**), the largest deviations of $\boldsymbol{\langle u_i \rangle}$ were expected to be maxima within 20 ms of the alignment stimulus pulse, which is a long enough period to

account for polysynaptic activity. Therefore, the amplitude at which $\langle u_i \rangle$ reached a maximum value was determined in epochs ranging from -20 ms to -4 ms (PRE), and 4 ms to 20 ms (POST), relative to the alignment stimulus pulse. The 4 ms gap was imposed to reflect the stimulus artifact rejection blanking period, and maintained prior to the stimulus to preserve symmetry in the durations of the PRE and POST epochs. In practice, similar results were obtained by varying both bounds of the PRE and POST epochs by several milliseconds, as long as they were maintained within the 28 ms blanking period. Group effects of epoch (PRE vs. POST) and stimulation regimen (ADS vs. OLS) were compared using two-way repeated measures ANOVA.

Results

Summary of Compared Recordings

In total, 19,697 stimuli were delivered in the ADS recording, and 37,265 stimuli were delivered in the OLS recording. In the ADS recording, 43 units were isolated after manual sorting and exclusion of units with spikes in less than 10% of trial-aligned epochs. Typically, a few units were strongly correlated to one another around the time of the stimulus trigger spike (**Figure 2.5c**). Using the same exclusion criteria as for ADS, 30 units were identified in the OLS recording. Visual inspection indicates that stimulation evokes some activity in both stimulus regimes (**Figures 2.5c, 2.5d**).

Figure 2.6A

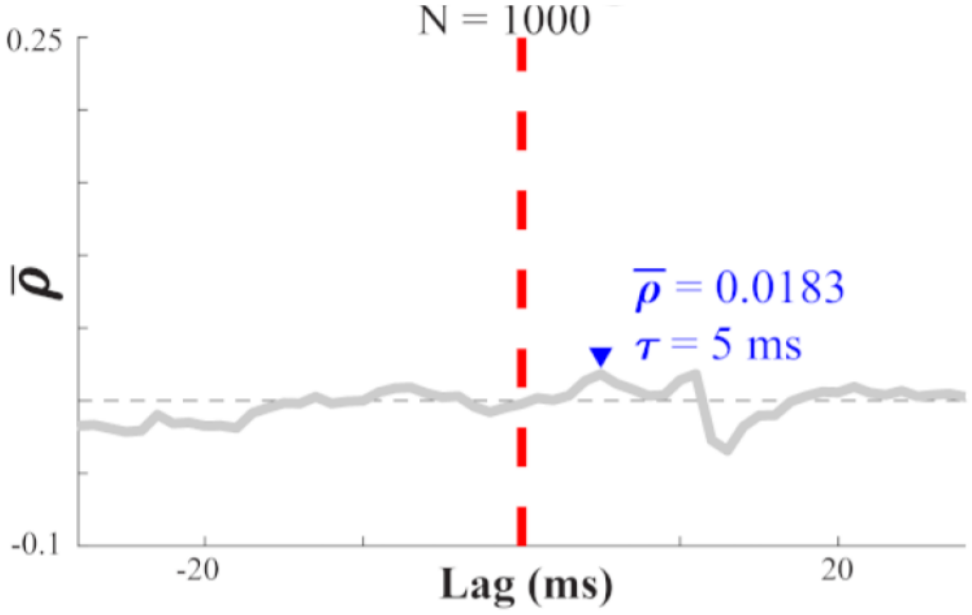

Figure 2.6B

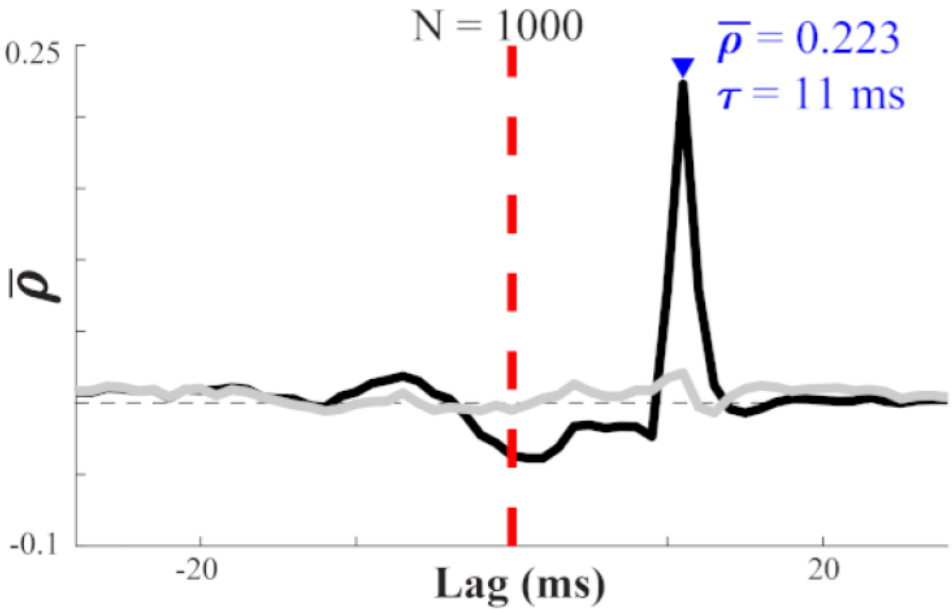

Figure 2.6C

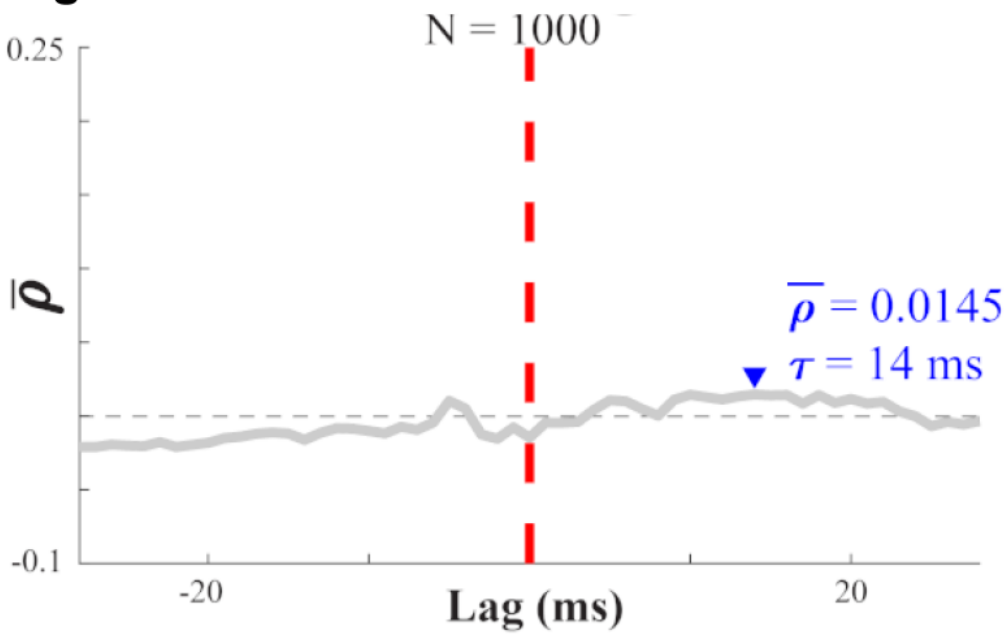

Figure 2.6D

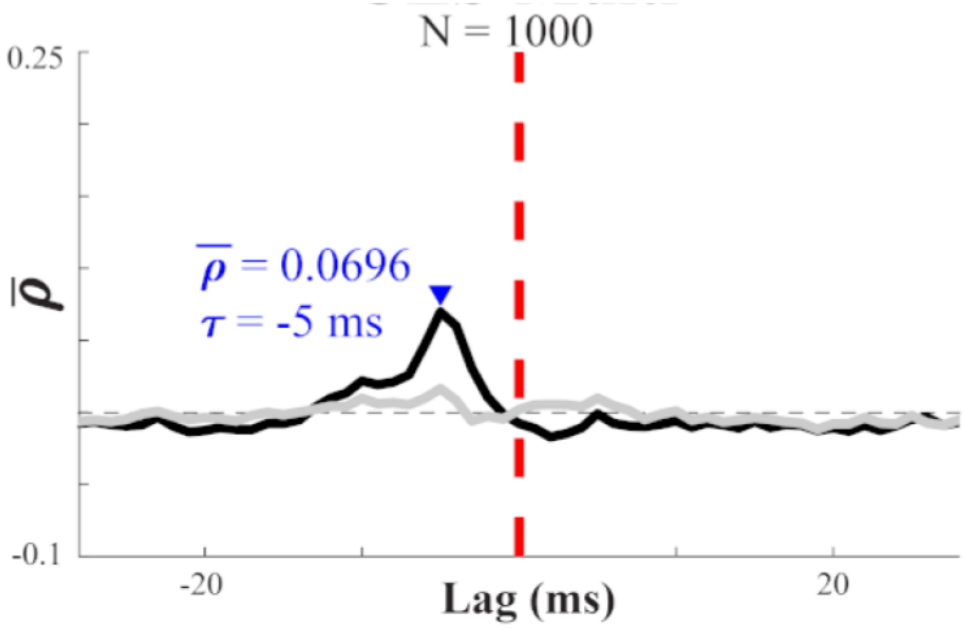

Figure 2.6: Cross-correlation for stimulus times and controller inferences.

Grey line is the average cross-correlation of controller inferences with stimulus times from

random trials of the same class (single vs. multiple stimuli). Each line represents the average from N = 1,000 such pulses. **A)** Activity-dependent stimulation (ADS) with a single ICMS pulse. **B)** ADS with multiple ICMS pulses. Black line represents average cross-correlation coefficient for single-trial stimulus times with matched inferences made by the controller. **C)** Open-loop stimulation (OLS) with a single ICMS pulse. **D)** OLS with multiple ICMS pulses.

Correlation Between Stimuli and Inferences

Cross correlations of s_i with $\langle u_i \rangle$ reveal that $\langle \square \rangle$ only demonstrated peaks in the multi-stim trials (Figure 2.6b, 2.6d). The timing of $\langle \square_{max} \rangle$ differs in causality with respect to s_i, depending on stimulus regimen. In the ADS recording, $\langle \square_{max} \rangle$ occurs when s_i led $\langle u_i \rangle$ by 11 ms (Figure 2.6b), approximately corresponding to the latency between spike trigger and stimulus pulse. By contrast, OLS occured when $\langle u_i \rangle$ led s_i by a lag of 5 ms (Figure 2.6d).

Figure 2.7

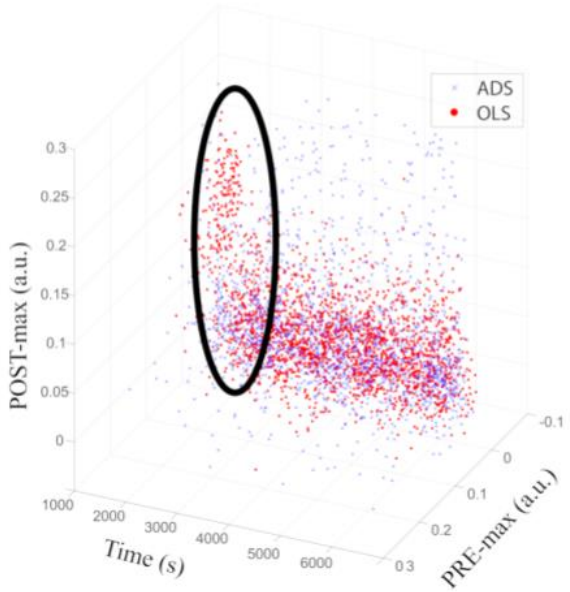

Figure 2.7: Evolution of inferred perturbations.

LFADS infers larger perturbations to the generator dynamics after stimuli at the beginning of the OLS experiment (red), but those effects diminish with time (black ellipse). By comparison, during the ADS experiment there are large perturbations both before and after the stimulus for the duration of the experiment (blue).

Pre- and Post-Stimulus Controller Output Maxima

Using the pre- and post-stimulus max[$\langle u_i^{epoch} \rangle$] as coordinate pairs, a qualitative assessment of peri-stimulus inferred perturbations indicates a rapid change in OLS perturbations that is not present during the ADS recording (**Figure 2.7**). The two-way repeated measures ANOVA indicates significant effects of epoch ($p = 2.0 \times 10^{-35}$) and stimulation type ($p = 2.0 \times 10^{-7}$), and a trending significance of their interaction ($p = 0.062$). Based on the lag □ at which $\langle \square_{max} \rangle$ was obtained for ADS and OLS, these results make sense; causality of the inferred perturbations are opposite with respect to the stimulus time for the two groups. The weaker interaction effect may reflect the relative spread maintained by ADS in terms of the controller maxima values throughout the experiment (**Figure 2.7**).

Discussion

Neural activity is obscured by the stimulus artifact and therefore dynamics inferred by LFADS during and nearby the artifact should be interpreted conservatively. However, LFADS inferences do correlate with electrical stimuli (**Figure 2.6**). This suggests that the LFADS inferences can be used as indicators for detecting the timescale of reorganization of network dynamics in response to random electrical microstimulation. For OLS, large post-stimulus inferred perturbations subside rapidly (within the first 15-minutes of the stimulation session; **Figure 2.7**).

By contrast, perturbations associated with ADS continue for the duration of the experiment, indicating that ADS may provide a more salient and sustained alteration to network dynamics than OLS. This difference may help explain the improvements in functional behavior evident in rats treated with ADS relative to OLS treatment (Guggenmos et al 2013).

LFADS provides new options for exploring population plasticity. For example, removing subsets of units from the training data could be informative in interpreting LFADS inferences. Removing the trigger unit from the ADS training set could be a way to explore how robust the trigger representation is within the rest of the population dynamics. Linearizing around the dynamics of fixed or slow points in the activations of the controller network, as suggested in (Sussillo & Barak 2013), could provide insights into the aspects of network computations that change resulting from internal and external stimuli. LFADS provides a new way to study cortical dynamics, and may represent an important advance for relating neuroplasticity and neurostimulation.

Conclusion

An ideal high-fidelity BCI would both sample and allow stimulation of precise neural features non-invasively. In reality, such a combination is unlikely. Nonetheless, current work across several types of BCIs provides promising results for the clinical applicability of these technologies. Despite the positive outlook for the future of BCIs, several challenges remain before high fidelity recording and stimulating devices are made available for common clinical use. For MEA recordings, two major challenges remain. The first is to improve the patency of chronically implanted microelectrodes so that they can continue to be used for recordings for the duration of the patient's lifespan. The second challenge is to find reliable recording sites and decoding algorithms that do not need to be recalibrated on a daily or weekly basis, and adaptive

decoders that would allow for automatic recalibration as patients learn to use implanted BCIs more efficiently.

For ECoG and EEG, the challenge is less from a materials perspective, and more from a computational perspective. The primary goal remains similar to MEA-based BCIs: it is most important to find regions from which task-related information can be reliably decoded and translated into repeatable intent. It may first be necessary to find a means to identify reliable neural substrates for BCI learning using MEAs, then demonstrate that the activity patterns of these substrates can be reliably decoded using less invasive measures. Emerging methods incorporating structural and metabolic information into current source estimates may provide the additional information necessary to increase decoding accuracy (Aihara et al., 2012). Additionally, as frequency-domain based decoders improve in accuracy, it will be important to continue to incorporate signals with greater numbers of independent features into BCI decoders in order to improve the ease of adaptation for implanted patients. In ECoG, this could potentially be improved by optimizing location and spacing.

In terms of decoded output, goal-tuned single units in MEA-based BCIs have shown great promise for decoding intent in complex movements. Meanwhile, work involving less-invasive approaches such as ECoG and EEG continues to improve in decoding accuracy. The future combination of these lines of work will be critical for progress towards increased clinical use of neural prosthetics. In order to demonstrate the complete neural electrophysiological basis for learned BCI behavior, elements from all types of recording paradigms may be necessary. Such an understanding may lead to new therapeutic targets for BCI devices.

As non-invasive electrical stimulation becomes a more realistic possibility in restorative devices that use overt, extrinsic goals for patient rehabilitation, combination stimulation approaches may increase the utility and effectiveness of BCIs. Devices controlling intrinsic operations, which

offer a more subtle form of closed-loop stimulation, face a different set of challenges going forward. The primary challenge will be to find a way to generalize their use to many parts of the CNS. Whether that is finding the optimal delay for activity-dependent stimulation between two areas, or finding the right recorded or computed pattern of neural stimulation to recreate lost functionality, the challenges facing internally interfaced devices are also numerous.

Thus, the current state of progress in implementing a high fidelity BCI depends on the type of device. Restorative closed-loop devices for rehabilitation therapy have already demonstrated some clinical effect in paretic patients (Ramos-Murguialday et al., 2013), but are limited to treatment of patient populations that retain spared neural pathways following injury. Devices that control extrinsic operations have attained clinical use in the sense that they have been implemented in limited human trials (Aflalo et al., 2015; Hochberg et al., 2012). However, the practicality of such devices for widespread use remains questionable until such time that costs are reduced and devices made more widely available. In addition, decoders must be made generalizable and receive more accurate input from a higher density of sources. Completely intrinsic closed-loop devices offer tantalizing possibilities due to the possibility of not only use in motor recovery (Guggenmos et al., 2013; McPherson et al., 2015), but potentially cognitive therapy as well (Berger et al., 2012). Still, many important questions remain unanswered about these devices. Can they show reliability in animal models at a large scale? How long must such a therapeutic device remain in effect before clinical results are demonstrated? Thus, each type of device has its potential benefits and drawbacks, but importantly, an abundance of paths remain toward a future where BCIs are commonplace in a variety of clinical settings.

Acknowledgment

Maxwell D. Murphy was supported by the National Institutes of Health under Ruth L. Kirschstein National Service Award T32 HD057850 (R.J.N., PI) from the National Institute for Child Health and Human Development.

References

Aflalo, T., Kellis, S., Klaes, C., Lee, B., Shi, Y., Pejsa, K., . . . Andersen, R. A. (2015). Neurophysiology. Decoding motor imagery from the posterior parietal cortex of a tetraplegic human. *Science, 348*(6237), 906-910. doi:10.1126/science.aaa5417

Aihara, T., Takeda, Y., Takeda, K., Yasuda, W., Sato, T., Otaka, Y., . . . Osu, R. (2012). Cortical current source estimation from electroencephalography in combination with near-infrared spectroscopy as a hierarchical prior. *Neuroimage, 59*(4), 4006-4021. doi:10.1016/j.neuroimage.2011.09.087

Ajiboye, A. B., Simeral, J. D., Donoghue, J. P., Hochberg, L. R., & Kirsch, R. F. (2012). Prediction of imagined single-joint movements in a person with high-level tetraplegia. *IEEE Trans Biomed Eng, 59*(10), 2755-2765. doi:10.1109/tbme.2012.2209882

Azin, M., Guggenmos, D.J., Barbay, S., Nudo, R.J., and Mohseni, P.: 'A miniaturized system for spike-triggered intracortical microstimulation in an ambulatory rat', IEEE Trans Biomed Eng, 2011a, 58, (9), pp. 2589-2597

Azin, M., Guggenmos, D.J., Barbay, S., Nudo, R.J., and Mohseni, P.: 'A battery-powered activity-dependent intracortical microstimulation IC for brain-machine-brain interface', IEEE Journal of Solid-State Circuits, 2011b, 46, (4), pp. 731-745

Bajaj, S., Butler, A. J., Drake, D., & Dhamala, M. (2015). Functional organization and restoration of the brain motor-execution network after stroke and rehabilitation. *Front Hum Neurosci, 9*, 173. doi:10.3389/fnhum.2015.00173

Bensch, M., Karim, A. A., Mellinger, J., Hinterberger, T., Tangermann, M., Bogdan, M., . . . Birbaumer, N. (2007). Nessi: an EEG-controlled web browser for severely paralyzed patients. *Comput Intell Neurosci*, 71863. doi:10.1155/2007/71863

Berger, T. W., Hampson, R. E., Song, D., Goonawardena, A., Marmarelis, V. Z., & Deadwyler, S. A. (2011). A cortical neural prosthesis for restoring and enhancing memory. *J Neural Eng, 8*(4), 046017. doi:10.1088/1741-2560/8/4/046017

Berger, T. W., Song, D., Chan, R. H., Marmarelis, V. Z., LaCoss, J., Wills, J., Granacki, J. J. (2012). A hippocampal cognitive prosthesis: multi-input, multi-output nonlinear modeling and VLSI implementation. *IEEE Trans Neural Syst Rehabil Eng, 20*(2), 198-211. doi:10.1109/tnsre.2012.2189133

Birbaumer, N., Ghanayim, N., Hinterberger, T., Iversen, I., Kotchoubey, B., Kubler, A., . . . Flor, H. (1999). A spelling device for the paralysed. *Nature, 398*(6725), 297-298.

Blankertz, B., Muller, K. R., Curio, G., Vaughan, T. M., Schalk, G., Wolpaw, J. R., Birbaumer, N. (2004). The BCI Competition 2003: progress and perspectives in

detection and discrimination of EEG single trials. *IEEE Trans Biomed Eng, 51*(6), 1044-1051. doi:10.1109/tbme.2004.826692

Benjamin, R.C., Matthew, T.K., Zachary, S.B., Mark, M.C., Stephen, I.R., Krishna, V.S., and Byron, M.Y.: 'DataHigh: graphical user interface for visualizing and interacting with high-dimensional neural activity', Journal of Neural Engineering, 2013, 10, (6), pp. 066012

Bleichner, M. G., Freudenburg, Z. V., Jansma, J. M., Aarnoutse, E. J., Vansteensel, M. J., & Ramsey, N. F. (2014). Give me a sign: decoding four complex hand gestures based on high-density ECoG. *Brain Struct Funct*. doi:10.1007/s00429-014-0902-x

Bonifazi, P., Difato, F., Massobrio, P., Breschi, G. L., Pasquale, V., Levi, T., Chiappalone, M. (2013). In vitro large-scale experimental and theoretical studies for the realization of bi-directional brain-prostheses. *Front Neural Circuits, 7*, 40. doi:10.3389/fncir.2013.00040

Bouchard, K. E., & Chang, E. F. (2014). Neural decoding of spoken vowels from human sensory-motor cortex with high-density electrocorticography. *Conf Proc IEEE Eng Med Biol Soc, 2014*, 6782-6785. doi:10.1109/embc.2014.6945185

Bulea, T. C., Prasad, S., Kilicarslan, A., & Contreras-Vidal, J. L. (2014). Sitting and standing intention can be decoded from scalp EEG recorded prior to movement execution. *Front Neurosci, 8*, 376. doi:10.3389/fnins.2014.00376

Capogrosso, M., Milekovic, T., Borton, D., Wagner, F., Moraud, E.M., Mignardot, J.-B., Buse, N., Gandar, J., Barraud, Q., Xing, D., Rey, E., Duis, S., Jianzhong, Y., Ko, W.K.D., Li, Q., Detemple, P., Denison, T., Micera, S., Bezard, E., Bloch, J., and Courtine, G.: 'A brain–spine interface alleviating gait deficits after spinal cord injury in primates', Nature, 2016, 539, pp. 284

Carmena, J. M., Lebedev, M. A., Crist, R. E., O'Doherty, J. E., Santucci, D. M., Dimitrov, D. F., Nicolelis, M. A. (2003). Learning to control a brain-machine interface for reaching and grasping by primates. *PLoS Biol, 1*(2), E42. doi:10.1371/journal.pbio.0000042

Chao, Z. C., Nagasaka, Y., & Fujii, N. (2010). Long-term asynchronous decoding of arm motion using electrocorticographic signals in monkeys. *Front Neuroeng, 3*, 3. doi:10.3389/fneng.2010.00003

Cheney, P.D., and Fetz, E.E.: 'Comparable patterns of muscle facilitation evoked by individual corticomotoneuronal (CM) cells and by single intracortical microstimuli in primates: evidence for functional groups of CM cells', J Neurophysiol, 1985, 53, (3), pp. 786-804

Chestek, C. A., Gilja, V., Blabe, C. H., Foster, B. L., Shenoy, K. V., Parvizi, J., & Henderson, J. M. (2013). Hand posture classification using electrocorticography signals

in the gamma band over human sensorimotor brain areas. *J Neural Eng, 10*(2), 026002. doi:10.1088/1741-2560/10/2/026002

Collinger, J. L., Wodlinger, B., Downey, J. E., Wang, W., Tyler-Kabara, E. C., Weber, D. J., . . . Schwartz, A. B. (2013). High-performance neuroprosthetic control by an individual with tetraplegia. *Lancet, 381*(9866), 557-564. doi:10.1016/s0140-6736(12)61816-9

Cooper, R., Winter, A. L., Crow, H. J., & Walter, W. G. (1965). COMPARISON OF SUBCORTICAL, CORTICAL AND SCALP ACTIVITY USING CHRONICALLY INDWELLING ELECTRODES IN MAN. *Electroencephalogr Clin Neurophysiol, 18*, 217-228.

Chung, J., Gulcehre, C., Cho, K., and Bengio, Y.: 'Empirical evaluation of gated recurrent neural networks on sequence modeling', arXiv preprint arXiv:1412.3555, 2014

Churchland, M.M., Cunningham, J.P., Kaufman, M.T., Foster, J.D., Nuyujukian, P., Ryu, S.I., and Shenoy, K.V.: 'Neural population dynamics during reaching', Nature, 2012, 487, (7405), pp. 51-56

Cunningham, J. P., Gilja, V., Ryu, S. I., & Shenoy, K. V. (2009). Methods for estimating neural firing rates, and their application to brain-machine interfaces. *Neural Netw, 22*(9), 1235-1246. doi:10.1016/j.neunet.2009.02.004

Cunningham, J. P., Nuyujukian, P., Gilja, V., Chestek, C. A., Ryu, S. I., & Shenoy, K. V. (2011). A closed-loop human simulator for investigating the role of feedback control in brain-machine interfaces. *J Neurophysiol, 105*(4), 1932-1949. doi:10.1152/jn.00503.2010

De Faveri, S., Maggiolini, E., Miele, E., De Angelis, F., Cesca, F., Benfenati, F., & Fadiga, L. (2014). Bio-inspired hybrid microelectrodes: a hybrid solution to improve long-term performance of chronic intracortical implants. *Front Neuroeng, 7*, 7. doi:10.3389/fneng.2014.00007

Donoghue, J. P., & Parham, C. (1983). Afferent connections of the lateral agranular field of the rat motor cortex. *J Comp Neurol, 217*(4), 390-404. doi:10.1002/cne.902170404

Endo, W., Santos, F. P., Simpson, D., Maciel, C. D., & Newland, P. L. (2015). Delayed mutual information infers patterns of synaptic connectivity in a proprioceptive neural network. *J Comput Neurosci, 38*(2), 427-438. doi:10.1007/s10827-015-0548-6

Ersen, A., Elkabes, S., Freedman, D. S., & Sahin, M. (2015). Chronic tissue response to untethered microelectrode implants in the rat brain and spinal cord. *J Neural Eng, 12*(1), 016019. doi:10.1088/1741-2560/12/1/016019

Ethier, C., Oby, E. R., Bauman, M. J., & Miller, L. E. (2012). Restoration of grasp following paralysis through brain-controlled stimulation of muscles. *Nature, 485*(7398), 368-371.

doi:http://www.nature.com/nature/journal/v485/n7398/abs/nature10987.html#supplementary-information

Evarts, E. V. (1966). Pyramidal tract activity associated with a conditioned hand movement in the monkey. *J Neurophysiol, 29*(6), 1011-1027.

Evarts, E.V.: 'Relation of pyramidal tract activity to force exerted during voluntary movement', J Neurophysiol, 1968, 31, (1), pp. 14-27

Felix, S. H., Shah, K. G., Tolosa, V. M., Sheth, H. J., Tooker, A. C., Delima, T. L., . . . Pannu, S. S. (2013). Insertion of flexible neural probes using rigid stiffeners attached with biodissolvable adhesive. *J Vis Exp*(79), e50609. doi:10.3791/50609

Felton, E. A., Wilson, J. A., Williams, J. C., & Garell, P. C. (2007). Electrocorticographically controlled brain-computer interfaces using motor and sensory imagery in patients with temporary subdural electrode implants. Report of four cases. *J Neurosurg, 106*(3), 495-500. doi:10.3171/jns.2007.106.3.495

Fetz, E. E. (1969). Operant conditioning of cortical unit activity. *Science, 163*(3870), 955-958.

Flint, R. D., Lindberg, E. W., Jordan, L. R., Miller, L. E., & Slutzky, M. W. (2012). Accurate decoding of reaching movements from field potentials in the absence of spikes. *J Neural Eng, 9*(4), 046006. doi:10.1088/1741-2560/9/4/046006

Flint, R. D., Wang, P. T., Wright, Z. A., King, C. E., Krucoff, M. O., Schuele, S. U., . . . Slutzky, M. W. (2014). Extracting kinetic information from human motor cortical signals. *Neuroimage, 101*, 695-703. doi:10.1016/j.neuroimage.2014.07.049

Flint, R. D., Wright, Z. A., Scheid, M. R., & Slutzky, M. W. (2013). Long term, stable brain machine interface performance using local field potentials and multiunit spikes. *J Neural Eng, 10*(5), 056005. doi:10.1088/1741-2560/10/5/056005

Gavins, F. N., & Smith, H. K. (2015). Cell tracking technologies for acute ischemic brain injury. *J Cereb Blood Flow Metab*. doi:10.1038/jcbfm.2015.93

Georgopoulos, A. P., Schwartz, A. B., & Kettner, R. E. (1986). Neuronal population coding of movement direction. *Science, 233*(4771), 1416-1419.

Gerstein, G.L., and Kiang, N.Y.S.: 'An Approach to the Quantitative Analysis of Electrophysiological Data from Single Neurons', Biophysical Journal, 1960, 1, (1), pp. 15-28

Grimaldi, G., Manto, M., & Jdaoudi, Y. (2013). Quality parameters for a multimodal EEG/EMG/kinematic brain-computer interface (BCI) aiming to suppress neurological tremor in upper limbs. *F1000Res, 2*, 282. doi:10.12688/f1000research.2-282.v2

Guggenmos, D.J., Azin, M., Barbay, S., Mahnken, J.D., Dunham, C., Mohseni, P., and Nudo, R.J.: ‘Restoration of function after brain damage using a neural prosthesis’, Proc Natl Acad Sci U S A, 2013, 110, (52), pp. 21177-21182

Hall, T. M., Nazarpour, K., & Jackson, A. (2014). Real-time estimation and biofeedback of single-neuron firing rates using local field potentials. *Nat Commun, 5*, 5462. doi:10.1038/ncomms6462

Hampson, R. E., Gerhardt, G. A., Marmarelis, V., Song, D., Opris, I., Santos, L., . . . Deadwyler, S. A. (2012). Facilitation and restoration of cognitive function in primate prefrontal cortex by a neuroprosthesis that utilizes minicolumn-specific neural firing. *J Neural Eng, 9*(5), 056012. doi:10.1088/1741-2560/9/5/056012

Hashimoto, Y., Ota, T., Mukaino, M., Liu, M., & Ushiba, J. (2014). Functional recovery from chronic writer's cramp by brain-computer interface rehabilitation: a case report. *BMC Neurosci, 15*, 103. doi:10.1186/1471-2202-15-103

Heck, C. N., King-Stephens, D., Massey, A. D., Nair, D. R., Jobst, B. C., Barkley, G. L., . . . Morrell, M. J. (2014). Two-year seizure reduction in adults with medically intractable partial onset epilepsy treated with responsive neurostimulation: final results of the RNS System Pivotal trial. *Epilepsia, 55*(3), 432-441. doi:10.1111/epi.12534

Hochberg, L. R., Serruya, M. D., Friehs, G. M., Mukand, J. A., Saleh, M., Caplan, A. H., Donoghue, J. P. (2006). Neuronal ensemble control of prosthetic devices by a human with tetraplegia. *Nature, 442*(7099), 164-171. doi:10.1038/nature04970

Hochberg, L. R., Bacher, D., Jarosiewicz, B., Masse, N. Y., Simeral, J. D., Vogel, J., Donoghue, J. P. (2012). Reach and grasp by people with tetraplegia using a neurally controlled robotic arm. *Nature, 485*(7398), 372-375. doi:10.1038/nature11076

Holz, E. M., Botrel, L., Kaufmann, T., & Kubler, A. (2015). Long-term independent brain-computer interface home use improves quality of life of a patient in the locked-in state: a case study. *Arch Phys Med Rehabil, 96*(3 Suppl), S16-26. doi:10.1016/j.apmr.2014.03.035

Hosseini, S. M., Farahmandnia, M., Razi, Z., Delavari, S., Shakibajahromi, B., Sarvestani, F. S., Semsar, M. (2015). Combination cell therapy with mesenchymal stem cells and neural stem cells for brain stroke in rats. *Int J Stem Cells, 8*(1), 99-105. doi:10.15283/ijsc.2015.8.1.99

Hubel, D.H., and Wiesel, T.N.: ‘Receptive fields, binocular interaction and functional architecture in the cat's visual cortex’, The Journal of Physiology, 1962, 160, (1), pp. 106-154.102

Izhikevich, E. M., Gally, J. A., & Edelman, G. M. (2004). Spike-timing dynamics of neuronal groups. *Cereb Cortex, 14*(8), 933-944. doi:10.1093/cercor/bhh053

Jackson, A., Mavoori, J., and Fetz, E.E.: ‘Long-term motor cortex plasticity induced by an electronic neural implant’, Nature, 2006, 444, (7115), pp. 56-60

Kasashima-Shindo, Y., Fujiwara, T., Ushiba, J., Matsushika, Y., Kamatani, D., Oto, M., . . . Liu, M. (2015). Brain-computer interface training combined with transcranial direct current stimulation in patients with chronic severe hemiparesis: Proof of concept study. *J Rehabil Med, 47*(4), 318-324. doi:10.2340/16501977-1925

Kellis, S., Hanrahan, S., Davis, T., House, P. A., Brown, R., & Greger, B. (2012). Decoding hand trajectories from micro-electrocorticography in human patients. *Conf Proc IEEE Eng Med Biol Soc, 2012*, 4091-4094. doi:10.1109/embc.2012.6346866

King-Stephens, D., Mirro, E., Weber, P. B., Laxer, K. D., Van Ness, P. C., Salanova, V., Morrell, M. J. (2015). Lateralization of mesial temporal lobe epilepsy with chronic ambulatory electrocorticography. *Epilepsia*. doi:10.1111/epi.13010

Laitinen, T., Sierra, A., Bolkvadze, T., Pitkanen, A., & Grohn, O. (2015). Diffusion tensor imaging detects chronic microstructural changes in white and gray matter after traumatic brain injury in rat. *Front Neurosci, 9*, 128. doi:10.3389/fnins.2015.00128

Leuthardt, E. C., Schalk, G., Wolpaw, J. R., Ojemann, J. G., & Moran, D. W. (2004). A brain-computer interface using electrocorticographic signals in humans. *J Neural Eng, 1*(2), 63-71. doi:10.1088/1741-2560/1/2/001

Leuthardt, E. C., Schalk, G., Roland, J., Rouse, A., & Moran, D. W. (2009). Evolution of brain-computer interfaces: going beyond classic motor physiology. *Neurosurg Focus, 27*(1), E4. doi:10.3171/2009.4.focus0979

Leyton, A.S.F., and Sherrington, C.S.: ‘OBSERVATIONS ON THE EXCITABLE CORTEX OF THE CHIMPANZEE, ORANG-UTAN, AND GORILLA’, Quarterly Journal of Experimental Physiology, 1917, 11, (2), pp. 135-222

Little, S., Pogosyan, A., Neal, S., Zavala, B., Zrinzo, L., Hariz, M., . . . Brown, P. (2013). Adaptive deep brain stimulation in advanced Parkinson disease. *Ann Neurol, 74*(3), 449-457. doi:10.1002/ana.23951

Marathe, A. R., & Taylor, D. M. (2013). Decoding continuous limb movements from high-density epidural electrode arrays using custom spatial filters. *J Neural Eng, 10*(3), 036015. doi:10.1088/1741-2560/10/3/036015

McCarthy, P. T., Otto, K. J., & Rao, M. P. (2011). Robust penetrating microelectrodes for neural interfaces realized by titanium micromachining. *Biomed Microdevices, 13*(3), 503-515. doi:10.1007/s10544-011-9519-5

McFarland, D. J., Sarnacki, W. A., & Wolpaw, J. R. (2010). Electroencephalographic (EEG) control of three-dimensional movement. *J Neural Eng, 7*(3), 036007. doi:10.1088/1741-2560/7/3/036007

McPherson, J.G., Miller, R.R., and Perlmutter, S.I.: ‘Targeted, activity-dependent spinal stimulation produces long-lasting motor recovery in chronic cervical spinal cord injury’, Proceedings of the National Academy of Sciences, 2015, 112, (39), pp. 12193-12198

Michel, C. M., Murray, M. M., Lantz, G., Gonzalez, S., Spinelli, L., & Grave de Peralta, R. (2004). EEG source imaging. *Clin Neurophysiol, 115*(10), 2195-2222. doi:10.1016/j.clinph.2004.06.001

Mukaino, M., Ono, T., Shindo, K., Fujiwara, T., Ota, T., Kimura, A., . . . Ushiba, J. (2014). Efficacy of brain-computer interface-driven neuromuscular electrical stimulation for chronic paresis after stroke. *J Rehabil Med, 46*(4), 378-382. doi:10.2340/16501977-1785

Murphy, J., Kwan, H., & Wong, Y. (1985). Cross correlation studies in primate motor cortex: synaptic interaction and shared input. *The Canadian journal of neurological sciences. Le journal canadien des sciences neurologiques, 12*(1), 11-23.

Murphy, M.D., Guggenmos, D.J., Bundy, D.T., and Nudo, R.J.: ‘Current Challenges Facing the Translation of Brain Computer Interfaces from Preclinical Trials to Use in Human Patients’, Frontiers in Cellular Neuroscience, 2015, 9, pp. 497

Murphy, Maxwell D., et al. "Assessing Perturbations to Neural Spiking Response Dynamics Caused By Electrical Microstimulation." *2018 IEEE International Symposium on Circuits and Systems (ISCAS)*. IEEE, 2018.

Nakanishi, Y., Yanagisawa, T., Shin, D., Fukuma, R., Chen, C., Kambara, H., Koike, Y. (2013). Prediction of three-dimensional arm trajectories based on ECoG signals recorded from human sensorimotor cortex. *PLoS One, 8*(8), e72085. doi:10.1371/journal.pone.0072085

Nudo, R. J., & Friel, K. M. (1999). Cortical plasticity after stroke: implications for rehabilitation. *Rev Neurol (Paris), 155*(9), 713-717.

Nudo, R.J., Jenkins, W.M., and Merzenich, M.M.: ‘Repetitive microstimulation alters the cortical representation of movements in adult rats’, Somatosensory & motor research, 1990, 7, (4), pp. 463-483

Nudo, R. J., Milliken, G. W., Jenkins, W. M., & Merzenich, M. M. (1996). Use-dependent alterations of movement representations in primary motor cortex of adult squirrel monkeys. *J Neurosci, 16*(2), 785-807.

Nuyujukian, P., Kao, J. C., Fan, J. M., Stavisky, S. D., Ryu, S. I., & Shenoy, K. V. (2014). Performance sustaining intracortical neural prostheses. *J Neural Eng, 11*(6), 066003. doi:10.1088/1741-2560/11/6/066003

Obien, M. E., Deligkaris, K., Bullmann, T., Bakkum, D. J., & Frey, U. (2014). Revealing neuronal function through microelectrode array recordings. *Front Neurosci, 8*, 423. doi:10.3389/fnins.2014.00423

Opris, I., Fuqua, J. L., Huettl, P. F., Gerhardt, G. A., Berger, T. W., Hampson, R. E., & Deadwyler, S. A. (2012). Closing the loop in primate prefrontal cortex: inter-laminar processing. *Front Neural Circuits, 6*, 88. doi:10.3389/fncir.2012.00088

Orsborn, A. L., Moorman, H. G., Overduin, S. A., Shanechi, M. M., Dimitrov, D. F., & Carmena, J. M. (2014). Closed-loop decoder adaptation shapes neural plasticity for skillful neuroprosthetic control. *Neuron, 82*(6), 1380-1393. doi:10.1016/j.neuron.2014.04.048

Pazienti, A., & Grun, S. (2006). Robustness of the significance of spike synchrony with respect to sorting errors. *J Comput Neurosci, 21*(3), 329-342. doi:10.1007/s10827-006-8899-7

Pandarinath, Chethan, et al. "Inferring single-trial neural population dynamics using sequential auto-encoders." *Nature methods* 15.10 (2018): 805-815.

Penfield, W., and Jasper, H.: 'Epilepsy and the functional anatomy of the human brain', 1954

Peng, Z., Xuan, M., Hailong, H., & Jiping, H. (2014). Predicting hand orientation in reach-to-grasp tasks using neural activities from primary motor cortex. *Conf Proc IEEE Eng Med Biol Soc, 2014*, 1306-1309. doi:10.1109/embc.2014.6943838

Perge, J. A., Homer, M. L., Malik, W. Q., Cash, S., Eskandar, E., Friehs, G., Hochberg, L. R. (2013). Intra-day signal instabilities affect decoding performance in an intracortical neural interface system. *J Neural Eng, 10*(3), 036004. doi:10.1088/1741-2560/10/3/036004

Perkel, D. H., Gerstein, G. L., & Moore, G. P. (1967). Neuronal spike trains and stochastic point processes. II. Simultaneous spike trains. *Biophys J, 7*(4), 419-440. doi:10.1016/s0006-3495(67)86597-4

Pfurtscheller, G., & Cooper, R. (1975). Frequency dependence of the transmission of the EEG from cortex to scalp. *Electroencephalogr Clin Neurophysiol, 38*(1), 93-96.

Pfurtscheller, G., Muller, G. R., Pfurtscheller, J., Gerner, H. J., & Rupp, R. (2003). 'Thought'--control of functional electrical stimulation to restore hand grasp in a patient with tetraplegia. *Neurosci Lett, 351*(1), 33-36.

Pfurtscheller, G., Neuper, C., Flotzinger, D., & Pregenzer, M. (1997). EEG-based discrimination between imagination of right and left hand movement. *Electroencephalogr Clin Neurophysiol, 103*(6), 642-651.

Pistohl, T., Ball, T., Schulze-Bonhage, A., Aertsen, A., & Mehring, C. (2008). Prediction of arm movement trajectories from ECoG-recordings in humans. *J Neurosci Methods, 167*(1), 105-114. doi:10.1016/j.jneumeth.2007.10.001

Popovic Maneski, L., Jorgovanovic, N., Ilic, V., Dosen, S., Keller, T., Popovic, M. B., & Popovic, D. B. (2011). Electrical stimulation for the suppression of pathological tremor. *Med Biol Eng Comput, 49*(10), 1187-1193. doi:10.1007/s11517-011-0803-6

Ramos-Murguialday, A., & Birbaumer, N. (2015). Brain oscillatory signatures of motor tasks. *J Neurophysiol*, jn 00467 02013. doi:10.1152/jn.00467.2013

Ramos-Murguialday, A., Broetz, D., Rea, M., Laer, L., Yilmaz, O., Brasil, F. L., . . . Birbaumer, N. (2013). Brain-machine interface in chronic stroke rehabilitation: a controlled study. *Ann Neurol, 74*(1), 100-108. doi:10.1002/ana.23879

Reddy, C. G., Reddy, G. G., Kawasaki, H., Oya, H., Miller, L. E., & Howard, M. A., 3rd. (2009). Decoding movement-related cortical potentials from electrocorticography. *Neurosurg Focus, 27*(1), E11. doi:10.3171/2009.4.focus0990

Rey, H. G., Pedreira, C., & Quian Quiroga, R. (2015). Past, present and future of spike sorting techniques. *Brain Res Bull*. doi:10.1016/j.brainresbull.2015.04.007

Rousche, P. J., & Normann, R. A. (1999). Chronic intracortical microstimulation (ICMS) of cat sensory cortex using the Utah Intracortical Electrode Array. *IEEE Trans Rehabil Eng, 7*(1), 56-68.

Rouse, A. G., Williams, J. J., Wheeler, J. J., & Moran, D. W. (2013). Cortical adaptation to a chronic micro-electrocorticographic brain computer interface. *J Neurosci, 33*(4), 1326-1330. doi:10.1523/jneurosci.0271-12.2013

Sanchez, J. C., Gunduz, A., Carney, P. R., & Principe, J. C. (2008). Extraction and localization of mesoscopic motor control signals for human ECoG neuroprosthetics. *J Neurosci Methods, 167*(1), 63-81. doi:10.1016/j.jneumeth.2007.04.019

Schalk, G., Kubanek, J., Miller, K. J., Anderson, N. R., Leuthardt, E. C., Ojemann, J. G., Wolpaw, J. R. (2007). Decoding two-dimensional movement trajectories using electrocorticographic signals in humans. *J Neural Eng, 4*(3), 264-275. doi:10.1088/1741-2560/4/3/012

Schalk, G., Miller, K. J., Anderson, N. R., Wilson, J. A., Smyth, M. D., Ojemann, J. G., Leuthardt, E. C. (2008). Two-dimensional movement control using electrocorticographic signals in humans. *J Neural Eng, 5*(1), 75-84. doi:10.1088/1741-2560/5/1/008

Sharma, A., Sane, H., Kulkarni, P., Yadav, J., Gokulchandran, N., Biju, H., & Badhe, P. (2015). Cell therapy attempted as a novel approach for chronic traumatic brain injury - a pilot study. *Springerplus, 4*, 26. doi:10.1186/s40064-015-0794-0

Shimazaki, H., Amari, S.-i., Brown, E.N., and Grün, S.: 'State-Space Analysis of Time-Varying Higher-Order Spike Correlation for Multiple Neural Spike Train Data', PLoS Comput Biol, 2012, 8, (3), pp. E1002385

Shindo, K., Kawashima, K., Ushiba, J., Ota, N., Ito, M., Ota, T., Liu, M. (2011). Effects of neurofeedback training with an electroencephalogram-based brain-computer interface for hand paralysis in patients with chronic stroke: a preliminary case series study. *J Rehabil Med, 43*(10), 951-957. doi:10.2340/16501977-0859

Slutzky, M. W., Jordan, L. R., Lindberg, E. W., Lindsay, K. E., & Miller, L. E. (2011). Decoding the rat forelimb movement direction from epidural and intracortical field potentials. *J Neural Eng, 8*(3), 036013. doi:10.1088/1741-2560/8/3/036013

Soekadar, S. R., Witkowski, M., Garcia Cossio, E., Birbaumer, N., & Cohen, L. (2014). Learned EEG-based regulation of motor-related brain oscillations during application of transcranial electric currents: feasibility and limitations. *Frontiers in Behavioral Neuroscience, 8*. doi:10.3389/fnbeh.2014.00093

Soekadar, S. R., Witkowski, M., Mellinger, J., Ramos, A., Birbaumer, N., & Cohen, L. G. (2011). ERD-based online brain-machine interfaces (BMI) in the context of neurorehabilitation: optimizing BMI learning and performance. *IEEE Trans Neural Syst Rehabil Eng, 19*(5), 542-549. doi:10.1109/tnsre.2011.2166809

Soekadar, S. R., Witkowski, M., Robinson, S. E., & Birbaumer, N. (2013). Combining electric brain stimulation and source-based brain-machine interface (BMI) training in neurorehabilitation of chronic stroke. *Journal of the Neurological Sciences, 333, Supplement 1*, e542. doi:http://dx.doi.org/10.1016/j.jns.2013.07.1906

Soekadar, S. R., Witkowski, M., Vitiello, N., & Birbaumer, N. (2015a). An EEG/EOG-based hybrid brain-neural computer interaction (BNCI) system to control an exoskeleton for the paralyzed hand. *Biomed Tech (Berl), 60*(3), 199-205. doi:10.1515/bmt-2014-0126

Soekadar, S. R., Witkowski, M., Birbaumer, N., & Cohen, L. G. (2015b). Enhancing Hebbian Learning to Control Brain Oscillatory Activity. *Cereb Cortex, 25*(9), 2409-2415. doi:10.1093/cercor/bhu043

Sullivan, R., Duncan, K., Dailey, T., Kaneko, Y., Tajiri, N., & Borlongan, C. V. (2015). A possible new focus for stroke treatment - migrating stem cells. *Expert Opin Biol Ther*, 1-10. doi:10.1517/14712598.2015.1043264

Sussillo, D., and Barak, O.: 'Opening the black box: low-dimensional dynamics in high-dimensional recurrent neural networks', Neural computation, 2013, 25, (3), pp. 626-649

Taghva, A., Song, D., Hampson, R. E., Deadwyler, S. A., & Berger, T. W. (2012). Determination of relevant neuron-neuron connections for neural prosthetics using time-delayed mutual information: tutorial and preliminary results. *World Neurosurg, 78*(6), 618-630. doi:10.1016/j.wneu.2011.09.002

Taylor, D. M., Tillery, S. I., & Schwartz, A. B. (2002). Direct cortical control of 3D neuroprosthetic devices. *Science, 296*(5574), 1829-1832. doi:10.1126/science.1070291

Todorova, S., Sadtler, P., Batista, A., Chase, S., & Ventura, V. (2014). To sort or not to sort: the impact of spike-sorting on neural decoding performance. *J Neural Eng, 11*(5), 056005. doi:10.1088/1741-2560/11/5/056005

Tooker, A., Tolosa, V., Shah, K. G., Sheth, H., Felix, S., Delima, T., & Pannu, S. (2012). Polymer neural interface with dual-sided electrodes for neural stimulation and recording. *Conf Proc IEEE Eng Med Biol Soc, 2012*, 5999-6002. doi:10.1109/embc.2012.6347361

Velliste, M., Perel, S., Spalding, M. C., Whitford, A. S., & Schwartz, A. B. (2008). Cortical control of a prosthetic arm for self-feeding. *Nature, 453*(7198), 1098-1101. doi:10.1038/nature06996

Wang, W., Collinger, J. L., Degenhart, A. D., Tyler-Kabara, E. C., Schwartz, A. B., Moran, D. W., Boninger, M. L. (2013). An electrocorticographic brain interface in an individual with tetraplegia. *PLoS One, 8*(2), e55344. doi:10.1371/journal.pone.0055344

Wang, Z., Gunduz, A., Brunner, P., Ritaccio, A. L., Ji, Q., & Schalk, G. (2012). Decoding onset and direction of movements using Electrocorticographic (ECoG) signals in humans. *Front Neuroeng, 5*, 15. doi:10.3389/fneng.2012.00015

Ward, M. P., Rajdev, P., Ellison, C., & Irazoqui, P. P. (2009). Toward a comparison of microelectrodes for acute and chronic recordings. *Brain Res, 1282*, 183-200. doi:10.1016/j.brainres.2009.05.052

Warnecke, J., Devine, N., & Olen, C. (2015). Inpatient physical therapy rehabilitation provided for a patient with complete vision loss following a traumatic brain injury. *Brain Inj*, 1-7. doi:10.3109/02699052.2015.1022877

Wessberg, J., Stambaugh, C. R., Kralik, J. D., Beck, P. D., Laubach, M., Chapin, J. K., Nicolelis, M. A. (2000). Real-time prediction of hand trajectory by ensembles of cortical neurons in primates. *Nature, 408*(6810), 361-365. doi:10.1038/35042582

Wilde, C., Bruder, R., Binder, S., Marshall, L., & Schweikard, A. (2015). Closed-loop transcranial alternating current stimulation of slow oscillations. *Current Directions in Biomedical Engineering, 1*(1), 85-88. doi:10.1515/cdbme-2015-0022

Willett, F. R., Suminski, A. J., Fagg, A. H., & Hatsopoulos, N. G. (2013). Improving brain-machine interface performance by decoding intended future movements. *J Neural Eng, 10*(2), 026011. doi:10.1088/1741-2560/10/2/026011

Williams, J. C., Hippensteel, J. A., Dilgen, J., Shain, W., & Kipke, D. R. (2007). Complex impedance spectroscopy for monitoring tissue responses to inserted neural implants. *J Neural Eng, 4*(4), 410-423. doi:10.1088/1741-2560/4/4/007

Wilson, J. A., Felton, E. A., Garell, P. C., Schalk, G., & Williams, J. C. (2006). ECoG factors underlying multimodal control of a brain-computer interface. *IEEE Trans Neural Syst Rehabil Eng, 14*(2), 246-250. doi:10.1109/tnsre.2006.875570

Wolpaw, J. R., & McFarland, D. J. (2004). Control of a two-dimensional movement signal by a noninvasive brain-computer interface in humans. *Proc Natl Acad Sci U S A, 101*(51), 17849-17854. doi:10.1073/pnas.0403504101

Wolpaw, J. R., McFarland, D. J., Neat, G. W., & Forneris, C. A. (1991). An EEG-based brain-computer interface for cursor control. *Electroencephalogr Clin Neurophysiol, 78*(3), 252-259.

Wu, W., Shaikhouni, A., Donoghue, J. P., & Black, M. J. (2004). Closed-loop neural control of cursor motion using a Kalman filter. *Conf Proc IEEE Eng Med Biol Soc, 6*, 4126-4129. doi:10.1109/iembs.2004.1404151

Yamamoto, T., Katayama, Y., Ushiba, J., Yoshino, H., Obuchi, T., Kobayashi, K., Fukaya, C. (2013). On-demand control system for deep brain stimulation for treatment of intention tremor. *Neuromodulation, 16*(3), 230-235; discussion 235. doi:10.1111/j.1525-1403.2012.00521.x

Yanagisawa, T., Hirata, M., Saitoh, Y., Goto, T., Kishima, H., Fukuma, R., Yoshimine, T. (2011). Real-time control of a prosthetic hand using human electrocorticography signals. *J Neurosurg, 114*(6), 1715-1722. doi:10.3171/2011.1.jns101421

Yanagisawa, T., Hirata, M., Saitoh, Y., Kato, A., Shibuya, D., Kamitani, Y., & Yoshimine, T. (2009). Neural decoding using gyral and intrasulcal electrocorticograms. *Neuroimage, 45*(4), 1099-1106. doi:10.1016/j.neuroimage.2008.12.069

Yoshimura, N., Dasalla, C. S., Hanakawa, T., Sato, M. A., & Koike, Y. (2012). Reconstruction of flexor and extensor muscle activities from electroencephalography cortical currents. *Neuroimage, 59*(2), 1324-1337. doi:10.1016/j.neuroimage.2011.08.029

Zhang, Z. W., & Deschenes, M. (1998). Projections to layer VI of the posteromedial barrel field in the rat: a reappraisal of the role of corticothalamic pathways. *Cereb Cortex, 8*(5), 428-436.

Zrenner, C., Tünnerhoff, J., Zipser, C., Müller-Dahlhaus, F., & Ziemann, U. (2015). V38. Brain-state dependent non-invasive brain stimulation using closed-loop real-time EEG signal analysis to trigger a TMS pulse with millisecond accuracy. *Clinical Neurophysiology, 126*(8), e85. doi:http://dx.doi.org/10.1016/j.clinph.2015.04.116

CHAPTER 3

Tools for the preclinical rehabilitation engineer

Introduction

This chapter provides a perspective on different approaches to the study of motor control during movement. It also makes an argument for the utility of the systems approach in studying motor control and motor reorganization in a preclinical animal model of injury. The next section describes considerations for the use of both kinematic markers of position and metrics of neural activity as either the system measurement[19] or system state[20]. A brief historical perspective shows why this is an important consideration. The final sections describe tools that either the author developed or which can be obtained freely by any investigator in order to accurately parse the relevant measured quantities[21] from acquisition instruments.

[19] The terms *measurement* and *observation* may be used interchangeably. *Output* is slightly more specific, but in the systems context and particularly the Kalman formulation used in the final chapter, all three may be considered synonymous.

[20] The term *state* typically implies some value of the system which defines its behavior, but which cannot be observed directly and must be estimated in some fashion that requires a model of the system architecture.

[21] For kinematics in the reaching rat, this is the 3D world-coordinate position time-series of markers distributed around the paw (along the digits and wrist). For neural activity, this corresponds to the times of spikes in the extracellular field potential, the local field potential (LFP) amplitude, and measures of correlation between such endpoints.

Perspectives on the study of motor behavior

According to Horak, there are three schools of thought when it comes to the study of motor behavior: Reflex Theory, Hierarchical Theory, and Systems Theory (Horak 1991). Horak wisely indicates that all three approaches are not only useful but necessary in experimental design for the motor systems scientist with an emphasis in rehabilitation.

While the author agrees with this strategy, this work makes a case for Systems Theory--to the exclusion of Reflex Theory or Hierarchical Theory--due to the highly-specific nature of the measurements and experimental designs that are possible in preclinical animal models of rehabilitation and motor behavior. Furthermore, each of these three "modes" of thought may not be as different as they are traditionally described to be. Instead, Systems Theory may simply represent a more flexible framework for accommodating the other two modalities.

Reflex Theory

The original reflex theorist was none other than the famous Sir Charles Sherrington. Although the knee-jerk reflex[22] was first discovered independently by Erb and Westphal in 1875 (Fine & Darkhabani 2009), the significance of this reflex arc with respect to the discovery of the inhibition of skeletal muscle did not occur until nearly 20 years later. In a one-page note, John Hughlings Jackson described the exaggerated knee-jerks and knee-clonus in a dog model of asphyxiation, which he speculatively attributed to the loss of excitability in the motor cortex and subsequent "loss of cerebral control upon lumbar centres" (Jackson 1892). In an excited response published less than a month later, Sherrington, who noted similar results published in

[22] Referred to as the "knee-jerk" directly in papers by Sherrington and Hughlings Jackson, this phenomenon is sometimes also called the patellar reflex or the knee reflex.

recent years in the rabbit model, described his replication of such findings in cats and macaques (Sherrington 1892).

Sherrington was adamant that the knee-jerk described by Jackson bore an “intimate dependence on the integrity of a reflex arc,” and, critically, he observed that the fact that “the knee-jerk should be related to only one nerve-root is singular when one remembers that the limb muscles are for the most part supplied by more than one spinal nerve” (Sherrington 1892). His studies of decerebrate rigidity in the cat would go on to show that patterns of inhibition were involved in the reflex arc (Sherrington 1898). Using the decerebrate model, Sherrington provided many findings that remain critical to current understanding of motor control mechanisms, such as the description of the stretch reflex (Liddell & Sherrington 1924). During these studies, Sherrington pioneered the idea of reciprocal innervation: when a muscle contracts in order to exert the force required for the movement of a body part in an intended direction, an antagonist muscle that directly opposes the movement of said body part in that direction is inhibited (Sherrington 1909, Sherrington 1910). This mechanism is so fundamental to movement that even though this work implements a Systems Theory approach, the strategy for designing the optimization required for regressing the linearized estimate of neural state dynamics, which is discussed in detail in **Chapter 5**, is based on the assumed requirement that the phasic activity of such agonist and antagonist pairs must be represented somehow in the strongest features of the neural population state during movement.

While the works of Sherrington revealed fundamental and ubiquitous mechanisms of motor control that primarily reside in circuitry organized below the level of the cerebral cortex, it is worth noting that the field of Reflex Theory bears necessary limitations when it comes to the problematic questions that behavior tends to raise. Fundamentally, since behavior is continuous and requires the binding of events through time, a theory of movement that relies only upon peripheral integration of responses to stimuli is likely insufficient to explain all manners of

movement, particularly those arising during voluntary and coordinated movement such as during upper-extremity movement. Nonetheless, the wealth of important insights that the theory has accounted for is a testament to the importance of dissecting a motor circuit under consideration in order to examine its most-basic elements.

Hierarchical Theory

Horak attributes John Hughlings Jackson with the first articulation of Hierarchical Theory in 1931 (Horak 1991). In assigning that date, she cites anecdotal praises that are quoted from the introduction in a textbook devoted to Jackson's teachings (Walsche, 1961). There is both good reason for such an attribution[23] and also a certain pedagogical appeal to crediting Jackson as the founder of Hierarchical Theory. However, while crediting with such a thing is convenient, it is somewhat unfair to a developmental neurobiologist by the name of George Ellett Coghill[24]. Furthermore, such an attribution might also be unfair to Jackson: while he suggested the role of the cerebral cortex in movement as early as 1876, he also adamantly disavowed metaphysics and emphasized that he could care less about mechanisms of movement (Jackson 1876).

On the other hand, Coghill was obsessed with such things. Over the course of his life's work, Coghill painstakingly studied the nervous system of amphibians[25] during development. As the salamander or newt larvae develops, it remains relatively motionless in its aquatic environment until stereotyped phases of movement emerge. The first movements are a result of reflex response to touch and range from slight flexion of the rostral-most muscles to an eventual "S-reaction" reflex that serves to propel the specimen away from the source of contact. In his

[23] The Jackson quote provided in the previous section shows that the famous physician clearly entertained the possible role of cortex in motor control of "lumbar centres" as early as 1892.
[24] This claim is nepotistic. The fixation of both the author of this work and Coghill on neuromotor generation of complex movement seems to run in the family.
[25] Coghill's model of choice was *Amblystoma Punctatum*, although some of his initial work was conducted in the Pacific newt. His research ultimately made use of several different salamander species, which may have been due in part to specimen availability.

earliest works, Coghill catalogues the progression of specimens through each of these stages in such extraordinary detail that he even expresses in the manuscript itself that he no longer plans to document future studies in this manner due to the impossibility of automation and impractical burden such annotation imposed on him (Coghill 1909). In a subset of experiments, when a specimen first produced movements corresponding to a specific developmental stage[26] Coghill prepared it immediately for histological analysis (Coghill 1913). This enabled him to observe the nervous system as it developed in order to coregister as accurately as possible the generation of each new type of movement with comparative neuroanatomical patterns of innervation.

It should be noted that Coghill was not only aware of Sherrington, but seemed to admire him. This made sense, as citing the work of Sherrington allowed Coghill to defend the use of his preferred model organisms. This was particularly evident in his discussions condemning a peer who used a fish model: while the amphibians tended to be relatively lethargic until the larvae reached a stage at which vigorous and stereotyped "S-reaction" was observed in response to cutaneous stimuli, the fish model generated poorly-described behavior that was less-stereotyped (Coghill 1909). However, even in his early works, Coghill diverges from the Reflex Theorists, with discussions indicating his skepticism that all of behavior could be explained on the basis of "simple reflexes." In later years, his initial descriptions of the difficult-to-quantify "instinct," were replaced by the suggestion that a central "mechanism of total integration," is related to motor output as it forms over the course of development (Coghill 1933). Coghill is perhaps most well-known for his book entitled "Anatomy and the Problem of Behavior," which suggests his rejection of Reflex Theory by virtue of the interesting question it raises: how does behavior, which is heterogeneous and specific to individuals, arise from anatomical elements with such homogeny (Coghill 1929)? If constituent reflexes are expected to otherwise behave

[26] A family rumor is that Coghill kept at least one hapless research assistant on duty watching salamanders on a 24/7 schedule when it was required to fix the specimen upon the first sign of spontaneous movement. Coghill's later works abandoned such lengths, probably due to feasibility.

similarly in response to a given stimulus, then the apparent coordination of such reflexes must require some “higher center” where behavior is “consolidated” or “integrated.”

The story of George Ellett Coghill is just an example from developmental neurobiology that suggests each theory of motor control is not so much a distinct, cut-and-dry philosophy so much as a series of natural trends in thinking that arose from common interests in motor behavior. These trends in thought arose from different sources, which were predicated upon the field of study of the investigators who espoused them. While the emphasis on Coghill should not detract from the incredible insight and observations made by John Hughlings Jackson[27], it seems more probable that Hierarchical Theory emerged gradually and inevitably as developmental neurobiologists and embryologists began to speculate about how movements develop[28].

This apparent discrepancy regarding the progenitor of Hierarchical Theory may simply reflect heuristics for teaching the theory of motor control. Over the entirety of the author’s education on the subject, which ranges from superficial discussions during high school psychology to graduate coursework in motor control theory, the two views were always presented as competing all-or-nothing theories. In Reflex Theory, it is taught, the role of the nervous system in motor control is strictly exerted by automatic closed-loop control of muscles and sensory receptors. Hierarchical Theory is then conveniently described in opposition: driven by “western thought” and the philosophical treatises of Descartes, the Hierarchical Theorists believed that nervous control of movement resulted purely from the voluntary specification of muscle activation patterns[29] that were generated by some “integrative” central center.

---

[27] Even as of 2020, breakthroughs continue to suggest the role of the cerebral cortex in the simultaneous modulation of excitation and inhibition of agonist and antagonist pairs via its projections to the “lumbar centres” (Griffin & Strick 2020).

[28] Despite Coghill’s repeated arguments for the model’s significance (Coghill 1930), the author thinks that probably not everyone shared the same enthusiasm for the wriggling of salamanders and newts.

[29] Sometimes referred to as *motor programs*. The author finds this terminology a helpful heuristic, although it is avoided if possible in order to semantically distinguish the manner in which information is encoded and decoded by the brain by comparison to the digital registers of a computer.

Taken holistically, we see that Hierarchical Theory and Reflex Theory emerged, at least to some degree, in parallel. While a traditional oversimplification suggests that Hierarchical Theory only considers the role of the central nervous system as a generator of movement patterns, when context for the emergence of such a theory is given, it can be seen that this is actually not the case. Returning to the sage advice of Horak, it is suggested that a limitation of the hierarchical model, as with the reflex model, is the "inability to account for the increasingly blurred distinction between voluntary and reflex control" (Horak, 1991). It is hoped that this discussion provides some concept of why such a blurring may be apparent if on no other basis but the shared roots of both modes of thought. As it will be seen in the ensuing chapters, the role of Hierarchical Theory is felt strongly in the interpretation of these empirical data, which were gathered from the cerebral cortex of the rat.

Systems Theory

Contextualizing Reflex Theory and Hierarchical Theory is critical, because it allows the physiologist to understand that an argument for Systems Theory is not actually an argument against the other two "schools." Instead, Systems Theory simply integrates Reflex Theory and Hierarchical Theory, while placing constraints on the roles of each that are grounded in parametric elements of the modeled system. Systems Theory subtly differs from Hierarchical Theory in that it does not necessarily require a fixed controller hierarchy; rather, it allows that movement genesis is probably related to reciprocal interactions between factors both within and outside of the scope of the nervous system. In the Systems Theory formulation, behavior at any given instant is predicated on its past and future states: neuromotor generators at multiple levels of the nervous system are simultaneously involved in the recursive prediction and feedback control required at all times for such a continuous process to propagate with stability.

Figure 3.1

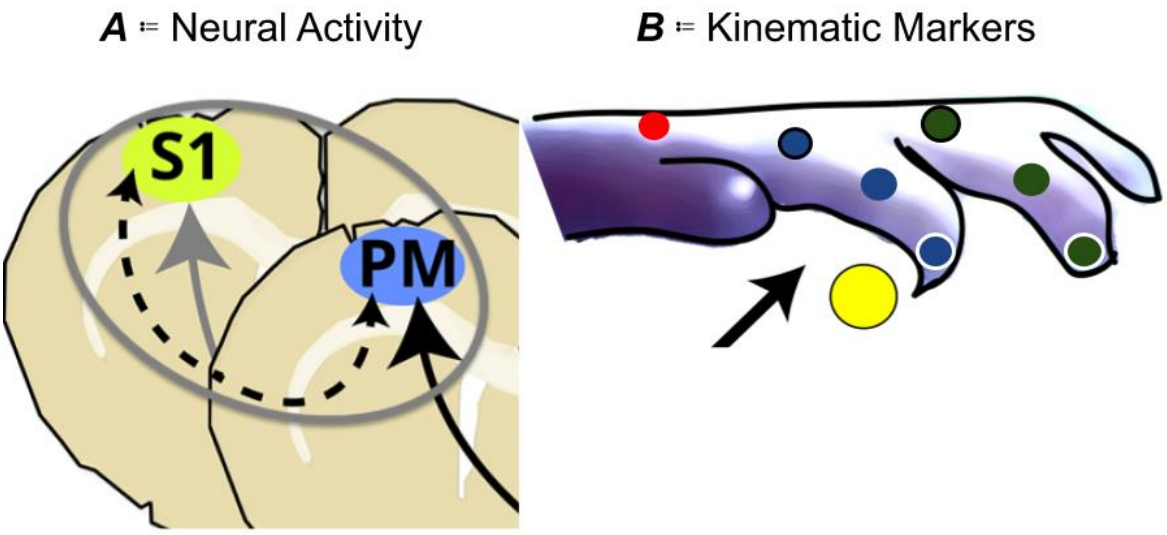

Figure 3.1: Example measurements under consideration.

Illustration of example components to be modeled under Systems Theory approach. *Left:* neural activity is recorded from electrodes embedded in approximately layer 5 (placed near cell bodies with descending spinal outputs) in premotor (PM; in rats this is Rostral Forelimb Area or RFA) and primary sensory cortex (S1). The electrodes measure the extracellular electrical field potential with respect to a reference site tied to a metal screw on the skull. *Right:* kinematic markers are reconstructed in 3D world coordinates using calibrated stereo cameras and a deep learning network trained to identify the pellet (yellow), wrist (red), distal-to-proximal parts of the first digit (blue; white to black outlines represent distal-to-proximal gradient), and distal-to-proximal parts of the second digit (green).

What is meant by "neuromotor generators at multiple levels of the nervous system"?

A simple example of Systems Theory in practice is the application of the laws of physics in predicting the state of a limb during voluntary movement. Figure 3.1 shows the sets of neural and kinematic measurements that might be used during such predictions. Considering such measurements, we see that aside from any mathematical formulations regarding their relation,

an immediate and non-trivial choice in model selection is the arrangement of the system components in a simple block diagram (Figure 3.2). Note that the figure intentionally uses a black box (***H***) to denote any transformation (linear or nonlinear) involved in prediction. With respect to the laws of physics in estimation of limb position, we suspect that Newton's laws of motion might be a good place to start in designing a linear matrix that relates the limb position at some time in the future to its present and past states (therefore, a linear system design for ***H*** in Figure 3.2ii might reflect such equations).

Figure 3.2

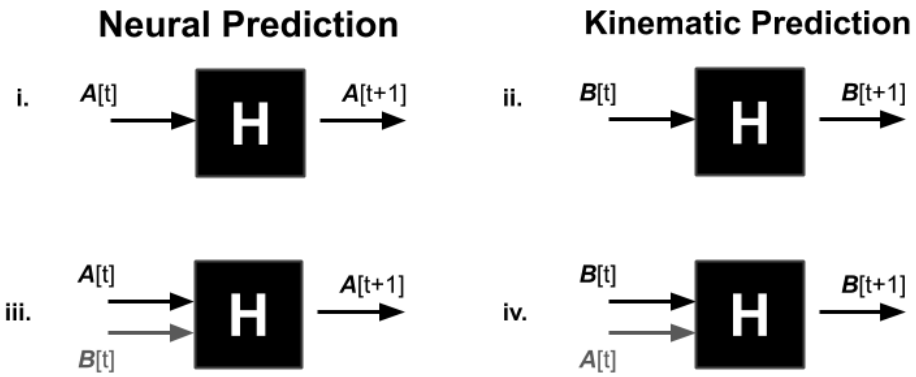

Figure 3.2: Examples of possible Systems schema.

Illustration of possible system model schematics. Each of panels *i* - *iv* represent a viable possible strategy for studying movement depending on which measurements shown in **Figure 3.1** are available. For the sake of generality, in each case, **H**, the filter (or alternatively thought of as the system transfer function) is kept as a black box, so that only the general configuration of measurements is considered.

i. Neural activity measurements predict the future measurements of neural activity.
ii. Kinematic measurements predict the future kinematic measurements.
iii. Neural activity measurements, augmented by kinematic measurements, predict future neural activity.
iv. Kinematic measurements, augmented by neural activity measurements, predict future

kinematic measurements.
Note that in the last two cases, if ***H*** is allowed to vary on some timescale, then the adaptive weightings (matched matrix elements of ***H***) contain information about the contribution of the secondary set of signals to prediction. Such information does not imply causation, but may be informative--particularly when very little is known about operational modes of the system.

The movement of a limb during volitional behavior probably can't be solely explained by its past states: behavior is a compound of smaller sub-movements. The combination of such movements is nonlinear, probably depends on circumstances external to the nervous system or the limb (e.g. reacting to an opponent while playing a sport), and involves changes in acceleration due to the combined contraction and relaxation of specific agonist and antagonist muscles in such a way as to alter the course of the limb in flight. Depending on the behavior, such deviations from the expectation of simple ballistic movement may be small and only most-evident in a phasic manner[30]. In the context of rats retrieving pellets, the most-likely instances requiring cortical mediation would then be near the moment of the attempted grasping of the pellet, and may also occur close to toe-off or immediately following the first sniff (Whishaw et al. 1986, Whishaw et al. 1992, Hyland 1998). It is unknown to what extent rats accurately perceive depth through vision, but it does not take too large of a leap in imagination to consider that, similar to a human reaching for a cell phone on the bedside stand in the dark, a weighting on neural activity relating to cutaneous sensation might also immediately precede grasping. This scenario is described by **Figure 3.2iii**. Both the present **neural state** and the present **limb state** combine in some way (again, allowing ***H*** to denote a generic "black box" yet to be addressed) to estimate the future neural state. As the **neural state** *estimate* of the **limb state** draws nearer to

[30] The engineer is recommended to take this as a first principle, regardless of the behavior! Due to probable bandwidth limitations on filtering in the cerebral cortex, it would be wasteful (and probably evolutionarily disadvantageous) if the cortex had to attend to every single aspect of a movement. The more that a movement could be offloaded to mechanisms not requiring attention, or even better--not even under nervous control at all but simply a product of mechanical properties of the system once the limb reaches a threshold *state*--the more that cortex might focus on other more nuanced parts of behavior or otherwise. Gait is an excellent example of such a case (Craig et al. 2016).

the pellet, the expectation of cutaneous contact increases. Distinguishing between activity related to the estimation process, and activity that occurs in anticipation of cutaneous contact would be a critical component for experimental design in this context: a behavioral task in which motor output can be executed in both the presence and absence of the hypothesized dominant sensory strategy would provide a causal manipulation that could help distinguish such a thing. Unfortunately, rats tend to spend an inordinate amount of time grooming the digits and forelimb once topical lidocaine is applied; it is noted that a habituation strategy in which the rats gradually acclimate to the lidocaine application has not been tested.

Systems Theory helps identify necessary "pre-experiments" during experimental design. It is most helpful when biologists and engineers collaborate prior to the collection of experimental data, so that an interesting hypothesis is not rendered useless by missed considerations during experimental design. Returning to the previous example of the rat reaching to retrieve pellets, consider the case in which only the neural data and not the kinematic reconstruction is available. This means that the investigator is forced to use the design illustrated in **Figure 3.2i**. It becomes difficult (*but not impossible*, as is shown in **Chapter 5**) for the investigator to derive an objective metric of error that relates to a measurable component of the behavior aside from the use of functional outcomes as a binary regressor. Clearly, the optimal alternative is illustrated by **Figure 3.2iv**: for example, if the filter is allowed to adapt in relation to some error term over the course of each trial, then perhaps the speculative "re-weighting" on cutaneous sensation mentioned previously is evident in the time-series of the relevant filter matrix coefficients. This generates a meaningful conversation between the biologist and the engineer: what is a meaningful error term in this situation? A short discussion may lead the biologist to the realization that he or she has already collected a wealth of publishable material. A simple empirical characterization of the process noise that occurs at both an individual and cohort level during the thousands of pellet retrievals that naive, Intact rats

perform while being trained to proficiency would have significance for future investigators using the reaching rat model to a variety of ends.

Similarly, to avoid an overly-elaborate model[31] that unduly emphasizes error terms which don't matter, the target model should be confirmed by all parties from the outset. The alternative is that the engineer begins to fret about "getting it wrong." Constraints imposed by measurable tissue properties of the effector limb, such as the viscoelasticity of muscles and tendons, might make the model more realistic; the engineer does a literature review and finds plausible values, inserting more terms and equations. The engineer begins to agonize about digit marker reconstructions that violate range-of-motion constraints. Each newly-conceived noise source haunts the engineer's dreams until addressed. Unfortunately, after countless hours spent on writing new code and tuning model parameters, which require waiting for the increasingly burdensome calculations to complete, it is found that the model only offers minimal or no improvements in accuracy with respect to the metrics of interest.

Instead, a simple conversation with a physiologist might have indicated that treating the digit markers as a "cloud" of noisy points about some centroid was sufficient for the correlative purposes to which it would be used in the model. Unfortunately, the physiologist who has not done the no-nonsense experiment characterizing process noise during reaching could not provide such intuition. It is also noted that, once again, such a discussion could generate other more meaningful and purposeful uses of the engineer's time: is it possible to simulate bounds on how the magnitude of such measurement noise could impact a model, and specifically, which parts of the model might be most-affected? Are there features of both the neural signal

[31] As model complexity increases, interpretability decreases: in the case of the most-complicated nonlinear dynamical system estimates (such as the metric described at the end of last chapter; Murphy et al. 2018), it may become altogether impossible to derive useful intuition from results. In other instances, key constraints are missing such that the oversimplified procedure for recovering system coefficients leads to converged endpoints with no basis in reality.

and the reaching movement of the limb that cause this behavior to become more robust to noise; and if so, when do they occur?

As a final point, hopefully at least one party in the collaboration already has application-specific knowledge. In this case, it is the job of that collaborator to provide specific parametric values; this should take the form of (preferably) summary statistics from past data or else a best-guess estimate based on clearly-stated assumptions. The use of fixed constant parametric values often simplifies the system identification problem, which as it can be seen, can be readily made over-complicated. An immediate practical benefit of providing such values is that their suitability for use in models can be tested: this not only gives the model the best chance of providing useful insight, but when conducted correctly, such tests almost always yield empirical results that are publishable in their own right, as shown in the next chapter (Murphy et al. 2019).

Figure 3.3

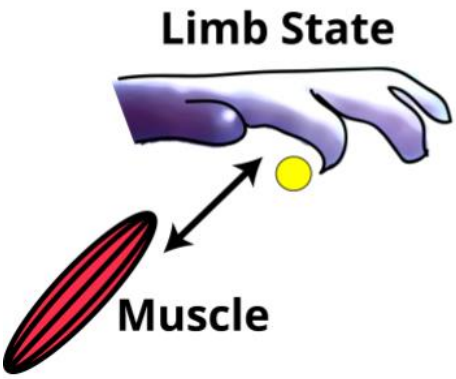

Figure 3.3: Limb state relates to muscle contraction.
The limb state is an approximation of the muscle co-contractions and relaxations of interest. Because it is technically quite challenging to obtain accurate electromyographical (EMG) readings from the rat forelimb even when the wires are inserted in the anesthetized preparation, direct measurement of the limb state is difficult in this model. Aside from the nontrivial issue of targeting the fine forelimb muscles (and subsequently hoping that this does not impair the

behavior), without proper precautions the rat is likely to remove such wires during grooming. Realizing this, the next-best option to direct EMG recordings is to record positional markers along the limb, which offer informative degrees of freedom with respect to movements generated during the behavior of interest. For example, markers on the tips of the digits would be of interest during digit flexion such as during grasping; the wrist may be interesting as a more proximal marker and "central" landmark for the others.

What is the **system state** specifically?

In the context of motor systems and strictly considering voluntary upper extremity limb movements, the **system state** comprises two state variables that the investigator typically wishes to relate in some way: the **limb state** and the **neural state**. When the limb moves from a resting position, or deviates from its ballistic trajectory in some intended manner, it requires the exertion of force in proportion to its mass and the amount of acceleration that is to be applied during such a change. With this in mind, the **limb state** must be defined as the combined electromyographical (EMG) activity of the muscles pertaining to movements of the effector limb of interest, as shown in **Figure 3.3**. The **neural state** is the combined activity of all nervous elements and is therefore never completely observed due to the limits of what is feasible to record from the nervous system given current electrode technology. In the narrower context of these experiments, the **neural state** is estimated in relation to processes of interest relative to the behavior; with respect to the sensorimotor areas of the cerebral cortex, this means that it is activity of neurons related to the filtering of input sensory measurements, prediction of future sensory inputs, prediction of the current state of the effector limb, and output command signals to the motoneuron pools and modulatory spinal interneurons (**Figure 3.4**).

Figure 3.4

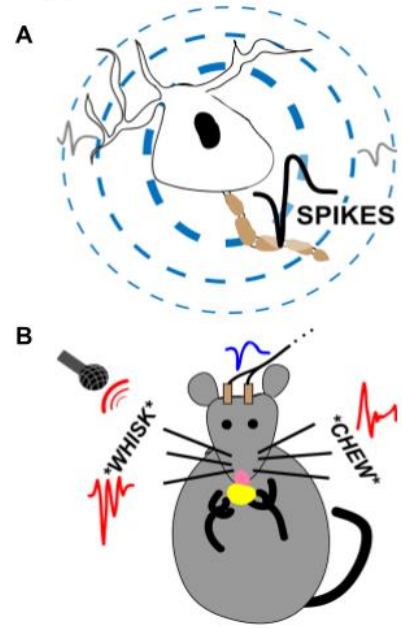

Figure 3.4: Neural state is task-specific and never observed completely.

The neural state is the combined activity of neurons in the nervous system which relate in some way to the filtering of motor information and generation of subsequent motor output. **A**) The neural "unit" is a characteristic spike that corresponds to the generation of an action potential by a single neuron (concentric circles denote that the amplitude decreases proportionally with the square of distance from the cell). The term "unit" refers to both the spike and the cell generating it: when represented as a point-process, the spike is typically denoted mathematically by shifted sums of the dirac delta function, (t), which is infinitesimally narrow, has infinite amplitude, and integrates to have unit area. While it is impossible to accurately identify actual single-unit activity from extracellular recordings of cortical cells during behavior without dense spatial arrays that enable the spatial triangulation of individual spike sources, "multi-unit" cortical activity appears to contain robust movement-related information. **B**) In this context, the neural state relates to the rat as it reaches to grasp and retrieve a pellet. Given that recordings are made from cortical units, the neural state under consideration is really the input and output filtering related to voluntary aspects of the reach-to-grasp maneuver. As shown by the non-neural noise sources, denoising the neural state is a non-trivial technical challenge, and failure to adequately do so not only generates erroneous results, but ones that are potentially misleading in that they may be conflated with biological noise sources that are behaviorally-related but not generated by the nervous elements under experimental manipulation.

Origins of a muscle-based **limb state**.

The subject of whether the **limb state** should be considered with respect to the muscular production of force or the position of the limb itself is somewhat controversial in motor systems neuroscience. In the late 1960's, a remarkably dedicated investigator by the name of Edward Evarts conducted a series of experiments in macaques trained to conduct a stereotyped hand movement, which would be formative in shaping the understanding of those studying the role of cerebral cortex in voluntary movements (Evarts 1966). Evarts recorded the extracellular field potentials from single electrode recordings taken from Layer 5 of the motor cortex contralateral to the arm during a task requiring the monkey to flex and extend its arm in order to receive a juice reward. He related the timing of behavior elements such as movement onset and force generation to the timing of activity generated by presumptive cortical pyramidal tract neurons (PTN) thought to project to the spinal motoneuron pools. He noted that the onset of PTN activity typically preceded EMG or movement onset. In a separate experiment, Evarts changed the force required to conduct a movement (Evarts 1968). He was able to identify PTNs that modulated activity on the basis of the load required by the effector: when flexion was opposed, the rate of PTN spikes (action potentials)[32] increased; when extension was opposed (i.e. flexion was facilitated), hardly any spikes were observed from the same PTN.

Later works that relied upon precisely summing snippets of rectified EMG waveforms (spike-triggered averages) based on the timing of detected PTN spikes strengthened the finding that PTNs directly modulate EMG output (Fetz & Cheney 1980). If such snippets demonstrated ergodicity on short timescales relative to a coherent event (i.e. the trigger spike), phenomena

[32] Spike detection in those days was considerably more challenging than it is today: most acquisition circuits still primarily consisted of analog components. Today, digital amplifier chips that scale programmable hardware filters to tens or hundreds of channels simultaneously are relatively inexpensive. It is also standard for acquisition circuits to facilitate synchronization of digital or analog logic from other circuits via (typically 5-V TTL) BNC ports.

such as “post-spike facilitation” might be seen as the bias over many averaged trials toward an increase in the rectified EMG at some latency relative to the spike. These biases are presumed to relate to the movement in a similarly coherent manner. The systems engineer should note that these averages are correlative; however, the model is predicated upon important calibrations that suggest the causality of PTN activity in this case. Specifically, the measured conduction velocity and estimated synaptic delays correspond to the latency between spikes detected from PTNs and the onset of average EMG increases (Cheney & Fetz 1980). Evarts, who was so dedicated to his work that he actually passed away while still in the laboratory, confirmed the identity of putative PTNs using antidromic stimulation[33] in the medullary pyramids (Evarts 1969). Collectively, these works suggest the significance of considering any metric of **limb state** that is derived from position in light of the underlying physiological engines that exert the forces required to engage in allowing the limb to reach such a state to begin with, particularly when considering the voluntary control of movement at the level of cortical neurons.

Limb position, population dynamics, and rise of the **neural state**

In 1982, not long after the studies of Cheney and Fetz refined the works of Evarts using coherent averages, a new perspective regarding the **neural state**[34] emerged in the works of

[33] Action potentials are conducted toward the axon terminal (end of the long projection, typically where it synapses onto some target) by *orthodromic* ionic currents. However, extracellular injection of high-frequency current pulses tends to preferentially recruit axons due to their lower effective capacitance compared to the soma (cell bodies). When recruited in a non-natural way, the current flow spreads away from the point of recruitment so that *antidromic* stimulation refers to currents carried back up the axon toward the cell body. This property is manipulated by electrophysiologists: *antidromic* stimulation in the medullary pyramids, where the bulk of the descending corticospinal fibers cross, at a latency corresponding to the arriving *orthodromic* nervous impulses causes a “collision” that silences the typical output. While potentially informative, such a technique is not without its own issues in interpretation (Fuller & Schlag 1976).

[34] This is often taught as a debate, although maybe this is only because of the deliberately provocative Introduction provided by Georgopoulos in his 1982 paper, coupled with his refusal to acquire or provide electromyography (EMG) measurements despite a Results section entitled *Other observations,* which is clearly a response to requests by a peer, in which cell discharge in response to muscle contraction is mentioned. Observations by both groups tend to otherwise align. The muscle-centrists acknowledge that only a small fraction of cortical cells demonstrate the properties they describe, while the movement-

Apostolos Georgopoulos (Georgopoulos 1982). Georgopoulos suggested that when the task paradigm shifted from a simple flexion-extension behavior to a "two-dimensional movement" that neural activity in the monkey motor cortex correlated with limb position. Subsequent collaboration with Ronald Kettner and Andy Schwartz resulted in a series of three important articles published in Journal of Neuroscience in 1988 elaborating upon these findings (Schwartz et al. 1988, Georgopoulos et al. 1988, Kettner et al. 1988). Schwartz generalized the prior findings from individual unit activity to decoding in three-dimensional space, Georgopoulos described a resampling procedure for use with a database of all units (recorded one or few at a time, as allowed by each electrode insertion) in which subsets of units were combined to regress a population vector of neural responses, based on their weights and "preferred direction,"[35] and Kettner attempted to recover a 3D phase space for spike rates as well as whether the population vector followed parallel trajectories when movements were initiated from different initial positions.

In hindsight, it seems that Georgopoulos (particularly in his 1982 study) may have wanted to oversell the significance of his findings: for example, his conjecture in the Discussion section that the orderly recruitment of spiking activity in response to a preferred direction represented a generalization of Evarts' findings is just not true. In 2015, Griffin & Strick showed what Georgopoulos might have if he had taken his peers' recommendation to acquire EMG recordings synchronously with the cortical and movement records: corticomotoneuronal cells are functionally tuned during motor behavior. Furthermore, a recent 2020 study by Griffin provides a key observation based on neuroanatomical arrangement: corticospinal cells play a

centrists allow that a majority of cells in the motor cortex lack direct descending spinal projections to motoneuron pools. When posed as a problem of model specification, the point of contention becomes clearer: should the hypothesis model assign the neural state as output, or is the output the limb state? Since brain and behavior form a chaotic, recursive system, the answer will always remain: the correct model output depends upon the question to be tested.

[35] "Directional tuning" equations similar or identical to the one presented by Schwartz (Schwartz et al. 1988) are a hallmark of the center-out reaching task. All such tuning procedures essentially recover coefficients that relate the number of spikes acquired during each trial to its direction.

dual role in “sculpting” movement via combinations of axonal terminal targets arising from the same pyramidal cell body. Excitatory synapses onto agonist motoneuron pools are coupled with excitatory synapses onto inhibitors of antagonist motoneuron pools, providing an intrinsic mechanism to prevent agonist/antagonist co-contraction.

Despite this, the grain of truth (or perhaps the honest question) behind Georgopoulos’ early work[36] excited the field and resulted in the future collaboration with Kettner and Schwartz that continues to influence the thinking of engineers developing brain computer interfaces to this day. While the 1986 experiment of Georgopoulos asked: “does the weighted population spike rate preferred direction reflect the movement direction on a given trial,” it is actually the Kettner paper[37] which offers the specific formulation describing “discharge rate of a single cell” as a weighted sum related to hand position. To emphasize this semantic distinction and why it is critical: consider that in sensory systems, it is much more straightforward to pose the question this way since the stimulus is causal with respect to the observed neurometric response curves. However, although tuning curves were already described (suggesting that the formulation for considering **neural state** existed in the motor systems “toolbox”), the works of Evarts and his students, while incredibly important, were necessarily limited by the emphasis placed on pinpointing precise system outputs in the form of pyramidal activity related to muscle activity. Knowing that output cells exist and the general form of their neuroanatomical arrangement and timing with respect to behavior is extremely useful information. However, the view is inflexible in that it refuses to acknowledge the possibility that the brain does other things than generate movement. In years following the 1988 trio of papers, the reformulated approach to motor systems neuroscience allowed the elaboration of new questions, such as whether both hand

[36] Which is specifically: what exactly are all these other cortical cells that do not have descending output projections doing during behavior?
[37] Probably specific to the author’s graduate studies, but Kettner for whatever reason seemed to come up less frequently in conversation than Schwartz or Georgopoulos.

position and velocity explain spike responses observed from the contralateral motor cortex (Moran & Schwartz 1999).[38]

Considerations regarding system architecture

Which state initializes the system? What is the input?

Between 2004 and 2006, Wei Wu and colleagues found a resolution to the evident controversy regarding whether the **limb state** encoded the **neural state** or was decoded from it. In the description of their solution, Wu cites the hypothetical problem identified by Zhang and colleagues in 1998. The problem is actually quite a simple one: suppose two units exert some control over movement on a hypothetical and idealized 2-dimensional plane. Unit A drives muscles that cause movements in the direction “up”. Unit B drives muscles that cause movements in the direction “right + up”. Weighted summation of the impulses caused by each unit results in some direction that is intermediate to “up” and “right + up.” Then the apparent “preferred direction” of both A and B will result in a reciprocal basis with respect to the driving directions: A will appear to prefer the direction “left + up” and B will appear to prefer the direction “right”. This result is simple algebra that relates to the definition of unit tunings (see Zhang et al 1998, Fig. 4 and associated section *Simple example of reciprocal basis* for details). The only case in which the preferred and driving directions are equivalent is when the driving directions are orthogonal.

These predictions, which could have been made with pen and paper, were reflected experimentally by the work of Moran & Schwarz (1999), and later by the findings of Griffin (2015). Realizing that this meant that a brain computer interface (BCI) decoder with a basis that depended on the recovery of unit tunings was impractical, Wu implemented efficient variants of

[38] Regression relating spike rate to movement speed and velocity captures a large portion of the fluctuations in spike rates.

the Kalman filter (generalized in a flow chart diagram in **Figure 3.5**). For example, the model could be calibrated for use on a 2-dimensional pinball tracking task fairly accurately using only 2.5 minutes of data (Wu et al 2006). Notice that in **Figure 3.5**, there really isn't a "system input;" rather, the system is initialized at some initial state and runs perpetually. Further discussion of the Kalman filter is provided in **Chapter 6**.

Figure 3.5

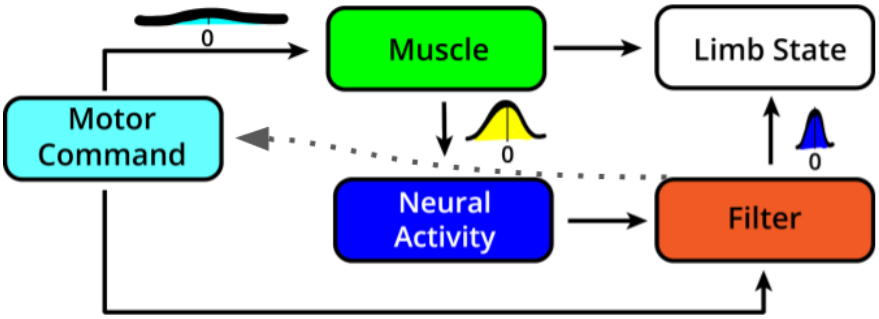

Figure 3.5: The ambiguous "input."

Due to the recursive nature of neural activity, it is challenging to abstract the correct part of the system to consider as an input. This relates to the unresolved issue of *temporal binding of behavior* in neuroscience; at a very high-level, most experiments ask questions that address very specific stimuli, their associated behavior, and neurophysiological or neuroanatomical correlators related to the response of interest. In order to use predictive models that relate temporal encoding and decoding of neural signals to the response of interest, there is a necessary calibration for setting good model parameters such as *initial conditions* that accurately allow a given model to reconstruct the response. The quantities used for calibrating the *initial conditions* (in this case, multi-unit spike rates occurring prior to lift and extension of the reaching forelimb) are the "inputs;" however, since the system must affect its own future state by necessity, this means that the whole thing becomes a recursion, as demonstrated by the Kalman formulated shown above. The formulation can be applied by the engineer in different ways to generate statistically optimal noise estimates (cyan, yellow, or blue Gaussian distributions) depending on the predicted output. With respect to the biology, the brain applies a predictive filter (red block) as shown in **Figure 3.2b** while issuing output commands (green block); the output is measured and values of its past state are incorporated to the prediction (blue block). This process repeats itself (grey dotted arrow) as the filter influences the future motor command and the movement proceeds continuously through time.

When is the **neural state** estimate adequate?

As was mentioned, the true **neural state**, which describes the simultaneous activity of all the nervous tissue related to the task at hand, is probably never measured. However, there are reasonably straightforward methods to check if the estimate is adequate. Ultimately, any such strategy relies upon the decomposition of the neural data into orthogonal bases in a high-dimensional space, where each dimension corresponds to a different spatial channel. There are many such decomposition methods, and describing them all is not the purpose of this section, but to name two: principal components analysis (PCA) is popular due to its speed and linearity (Chapin & Nicolelis 1999); or, particularly when EMG and muscle synergies are involved, non-negative matrix factorization (NNMF) may be appropriate (Ranaldi et al 2018). Note that interpreting features that relate to this decomposition depends upon marginalizations performed on the data prior to the decomposition step: for example, it may be necessary to strictly decompose the components of only highly-stereotyped behaviors. This is done by curating the behavioral dataset (e.g. watching each trial video) to make sure that behavior proceeds as expected.

Figure 3.6

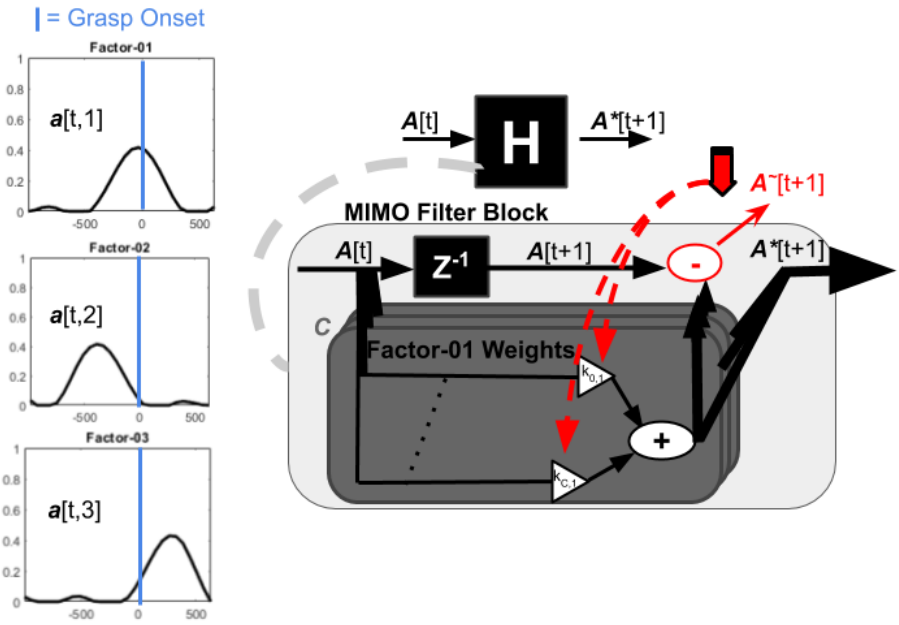

Figure 3.6: Concurrent state and observation variables.

As spatial channel counts increase, with respect to the behavior under consideration there is likely redundancy in linear relations between the observed neural data and the output behavior. *(Left)* Prior to regression using the full trial-aligned spike rate time-series, the neural data is compressed to its most-salient population-level "factors" (here: using non-negative matrix factorization; often: using PCA or ICA). (*Right*) even after compression, the first-order dynamics represent a system with multiple inputs and multiple outputs (MIMO). (*Inset*) The abstracted filter and its estimation procedure. Each dark grey box corresponds to one of *C* compressed factors representing the multi-unit spike rate population state. The $\mathbf{Z}^{-1}$ block represents a single-sample delay, which is used to fit multiple least-squares regression by minimizing the residual error squares (*$A\tilde{}[t+1]$; red arrow denotes minimization process, which determines $k_{0,i}$ through $k_{C,i}$ for factor* i). The filter output predicts the future state of each neural factor using weighted sums of the current value of each factor (coefficients in white triangles). It is not uncommon that between 6-12 "factors" explain the majority (more than 95-99%) of the multi-unit rate population state when using a 32-channel recording array. For comparison, if each channel were observed due to independent and normally distributed processes (i.e. purely due to noise), the corresponding expectation on the percent of data explained would be approximately 18-36%.

After the data has been decomposed to a new basis, resolving the question of *is this an adequate sample* depends on the model prior regarding **limb state:** how many meaningful

dimensions do we expect the limb state to take? More specifically, how many dimensions of freedom do we expect in the movements required of the behavior (since movements are likely to covary along different world-coordinate axes, and markers at points along the body are intrinsically correlated)? Past work suggests that between 6-12 dimensions are sufficient to account for behavior during a unilateral upper-extremity movement (Churchland et al 2007, Churchland et al 2012). Once the target dimension has been selected, this choice can be used either to reduce the basis to its top components (PCA), or to set the number of factors during the decomposition (NNMF; **Figure 3.6** *left panels*). In both cases, the accuracy in regressing the reduced data onto its original values should be used to assess whether such a decomposition makes sense. As a heuristic, one strategy is to simply specify that at least 95% of the original data must be explained by the reduced factors, and then use the corresponding number of principal components or iteratively determine the number of factors for NNMF. Once the factors are recovered, they can be used for prediction of either the future **neural state** (i.e. future factor values; **Figure 3.6** *right panels*), or the future **limb state** (for example, relating to independent sensory and motor factors for prediction as shown in **Figure 3.7**).

Figure 3.7

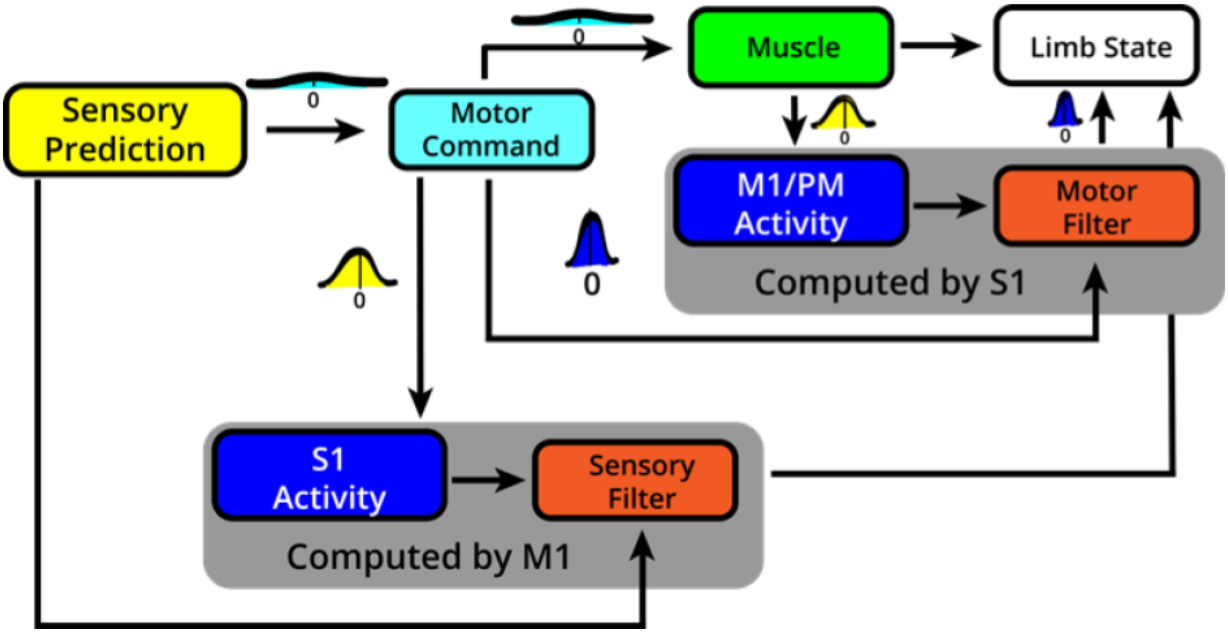

Figure 3.7: A more complicated realization.

Returning to the Kalman formulation of **Figure 3.5**, an attempt to reverse-engineer the likely sources of actual biological computation begins to quickly complicate the model. In **Chapter 6**, some simplifying assumptions are made: for example, the S1 sensor computed by M1 is instead just included to the neural state variable as the cross-correlation between the M1 and S1 mean LFP signals based on preliminary results indicating this as a good choice that were obtained from the anesthetized rat subjected to cutaneous solenoid stimuli of the distal forelimb.

Note that such estimates form a useful prior on how many electrodes might be sufficient for a given experiment, which is not only dependent upon how many task-relevant dimensions are expected, but also the spatial correlation and desired spatial resolution for sampling the brain. Depending on how correlated the neural signals will be: as electrodes in the brain are placed more closely together, they become more likely to detect similar or identical signal sources

(cells); with a site spacing of 250 □m, 32 channels distributed across bilateral motor areas was observed to be sufficient (**Chapter 5**). Other configurations, such as the array designs that are possible when using commercially-fabricated flexible polymer-based electrodes (i.e. NeuroNexus), which allow site spacing on the order of 100-150 □m, may require even higher channel counts.

Figure 3.8

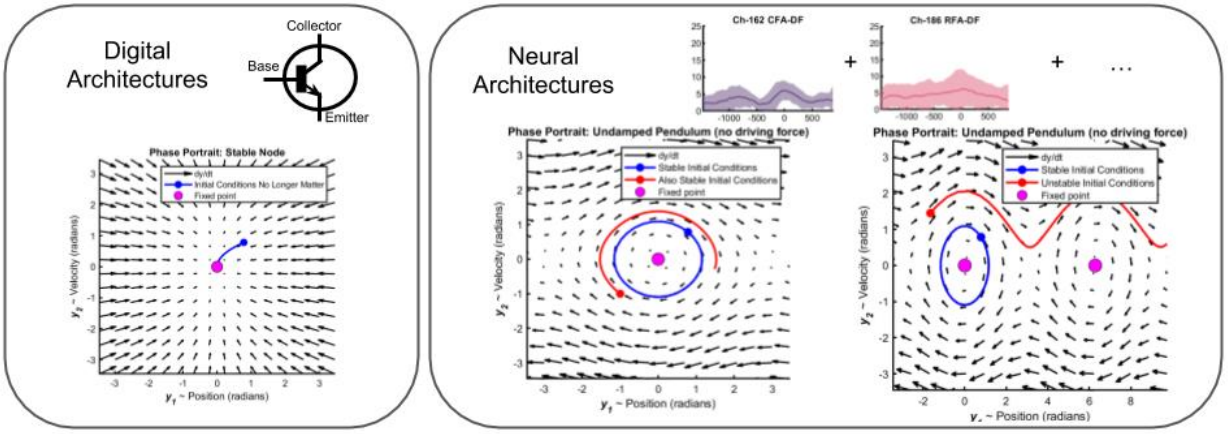

Figure 3.8: A consideration regarding critical difference between brains and computers.

A key conceptual point is that the brain is different from a computer. In a digital architecture (*left group*), information storage and retrieval is typically achieved in some fashion using logical operations (i.e. transistor state; *top-right inset*). Stable data storage typically involves the use of "latch" architectures (not shown); when such an operation occurs, the field potential of the transistor will always converge and remain in a single fixed point, which is meaningful in that context (*stable node*). In neural architectures (*right group*), temporal propagation of highly volatile membrane potentials of individual neurons and the related stochastic generation of action potentials is necessarily erratic, even in relation to an event that makes the expectation of "relative" stationarity more likely (i.e. motor behavior; *top inset: 95% confidence bounds of spike counts aligned to grasp*). For neural networks, the physical realization of a system that encodes information requires transient convergence to trajectories that "fleetingly" orbit some fixed point (*center pendulum example*); while analysis is limited by statistical power to focus on transient behavior, it is most likely that such behavior carries its "momentum" into subsequent fixed point orbits, allowing propagation of coherent activity (*right pendulum example; major and fundamental unresolved problem in neuroscience at large*).

Model selection should address the appropriate neural state code

A benefit of Systems Theory is that the model can generate meaningful qualitative descriptions of behavior that necessarily depend upon model architecture. At the risk of pointing out the obvious: information that is filtered by neurons in the brain is necessarily stored and retrieved in a different way than it would be in an architecture of interconnected transistors. The latch--a common logical arrangement scheme for stably encoding and manipulating the binary state of a single transistor--cannot function the same way in a neuron as in a transistor. **Figure 3.8** illustrates this. The transistor encodes states through the use of semiconductors: a voltage across the semiconductor changes its resistance and thereby allows or disallows the flow of electrical current. If we focus on the state of the transistor around some encoding event[39] in which it is desired for the transistor to move to the state "0" in which no current flows, then regardless of the prior state of the transistor, we can manipulate the system[40] so that the state "0" will be held for any arbitrary amount of time (**Figure 3.8, *left***). Similarly, a known manipulation of the system can reliably change or hold the value of the transistor state to "1."

On the contrary, the membrane voltage of the neuron is in a constant state of flux. If we consider the neuron as a unit[41], then the topology of its state space is approximately comparable to the transistor. However, since the neuron will only ever transiently hold the state "1," it should be clear why a latch scheme cannot work the same way in neurons as in

[39] For example, a register holding the value of an infrared sensor might take the value of "0" when the beam is broken, indicating the presence of an object such as a pellet in some target location; a value of "1" would indicate an unbroken beam--that the target is no longer present in that location.
[40] In an N-P-N transistor as shown in **Figure 3.8**, this corresponds to changing the voltage between the base and ground.
[41] This means we reduce all properties of the neuron so that we create a binary state that takes a value of "0" most of the time when the membrane voltage of the neuron at the axon hillock is below a threshold, and "1" only when membrane voltage at the same point exceeds the threshold, which corresponds to the propagation of an action potential along the axon and subsequent release of neurotransmitters at synapses along the axon.

transistors: the only reliable state value capable of propagating itself through time is “0,” which means that the neuron cannot encode information by itself[42].

As we know, neurons do not exist in isolation. If we consider that the binary state of a single neuron in the motor cortex cannot encode information (even cells that are intrinsically capable of rhythmogenesis still have a refractory period during which they cannot elicit the “1” state after an action potential), then the scheme must change: it is the pattern of “0” and “1” states that the neuron takes with some arbitrary reference to time, which endows the neuron with its capacity to encode information. Therefore, it is only natural to wonder: how do such patterns depend on time? Do neurons encode information in a serial code, so that precisely patterned sequences of binary events correspond to a *hidden state*; or, do neurons continuously encode information in their membrane voltage or some other network feature, in which case the *hidden state* is the conditional likelihood of a neuron generating an action potential at any particular instant in time?

The answer is: it depends on the brain area under consideration. In practice, the best solution is probably to choose the estimator that is computationally least-expensive. The true solution, while interesting to consider, will probably not be finalized any time soon: opinions in motor systems neuroscience seem to fluctuate between acknowledging the importance of timing or eschewing it every few years. The following sections elaborate slightly on this issue that was more intensely scrutinized during the late 1980’s and early 1990’s.

Premotor synchrony: the case for precise timing as the neural state code

In the late 1980’s and through the 1990’s, Alexa Riehle and her computational collaborators designed a clever experiment in macaques to test the importance of *precise timing* of spikes

[42] There are exceptions. Gyorgy Buzsaki famously summarizes things like pacemaker neurons, whose endogenous biophysical characteristics endow them with the ability to sustain rhythmic generation of action potentials, in his influential book which is well worth a read (Buzsaki 2006). However, most if not all neuron subtypes in the motor areas of the cerebral cortex do not exhibit such properties.

from sorted single-unit activity observed from multiple locations in the macaque premotor cortex simultaneously. The task required holding a ready position for a variable duration until a target cue was issued at one of a few fixed latencies relative to reaching the ready state (Riehle & Requin 1989, Riehle et al. 1997). They noticed that short epochs, which aligned with the set of possible discrete cue latencies, contained a significant increase in the likelihood of synchronous spiking between multiple cells. Riehle suggested that the macaque had learned these latencies, and that the number of synchronous events reflected a physiological process. To substantiate this argument, the number of synchronous events was estimated using an assumption of linearity on the expected spike rate during each epoch. If the number of spike times that were coincident within some time-window significantly exceeded what would be expected by chance on the basis of random stochastic realizations of the rates during these windows, as was observed, it was hypothesized to substantiate the importance of timing at least with respect to features of the reach. A notable observation was that when the number of synchronous events was higher, it seemed to correlate with trials on which the monkey was paying better attention to the task, which was evident in its performance (Riehle et al. 1997).

Premotor variability: the case for counts or rates as the neural state code

At the same time as the experiments of Riehle and colleagues, due to the possibility of recording from multiple spatial channels distributed throughout the motor areas of cerebral cortex simultaneously, there was a rising interest in the development of brain computer interfaces (BCI) for a variety of applications (some of which were discussed in **Chapter 2**). In general, the use of counts or instantaneous rate estimates, at least in motor systems and particularly by investigators such as Evarts or Georgopoulos, was common. Such strategies accepted the limitations of experimental regimes that made it impossible to rely upon manual curation and meticulous sorting of spike waveform snippets to isolate or differentiate between single-unit and multi-unit activity on the basis of characteristic spike shapes. Peri-event time

histograms (PETH) were seen as an acceptable endpoint: the spikes were a stochastic realization of noisy processes that were biased towards more-frequent observation at specific times relative to behavior due to some relation to it. If more than one unit was under consideration simultaneously, then the simplest way to describe the experiment was by constructing a joint probability estimate relating the conditional likelihood of observing a particular count of spikes from the first unit at some instant relative to the behavior to the expected number of spikes from the second unit at the same or different instant relative to the same behavior (Gerstein 1969).

The two modes of thought might be summarized as treating spike times as either deterministic processes or stochastic reflections of some underlying generative process. Eventually, efforts were made to reconcile discrepancies: since the true coding formulation could not be determined definitively, computational calibrations were introduced by a number of groups (Gabbiani & Koch 1998). For example, spike counts could be considered as doubly stochastic with respect to the uncertainty of the time window over which the count should occur (which might reflect a faster or slower behavior; such a thing might even be related to the observed spike rate intrinsically). Such characteristics became characterized by putative unit subtype, so that a calibration could be made to compute modified higher order statistics such as variants on the Fano Factor that were more reliable for high spike rates (Shinomoto et al. 2005).

Returning to the issue of spike synchrony prior to movement: by applying a principled approach to recover variance using statistical assumptions related to the assumption that spike counts should demonstrate Poisson characteristics, it was found that premotor variability at a population level was intrinsically higher prior to movement execution (Churchland et al. 2006a). In addition, increases in premotor variability correlated with greater movement speed (Churchland et al. 2006b). These findings suggest that the results of Riehle may have been due

to an underestimate on the probability of coincident spike detection, rather than indicating some other timing mechanism.

Which version of **neural state** should be used?

At least insofar as the motor cortex[43], it is probably the case that a simple kernel smoothing to approximate the instantaneous firing rate, which essentially requires the convolution of a 20- or 30-ms rectangle or weighted kernel function with similar bandwidth, serves as a suitable estimate (Manwani 2002). There are many rate estimators that have statistically optimal properties under different assumptions and considerations (Shimazaki 2007, Shimazaki 2010). The marginal benefit of using such an estimator is probably quite low given the current state of this type of experiment in the reaching rat model as it is used within the field of rehabilitation medicine.

Supposing that spike rate, or the instantaneous likelihood of observing a spike, is used to estimate the **neural state** at the level of individual units. Recall that this does not resolve the issue of information encoding (at least for neurons in the motor cortex): the neuron at an individual cell level cannot maintain a fixed rate for an arbitrary period of time without network interactions. However, consider the idea that (transiently) it is wished to encode a *target* for the behavior, such as the pellet to be retrieved by the rat. The pellet may not be placed yet, or the door allowing the rat to retrieve the pellet may be occluded. As the rat prepares to retrieve the pellet as quickly as is allowable given the retrieval setup, the *target* must be encoded somehow to the cortical neurons that exert influence on the voluntary motor output of the forelimb. The information that allows this *target* to manifest as a goal against which the firing state of the

[43] Response properties of neurons in the forelimb and hindlimb areas of the rat primary sensory cortex have been characterized by Karen Moxon and colleagues (Tutunculer et al. 2006, Moxon et al. 2008).Their work suggests that there might be two relevant codes: a time-to-first-spike code that indicates a particular cortical representation receives the earliest nervous impulses related to a particular sensory stimulus, and an aggregate amplitude code that may relate to the intensity of the stimulus. It is not hard to imagine how such signals could be coded in an orthogonal fashion, which makes sense intuitively.

neural population continually optimizes must persist for some arbitrary period of time. Therefore, the **neural state**, as it relates to information regarding the *target* specifically, is probably more accurately described by the simultaneous spike rates of many cortical neurons simultaneously. Note that some of these cells may contain descending corticospinal output projections: while the cells might become active transiently, the activations must be balanced in such a way that results in no movement.[44]

An analogy that is commonly invoked by Systems Theorists when explaining the neural population dynamics is to describe the phase portrait of the differential equations pertaining to an undamped pendulum without forcing (**Figure 3.8**, *neural architectures box*). Once any position along the phase portrait is identified, the rest of the points and all future trajectories are defined completely unless the system is subjected to an external influence (**Figure 3.8**, *central phase portrait*). Concretely, if there is no damping and no forcing, then as long as the pendulum is dropped from a low enough point and a small enough initial velocity is supplied, the pendulum will continue to swing back and forth forever. Analogously, despite change in its constituent firing rates through time, the neural population state could be maintained in such a trajectory for an arbitrary period of time in order to "hold" a *target*. Furthermore, if a sufficient perturbation or increase in velocity is supplied, the behavior of the system changes (**Figure 3.8,** *right phase portrait*): instead of reaching some point and changing direction, it enters orbit, spinning indefinitely about the idealized point of fixation. This means that such a population state represents a potentially efficient mechanism wherein only a small (external) input is required to shift the *target* to a new point. What circuit elements would be required for such a population state to stably perpetuate in a metabolically efficient manner, and how long such a system could plausibly retain a *target* in practice, are each open questions that are probably both model- and behavior-specific. However, such rotations of the population space are observed in the reaching

[44] This is known as the "cortical null space" hypothesis (Kaufman et al. 2014).

rat model and do seem to relate to motor performance (**Chapter 5**). Fortunately, the process for recovering such a state space from the neural firing rates is well-described (Churchland et al. 2012; **Figure 3.6** *right panel MIMO filter block*).

Tools for measuring the **limb state**

Data acquisition

A list of methods that do not work in the reaching rat model.

As mentioned previously, technical challenges with acquiring the EMG signal directly from forelimb muscles of the rat during pellet retrieval means that the **limb state** must be estimated indirectly. The experiments of Evarts made use of a force transducer in order to provide a correlator to both EMG and cortical spike rates (Evarts 1968); however, aside from ground forces relating to postural support from the non-reaching forelimb, the use of force measurements is impractical for the reaching rat as well. The experiments of Georgopoulos, which measured position, made use of a system of ultrasonic sensors for triangulating an emitter attached to the dorsal surface of the monkey's distal forelimb (Georgopoulos 1982). This might be a possibility in rats, but would probably fail for reasons common to most systems requiring the attachment of some marker to the forelimb. In the author's experience, the reflective marker system (Optitrack) used previously by the cortical plasticity lab for measuring gait kinematics in ambulatory rats after spinal cord injury (Borrell 2020) proved ineffective for capturing 3D kinematics in reaching rats due to the tendency of rats to remove the reflective markers. The infrared cameras used in combination with these markers also suffered in performance due to reflections caused by surfaces of the experimental box. Similarly, application of green nail polish in an attempt to define fixed marker positions for post hoc extraction led to the rats mostly misbehaving.

Recovery of markers using stereo-calibration and post-hoc detection

Camera setup

The recommended method for recovering 3D kinematics in the reaching rat requires an initial calibration. The first step is to define a placement of cameras from a series of angles as required to capture dimensions of relevant variance to the reaching movement (for example, a

camera perpendicular to the box opening is helpful; **Figure 3.9A**). The video cameras must be placed in a fashion that also captures an LED or other element that allows the approximate post-hoc synchronization of the offset for the start of each recording record; due to drift in camera frame rate and the fact that cameras typically break recordings into multiple data files over the course of a single session, it is recommended that this synchronization calibration can be applied for each individual pellet retrieval trial. It is also recommended to attach a checkerboard pattern to a surface that can be seen for each trial, from each camera, so that if necessary a calibration can be recovered for each trial (which is important for example if a camera is bumped even slightly by the experimenter). It is recommended if at all possible to use a camera with a minimum sample rate of 60 frames per second; a camera with 30 frames per second was used in the experiments described in **Chapter 5** and based on the time scales of phases of behavior it might barely be sufficient but the behavior is better-served by 60 frames per second at a minimum. The movements in **Chapter 6** were captured using a camera sampled at 240 frames per second; the movement was well-handled at this frame rate, although with such low frame rates, ambient lighting becomes a non-trivial issue. Critically, increased ambient lighting by using high-intensity search and rescue flashlights does provide an increase in light, but they did have a noticeable impact on reach accuracy.

Figure 3.9

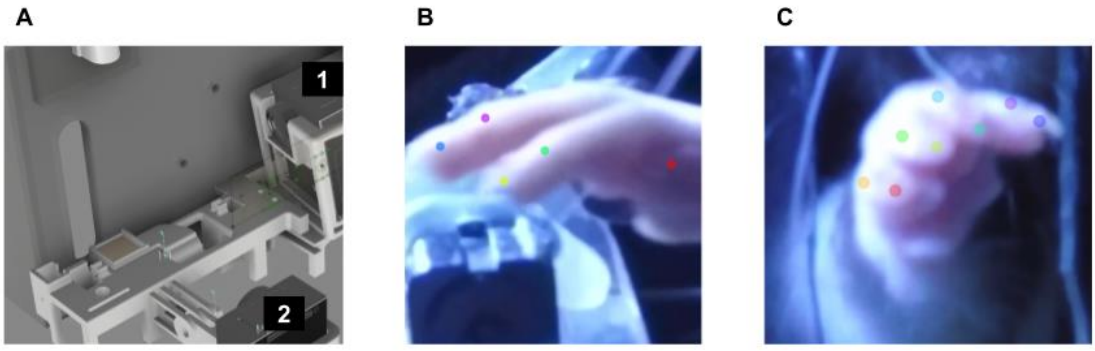

Figure 3.9: Post-hoc recovery of kinematics.

While calibration and collection of kinematic measurements using commercial devices such as the OptiTrack equipment used for gait studies in spinally injured rats is both more accurate and less cumbersome, repeated attempts to apply reflective markers to the digits and paw in order to make such measurements during pellet retrievals proved fruitless. **A)** Instead, 3D reconstructions of kinematic estimates could be obtained by using stereo-calibrated camera pairs or triplets. **B)** Markers used in training a deep network on still frames acquired from camera-1 (shown in **A**). **C)** Same as **B**, but for camera-2. Matched points could then be triangulated, although this was more accurate when measurements from multiple sets of cameras were used due to the occasional occlusion of marker target regions.

Training post-hoc markerless tracker

Once videos have been acquired from the desired angles, the author found that it was easiest to train a separate marker detector for each camera angle using the DeepLabCut interface provided by Mathis and colleagues (Mathis et al. 2017). Initial training typically only requires 15-20 labeled frames, for which the desired marker labels should be applied in a manner consistent across cameras in order to coregister them later (**Figures 3.9B** and **3.9C** provide examples from two cameras capturing the forelimb on the same reach trial). Depending on the arrangement of cameras, in certain frames, some of the digits may not be visible; documentation on the repository associated with the Mathis study explains how to account for this during the initial labeling procedure.

Recovery of marker position estimates using trained network output

After the initial training, the network is then used to recover marker estimates for each video frame. The output of the network gives pixel coordinates for each marker, along with the associated likelihood that the output actually is the marker (the network detects candidate pixels and returns the most likely pixel as the marker position). At this stage, the output may already

be good enough depending on the quality of the video and accuracy of the training labels, as well as how the training labels were distributed over the course of the behavior. Ideally, the training labels reflect the hand in a variety of configurations, so that some peculiarity of the hand conformation is not overlearned by the network, causing problems with generalized labeling. Alternatively, after reviewing the output kinematic errors by visual inspection of the markers superimposed on the original video frames, parts of the behavior where the network consistently underperforms should be identified; more training images can be extracted from those segments and labeled; and then these training images can be used to retrain the network, initializing the network weights using the previously learned configuration.

Once all the video frame kinematic labels have been exported and aligned to satisfaction, the pixel coordinates for each camera pair can be used to triangulate an estimate of the world coordinate system. This stage benefits from de-noising: for example, a Kalman filter can be applied as an initial step to simply exclude large “jumps” in the observed kinematic series that are most likely due to mislabeled pixels returned by the network output.

Limb State: related repository links and brief descriptions

- **DeepLabCut**: this is a tool developed and described by the Mathis group (Mathis et al. 2017). Because the group actively maintains this tool, it makes more sense to get the version they have maintained, as the group has also suggested that at some point in the future they will implement a Kalman filter to automate some of the de-noising described above.
- **Kalman-Thesis**: This repository contains code that was used to de-noise the kinematic data used in **Chapter 6**. As a rule of thumb, most application-specific repositories are written with Matlab version R2017a+ in mind, and should contain a **main.m** script that organizes or gives examples for the use of repository contents. Repositories that were

created later in the author's graduate career also contain **Contents.m** files, so that those tools are compatible with the Matlab built-in `help` and `doc` features.

- **rc-proj**: **Limb state** analyses (specifically, tools used to score videos and curate behavior to tag movement phase delimiters) are contained in the subfolder **videoAnalyses**. It was used in the manuscript under preparation that serves as the bulk of **Chapter 5** (Pack et al. 2020; *note that this is technically a co-first-authorship*).

Tools for measuring the **neural state**

The **neural state**, as previously mentioned in this Chapter, is application-specific. This section describes steps taken to obtain typical **neural state** features such as spikes and LFP spectral content. It also provides consideration regarding the cost-benefit tradeoff when using in-house fabricated custom electrode designs compared to arrays from a commercial vendor. The acquisition circuit is a critical and experiment-specific component, so some considerations when setting this circuit up are raised, as well as a brief discussion of the 3D-printed automated box for scaling up rat training. Finally, during experimentation, data is saved in a device-specific binary format, which must then go through subsequent processing and cleaning stages that are specific to both the acquisition circuit and the desired experimental endpoints (example overview in **Figure 3.10**).

Figure 3.10

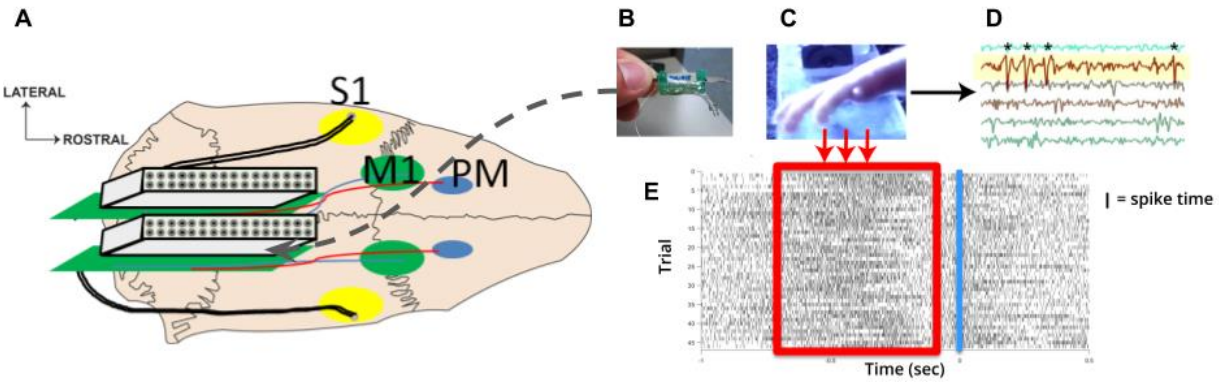

Figure 3.10: Bilateral sensorimotor field potentials.
Overview of acquisition scheme for experiments involving bilateral recordings from sensorimotor cortex. **A)** Dorsal view of the skull with cartoon illustrations of electrodes (**B)** and indicating skull regions to remove based on cortical targets. **B)** Custom electrodes use 40-□m diameter polyimide-coated tungsten wire that were individually hand-soldered to copper pads on custom electrode interface boards (EIB). Each electrode is attached to a 36-pin connector, with 2 pairs of pins tied to reference and ground sites. Black wires indicate "floating" leads that were inserted to the sensory cortex to acquire LFP signals. **C)** Example of contact with foreign surface prior to the closing of digits, a typical alignment event. **D)** Example of signal on a subset of 6 channels; asterisks denote spikes that correspond to action potentials on the highlighted channel. **E)** Raster indicates timing of spikes on highlighted channels relative to the alignment event (blue vertical line). Red box indicates a large increase in spikes that correlates temporally with cutaneous surface contact (example shown in **C**).

Electrode array design considerations

The selection of electrode array design is a critical consideration regarding measurement of the **neural state**. The very first decision is non-trivial: should the investigator fabricate custom electrodes by hand (e.g. **Figure 3.10B**), or order them from a commercial vendor? This is typically dictated by budget constraints and the number of rats and recording targets required to power an experimental aim. An initial cohort of rats implanted bilaterally with custom in-house 32-channel polyimide-coated tungsten microwire arrays that spanned sensorimotor cortex produced viable spike and LFP activity. By the end of the experiments, the author was able to fabricate electrodes (such as pairs of double-bundled 16-channel bundles for bi-hemispheric targets described by **Figure 3.11**) with mean fabrication time of roughly 1.75 hours and standard deviation of probably 30 minutes (best assembly time was probably 1.5 hours). The fabrication process itself will inevitably be specific to experimental design; taking this into

consideration will also yield an improved and more practical final electrode array design (for example, in a bi-hemispheric configuration, the assembly in **Figure 3.12** ends up being more useful).

There was one key process improvement step and two key reagent improvements that greatly increased the viability of electrodes fabricated in this fashion and so are described here for posterity. The first step was switching from silver paint to hand-soldering each wire to the exposed copper pads. This means that the first step is to hand-solder the Omnetics connector headpins to the electrode interface (EIB) pads. Obtain a clean 28-gauge (or highest-available gauge) hypodermic needle and modeling clay that will be used to hold the needle, and place these where they will be easily accessible along with a small aliquot of the silver and flux paste mixture that will be applied using the needle. Using the needle, apply the silver and flux paste mixture along the EIB pads with the Omnetics connector headpins clipped into alignment with the pads: you should only need a grain or two per pad.

Figure 3.11A

32-microwire array (Right Hemisphere)

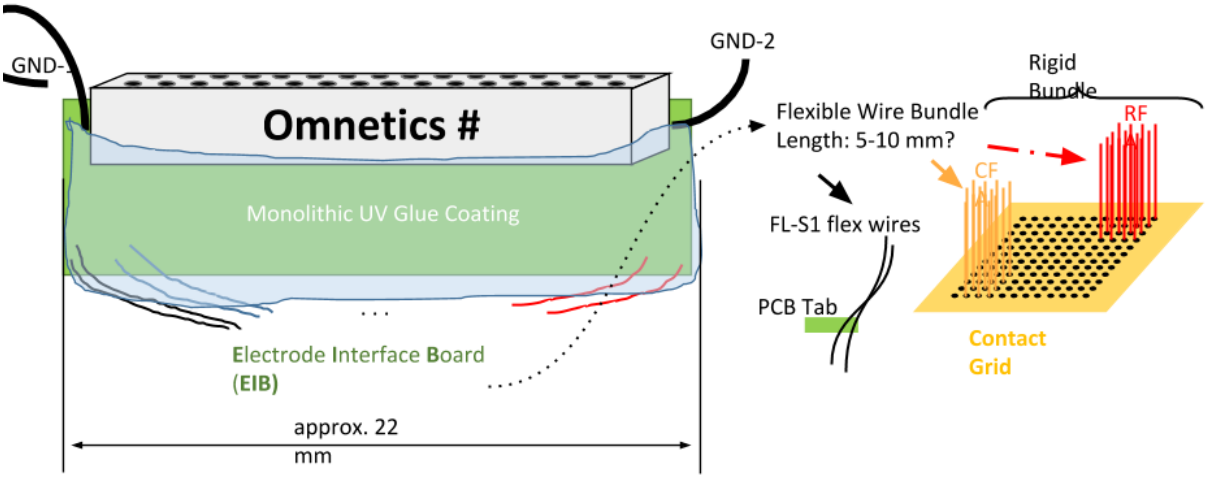

Figure 3.11B

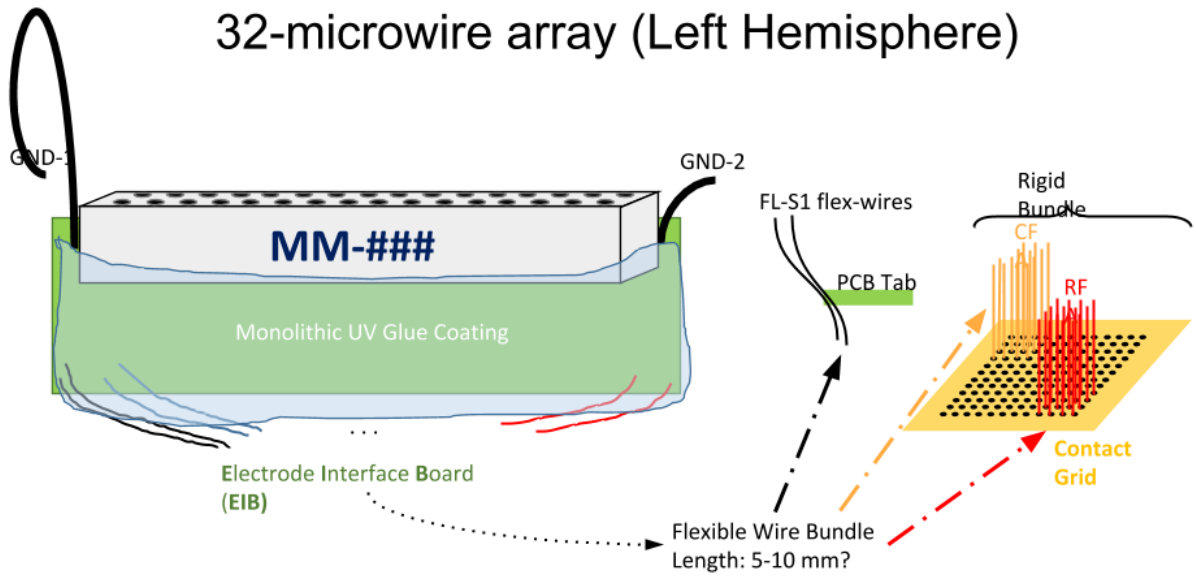

Figure 3.11: Building microwire array bundles

Overview of example contact grid schematic and setup for construction of microwire array bundles to target stereotaxically defined rostral forelimb area (RFA) and caudal forelimb area (CFA).

A) Right-hemisphere array. Critical considerations are the spacing between bundle centers, which are defined by site spacings of the Contact Grid array. The length of wire bundle that remains flexible (i.e. non-encapsulated by UV glue) is also an important determinant in likelihood of implantation success; however, leaving this part too long may also lead to degradation of electrode signal or ultimate electrode failure. **B)** Left-hemisphere array. This is essentially a mirror-image of what is shown in **Panel A**, but note the reversed orientation of the electrode interface board (EIB); the omnetics part number no longer faces upward during electrode construction.

Once the connector is bonded to the EIB, use a helping-hand device or similar (anything with alligator clips to suspend small parts) so that the Omnetics header pins are used to suspend the rest of the EIB with the wire holes exposed. Critically, at this part make sure the orientation is as expected; a systematic method for bonding the wires means that they will take a stereotyped grid pattern and speed the process up by preventing the need to write the grid orientation of each wire unless a mistake is made. Note that the pattern which makes this process most-accessible (at least to the right-handed investigator) starts with the far-bottom-left hole on the EIB copper rings, then the second-to-the-left bottom hole, then the far-left top-hole, and then continues alternating between bottom and top in this manner until all the wires are bonded. A secondary clip should be used to suspend a pair of guide boards, clamped together so that they are immediately stacked and all the holes are perfectly aligned, at the desired offset distance from the EIB. This should approximately correspond to the envisioned distance between the eventual connector offset on the head relative to where the wire bundles will be inserted.

Figure 3.12

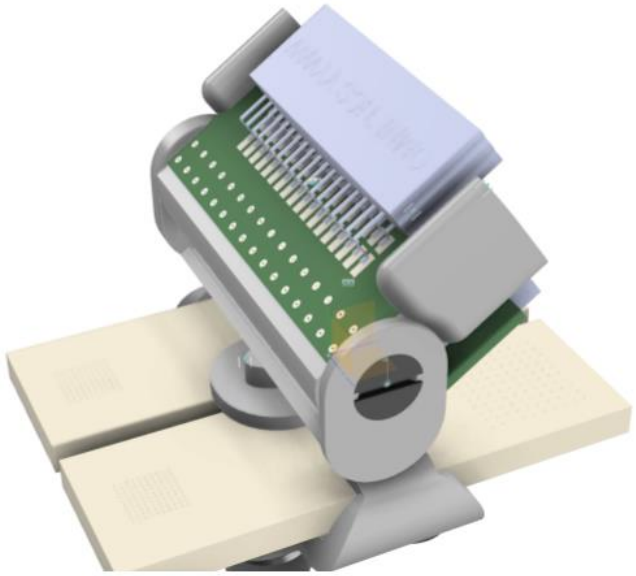

Figure 3.12: Reorienting microwire bundles.

Example of a stereolithographically printed assembly housing for a different orientation of the bilateral custom array layout. Because of the protrusion of the microwire array (the 32-channel connectors are relatively large by comparison to the entire size of the rat's head to begin with), the rats sometimes get stuck during the task near the front of the box, or have to alter their learned behavior and ultimately generate unwanted motor output. To mitigate this, a new configuration of electrodes was conceived, whereby the electrodes are oriented at approximately a 45 degree angle with respect to the skull, and bundles are built specifically in lateralized pairings so that paired electrode microwire arrays are used for a given animal.

The thicker contact grid for microwire spacing was added in the hopes of making the spacing more uniform after the final cutting procedure once all the microwires had been set in place; however, in practice this did not work much better than the original thin contact grids.

Each individual microwire is cut to a length of approximately 1.5-inches and at an angle so that one end will be the sharp side. The wires should be arranged along a piece of white paper so that a slightly-blunted number-15 scalpel blade (typically re-used) is used to scrape approximately 100 to 200-mm of the polyimide coating from the end of each wire opposite the diagonal cut. Similar to a ribbon on a gift, this will cause the wire to curl; this is good because it provides an easy point to grab individual microwires using the forceps. The next part requires a benchtop scope focused on the suspended EIB apparatus (make sure to adjust prior to starting to avoid neck cramps). Make sure that the finest tip available is attached to the soldering iron and set it to 650F. Changing the desktop light supply is also critical to give an angle that lights both the EIB holes and the guide grid.

The next part is hardest and the investigator should not be discouraged but might expect some minor cutaneous injuries to occur, so please be very careful if you find yourself following these instructions for whatever reason[45]. Once the microwire is grasped with forceps by one hand,

[45] Surely, there is a better way of doing this.

manipulate the hook so it faces toward the holes on the EIB and grasp it approximately 0.5-inches from the hook with the non-forcep hand. Setting down the forceps with the other hand, retrieve the needle from the modeling clay and dab a tiny bit of the flux paste onto the tip. The needle can be used to help guide the hooked end of the microwire through one of the EIB copper-ringed holes; make sure that some of the flux paste and silver granules are deposited along with the hooked wire. Now, keeping the hand with the wire looped in place very carefully, put the needle back in the clay and retrieve the heated soldering iron. Be careful about holding the wire too close to the EIB. Just a very light touch should immediately cause the silver and flux paste to glisten indicating that it has melted; the hole should become completely covered. At this point a common error is to put the hook through too far so that the polyimide obstructs bonding of the wire to the copper pads; should this happen, you may need to reheat the silver paste and withdraw the wire slightly. If the wire does not move in or out of the hole when a light tug is applied, then the silver paste has bonded correctly. When done correctly, there should be enough remaining wire to now thread through the grid array guide on the second clip as dictated by the desired spatial arrangement of electrodes.

Once all electrodes are bonded and arranged as desired through the guide array, the next step is to fix things in place. Small bundles formed by sets of wires together using suture silk helps keep the wires together in a tight bundle. First, the back part of the EIB should be checked and excess wires sticking out the opposite side should be trimmed so that they are less likely to flex in some odd way and cause a short. Using the thicker silver ground wire, add grounds to the reference/ground pads that are tied together on either side of the array. Finally, use the *Standard* UV glue (*Riverruns brand*) to mechanically secure all the bonded leads in place. During this process, you can affix clipped approximately 1-inch long segments of carbon rod to the EIB assembly near the headstage. This allows you to use dental acrylic to ensure that a

point-of-purchase will remain secure on the electrodes so that dental rubber bands can be used to secure the recording headstage to the electrode connector during behavior.

After a coat of *Standard*, the *Thin* UV glue produced by the same company can be applied lightly to give the electrode a harder outer shell for protection. The *Thin* UV glue is somewhat runny so be careful that it does not drip down onto the precious array, or into the connector holes, at this point. This property is useful however, in that it helps seal any gaps in insulation of the EIB. Finally, carefully (making sure not to dislodge inserted wires from their grid positions) tie the bundles as desired just above the guide grid held by the second clip. Once tied, the suture helps prevent the UV glue from running down onto the guide grid, but that seems to occur more-often than not, which is why 2 guide grid array boards are suggested for use. Once the bundle is sufficiently glued together (probably do not glue the entire bundle, as then the whole thing will become rigid and almost impossible to insert during surgery in a way that feasibly allows a second array), carefully re-sharpen the best pair of carbon-tipped scissors available. The final stage is to re-cut the angled ends of the wire bundle (below the grid) so that they are arranged at approximately the same planar depth. This is a noted limitation of such custom in-house arrays: the spatial grid is not as accurate as a commercially-fabricated array, and if precision in that regard is important for the experiment, then commercial arrays must be used.

While tedious, when fabricated in this fashion, electrode impedances were almost always consistent with the 100-to-400 kΩ range expected given the 40-μm wire diameter and anticipated exposed surface area. Total number of viable channels was animal-specific and the sample size was probably too low to get a meaningful estimate; however, overall it probably tends to be not as good as with commercial arrays (in the pilot data used for **Chapter 6**, 14 of the channels were rejected outright during acquisition; a remaining 25 channels were subsequently rejected because they did not contain viable spike activity).

Data acquisition

At the cortical plasticity lab, as of the time of this writing, there are two primary commercial acquisition systems for which tools were developed (TDT and Intan). Experiments in **Chapter 4** and **Chapter 6** make use of the Intan system. The experiment in **Chapter 5** used the TDT system. The author recommends using how to learn the Intan system: it is ultimately more flexible and also components are much cheaper than the TDT system. However, prototyping hardware components for closed-loop applications is probably easier using the TDT system due to the graphical interface provided to create custom acquisition circuits.

When designing an acquisition circuit, the primary considerations should be the type of neural data to be collected, and whether there will be any timing components to the experiment that will require synchronization of events or epochs with the neural time-series. It is typically a good idea to have some sort of digital logic signal that can be manually manipulated by the experimenter (i.e. a simple button-press circuit), and this circuit would ideally also have an LED attached to it so that it could easily be used to synchronize video cameras. While an ideal workflow would integrate some graphics unit or FPGA modification that allowed streaming video signals to be converted and remove the bulk of the image data that is saved with the large behavioral videos in an automated and online fashion, such a project was beyond the scope of this thesis.

Regarding the neural data to be acquired, if measuring spike activity, sample rates of 20 kHz or greater are sufficient; the author did not experience noticeable improvements in spike detection or automated clustering procedures using 30 kHz. If only the LFP or only EMG is to be measured, then 1 kHz is a recommended sample rate.

Regarding the automated box described in a preliminary form in (Bundy et al. 2019), a key consideration in the reaching rat is the fact that unlike monkey experiments, which can isolate

premotor activity well due to the presence of cues that do not elicit immediate behavior, the reaching rat model poses the problem of distinguishing premotor from motor activity particularly because one of the hypotheses specifically involves the expectation that activity in a premotor area will shift after injury to resemble activity from a motor one. The author attempted to teach rats an experimental paradigm in which the rats learned to associate one of two tone cues with either a left or a right door. This experimental configuration was part of ambitious[46] experiments outside the scope of the thesis, but worth describing in case the collected data are of interest to a future student or other lab member. In general, a setup in which the rats learned to perform a nose poke seems to be too difficult for the rats to distinguish a tone and run to the correct door consistently, an effect that becomes exacerbated after implant and associate recovery given the size of the large arrays even in Intact animals. It is speculated that such experiments could succeed and would probably be informative if restricted in scope: instead of training rats to use both doors, simply training rats on a unilateral task and focusing on one hemisphere would still be quite interesting in rats that learned the nose poke task. Unlike the behavior described by Bundy and colleagues, which involves pressing a button and so represents a distinction between a *simple* and *complex* behavior, wherein the pellet retrieval represents the latter; the nose poke could be used to train the rats to hold at the hole for variable periods of time, which would present clear alignments for premotor activity. The recommended structure for such variable hold periods would reflect the experimental design of Alexa Riehle and colleagues, but on a shorter time scale (Riehle et al. 1997); anecdotally it seems like rats do not have as much patience as monkeys.

To a graduate student reading this, many of these recordings have been processed and metadata are kept in a log with all animal records and notes of this author during his time in the

[46] One of the main things learned during the course of the author's graduate career is to avoid this word if at all possible.

cortical plasticity lab. There is a wealth of data associated with these recordings that is untapped and unpublished that is sitting on the `P:/Processed_Data` lab server in `BilateralReach` or at the very least in `R:/Raw_Data`. A shareable **online document**[47] with more notes, observations, and preliminary findings is happily made available upon request. Knowing that sometimes there is some amount of momentum to be built up prior to the collection of one's own animal recordings, these data might be a great starting place for a new graduate engineering student who has recently joined the laboratory.

File organization and conversion

In general, a standardized method for naming experimental recordings and assigning surgical identification numbers is followed in the cortical plasticity lab. This allows tracking of associated animal behavioral logs, surgical records, and other types of metadata. Critically, **nigeLab**, which is the synthetic version[48] containing features of most other repositories described in the following sections. The **nigeLab wiki** contains more information regarding file naming conventions in place at the cortical plasticity laboratory, although it also allows the user to change name conventions using different configuration files to provide a flexible and experiment-specific framework. In general, **nigeLab** should just be thought of as a tool that allows efficient access, organization, and association of neural recordings to other experimental metadata.

Once experimental data is saved, it can be converted to a hierarchical format using **CPLTools** (described below) or **nigeLab** that makes it easier to access and manipulate in a consistent manner that creates an expectation of organizational structure between collaborators.

[47] The linked OneNote document may cease to point to a viable location, but should remain available while relevant.

[48] Continually under development, **nigeLab** remains an ongoing collaboration with Federico Barban from Istituto Italiano d'Tecnologia. Neither collaborator could think of a good name, so it was named as a portmanteau of the author's cat (Nigel) and Matlab.

Filtering and De-noising

All pipelines described are designed to automatically save a separate set of data with a 300-Hz high pass state filter applied to each channel, and a secondary set of “re-referenced” and filtered data which subtracts the mean time-series from all channels on a single probe from the individual channel values (common average re-reference; CAR). This procedure was found to be quite important for improving spike detection; commonly there is probably a slight impedance mismatch between reference and recording electrodes that results in not only 60-Hz line noise, but also demodulated AM radio signals, which occupy the frequency band of interest with respect to spike activity. The CAR procedure helps with each of these things, and it also helps to attenuate artifacts due to vibration or chewing.

Some investigators have reservations about applying the CAR to denoise their data, with the concern that it will add inappropriate spikes due to spuriously “loud” channels contaminating the other ones. This is a valid concern, but there is a practical solution: simply look at a short snippet of each channel and if more concerned, and discard any channels with clearly aberrant features (in the author’s experience this is almost always very clear, and so this perceived problem is the result of engineering trying to “over-automate” certain steps). A more cautious investigator might plot a distribution of RMS values for each channel in sliding 1-second windows from the entire signal or random sub-samples along the total signal length to assure themselves that they are only including channels with signal RMS values. Then, as long as the number of channels on an array is 8 or more[49], the CAR procedure is a safe way to remove spatially distant common noise sources.

[49] A large spike amplitude would be 200-μV in an extreme case. This would add 25-μV to the time-sample of non-spiking channels in the 8-channel case. If the RMS noise is on the order of 25-μV, there are other more serious concerns about the recording; using the Intan system a typical noise characteristic might be 10-13μV. A good rule of thumb is to require that spikes must be at least 50-μV in amplitude in order to get usable multi-unit activity. Therefore, it is unlikely even in this extreme example that the CAR procedure would lead to very many false positive apparent spikes. Typically, at least 13 or 14 channels are present on any given probe to begin with, and a large stereotyped spike might reach 150-μV on a good day.

Another consideration regards data that makes use of electrical microstimulation, such as is used in the cortical plasticity lab for certain closed-loop therapeutic experiments. The investigator in this situation must double-check what unit filter is applied during the data processing step[50]. An FIR bandpass filter with tight passband specifications might be useful in some instances, but when "short memory" of a recent large artifact that is orders of magnitude larger than the signal of interest is required, a short IIR filter with little or no memory is a much better choice. If the wrong filter is used during this stage, it will be clear: the filtered signal will look very "wavy," particularly around the stimulus artifacts.

Spike Detection and Sorting

A critical consideration is the method of spike detection, since the spikes typically form the baseline data points used in generating all other derived metrics in the experiment. This will not be covered extensively here, since **Chapter 4** provides an online spike detection algorithm and a little more context about spike detection in general. A method for computing the smoothed nonlinear energy operator and using it to pinpoint spike peaks is provided with both **CPLTools** and **nigeLab**; this method seems to be the most-robust. The alternative that would be recommended is a simple fixed amplitude threshold.

A usable recording typically has clean enough data that spikes "speak for themselves." More sophisticated detection (and clustering) algorithms will undoubtedly grow in importance with the advent of arrays such as NeuroPixels that offer incredible spatial resolution in terms of site spacing; however, for the purposes of most if not all experiments at the cortical plasticity such things are irrelevant. Furthermore, a benefit of a fixed amplitude threshold is that it provides an

[50] When the author first learned about digital signal processing, he realized he could very tightly control certain passband specifications using a long FIR filter. While this is true, this is actually a case where the filter specifications are mostly "guidelines" rather than "specifications," something which was not realized until later.

immediately contextualizing point of information when reported in either the methods or alongside the initial description of spike counts in an experimental manuscript.

While the author holds the opinion that spike sorting is not useful when recordings are made using the resolution of spatial arrays typically used in the reaching rat model, it is also recognized that sometimes it is helpful simply as a denoising process (particularly when large artifacts due to electrical microstimulation are present and cause “weird” signals in the few milliseconds while the amplifier rebounds from saturation). To that end, both **CPLTools** and **nigeLab** contain a spike sorting and curation interface, as described below.

Neural State: related repository links and brief descriptions

- **CPLTools** (Cortical Plasticity Lab Tools): an initial amalgamation of general-purpose tools used by the author before smaller and more application-specific repositories were made. The repository contains code written for use with Matlab R2017a+. It is split into three separate subfolders with the following general organization:
    - Conversion & de-noising on KUMC Isilon parallel computing (**MoveData_Isilon**)
        - Use **adHocExtract_Intan.m** for data acquired with any Intan system.
        - Use **adHocExtract_TDT.m** for data acquired using the TDT system.
        - After either of the above functions, data should be in a standardized hierarchical format, which is elaborated in the **nigeLab** documentation.
    - Spike detection on KUMC Isilon parallel computing (**_SD**)
        - Use **adHocCAR.m** to apply common-average re-reference (de-noising); use **qCAR.m** to run the CAR algorithm from the KUMC Isilon clusters (generally, code with q leading it indicates that it runs on the Isilon via the “job queue”).

        - Use **qSD.m** to queue spike detection jobs on the KUMC Isilon clusters. This requires that filtered data exists in the block folder (either `_Filt` or `_FiltCAR` should suffice), which must be on the `P:` drive in order to run.
    - Spike sorting and extraction of miscellaneous measurements (**Matlab_Addons**)
        - The spike sorting and cluster curation tool resulting in co-publication of manuscripts together with researchers in several collaborative projects is contained in this sub-folder, in the **Functions** sub-folder, in the **Spike Analyses** sub-folder, it is the function **CRC.m** (Bundy et al. 2019, Averna et al. 2019, Millighetti et al. 2020).
- **Intan-DAC-State-Machine-Detector**: Code associated with the manuscript and software/firmware upgrades described in **Chapter 4** reside in this repository. The repository Wiki contains additional documentation (Murphy et al. 2019).
- **Phase-Portrait-Example**: Code for generating **Figure 3.8** or phase portraits in similar simulations depending on hypothesized system fixed points.
- **Matlab_Utilities**: Code in this repository relates to some miscellaneous utilities that the author found useful, particularly for figure generation or creating less-annoying *alert* sounds to notify the end-user that some algorithm or batch process is completed. It is required for some of the other repositories listed on the author's repository profile. See documentation associated with the repository for details.
- **rc-proj**: **Neural state** analyses are contained in the sub-folder **spikeAnalyses**. It was used in the manuscript under preparation that serves as the bulk of **Chapter 5** (Pack et al. 2020; *note that this is technically a co-first-authorship*).

References

Averna, Alberto, et al. "Differential effects of open-and closed-loop intracortical microstimulation on firing patterns of neurons in distant cortical areas." *Cerebral Cortex* 30.5 (2020): 2879-2896.

Bundy, David T., et al. "Chronic stability of single-channel neurophysiological correlates of gross and fine reaching movements in the rat." *PloS one* 14.10 (2019): e0219034.

Buzsaki, Gyorgy. *Rhythms of the Brain*. Oxford University Press, 2006.

Borrell, Jordan A. *Inducing neural plasticity after spinal cord injury to recover impaired voluntary movement.* Doctoral Thesis, University of Kansas Bioengineering, 2020.

Chapin, John K., and Miguel AL Nicolelis. "Principal component analysis of neuronal ensemble activity reveals multidimensional somatosensory representations." *Journal of neuroscience methods* 94.1 (1999): 121-140.

Cheney, Paul D., and Eberhard E. Fetz. "Functional classes of primate corticomotoneuronal cells and their relation to active force." *Journal of neurophysiology* 44.4 (1980): 773-791

Churchland, Mark M., et al. "Neural variability in premotor cortex provides a signature of motor preparation." *Journal of Neuroscience* 26.14 (2006a): 3697-3712.

Churchland, Mark M., Gopal Santhanam, and Krishna V. Shenoy. "Preparatory activity in premotor and motor cortex reflects the speed of the upcoming reach." *Journal of neurophysiology* 96.6 (2006b): 3130-3146.

Churchland, Mark M., et al. "Techniques for extracting single-trial activity patterns from large-scale neural recordings." *Current opinion in neurobiology* 17.5 (2007): 609-618.

Churchland, Mark M., et al. "Neural population dynamics during reaching." *Nature* 487.7405 (2012): 51-56.

Coghill, G. E. "The reaction to tactile stimuli and the development of the swimming movement in embryos of Diemyctylus torosus, Eschscholtz." *Journal of Comparative Neurology and Psychology* 19.1 (1909): 83-105.

Coghill, G. E. "The primary ventral roots and somatic motor column of Amblystoma." *The Journal of Comparative Neurology* 23.2 (1913): 121-143.

Coghill, George Ellett. *Anatomy and the problem of behavior*. CUP Archive, 1929.

Coghill, George E. "The structural basis of the integration of behavior." *Proceedings of the National Academy of Sciences of the United States of America* 16.10 (1930): 637.

Coghill, George E. "The neuro-embryologic study of behavior: Principles, perspective and aim." *Science* 78.2016 (1933): 131-138.

Craig, Jordan J., Adam Bruetsch, and Jessie M. Huisinga. "Relationship between trunk and foot accelerations during walking in healthy adults." *Gait & posture* 49 (2016): 25-29.

Evarts, Edward V. "Pyramidal tract activity associated with a conditioned hand movement in the monkey." *Journal of Neurophysiology* 29.6 (1966): 1011-1027.

Evarts, Edward V. "Relation of pyramidal tract activity to force exerted during voluntary movement." *Journal of neurophysiology* 31.1 (1968): 14-27.

Evarts, Edward V. "Activity of pyramidal tract neurons during postural fixation." *Journal of Neurophysiology* 32.3 (1969): 375-385.

Fetz, Eberhard E. and Paul D. Cheney. "Postspike facilitation of forelimb muscle activity by primate corticomotoneuronal cells." *Journal of neurophysiology* 44.4 (1980): 751-772.

Fine, Edward J., and M. Ziad Darkhabani. "History of the development of the neurological examination." *Handbook of Clinical Neurology*. Vol. 95. Elsevier, 2009. 213-233.

Fuller, James H., and John D. Schlag. "Determination of antidromic excitation by the collision test: problems of interpretation." *Brain research* 112.2 (1976): 283-298.

Gabbiani, Fabrizio, and Christof Koch. "Principles of spike train analysis." *Methods in neuronal modeling* 12.4 (1998): 313-360.

Georgopoulos, Apostolos P., et al. "On the relations between the direction of two-dimensional arm movements and cell discharge in primate motor cortex." *Journal of Neuroscience* 2.11 (1982): 1527-1537.

Georgopoulos, Apostolos P., Ronald E. Kettner, and Andrew B. Schwartz. "Primate motor cortex and free arm movements to visual targets in three-dimensional space. II. Coding of the direction of movement by a neuronal population." *Journal of Neuroscience* 8.8 (1988): 2928-2937.

Gerstein, George L., and Donald H. Perkel. "Simultaneously recorded trains of action potentials: analysis and functional interpretation." *Science* 164.3881 (1969): 828-830.

Griffin, Darcy M., Donna S. Hoffman, and Peter L. Strick. "Corticomotoneuronal cells are “functionally tuned”." *Science* 350.6261 (2015): 667-670.

Griffin, Darcy M., and Peter L. Strick. "The motor cortex uses active suppression to sculpt movement." *Science Advances* 6.34 (2020): eabb8395.

Horak, Fay B. "Assumptions underlying motor control for neurologic rehabilitation." *Contemporary management of motor control problems: Proceedings of the II STEP conference*. Alexandria, Va: Foundation for Physical Therapy, 1991.

Hyland, B. "Neural activity related to reaching and grasping in rostral and caudal regions of rat motor cortex." *Behavioural brain research* 94.2 (1998): 255-269.

Jackson, J. Hughlings. "Clinical and physiological researches on the nervous system. I. On the localisation of movements in the brain." (1876).

Jackson J. H. (1892). Note on the Knee-Jerk in the Condition of Super-Venosity. *British medical journal*, *1*(1624), 326. https://doi.org/10.1136/bmj.1.1624.326

Kaufman, Matthew T., et al. "Cortical activity in the null space: permitting preparation without movement." *Nature neuroscience* 17.3 (2014): 440-448.

Kettner, Ronald E., Andrew B. Schwartz, and Apostolos P. Georgopoulos. "Primate motor cortex and free arm movements to visual targets in three-dimensional space. III. Positional gradients and population coding of movement direction from various movement origins." *Journal of Neuroscience* 8.8 (1988): 2938-2947.

Liddell, Edward George Tandy, and Charles Scott Sherrington. "Reflexes in response to stretch (myotatic reflexes)." *Proceedings of the Royal Society of London. Series B, Containing Papers of a Biological Character* 96.675 (1924): 212-242.

Manwani, Amit, Peter N. Steinmetz, and Christof Koch. "The impact of spike timing variability on the signal-encoding performance of neural spiking models." *Neural computation* 14.2 (2002): 347-367.

Mathis, Mackenzie Weygandt, Alexander Mathis, and Naoshige Uchida. "Somatosensory cortex plays an essential role in forelimb motor adaptation in mice." *Neuron* 93.6 (2017): 1493-1503.

Milighetti, Stefano, et al. "Effects of tDCS on Spontaneous Spike Activity in a Healthy Ambulatory Rat Model." *Brain Stimulation* (2020).

Moran, Daniel W., and Andrew B. Schwartz. "Motor cortical representation of speed and direction during reaching." *Journal of neurophysiology* 82.5 (1999): 2676-2692.

Moxon, K. A., et al. "Responses of infragranular neurons in the rat primary somatosensory cortex to forepaw and hindpaw tactile stimuli." *Neuroscience* 156.4 (2008): 1083-1092.

Murphy, Maxwell D., et al. "Assessing Perturbations to Neural Spiking Response Dynamics Caused By Electrical Microstimulation." *2018 IEEE International Symposium on Circuits and Systems (ISCAS)*. IEEE, 2018.

Murphy, Maxwell D., et al. "Improving an open-source commercial system to reliably perform activity-dependent stimulation." *Journal of neural engineering* 16.6 (2019): 066022.

Pack, Andrea, et al. “Restoration of rodent cortical dynamics after stroke.” *In Preparation* (2020).

Ranaldi, Simone, et al. "The effect of non-negative matrix factorization initialization on the accurate identification of muscle synergies with correlated activation signals." *2018 IEEE International Symposium on Medical Measurements and Applications (MeMeA)*. IEEE, 2018.

Riehle, Alexa, and Jean Requin. "Monkey primary motor and premotor cortex: single-cell activity related to prior information about direction and extent of an intended movement." *Journal of neurophysiology* 61.3 (1989): 534-549.

Riehle, Alexa, et al. "Spike synchronization and rate modulation differentially involved in motor cortical function." *Science* 278.5345 (1997): 1950-1953.

Schwartz, Andrew B., Ronald E. Kettner, and Apostolos P. Georgopoulos. "Primate motor cortex and free arm movements to visual targets in three-dimensional space. I. Relations between single cell discharge and direction of movement." *Journal of Neuroscience* 8.8 (1988): 2913-2927.

Sherrington C. S. (1892). Note toward the Localisation of the Knee-Jerk. *British medical journal*, *1*(1628), 545. https://doi.org/10.1136/bmj.1.1628.545

Sherrington, Charles S. "Decerebrate rigidity, and reflex coordination of movements." *The Journal of physiology* 22.4 (1898): 319.

Sherrington, Charles Scott. "Reciprocal innervation of antagonistic muscles. Fourteenth note.-On double reciprocal innervation." *Proceedings of the Royal Society of London. Series B, Containing Papers of a Biological Character* 81.548 (1909): 249-268.

Sherrington, Charles S. "Flexion-reflex of the limb, crossed extension-reflex, and reflex stepping and standing." *The Journal of physiology* 40.1-2 (1910): 28.

Shimazaki, Hideaki, and Shigeru Shinomoto. "A method for selecting the bin size of a time histogram." *Neural computation* 19.6 (2007): 1503-1527.

Shimazaki, Hideaki, and Shigeru Shinomoto. "Kernel bandwidth optimization in spike rate estimation." *Journal of computational neuroscience* 29.1-2 (2010): 171-182.

Shinomoto, Shigeru, Keiji Miura, and Shinsuke Koyama. "A measure of local variation of inter-spike intervals." *Biosystems* 79.1-3 (2005): 67-72.

Tutunculer, Banu, et al. "Structure of the excitatory receptive fields of infragranular forelimb neurons in the rat primary somatosensory cortex responding to touch." *Cerebral Cortex* 16.6 (2006): 791-810.

Walshe, Francis MR. "Contributions of John Hughlings Jackson to neurology: A brief introduction to his teachings." *Archives of neurology* 5.2 (1961): 119-131.

Whishaw, Ian Q., O'Connor, William T., and Dunnett, Stephen B. "The contributions of motor cortex, nigrostriatal dopamine and caudate-putamen to skilled forelimb use in the rat." *Brain* 109.5 (1986): 805-843.

Whishaw, Ian Q., Sergio M. Pellis, and Boguslaw P. Gorny. "Medial frontal cortex lesions impair the aiming component of rat reaching." *Behavioural Brain Research* 50.1-2 (1992): 93-104.

Wu, Wei, et al. "Modeling and decoding motor cortical activity using a switching Kalman filter." *IEEE transactions on biomedical engineering* 51.6 (2004): 933-942.

Wu, Wei, et al. "Bayesian population decoding of motor cortical activity using a Kalman filter." *Neural computation* 18.1 (2006): 80-118.

Zhang, Kechen, et al. "Interpreting neuronal population activity by reconstruction: unified framework with application to hippocampal place cells." *Journal of neurophysiology* 79.2 (1998): 1017-1044.

CHAPTER 4

Improving an open-source system to reliably perform ADS

Abstract[51]

Objective. Activity-dependent stimulation (ADS) is designed to strengthen the connections between neuronal circuits and therefore may be a promising tool for promoting neurophysiological reorganization following a brain injury. To successfully perform this technique, two criteria must be met: 1) spikes in the extracellular electrical field potential must be detected accurately at one site of interest, and 2) stimulation pulses generated at fixed (< 1ms jitter), low-latency (< 10ms) intervals relative to each detected spike must be delivered reliably to a second site of interest. Here, we aimed to improve noise rejection in a low-cost commercial system to reliably perform ADS in awake, behaving rats, while maintaining latency requirements.

Approach. We implemented a spike detection state machine on a field-programmable gate array (FPGA). Because the accuracy of spike detection can be heavily reduced in awake and behaving animals due to biological artifacts such as movement and chewing, the state machine tracks candidate spike waveforms, checking them against multiple programmable thresholds and rejecting any spikes that fail to meet a programmed threshold criterion.

[51] The contents of this chapter are quoted from a manuscript published in a peer-reviewed journal (Murphy et al. 2019). Readers requiring the use of this method are encouraged to visit the wiki associated with the freely available, open-source public code repository containing compiled executable and FPGA bitfiles. The easiest way to understand the point of this method is to watch the supplementary video (**Video S4.1**), which illustrates the capabilities of the state machine detector to create a logical gating signal to include or exclude arbitrary functions of interest by setting various thresholds and toggling their state to include or exclude ambient noise generated by a nearby computer monitor.

Main Results. A series of offline analyses showed that our implementation was able to appropriately trigger stimulation during epochs of biological artifacts with an overall accuracy between 72% and 97%, fixed computational latency of 167µs, and an algorithmic latency of 300µs to 800µs.

Significance. Our improvements have been made open-source and are freely available to all scientists working on closed-loop neuroprosthetic devices. Importantly, the improvements are easily incorporated into existing workflows that utilize the Intan Stimulation and Recording Controller.

Introduction

Recent preclinical work has investigated the feasibility and efficacy of intracortical microstimulation (ICMS) coupled to neural activity to promote rehabilitation after brain injury (Azin et al. 2011a, 2011b; Guggenmos et al. 2013). In brain-injured rats, constraining the timing of ICMS to within a few milliseconds of a detected extracellular action potential recorded in a second area improves motor skill beyond that achieved by randomly timed stimuli (Guggenmos et al. 2013). This ICMS paradigm, known as activity-dependent stimulation (ADS), has also been used in healthy macaques to pair sites within the motor cortex in order to alter the evoked EMG output (Jackson et al. 2006). The efficacy of these protocols relies both upon the accuracy of the spike detector and upon the reliability of subsequent low-latency (<10 ms) delivery of ICMS. Furthermore, because the invoked strengthening of connections between sites is thought to be generated by a Hebbian mechanism, low jitter in the delivery of stimuli (<1 ms) is critical; for example, the difference in timing between invoking maximal potentiation and maximal depression of synaptic efficacy in hippocampal cultures is <5 ms (Bi & Poo 1998). Depending upon the distance, type, and number of synapses that are putatively involved between the targets of ADS, it is also possible that the <10 ms latency constraint may be restricted to as low as <3-4 ms.

Historically, spike detection has been performed by applying a monopolar voltage threshold to the amplified and filtered neurophysiological signal, counting each rising edge of the resultant logical signal as the onset of a spike (Cheney & Fetz 1985). However, spike detection done in this way tends to conflate signals generated by movement and chewing with spikes from neural units when used in awake animal experiments, due to the similar frequency characteristics and larger amplitude of the former. For ADS, which relies upon the specific pairing of

neurophysiological activity between two sites, non-specific stimulation due to biological noise sources would be obviously problematic.

Although many algorithms that are superior to monopolar voltage thresholds now exist and are easily implemented in various software packages for spike detection and sorting, the latency required in communicating with a host device can be prohibitive for ADS. Previously, ADS had been implemented in lightweight telemetric devices using an application-specific integrated circuit (Azin et al. 2011a, 2011b). However, for a long-term neurophysiological data acquisition solution, a more flexible architecture that can simultaneously acquire signals from hundreds of channels would be desirable. In addition, due to the timing constraints mentioned previously (<10 ms latency between detection and stimulation; <1 ms jitter in stimulus delivery), software solutions that involve a USB chain cannot be used. Therefore, the most tenable solutions need to be implemented algorithmically in hardware, such as through a field programmable gate array (FPGA), a PCIe card interfaced through an ethernet connection, or some other comparable digital signal processing unit.

Recently, the commercial availability of high-gain, high-resolution custom amplifier integrated circuits (Harrison 2007; Harrison & Charles 2003), which interface to a host device through a serial parallel interface (SPI) has made it possible to construct relatively inexpensive neurophysiological acquisition systems that scale to high numbers of recording channels. These systems, such as the acquisition system provided by Intan or the Open-Ephys acquisition board (Siegle et al. 2017), use an FPGA to run the SPI that controls the amplifier chip while maintaining a buffer for USB communication with a host computer. Several proposed spike detection and spike sorting techniques take advantage of the FPGA, an integrated circuit that the end-user can reconfigure (Biffi et al. 2010, Gibson et al. 2013, Park et al. 2017, Vallicelli et al. 2017). Implementing the detection and sorting circuit on an FPGA allows the use of neurophysiological spiking as a reliable control signal in real-time, with low-latency; however,

most implementations require custom integration with respect to the design of the full data acquisition circuit, which typically varies from laboratory to laboratory.

Here, we implemented a spike detection state machine designed to provide multiple threshold windows, reducing the likelihood of activity from sources other than spiking neural units on a single channel leading to the delivery of stimulation. The algorithm reduces the erroneous detection of spikes during biological noise in awake animals using an intuitive algorithm that requires minimal computational power. The implementation is conveniently designed to work as a modification to the existing open-source code provided by Intan for use in conjunction with their low-cost commercial platform for neurophysiological data acquisition and stimulus delivery. Importantly, the system allows the application of ADS with a fixed minimum latency <1 ms and has the potential to scale to a high number of channels in future design iterations.

Figure 4.1

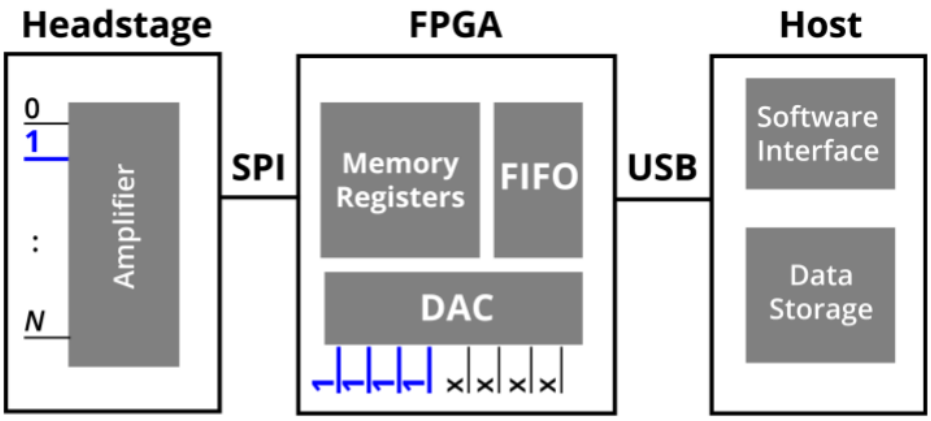

Figure 4.1: Overview of system architecture and implementation.
An amplifier chip is interfaced to the field-programmable gate array (FPGA), via a serial-parallel interface (SPI). *N* electrode channels are routed to a high-gain amplifier. On board the FPGA, amplifier data from the FIFO buffer are piped to the host device via a USB interface. The digitized signals from any selected combination of amplifier channels (blue) can also be routed to up to 8 digital-to-analog converter (DAC) channels, where threshold comparator

logic can be applied with sub-millisecond latency. In this example, 4 threshold windows are applied to the filtered data stream from amplifier channel 1.

Methods

Hardware architecture

The hardware architecture of the acquisition system and spike detector consists of three core components (**Figure 4.1**):

1. **Headstage**: an amplifier circuit connected to a microelectrode array with an arbitrary number N of physical microelectrode leads placed near the neural substrate of interest;
2. **FPGA**: an interface that allows the amplifier circuit to multiplex both the incoming microelectrode signals and any outgoing stimulation commands to the appropriate microelectrodes; and,
3. **Host**: a general-purpose computer that provides an interface to the system, allowing the user to select the desired microelectrode channels and how a closed-loop stimulation scheme will be implemented.

This implementation used a commercially available integrated circuit and pre-assembled headstage (RHS2116; Intan Technologies, Los Angeles, CA, USA) to connect to the microelectrodes. To interface with this circuit, we used the Intan Stimulation/Recording Controller, which consists of an FPGA evaluation board (XEM6010-LX45; Opal Kelly Inc., Portland, OR, USA) equipped with a Xilinx Spartan 6 FPGA (XC6SLX45-2; Xilinx Inc., San Jose, CA, USA), a 128-Mbyte SDRAM chip, a 100-MHz clock source, I/O connectors, and a USB 2.0 interface chip capable of streaming data to a host computer at rates exceeding 20

Mbyte/s. A desktop personal computer (Z230; Hewlett-Packard, Palo Alto, CA, USA) running Windows 7 (Microsoft, Redmond, WA, USA) was used to control the USB chain.

Intan provides a hardware design that embeds the open-source USB/FPGA interface developed by Opal Kelly. This design makes it possible to read and modify registers of the RHS2116 from a host computer. It consists of verilog Hardware Description Language (HDL) code written for the XEM6010-LX45 evaluation board. This code is synthesized using the free Xilinx ISE WebPack software. The resulting bitfile is locally stored on the board in a dedicated Flash memory and can be updated through the USB interface. It is loaded on the Spartan-6 FPGA at each power-up, allowing the FPGA to interpret commands and parameters issued by the user from the USB chain.

At its core, the USB/FPGA design provided by Intan is a state machine that controls SPI buses on up to eight peripheral RHS2116 amplifier circuits. The interface also contains a module that implements a short-latency threshold comparator on up to eight channels of digitized amplifier data streams routed to 16-bit digital-to-analog converters (DAC; AD5662; Analog Devices, Norwood, MA, USA) mounted on the evaluation board. The comparator logic state is routed to a TTL output wire that corresponds to the DAC channel number. The DAC module also implements a single-pole high-pass filter (HPF) on the selected amplifier data stream.

A second module, also included in the existing Intan USB/FPGA interface, contains a state machine that controls the delivery of ICMS to a selected amplifier channel. The module can be configured through the GUI to deliver stimuli on the rising or falling edge of a TTL input signal. Thus, by physically connecting pairs of TTL inputs and outputs, “closed-loop” stimulation based on the detection of threshold-crossing events (in this case, extracellular action potentials, or spikes) is already possible using the USB/FPGA interface as provided by the vendor.

The main contribution described herein is the addition of a state machine for spike detection that offers improved artifact rejection, while taking advantage of the short-latency comparator in the DAC module of the existing USB/FPGA interface. Importantly, we sought to make as few changes as possible to the existing toolkit provided and validated by the commercial vendor, in the hopes that any changes we introduced could be more easily integrated to existing workflows. Overall, the changes amount to an increase of 408 flip flops compared to the originally synthesized architecture, well within the bounds of the available resources on the XEM6010-LX45.

Software interface

Software was modified from the original open-source C/C++ code provided by Intan Technologies for use with the RHS2116 amplifier IC, retaining many similarities with the original. The software implements a GUI, which provides a front-end to the USB/FPGA interface. Modifications described in the present study were added using Qt (version 5.8). Applications were compiled for Windows 32- and 64-bit operating systems using compilers for Microsoft Visual Studio 2015. This modified GUI includes a tab that allows configuration of the DAC (**Figure 4.2A**, left panel) and the popup window for visualizing spikes is altered to accommodate online specification of each of the four parameters for each DAC channel used in the state machine detector, as described in **Figure 4.2A**.

Figure 4.2A

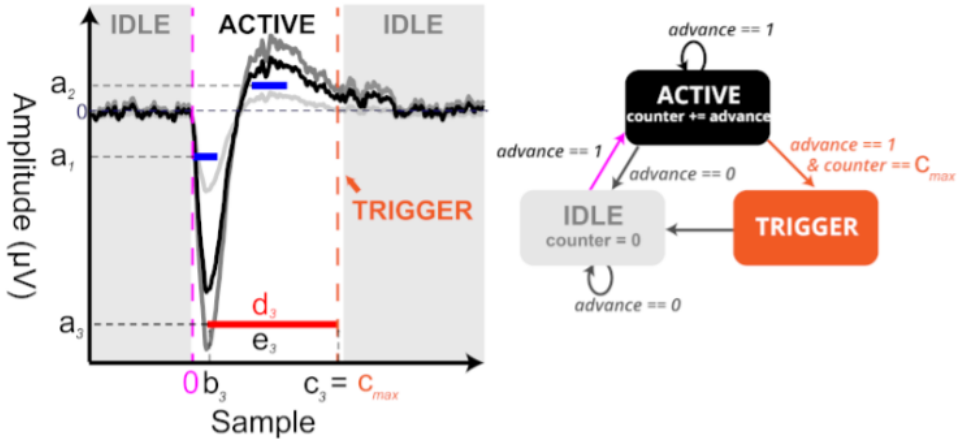

Figure 4.2B

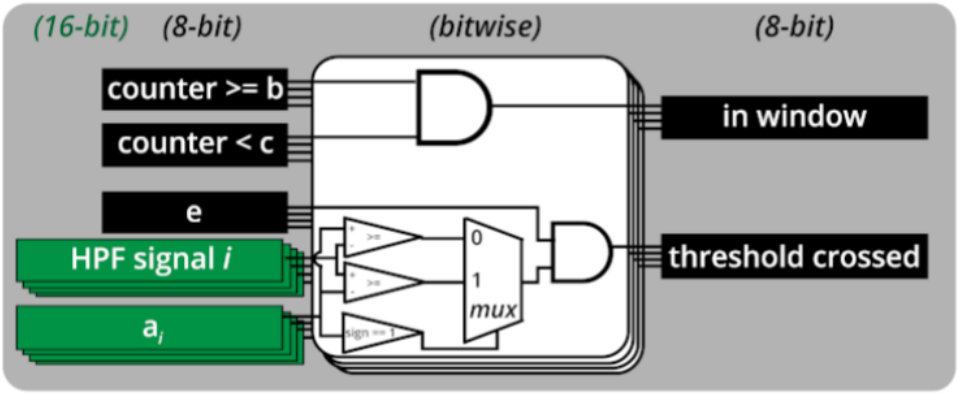

Figure 4.2C

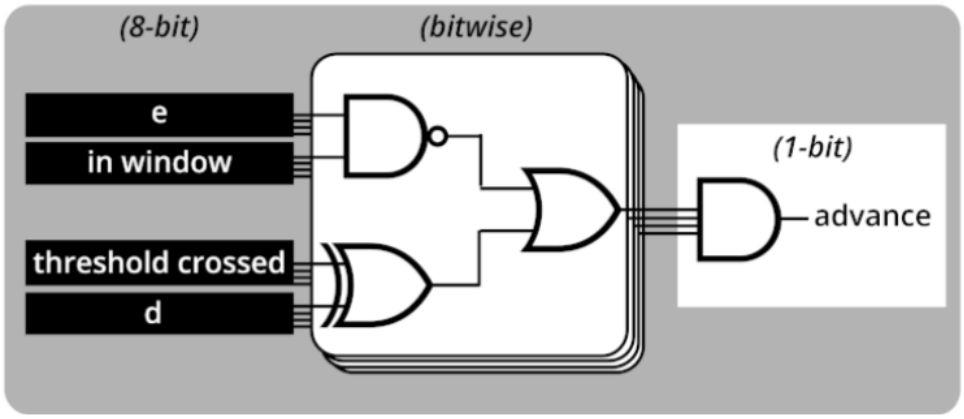

Figure 4.2: Spike detection state machine

A) *Left:* Example of a spike that would be included (black) and waveforms that would be rejected (grey) by the three state machine levels depicted (L_1, L_2, and L_3, denoted by corresponding thresholds a_1, a_2, and a_3). The dark-grey waveform exceeds the red exclusion threshold (a_3), while the light-grey waveform does not meet the second blue inclusion threshold (a_2). The black spike is included because the absolute value of its negative component does not exceed the absolute value set by a_3, while the absolute value of its positive component exceeds the level set by the second blue inclusion level a_2. The parameters (a-e) are defined by the user during acquisition and are illustrated for the red exclusion level shown. *Right:* state flow diagram for the spike detection state machine. By default, the detector is in the idle state (grey), but transitions to active (black) as soon as the data stream fulfils the parameters for the earliest window (magenta). If the waveform meets all criteria specified by the defined levels, the state switches to trigger (orange), then automatically reverts to idle.
B) Threshold logic in the DAC module. For each of the 8 DAC channels, the corresponding parameters determine if the machine is within the start and stop points of the window, relative to when the counter started, as well as whether it crossed the threshold (depending on threshold polarity).
C) Active and idle counter incrementing logic. If the data stream meets criteria of each enabled level that applies to the current counter value, the counter is advanced by 1.

Spike detection state machine

The core of the spike detection state machine is a simple logic cycle that runs in the main module of the USB/FPGA interface (**Figure 4.2A**, right). The state machine allows up to 8 threshold levels (L_i, where i is an integer from 1 to 8) with the following user-defined parameters (**Figure 4.2A**, left):

- **Threshold**, a_i, refers to the voltage value (μV) that the signal must pass through to count as a crossing. If the threshold is negative, then a crossing occurs when the signal value is less-than or equal-to the threshold value (**Figure 4.2B**, multiplex logic). If the threshold is positive, then a crossing occurs when the signal is greater-than or equal-to the threshold value. This number is an unsigned 16-bit integer, which is limited between -5,000 μV and +5,000 μV, based on the dynamic range and scaling of the amplifier and DAC.
- **Start**, b_i, refers to the (inclusive) onset sample of the window L_i. If the state machine counter is less than this value, the threshold conditions for the specified window will not be considered in the state machine logic. The state machine switches from idle to active (as defined below) once the filtered amplifier data stream routed to DAC channel i meets the criteria for L_i, if $b_i = 0$.
- **Stop**, c_i, refers to the (exclusive) end sample of the window L_i. If the state machine counter is equal or higher than this value, the threshold conditions for the specified window will not be considered in the state machine logic. The maximum stop value, c_{max}, defines the total duration of the spike detection state machine.
- **Type**, d_i, refers to the amplitude bounding for window L_i. It depends upon the polarity of the threshold. A value of zero corresponds to an “include” type window, which means that the signal must be less than a negative threshold or greater than a positive threshold while the state machine counter is within the range defined by the start and

stop samples (Figure 4.2C). A value of one corresponds to an “exclude” type window, which enforces the opposite conditions (signal must be greater than a negative threshold or less than a positive threshold).

- **Enable**, e_i, refers to whether window L_i is involved in the decision circuit for the state machine. The state machine can run with as few as 1 and as many as 8 windows enabled.

In the specific example of Figure 4.2A, we have defined three levels (e.g. L_1, L_2, and L_3), where a_1 and a_2 are the blue ‘inclusion’ thresholds ($d_1 = d_2 = 0$) and a_3 is the red exclusion threshold ($d_3 = 1$). Therefore, the dark-grey spike, which crosses threshold a_3, is excluded, but the black spike is not. Likewise, the light-grey spike, which does not cross the a_2 blue ‘inclusion’ threshold is also excluded. In total, the state machine runs for c_{max} samples, starting whenever the state is ‘idle’ and the filtered signal is less than a_1.

The state machine increments a counter on the rising edge of the sample clock depending upon its current state, which is always in one of these three conditions:

1. **idle**, when one or more of the level criteria is not met or no DAC channel is enabled (Figure 4.2A, grey);
2. **active**, when the criteria for each enabled DAC with a start value less than or equal to the current sample index and a stop value greater than the current sample index channel is true (Figure 4.2A, black); or,
3. **trigger**, when the counter equals the largest enabled DAC window stop value (Figure 4.2A, orange).

The counter increments only when the state machine is in the active state, and resets to zero any time it enters the idle state (Figure 4.2A; right). If the state machine reaches the trigger state, it returns to the idle state on the ensuing sample clock cycle. Each state of the machine is

reported by the high state on a unique pair of TTL output and input wires (see Supplementary section S4 for details).

Surgical implant and recording for in vivo testing

All protocols for animal use were approved by the Kansas University Medical Center Institutional Animal Care and Use Committee in compliance with the Guide for the Care and Use of Laboratory Animals (Eighth Edition, The National Academies Press, 2011). Briefly adult male Long Evans rats were anesthetized using a combination of ketamine and xylazine as described previously (Nishibe et al. 2010). A laminectomy was performed to minimize edema during the procedure. Five 00-80 stainless steel skull screws were fixed around the perimeter of the skull to improve attachment of the dental acrylic cap. Using stereotaxic coordinates, a craniectomy was made over the sensorimotor cortex of the left hemisphere. Microwire arrays were positioned to span the rostral forelimb area (RFA), caudal forelimb area (CFA), and forelimb sensory cortex (S1), which was confirmed by a brief ICMS mapping procedure before insertion to a depth of approximately 1500 μm. An external silver wire on each array was tied to the same skull screw placed in the interparietal bone, which acted as a common ground. In the rat used for session A (recording sessions described below), the microwire array was a custom in-house design consisting of 32 channels of 33 μm diameter polyimide-coated tungsten wire (California Fine Wire Co., Grover Beach, CA), which were distributed throughout RFA, CFA, and S1 in a non-uniform grid pattern. The rat used for sessions B and C was implanted with a commercial microwire array (MicroProbes for Life Science, Gaithersburg, MD) consisting of 16 channels of nickel-chromium alloy 50 μm diameter wires arranged in a 4x4 grid with 250 μm site spacing implanted in S1. Qualitatively, spiking activity from both datasets was similar, but session A contained a few channels with large, stereotyped spikes, while spikes tended to be smaller in amplitude for sessions B and C. Prior to each recording, the rat was placed under anaesthesia

via isoflurane induction, and subsequently one channel located within RFA was used for recording, while a single S1 channel was used in any stimulation sessions Electrode impedances ranged from 750 – 1,500 kΩ at recording sites. Recordings were made in 3- to 5-minute blocks during and after recovery from anaesthesia.

Recordings were made during three separate sessions. Recording sessions were assigned the codes ‘A,’ ‘B,’ and ‘C.’ The main features and how these data were used within the current work are summarized in **Table 4.1**. Session A was taken from a first rat, three days after implantation, and contains a single epoch in which no stimulation was performed, which was used for subsequent offline characterizations due to the presence of large, stereotypical spike waveforms and low noise floor (RMS 18.6 μV, rectified median 11.3 μV). Sessions B and C were taken from a second rat approximately three months after the implantation. Session B tested the latency between spike detection using the state machine and onset of stimulation. Session C tested the online performance of the spike detection state machine using ad hoc parameters selected while the experiment was ongoing (e.g. to mimic a typical use case). Specific parameters for each recording session are reported in detail in **Table S4.1**; sub-indices indicate identical recording data that was re-run offline using a simulated test bench to characterize performance. To identify chewing periods (which bias performance toward false positive spike detection due to the presence of high-amplitude biological noise), a simultaneous video stream was synchronized with the neurophysiological data from session C through co-registration of a flashing LED that was tied to a digital input on the acquisition board.

Table 4.1

Name	*Stim?*	*Feature*	*Use*
A	No	Large stereotypical spikes; low noise	Offline performance
B	Yes	Stimulus artifacts	Test latency of stimulation
C	No	Typical use case; synchronized video	Online performance

Table 4.1: Summary of recording data sets taken from rats.

Recordings were taken from awake, ambulatory rats implanted in RFA and S1. Columns describe whether stimulation was used, the main feature that distinguishes that recording dataset from the others, and the reason the recording was used in this study.

Offline performance testing

Performance of the spike detection state machine was evaluated by comparing offline detection of spikes from the in vivo data from session A, either using a monopolar threshold detector or the state machine detector. To ensure that the analyses accurately captured online performance, we first validated the fidelity of the reconstructed recorded signals by ensuring that the DAC amplifier data stream and digital logic state streams recorded in vivo during session C matched those generated by the offline DAC filter and state machine simulation. Simulations were performed using test benches compiled in verilog, MATLAB (R2017a+), and Simulink (R2018b), as described in the supplementary methods section. The test benches are included in the online code repository along with the modified software and hardware code. Once we verified that there was no difference in the simulated digital logic state signals and the recorded ones, we used the DAC amplifier data stream recorded from session A to simulate the spikes

detected using both a single-threshold detector (A0) as well as all events that entered the active and trigger states using the state machine detector (A1). For the monopolar threshold detector, spikes were only counted on the logical rising edge of the threshold crossing. Selection of a monopolar threshold was fixed at 40 μV, which was initially determined online by visual inspection of the spike scope to set a level that appeared qualitatively to reject noise while accepting most multi-unit spiking.

To characterize the ability of the spike detection state machine to reject artifact while still detecting viable spikes we calculated accuracy, defined as the ratio of the sum of correctly classified spikes (true positives; TP) and correctly classified artifacts (true negatives; TN) to the total number of spikes and artifacts detected. To determine whether spikes or artifacts detected during a simulation were correctly classified, a set of target classifications for spike and artifact waveforms were obtained offline using manual sorting to group similar waveforms. This consisted of a cluster cutting technique in which the spikes and artefactual waveforms were assigned iteratively through the manual selection of waveforms from the candidate set of waveforms detected as either spikes or artifacts by the detector, similar to the technique described in (Harris et al. 2000). While this method of classifying multi-unit spike waveforms has limitations depending on the amplitude of units under consideration (Harris et al. 2000), the purpose was to illustrate the ability of the spike detection state machine to reject artifactual waveforms, a situation for which an experienced operator is well-suited.

To verify our results on a dataset in which the ground truth spike times are already known, we synthesized an additional set of recordings (C3, in which a threshold detector was applied, and C4, in which the state machine detector was applied; parameters in **Table S4.1**). In these simulations, known spike waveforms were added to a non-spiking recording channel at 1,500 uniformly sampled random samples throughout the duration of the sample record. It should be noted that in these simulations, identical recordings can yield slightly different numbers of total

detected spike and artifact waveforms depending on which spike detection procedure was simulated even if the initial inclusion threshold is the same for the state machine detector and the threshold detector: because the state machine has a minimum duration that requires multiple samples in order to detect the spike, probabilistically there are more opportunities to identify candidate spike and artifact waveforms when using a single-threshold detector, potentially leading to a slightly higher number of total event classifications when using the monopolar threshold detector.

After either sorting the detected spike and artifact waveforms to obtain the target classifications or using the a priori known ground truth spike times as targets, performance was obtained using confusion matrices to compare the detected outputs (e.g. spikes or artifacts) against the target outputs (e.g. spike or artifact classifications of the detected outputs using offline sorting). Sensitivity (or true positive rate; TPR) was estimated as the ratio of correctly classified spikes to the sum of correctly classified spikes (true positives; TP) and outputs given as artifacts that were determined to be spikes by offline sorting (false negatives; FN). True negative rate (TNR) was estimated as the ratio of correctly classified artifacts (true negatives; TN) to the sum of correctly classified artifacts and outputs given as spikes that were determined to be artifacts by offline sorting (false positives; FP). Precision (positive predictive value) was estimated as the ratio of true positives to the sum of true positives and false positives. The false discovery rate (FDR) was estimated as the ratio of false positives to the sum of true positives and false positives. The false negative rate (FNR) was estimated as the ratio of false negatives to the sum of true positives and false negatives. These last two metrics (FDR and FNR) were of special interest, as we aimed to reduce FDR while maintaining a low FNR.

Figure 4.3A

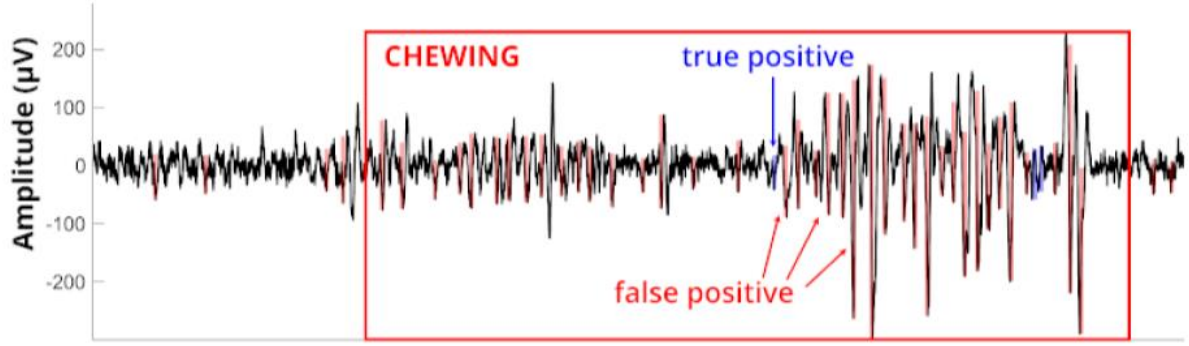

Figure 4.3B

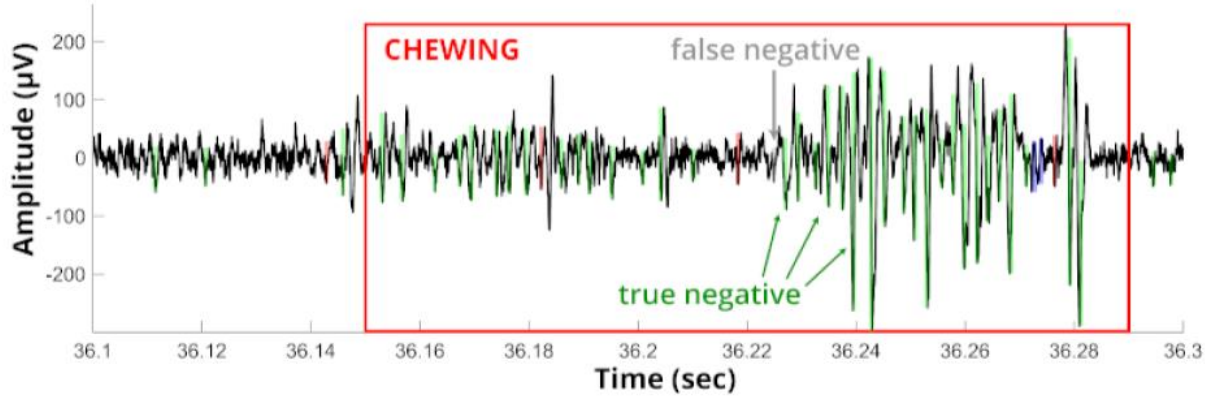

Figure 4.3C

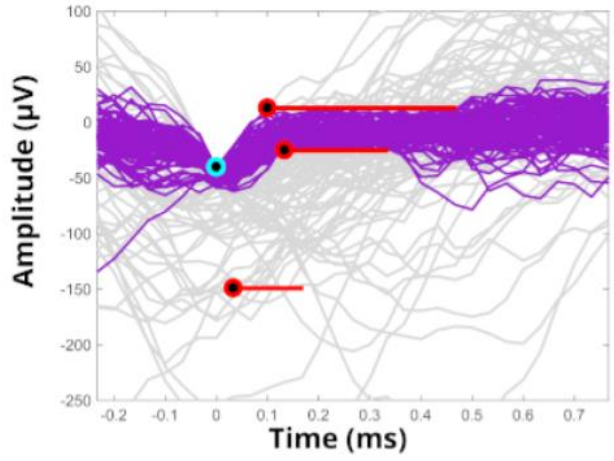

Figure 4.3D

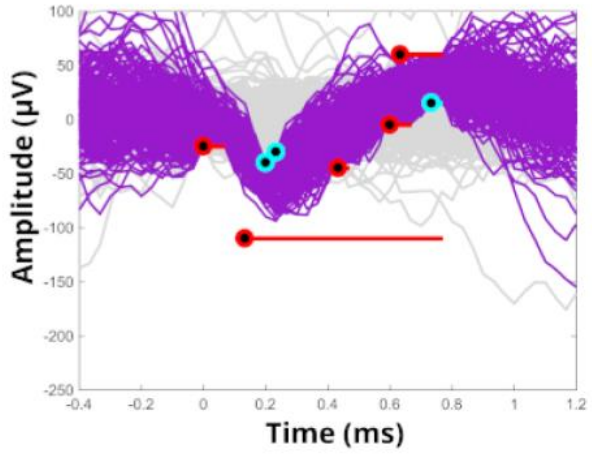

Figure 4.3: **Qualitative performance of the implemented spike detection.**

A) 200ms of high-pass filtered data from session *C* during single-threshold (-40μV; simulation *C2*) spike detection. Red box represents a 130-ms epoch of chewing. Red highlighting (false positive) indicates spikes that were wrongly detected. Blue highlighting (true positive) shows spikes that were correctly identified. **B)** Same data as in panel A with superimposed detections from the state machine spike detector. Green highlighting (true negative) indicates artifacts that were correctly rejected by the state machine. Grey highlighting (false negative) indicates a case of true spike not detected by the state machine. **C)** Random sub-sampling of 250 detected (magenta) and 250 rejected (grey) waveforms using the spike detection state machine in real-time (recording *C0*), using the digital outputs from the online state machine. Flat lines represent threshold levels. Black spots represent inclusive samples that must meet the threshold criteria, while ends of lines are open to represent the non-inclusive threshold criterion. Cyan thresholds must be exceeded, whereas red thresholds must not be exceeded. **D)** An offline reconstruction (recording *C1*) was used to simulate the state machine using different window parameters. This random sub-sampling of 250 detected and 250 rejected waveforms indicates how the parameters could be set differently to isolate spikes from a different unit. Note that increasing the duration of the state machine also increases the total time to detection.

Results

Ability to detect waveforms of interest

An important feature of the spike detector state machine is the ability to identify relatively low-amplitude spikes during epochs that contain periods of relatively high-amplitude biological artifact. Biological noise, such as arises from mechanical vibration and EMG that occur during chewing and whisking, leads to large-amplitude, high-frequency (>300 Hz) deflections in the signals observed on electrodes embedded within the cortex. To illustrate this, we isolated a short example epoch from recording session C in which the presence of chewing was verified by synchronizing the electrophysiological data stream with video of the rat moving freely in the recording chamber. While these epochs of activity are likely generated by biological sources, they may still be undesirable during motor recordings designed to study neurophysiological spiking of units related to other motor behavior (i.e. forelimb movement during pellet retrievals). Unfortunately, the simple threshold detector produces many false-positive spike detections during such epochs (**Figure 4.3A**, red highlighting). By contrast, the state machine detector is still able to correctly detect spikes (**Figure 4.3B**, blue highlighting) during the noisy periods without mistakenly triggering from the same waveforms that are problematic for the threshold detector (**Figure 4.3B**, green highlighting). Even within a single recording session and on a single recording amplifier channel, it was possible to distinguish between substantially different spike waveforms by customizing the parameters sent to the spike detection state machine online. Parameters that were selected online (recording C0, **Table S4.1**) captured the smaller multi-unit activity (**Figure 4.3C**), whereas offline adjustment of parameters led to the ability to isolate waveforms from the larger of the two units (**Figure 4.3D**). Importantly, the ability to set the level parameters in real-time, thanks to the modified GUI (**Figure S4.2**), improved ease-of-use compared to existing systems, in which a “training” recording must first be obtained and

analysed offline before allowing parameters to be set (Azin et al. 2011a, 2011b, Guggenmos et al. 2013).

Figure 4.4A

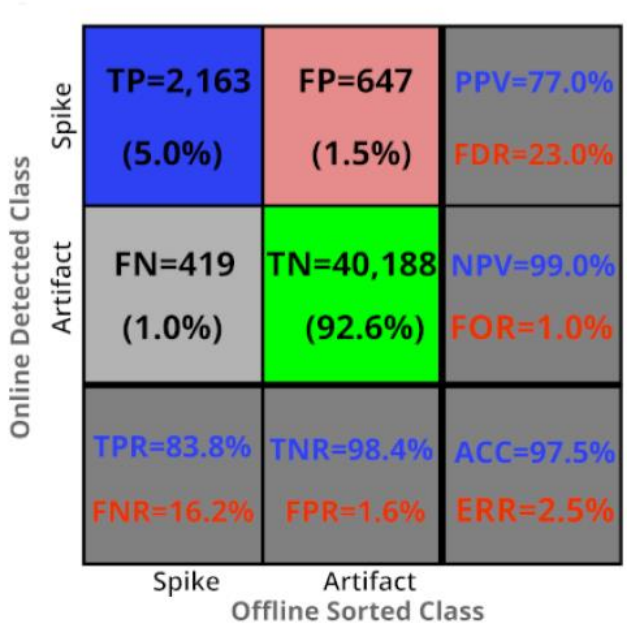

Figure 4.4B

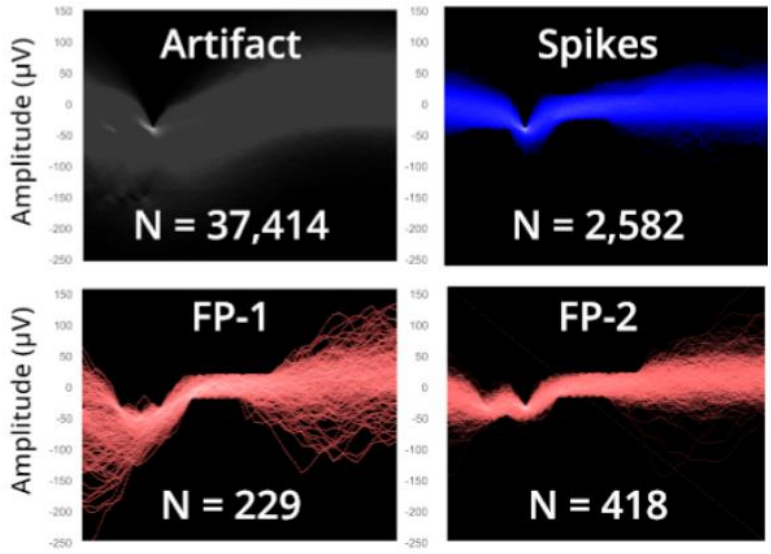

Figure 4.4: Typical performance compared to offline sorted spikes

A) Confusion matrix for comparison of online spike detection state machine performance after manual offline sorting of spike and artifact waveforms (recording *C0*). The blue box contains the number of true positive spikes and the percentage of the overall detected events that fit this category. The salmon box contains the number of false positive spikes detected by the algorithm, as determined by manual sorting. The grey box indicates the number of rejected spikes (which entered but did not complete the state machine) that were scored offline as spikes. The green box represents waveforms that were rejected by the state machine and were also classified manually offline as artifact. The top row on the far-right column show the positive predictive value (PPR) in blue and false discovery rate (FDR) in red. The second row on the far-right column shows the negative predictive value (NPV) in blue, and the false omission rate (FOR) in red. The first column on the bottom of the matrix show the sensitivity (or true positive rate, TPR) in blue and the false negative rate (FNR) in red. The second column on the bottom of the matrix shows the true negative rate (TNR) in blue and the false positive rate (FPR) in red. The box in the bottom right of the plot shows the overall accuracy (ACC) in blue and its complement (the error percentage, ERR) in red. **B)** Offline sorting used for comparison. Lighter regions indicate a higher density of waveforms passing through those voltage values. Spikes were manually sorted using cluster cutting to separate units into characteristic waveforms. Magenta outline indicates spike profile used for offline sorting in panel A. Bottom two panels (FP-1 and FP-2) are characteristic waveform types that sometimes passed the state machine conditions, contributing to the number of false positives.

Performance in awake ambulatory rats

To quantify the online performance of the state machine we performed manual offline sorting of spike and artifact waveforms (from session C). We considered the offline sorting as ground truth, which allowed us to compute confusion matrices comparing the online classification (e.g. spike or artifact) to the offline sorted classification for the same waveform for each monopolar threshold crossing (**Figure 4.4**). The number of spikes correctly detected by the online spike detector state machine was 2,163 out of 2,582 (meaning a sensitivity, or true positive rate, of 83.8%). The number of true negatives (i.e. artifacts not detected as spikes) was 40,188 out of 40,835 (meaning a specificity, or true negative rate, of 98.4%). The number of artifacts incorrectly classified as spikes was 647, resulting in a 23% false discovery rate (FDR) for the online spike detector state machine. Artifacts that led to false-positives contained qualitative similarities with the spikes of interest, which may account for this value (**Figure 4.4B**, FP-1 and

FP-2). Overall, the online accuracy of the spike detector state machine was 97.5% (**Figure 4A**; recording C0), which is inflated by a high number of true negative samples due to the relatively large number of artifacts passed by the monopolar threshold. In practice, this could be mitigated using a monopolar threshold set to a much higher value; however, while increasing the threshold could reduce the number of artifacts falsely detected as spikes, it would also reduce the number of true positive spikes and is therefore not a feasible solution. Indeed, even the synthetic insertion of large-amplitude (-150μV peak) spikes at known times to a non-spiking channel results in an FDR of 90.5% for a monopolar threshold of -100 μV, while the state machine detector yielded an FDR of 29.3% and overall accuracy of 72.2% (**Figure S4.3**).

Using a channel selected for its low noise floor and large-amplitude spike waveforms recorded in vivo (session A), we computed the same performance measures used in the previous case (**Figure 4.5A**). Performance overall was comparable (97.1% accuracy) due to the large number of correctly rejected waveforms. However, careful parameter selection also yielded an improved FDR (6.9%) and FNR (2.8%) for the state machine spike detector under these ideal conditions. We compared the best-case performance of our state machine detector to a monopolar threshold detector. Using identical recordings, there is a dramatic improvement in the FDR when using the state machine detector (189 artifacts characterized as spikes, of a total 2,075 spikes detected online, **Figure 4.5B**) compared to the monopolar threshold detector (2,770 artifacts characterized as spikes, of a total 7,075 detected spikes, **Figure 4.5B**). This improvement results from the rejection of artifactual waveforms, such as occur during epochs of biological noise (e.g. chewing, **Figures 4.3A, 4.3B**).

Figure 4.5A

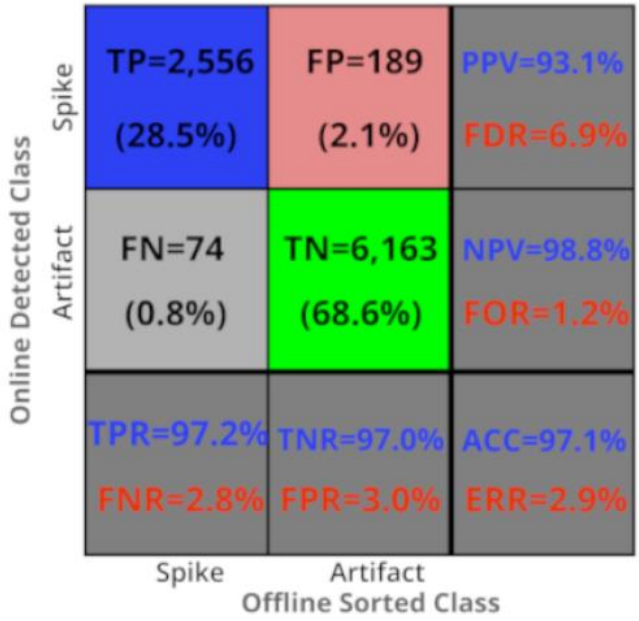

Figure 4.5B

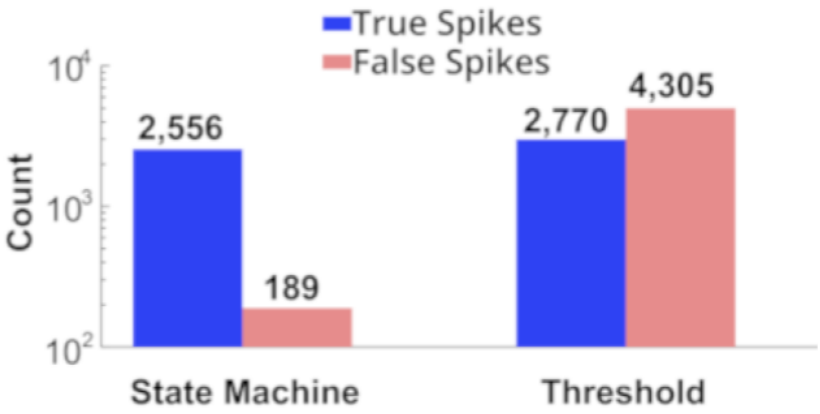

Figure 4.5: Ideal performance compared to offline sorted spikes and monopolar threshold detection.
A) Simulated performance using an ideal *in vivo* recording with large spikes (recording *A1*).

Although the simulated performance is applied to a channel with high-amplitude spike waveforms, the overall accuracy effectively remains consistent. This is due to the relatively large proportion of waveforms that are correctly rejected (middle box). **B)** Manual offline sorting performed for recording *A1* (presented in panel A), as well as a comparison to performance of true (blue) to false (salmon) discoveries for the state machine detector and a simple threshold detector for the same dataset (recording *A0*).

Mean latency from spike peak to stimulus delivery

The total latency for an activity-dependent stimulus can be considered as the sum of the algorithmic latency (to reliably detect an event) and the computational latency (due to the system). Algorithmic latency, in this case, depends on the maximum number of samples needed to detect a spike. In this work, spikes were detected using state machines that varied between 300µs (session B; 9 samples at 30 kHz sample frequency) and 800µs (session C; 24 samples at 30 kHz sample frequency). Therefore, the exact algorithmic latency is specific to the parameterization of the user-defined threshold levels. Our work did not alter the computational latency between the event detection and the delivery of the stimulus. During session B, the Intan Stimulation/Recording Controller stimulation sequencer module delay was set to zero milliseconds, allowing us to estimate the computational latency as the minimum latency between the rising edge of the virtual TTL input corresponding to the trigger state of the spike detection state machine and the onset of stimulus artifact. The computational latency obtained in this way was 167µs (5 samples at 30 kHz sample frequency; **Figure S4.1**). Therefore, the total latency of the system during spike detection was reliably less than 1 ms, mainly due to the algorithmic latency, and indicates that the detector is responsive on a timescale that is both fast and reliable enough to be used for performing ADS.

Discussion

We developed a modified version of an open-source commercial system to implement closed-loop stimulation with sub-millisecond latency. The main improvement is the implementation of a spike detection state machine with an interface that allows the application of eight reconfigurable thresholds to any combination of different or identical amplifier channels. The implemented state machine slightly reduces sensitivity (i.e. true positive rate, **Figure 4.4A**), but drastically improves specificity (i.e. reduced FDR; **Figures 4.5A, 4.5B**), which may be critical in designing closed-loop electrical stimulation paradigms in the central nervous system in vivo. This improvement in selectivity is particularly important when the stimulation paradigm must be implemented during ongoing natural behavior, such as chewing or whisking (**Figure 4.3**).

Although the focus of this study was on applying the improved detector for use in ADS, we envision that this type of low-latency, highly-selective discriminator could be useful in a range of closed-loop applications. For example, feedback needs not be delivered in the form of stimulation pulses but could instead be incorporated as a part of the experimental design itself, such as the delivery of a reward contingent upon the discrimination of a unique spike waveform (Koralek et al. 2012). However, the context of developing closed-loop neuroprostheses for applications such as neurorehabilitation provides important constraints. For example, a critical aspect of the ADS paradigm is the timing of stimuli based on the detection of a stereotyped waveform that represents a small group of cells near the recording microelectrode (Guggenmos et al. 2013). Therefore, it is desirable to minimize the FDR while maintaining a detection algorithm that can be implemented with low latency and customizable sensitivity to maximize the chances of invoking Hebbian mechanisms of plasticity between cells at the detection site and those at the stimulation electrode (Bi & Poo 1998). It is possible that such a stimulation regime could be augmented by incorporating multiple stimulation sites at offset latencies from a

single trigger source; this is also possible using the system presented in this study. Similarly, although not tested here, the modifications presented can apply simultaneous thresholds to several spatially distributed sites simultaneously. This provides a practical way to mitigate the large, non-neural sources of noise that result from a failure in the common-mode rejection, which are typically present on multiple channels simultaneously. Future versions of the discriminator presented here that scale to an arbitrarily large number of thresholds could then be useful in sorting using tetrodes or other high-density arrays.

With the rising interest in applications of closed-loop technologies for stimulation of the central nervous system (Levi et al. 2018), a number of methods for implementing closed-loop stimulation have been made openly available. These include software packages, such as Falcon (Ciliberti & Kloosterman 2017), the Open Ephys GUI (Siegle et al. 2017), and NeuroRighter (Newman et al. 2012); however, software implementations of online spike detection and triggered stimulation typically suffer from the latencies imposed when performing serial communication with the host computer. One exception is the Real-Time eXperiment Interface (RTXI, (Patel et al., 2017)); however, because the system is designed to operate using a National Instruments Data Acquisition card (NI-DAQ), it may be difficult to scale to a very high channel architecture. On the other hand, the ADC of the RHS2116 is scalable, and because digitization occurs very close to the source (on the headstage), yields improved noise characteristics.

Hardware implementations, such as the synthesized bitfile that can be readily uploaded to effectively transform an FPGA into a commercial neurophysiological acquisition system, are not as widely distributed. Because hardware implementations typically have very specific design constraints and are optimized to meet those constraints, it is impractical to develop and distribute open-source hardware for closed-loop neuroprosthetics. Just as the RTXI system is not readily compatible with the Intan amplifier chips, hardware implementations (Ambroise et al.

2017, Buccelli et al. 2019) are designed to interface with in vitro microelectrode arrays that interface to an FPGA with different input and output pin configurations, making it difficult to provide a ubiquitous hardware bitfile for every experimental setup. Alternatively, moving from a hardware implementation in an FPGA to a custom application specific IC (and subsequent commercialization) becomes more practical for individual applications.

To minimize changes to the existing open-source software provided by Intan, the spike detection state machine was implemented in the DAC module. This imposes the limitation that only one spike detection state machine can run at a time. At a maximum, up to eight different amplifier channels could be polled for synchronous or near-synchronous events, or eight threshold criteria could be applied to the waveform of a single amplifier channel. Making substantial modifications to the existing FPGA might allow scaling of a spike detection state machine module to any arbitrary number of thresholds on different channels. A natural extension of this work would be to scale up the number of trigger sources for multi-stream ADS, particularly as FPGA evaluation boards with increased on-board resources become available. Generalizing the state machine to a higher number of independent channels by running it as a module that is independent of the DAC, automating the process of setting threshold levels (e.g. using spike “templates”), and integrating independent state machines to allow concurrent detection of events in multiple frequency ranges are currently being investigated to improve their application in closed-loop neuroprosthetic interfaces. Automating the process of setting threshold levels, especially as channel counts scale up, will be important, as the improved rejection may also reduce sensitivity, depending upon the ad hoc parameters set by the operator. Algorithmically, the state machine is fundamentally similar to the one implemented in (Azin et al. 2011a); however, the state machine described here allows more flexibility in the parameterization of each threshold level by allowing the end-user to set each of the following four parameters while the application is running.

We have provided modifications to an existing interface for conducting electrophysiological experiments using closed-loop stimulation. These improvements allow spike detection to be performed with a higher selectivity at the expense of a reduced sensitivity. This trade-off is dependent upon the ad hoc selection of parameters, which can be adjusted by the experimenter in real-time. The architecture in which this improved spike detection state machine is implemented has the possibility to scale to a very high number of channels in the future, improving current and future functionality. Our contribution to the original design improves the accessibility of investigating closed-loop stimulation paradigms, which may be necessary for effective, therapeutic neuroprosthetic systems.

Acknowledgment

This study was made possible through the support of NIH grants R01NS030853 (RN), R03HD094608 (DG), T32HD057850 (MM, RN), and F32NS100339 (DB). Collaboration was made possible through the MAECI award (MC). The authors have no competing interests to disclose.

References

Ambroise, M., Buccelli, S., Grassia, F., Pirog, A., Bornat, Y., Chiappalone, M., & Levi, T. (2017). Biomimetic neural network for modifying biological dynamics during hybrid experiments. *Artificial Life and Robotics, 22*(3), 398-403.

Azin, M., Guggenmos, D. J., Barbay, S., Nudo, R. J., & Mohseni, P. (2011a). A battery-powered activity-dependent intracortical microstimulation IC for brain-machine-brain interface. *IEEE Journal of Solid-State Circuits, 46*(4), 731-745.

Azin, M., Guggenmos, D. J., Barbay, S., Nudo, R. J., & Mohseni, P. (2011b). A miniaturized system for spike-triggered intracortical microstimulation in an ambulatory rat. *IEEE Transactions on Biomedical Engineering, 58*(9), 2589-2597.

Bi, G., & Poo, M. (1998). Synaptic modifications in cultured hippocampal neurons: dependence on spike timing, synaptic strength, and postsynaptic cell type. *The Journal of Neuroscience, 18*(24), 10464-10472.

Biffi, E., Ghezzi, D., Pedrocchi, A., & Ferrigno, G. (2010). Development and Validation of a Spike Detection and Classification Algorithm Aimed at Implementation on Hardware Devices. *Computational Intelligence and Neuroscience, 2010*, 15.

Buccelli, S., Bornat, Y., Colombi, I., Ambroise, M., Martines, L., Pasquale, V., Chiappalone, M. (2019). A neuroprosthetic system to restore neuronal communication in modular networks. *bioRxiv*, 514836.

Cheney, P. D., & Fetz, E. E. (1985). Comparable patterns of muscle facilitation evoked by individual corticomotoneuronal (CM) cells and by single intracortical microstimuli in primates: evidence for functional groups of CM cells. *Journal of Neurophysiology, 53*(3), 786-804.

Ciliberti, D., & Kloosterman, F. (2017). Falcon: a highly flexible open-source software for closed-loop neuroscience. *Journal of Neural Engineering, 14*(4), 045004.

Gibson, S., Judy, J. W., & Markovic, D. (2013). An FPGA-based platform for accelerated offline spike sorting. *Journal of Neuroscience Methods, 215*(1), 1-11.

Guggenmos, D. J., Azin, M., Barbay, S., Mahnken, J. D., Dunham, C., Mohseni, P., & Nudo, R. J. (2013). Restoration of function after brain damage using a neural prosthesis. *Proceedings of the National Academy of Sciences of the United States of America, 110*(52), 21177-21182.

Harris, K. D., Henze, D. A., Csicsvari, J., Hirase, H., & Buzsáki, G. (2000). Accuracy of tetrode spike separation as determined by simultaneous intracellular and extracellular measurements. *Journal of Neurophysiology, 84*(1), 401-414.

Harrison, R. R. (2007). *A Versatile Integrated Circuit for the Acquisition of Biopotentials*. Paper presented at the IEEE Custom Integrated Circuits Conference, San Jose, CA.

Harrison, R. R., & Charles, C. (2003). A low-power low-noise CMOS amplifier for neural recording applications. *IEEE Journal of Solid-State Circuits, 38*(6), 958-965.

Jackson, A., Mavoori, J., & Fetz, E. E. (2006). Long-term motor cortex plasticity induced by an electronic neural implant. *Nature, 444*(7115), 56-60.

Koralek, A. C., Jin, X., Long Ii, J. D., Costa, R. M., & Carmena, J. M. (2012). Corticostriatal plasticity is necessary for learning intentional neuroprosthetic skills. *Nature, 483*(7389), 331-335.

Levi, T., Bonifazi, P., Massobrio, P., & Chiappalone, M. (2018). Editorial: Closed-Loop Systems for Next-Generation Neuroprostheses. *Frontiers in Neuroscience, 12*(26).

Murphy, Maxwell D., et al. "Improving an open-source commercial system to reliably perform activity-dependent stimulation." *Journal of neural engineering* 16.6 (2019): 066022.

Newman, J. P., Zeller-Townson, R., Fong, M.-F., Arcot Desai, S., Gross, R. E., & Potter, S. M. (2012). Closed-Loop, Multichannel Experimentation Using the Open-Source NeuroRighter Electrophysiology Platform. *Frontiers in Neural Circuits, 6*, 98.

Nishibe, M., Barbay, S., Guggenmos, D., & Nudo, R. J. (2010). Reorganization of motor cortex after controlled cortical impact in rats and implications for functional recovery. *Journal of Neurotrama, 27*(12), 2221-2232.

Park, J., Kim, G., & Jung, S. (2017). A 128-Channel FPGA-Based Real-Time Spike-Sorting Bidirectional Closed-Loop Neural Interface System. *IEEE Transactions on Neural Systems and Rehabilitation Engineering, 25*(12), 2227-2238.

Patel, Y. A., George, A., Dorval, A. D., White, J. A., Christini, D. J., & Butera, R. J. (2017). Hard real-time closed-loop electrophysiology with the Real-Time eXperiment Interface (RTXI). *PLOS Computational Biology, 13*(5), e1005430.

Siegle, J. H., López, A. C., Patel, Y. A., Abramov, K., Ohayon, S., & Voigts, J. (2017). Open Ephys: an open-source, plugin-based platform for multichannel electrophysiology. *Journal of Neural Engineering, 14*(4), 045003.

Vallicelli, E. A., De Matteis, M., Baschirotto, A., Rescati, M., Reato, M., Maschietto, M., Zeiter, R. (2017). *Neural spikes digital detector/sorting on FPGA*. Paper presented at the IEEE Biomedical Circuits and Systems Conference, Turin, Italy.

Supplementary Materials

Supplementary Figures

Figure S4.1

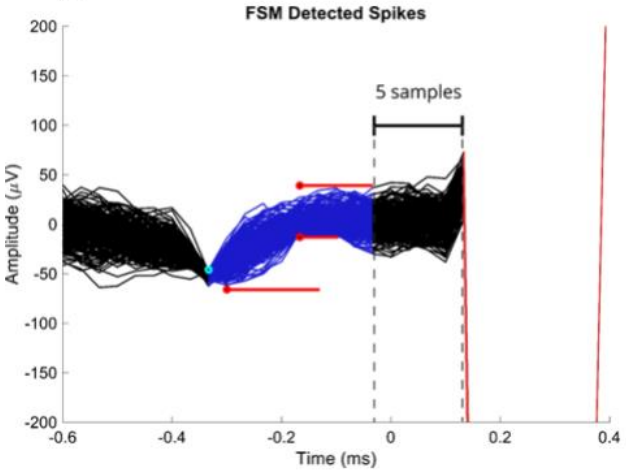

Figure S4.1: Random subsample of 250 triggered stimuli from recording B0

The Intan RHS Stimulation/Controller system has a built-in stimulation sequencer state machine, which limits the minimum latency from detection to stimulation to 5-samples, or 167 μs when sampling at 30 kHz. The trigger spikes used for stimulation are highlighted in blue. Red indicates the stimulus artifact (60 μV biphasic pulse, 100μs per phase), and rebound from amplifier saturation.

Figure S4.2A

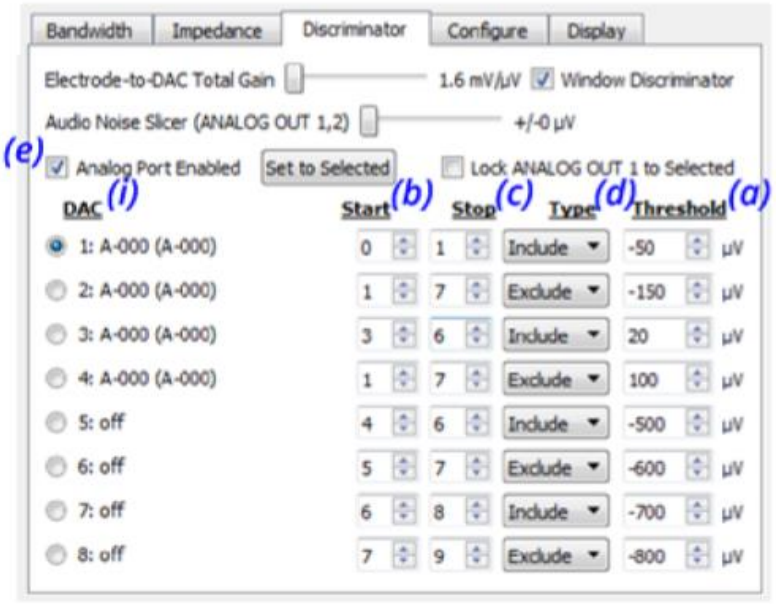

Figure S4.2B

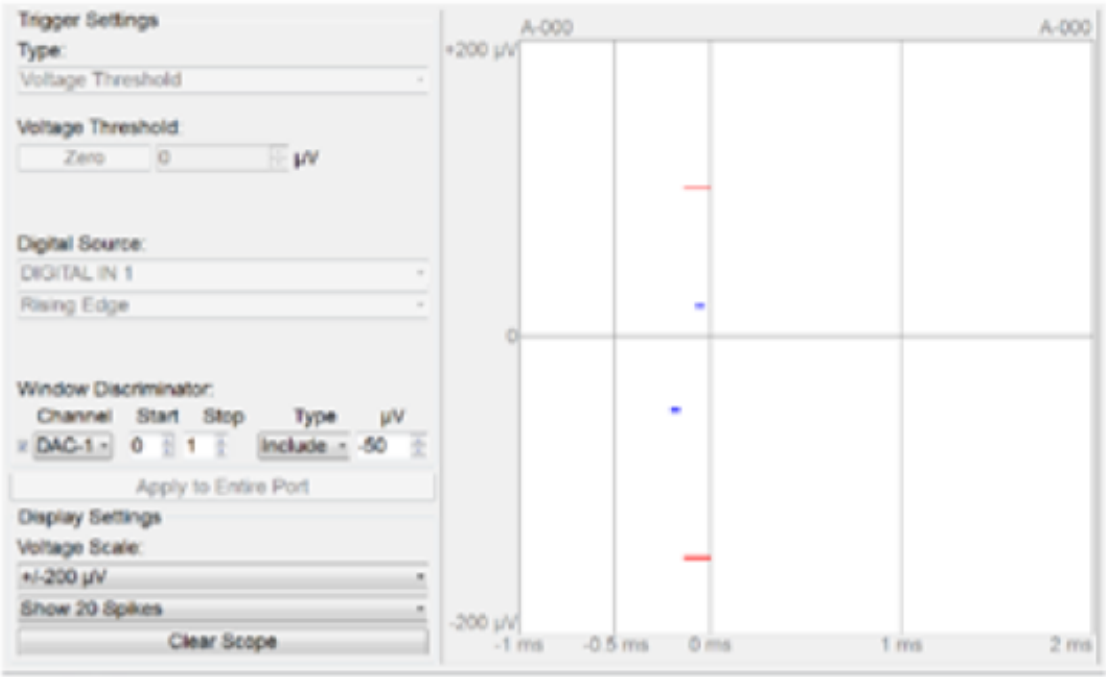

Figure S4.2: Modifications to the graphical user interface (GUI).

A) The original DAC tab was modified to create a new Discriminator tab. Parameters for the currently-selected DAC channel (*i*) are set using the spin box for start (*b*) and stop (*c*) samples, dropdown box that sets the type (*d*) as either "Include" or "Exclude," threshold (*a*) spin box, and check box to enable (*e*) the current DAC channel. Other elements, such as the button to "Set to Selected," are used in the same way as the previous interface (e.g. to route the selected amplifier channel to the highlighted DAC channel as indicated by the radio buttons on the left). **B)** (*Left)* The spike scope was modified as well, to accommodate the additional parameters described in **A**. (*Right)* Each enabled DAC channel has a corresponding window that is either blue ("Include") or red ("Exclude"). Window amplitude for the current channel can be set by clicking within the white window, which places the level for the currently selected DAC channel at the mouse cursor's current amplitude within the spike plot on the right. An "in-action" version of the interface is shown in **Video S4.1**.

Figure S4.3A

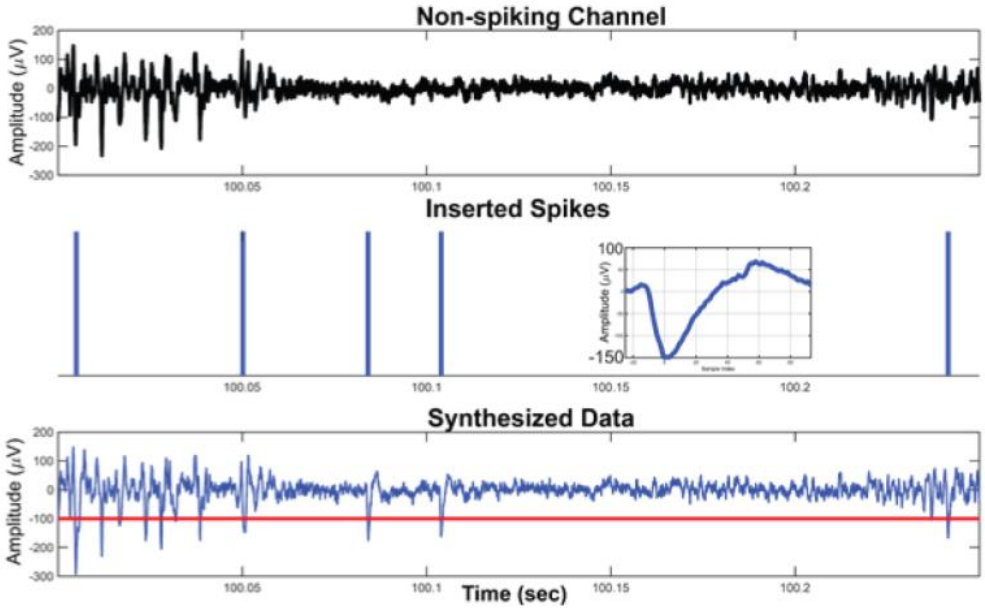

Figure S4.3B

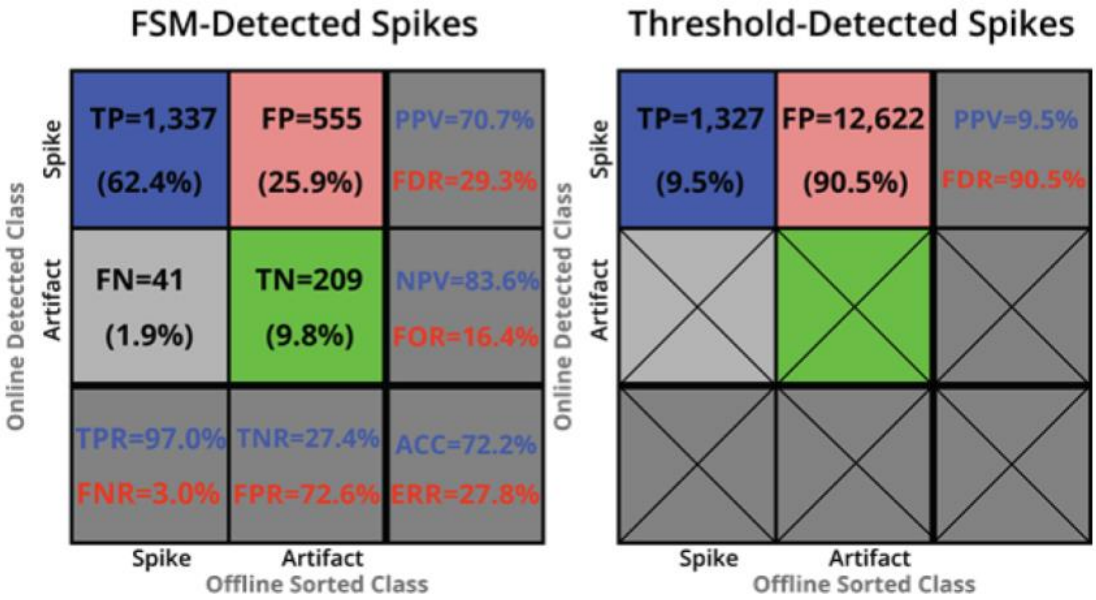

Figure S4.3: Performance on simulation using non-spiking channel with known spike profiles inserted.

A) Overview demonstrating original data (top), spike waveforms (inset) and blue bars indicating times of negative peak onset to superimpose (middle), and generated waveform with known spike times (bottom). Red line on the bottom panel denotes the threshold (-100μV) used in panel B (for the threshold-detected spikes, right panel). In total, 1,500 known spike waveforms were added to the synthetic dataset. **B)** Confusion matrix for performance of both the state machine detector (left) and standard threshold detector (right). The state machine detector is much more robust in picking out the spike waveform from noise. Parameters for both detectors are listed in table S1; although the initial inclusion threshold for the state machine detector is lower (-70μV), it still has a much lower false discovery rate (FDR; 29.3% vs 90.5%). The threshold detector was only allowed to detect spikes on the rising edge of a signal, but still identified many more candidate waveforms despite sharing the same initial inclusion threshold, since the state machine detector is longer (12 samples to completion). Note that the threshold detector only detects spikes (it cannot classify waveforms).

Supplementary Tables

Table S4.1

Date	ID	Duration	Start	Stop	Threshold	Type	Vid	Stim	Simulated
2018-04-27	A0	304.2 sec	0	1	-70 µV	Include	No	No	Yes
2018-04-27	A1	304.2 sec	0 0 1 8	1 5 2 15	-70 µV -200 µV -90 µV -50 µV	Include Exclude Include Exclude	No	No	Yes
2019-01-31	B0	181.1 sec	0 1 5 5	1 7 8 9	-46 µV -66 µV -13 µV 39 µV	Include Exclude Exclude Exclude	No	Yes	No
2019-02-01	C0	162.3 sec	0 1 4 3	1 6 11 15	-40 µV -149 µV -25 µV 13 µV	Include Exclude Exclude Exclude	Yes	No	No
2019-02-01	C1	162.3 sec	0 4 6 7 13 18 19 22	3 24 7 8 15 21 24 24	-25 µV -110 µV -40 µV -30 µV -45 µV -5 µV 60 µV 15 µV	Exclude Exclude Include Include Exclude Exclude Exclude Include	Yes	No	Yes

Table S4.1: Parameters used during *in vivo* recordings.

Three recordings ('A', 'B', and 'C') were taken during separate recording sessions from channels within RFA. Each column details parameters used online or during simulations. For recordings using the spike detection state machine, sub-rows within the 'Start,' 'Stop,' 'Threshold,' and 'Type' columns correspond to parameters given for each DAC channel. Recording *A* was used for simulated performance due to the low noise floor and large, stereotypical spike waveforms. Recording *B* was used to evaluate the latency from spike detection to stimulation. Recording *C* was used to evaluate performance in a "typical use" scenario, where online parameters were set quickly by the operator (*C0*) and compared to both a more stringent parameterization (*C1*) as well as a monopolar threshold simulation (*C2*). In addition, recording *C* contains asynchronized video record, that allowed the verification of manually identified epochs of biological artifact, such as chewing, so that qualitative performance of the different spike detector parameterizations could be assessed. Two additional recordings (*C3* and *C4*) were artificially generated by superimposing large spike waveforms onto an amplifier channel that did not generate much spiking activity. These recordings were used to allow for a known ground truth regarding spike times (Fig. S3).

CHAPTER 5

Recovery vs Restitution: a matter of filter stability

Abstract[52]

The purpose of this study was to characterize injury-related changes in layer 5 neural activity of bilateral motor cortices during movements in the postacute period following stroke. We recorded extracellular field potentials from microwire arrays embedded in the contralateral rostral forelimb area (RFA) and the ipsilateral caudal forelimb area (CFA) with respect to the preferred forelimb used during pellet retrievals by ambulatory rats. A subset of rats received a focal vasoconstrictive ischemia in CFA contralateral to the preferred reaching forelimb, which led to clear motor deficits on this task. Recordings were taken daily during behavior starting in the first week after the implant and continuing for four weeks. Multi-unit spiking activity was analyzed at the levels of individual channels, by area, and as an aggregate proxy for control dynamics that commonly occur during motor behavior. When the compound movements of the behavior were broken down into Reach and Retract phases, it was found that spike counts in RFA of the ipsilesional hemisphere exhibited small but statistically significant changes in average spike counts just prior to the Reach phase and also during the Retract phase when the Ischemia group was compared to Intact controls. There was no significant difference in predictive power for determining successful pellet retrievals when using units from either hemisphere. These findings suggested that while a few cells undergo changes consistent with motor learning during reorganization after stroke, as we had initially hypothesized, most cells do not. Surprisingly,

[52] A modified version of this chapter is in preparation for submission to Nature Communications (Pack et al. 2020). A manuscript that also considers these data but which did not discuss population dynamics is available on a public preprint server (Pack et al. 2020). It is likely that the contents of this dissertation will differ from the final manuscript in academic publication. The contents of this dissertation reflect the interpretation and opinions held by the dissertation author, which may dissent from co-authors on the relative importance or significance of experimental findings.

population-level multiple least-squares (MLS) regression to recover linearized first-order dynamics revealed that individual rats exhibit direct longitudinal trends between the amount of variance explained (R^2_{MLS}) by the dynamical system regression and time from surgery. MLS regression was then constrained to impose skew symmetry on the recovered coefficient matrix, and the amount of variance explained by this regression (R^2_{Skew}) was used together with R^2_{MLS} and total trial duration as a movement covariate to predict daily success rates. Interestingly, the interaction between R^2_{MLS} and R^2_{Skew} was strongly predictive of the pellet retrieval success rate on a given day, despite the inclusion of a movement covariate in the regression model. Optimal performance was not directly related to first-order recursive structure in population activity (R^2_{MLS} is large), but instead it required a specific kind of fixed point dynamics (R^2_{Skew} also large). This result suggests that benefits observed during behavioral interventions applied during the postacute window may arise from diverse mechanisms that are distributed bilaterally throughout the network. While further work will be required to identify which synapse subtypes are involved, it is noted that the timing of re-emerging dynamics coincides with the approximate period in which sprouting axons could be expected to terminate on cortical sensorimotor targets, suggesting this as a critical target for future preclinical experiments in neurorehabilitation.

Introduction

Despite progress in the past three decades, neurorehabilitation research has yet to pinpoint the system that determines the efficacy of behavioral therapy after stroke in modifying the cortical generation of movement. The past era was instead a period of exploration: associative animal models of stroke focused on the indirect correlation of time-dependent anatomical (e.g. Dancause et al. 2005) and physiological changes (e.g. Friel & Nudo 1998, Nudo et al. 2000) with behavioral covariates during the postacute window of increased plasticity that occurs over the course of the first several weeks after ischemia. Reorganization in such studies spans scales that range from transcriptional regulation (Li et al. 2010), to structural changes such as increases in dendritic branching (Withers & Greenough 1989, Jones et al. 1994), to shifts in motor map representation (Nishibe et al. 2010). Other studies of post-injury reorganization in animal models have described neurite outgrowth (Carmichael et al. 2001, Jones & Schallert 1992), dendritic branching (Brown et al. 2010, Bury & Jones 2002), increased expression of growth-associated proteins (Kawamata et al. 1997, Stroemer et al. 1995) and changes in synaptic density (Brown et al. 2008, Jones et al. 1999). Studies of cortical injury in the rat typically involve functional outcomes, such as the ability to successfully traverse a ladder without slipping (Jones et al. 1999); specific forelimb movements while handling pasta (Tennant et al. 2010); or the ratio between successful pellet retrievals and attempted reaches while retrieving a pellet from a pedestal outside of the experimental box (Whishaw et al. 1986, Whishaw & Kolb 1988, Whishaw et al. 1990, Whishaw et al. 1991, Whishaw et al. 1992, Whishaw et al. 1993). However, while these works set the stage for the system identification problem, the inability to directly associate mechanisms of plasticity to both movement and its generation by the cortical engine has precluded an answer.

The future of neurorehabilitation research depends upon the ability to relate these things directly. This is evident in apparent controversies arising from the desire to interpret different results from similar findings in the reaching rat (Alaverdashvili et al. 2008a, Allred et al. 2010, Kirkland et al.

2012). Similarly, it is now controversial to even use the terms *recovery* and *restitution* when describing post-stroke plasticity (Levin et al. 2009, Krakauer et al. 2012, Krakauer & Carmichael 2017). Fortunately, a more recent approach that involves the relation of movement directly to the cortical activity associated with it serves as an example of how this model might be used to describe *recovery* specifically (Ramanathan et al., 2018). Low-frequency oscillations in the local field potential (LFP) were observed during pellet retrievals, disappeared after small ischemic injuries, and re-emerged in rats that regained the ability to perform the behavior. The study focused on quasi-oscillatory activity and the use of alternating current stimulation based on the importance of phase-locked spiking, which is suggested to be an important population feature that intrinsically relates to the generation of movement by the motor cortex. However, a gap in knowledge persists: which circuit components allow such oscillations and the subsequent accurate volitional control of movement by the motor cortex? For example, to what extent do related changes at the level of unit activity pertain to tuning shifts in output or output-adjacent cells, such as is thought to occur during motor learning (e.g. Mitz et al. 1991, Wise et al. 1998, Peters et al. 2017a, Peters et al. 2017b, Papale & Hooks 2018)? Do these changes relate specifically to shifting cortical outputs, such as occurs in Layer 5b of mice during learning of a lever-pressing task (Masamizu et al. 2014)?

Figure 5.1A

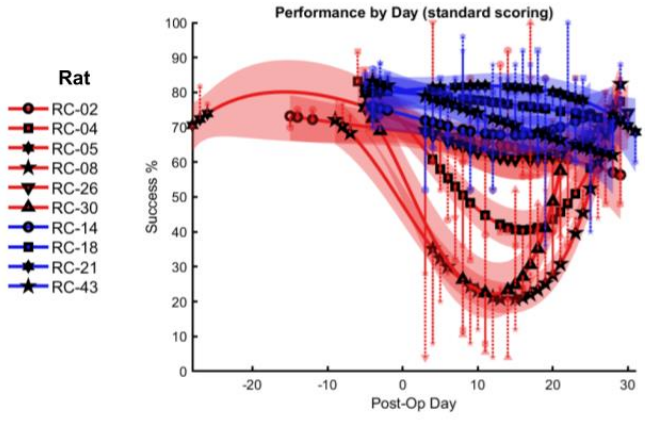

Figure 5.1: Experiment setup

A) Timeline of behavioral endpoints. After surgery, despite unavoidable heterogeneity at the level of individual animals, there was a statistically significant group-level difference in the main **functional outcome**: likelihood of successful pellet retrieval. There was also a significant group by post-op day interaction: rats eventually showed functional changes that allowed them to retrieve pellets successfully at levels that were comparable to pre-surgical baselines.

B) Spatial layout of bilateral cortical recordings and targeted ischemic injury. Recordings were made from the rostral forelimb area (RFA; PM homolog) contralateral to the preferred reaching limb ("contralateral" or "ipsilesional" hemisphere) and the caudal forelimb area (CFA; M1 homolog) ipsilateral to the preferred reaching limb ("ipsilateral" or "contralesional" hemisphere). Motor maps were defined using intracortical microstimulation (ICMS) mapping to identify the forelimb responsive areas, which were then targeted using stereotaxic methods and approximately co-registered on digital maps as shown in insets. Grey circles represent injection sites of Endothelin-1 (ET-1), which were only administered to the **Ischemia** group. Example comparisons of coronal sections corresponding to the targeted CFA territory are shown on the inset on the right. *Credit for data collection, surgical and animal care, and histological analysis described in this chapter goes to Andrea Pack and David Guggenmos; a bulk of these data were collected before the author joined the cortical plasticity lab.*

C) Motor-learning null hypothesis. The original null hypothesis was that units in spared territory of the ipsilesional hemisphere, such as those in RFA, would demonstrate shifts in activation that would more closely align to a particular motor event (*shown: **Grasp** onset*). This would cause individual unit "tunings" to appear to shift closer to the time of that particular event, or cause them to emerge when a given tuning was not initially present (*not shown*). Because the "tunings" would likely be closely associated to the output of the motor area, which exhibits descending corticospinal projections as does the injured CFA, this may be more likely to occur in "output" units so that changes might resemble tuning shifts observed in areas associated with learning.

D) Network reoptimization alternative hypothesis. The alternative hypothesis is that changes are more subtle, which mostly results in no apparent "shift" in tunings to motor events. Instead, plasticity is distributed throughout the network, leading to changes that are significantly evident in the temporal patterns of population activity (when the neural state is considered as a multivariate vector for a single instant in time, as opposed to as a single variable corresponding to the rate of a given cell under consideration). These changes would manifest subtly, as the network converges upon its new preferred state during a "motor re-optimization" process.

Figure 5.1B

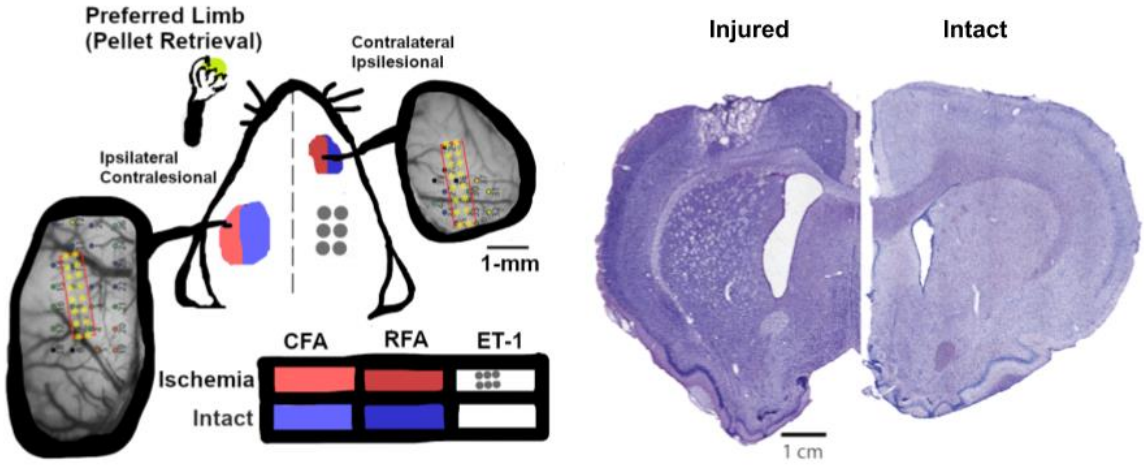

Figure 5.1C

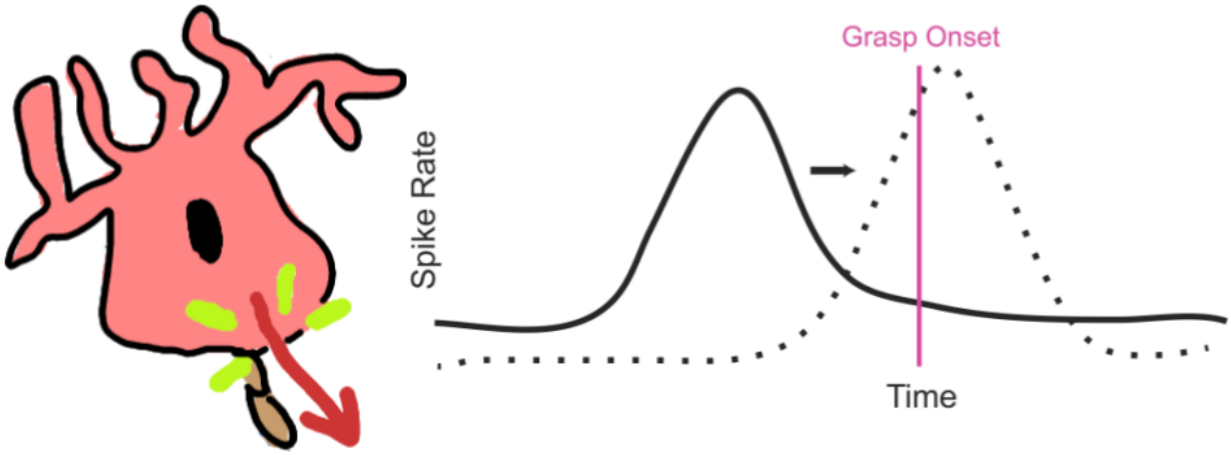

H_0 - "Output" or "output-adjacent" units cause motor *restitution* similar to motor-learning.

Figure 5.1D

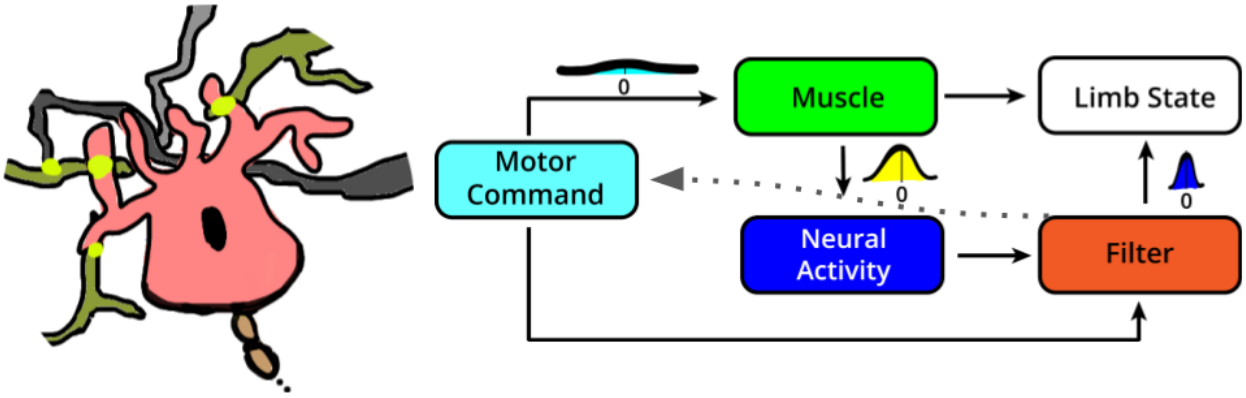

H_A - Network re-optimization convergence dictates *restitution* or *recovery*.

This study describes changes in the motor phenotype of rats retrieving pellets during the first four weeks after a focal, vasoconstrictive ischemia targeted to the caudal forelimb area (CFA) contralateral to the preferred forelimb (**Figure 5.1A,B**). Concurrent extracellular recordings collected from spared rostral forelimb area (RFA) in the same (*ipsilesional*) hemisphere and CFA in the opposite (*contralesional*) hemisphere were used to test the hypothesis that units shift their activity in a process that resembles motor learning (i.e. **Figure 5.1C**). While a statistically significant change in unit activity by group and area during specific movement phases distinguished units on the basis of injury group and area, the small effect size and lack of longitudinal trends differentiating unit spike counts when grouped this way indicates instead that such changes might be driven by a smaller subset of responsive units that do undergo tuning changes as might be expected during motor learning. However, if such a subset represents a relatively small proportion of all units under consideration, why does the majority of unit activity appear to be indifferent to the injury?

Modeling the bilateral unit population as a recursive system, we tested for indicators of fixed point dynamics (i.e. **Figure 5.1D**). This led to a surprising finding. Features of the neural population dynamics predicted daily behavioral performance even though all regressions used data from only stereotyped, successful pellet retrievals. Specifically, the ratio between the amount of variance explained by multiple-least-squares (MLS) optimal regression (R^2_{MLS}) of bilateral population features onto their first difference and the variance explained by the same regression with a skew-symmetry constraint (R^2_{Skew}; Churchland et al. 2012) predicted behavioral performance on a given day even when total trial duration was included in the regression model. These results support the interpretation that while a small portion of cortical units probably do shift tunings in a manner that resembles motor learning, the bulk of changes that differentiate between *restitution* and *recovery* are distributed among synapses throughout the cerebral cortex in both hemispheres.

Results

Trends in pellet retrieval performance

Young-adult (3-4 months) male Long-Evans rats were required to successfully retrieve[53] at least 42 of 60 pellets (70%) on three separate days prior to study inclusion (**Baseline**; **Figure 5.1A**, *postoperative days with values less than zero*). A binomial generalized linear mixed-effects (GLME) model with a logistic link function was used for the number of successfully retrieved pellets given the total number of pellets was fit to data from only **Baseline** sessions using a fixed intercept and the fixed effect of *Group* (**Intact** or **Ischemia**) and a random intercept by *Animal* (**Table S5.1**: *Model-1*). There was no statistically significant difference between the two levels of *Group* for pellet retrieval success rate during these criterion sessions (**Intact**, $n = 4$; **Ischemia**, $n = 6$; $R^2 = 0.14$, $p = 0.178$, $t(28) = 1.382$; **Figure S5.1A**), indicating that trends were not driven by an initial intrinsic difference in the capacity of individual rats to retrieve pellets.

A similar binomial GLME model with logistic link function was used to address all pellet retrieval sessions. This model added a categorical fixed-effect indicating if retrievals occurred during **Baseline** (*Pre-vs-Post*) as well as an interaction of this term with *Group* (**Table S5.1**: *Model-2*). In general, performance declined across groups after surgery ($R^2 = 0.50$, fixed effect of *Pre-vs-Post:* $p << 0.001$, $t(219) = -14.006$; **Figure 5.1A**), although this decline was significantly less in the **Intact** group (fixed effect interaction of *Pre-vs-Post*[**Post**] and *Group*[**Intact**]: $p << 0.001$, $t(219) = 5.63$).

A third binomial GLME model with logistic link function was fit to address trends in performance after the surgery (only *Pre-vs-Post*[**Post**] sessions were included; **Table S5.1**: *Model-3*). Because of the characteristic trend of **Ischemia** rats to show a large decline in performance

[53] Definitions of successful retrieval are elaborated in the **Methods** section. Pellet retrievals were scored for success using two different sets of criteria. Scoring to determine success rates used for initial inclusion and overall trends in behavioral performance (i.e. *Models 1-3*) allowed up to three reach attempts as long as the pellet was not dislodged from the platform before a trial was marked as unsuccessful.

during the first and second weeks after the injury (e.g. **Figure 5.1A**), the random effect of *Animal* included not only a random intercept term, but also a coefficient for *Day* and a cubic transformation[54] of *Day* (*Day-Cubed*). The fixed effects were an intercept term, and each main factor as well as the interaction between *Group* and *Day-Cubed*. The use of *Day-Cubed* in the fixed effect interaction reflects the motivation to distinguish between the tendency of one group to improve behavior by day, which typically occurred in a nonlinear fashion. As expected, the **Intact** rats were significantly better and more consistent across days at retrieving pellets, as indicated by a smaller coefficient for the interaction effect of *Group* and *Day-Cubed* (R^2 = 0.67, p = 0.019, $t(189)$ = -2.36). While there were significant differences between the stricter scoring required to ensure that only trials with stereotyped movements were used for the subsequent neural analyses (*Method:* R^2=0.79, p = 0.003, $t(358)$ = 8.89; **Table S5.1**: *Model-4*), **Intact** and **Ischemia** rats demonstrated comparable recovery trajectories by group and were still

[54] It should be noted that this precludes the utility of such a model in predicting behavior outside the range of days observed in these experiments. Such a use-case was not the intent in this experiment; the motivation was simply to fit individual rat trends in performance while addressing longitudinal correlations in the data.

differentiable on the basis of *Group* (p = 0.002, $t(358)$ = 10.1; Figure S5.1B).

Figure 5.2A

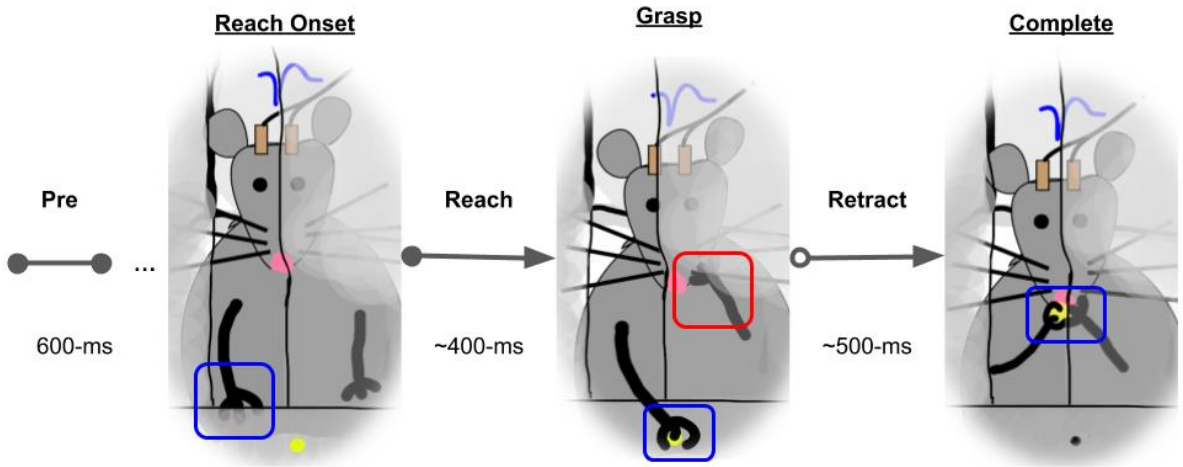

Figure 5.2: Spike count trends during specific phases of movement for individual channel activity.

A) Illustration of motor events and behavioral phases. The phases of the pellet retrieval rat behavioral model have been well-described elsewhere. In this study, we focused on key events that were required in order to define a trial for consideration in further analyses: ***Reach Onset***, ***Grasp***, and ***Complete***. These events relationally defined three phases of the behavior that formed epochs over which spikes were counted: ***Pre***, ***Reach***, and ***Retract***.

B) Aggregate detrended spike count differences during *Pre* phase. Multi-unit activity was counted during stereotyped phases of the reach, grasp, and retrieval behavior. Because no "preparatory" cue was used, premotor activity (**Pre** phase) was estimated as spike counts during a fixed 600-ms epoch beginning 1,350-ms prior to the Grasp event based on the distribution of reach/advance phase durations. This period was selected with the goal that, on average, it was temporally close to the rest of the behavior, far enough temporally to avoid overlap with motor phases, and long enough to observe enough spikes that a Poisson model could be accurately reconstructed.

C) Aggregate detrended spike count differences during *Reach* phase. The two phases, **reach/advance** and **retract** were defined using three tagged behavioral landmarks that could be readily identified during manual video scoring used to refine behavioral synchronizations obtained via digital or analog inputs collected from the same acquisition circuit as the extracellular field-potential time-series. ***Reach Onset*** was defined as the earliest frame in

which the rat began a forward motion of the forelimb from inside the behavioral box toward the pellet platform outside of the box. ***Grasp*** was defined as the first frame in which the digits began to clearly close around the pellet (a phenomenon that was notably lacking at early time-points for multiple rats in the ***Ischemia*** group). This was often preceded by a spreading of the digits that has been described elsewhere as ***Arpeggio***, although the close temporal proximity of this behavioral element relative to the camera frame-rate precluded it or other similar more-granular elements of behavior from further consideration in analyses of neural time-series. The **reach/advance** phase is defined as the times between and including the times corresponding to the tagged ***Reach Onset*** and ***Grasp***, meaning that there is a temporal jitter on the order of 30-ms around this epoch due to the camera frame rate.

D) Aggregate detrended spike count differences during *Retract* phase. The ***retract*** phase was bounded by the ***Grasp*** and the third tagged behavioral element: ***Complete***, which was the first frame in which the rat had fully returned its paw through the opening at the front of the box. Because all three tags were required for a reach to be considered in neural analyses, (common) trials that ended with a "functional success," in which the rat flailed multiple times prior to grasping the pellet, were excluded from consideration in neural analyses.

Figure 5.2B

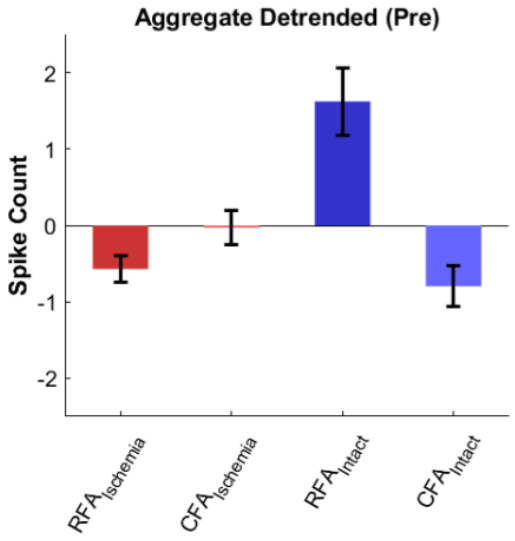

Figure 5.2C

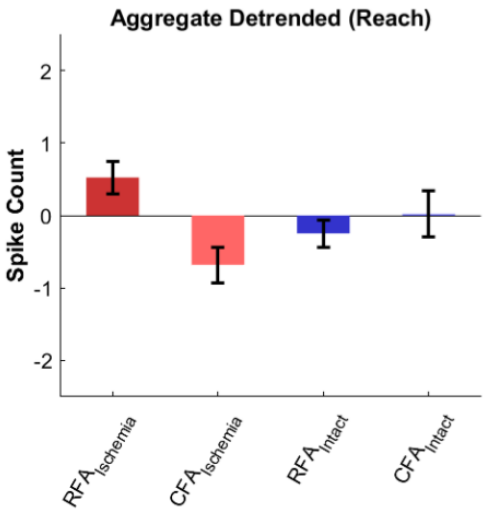

Figure 5.2D

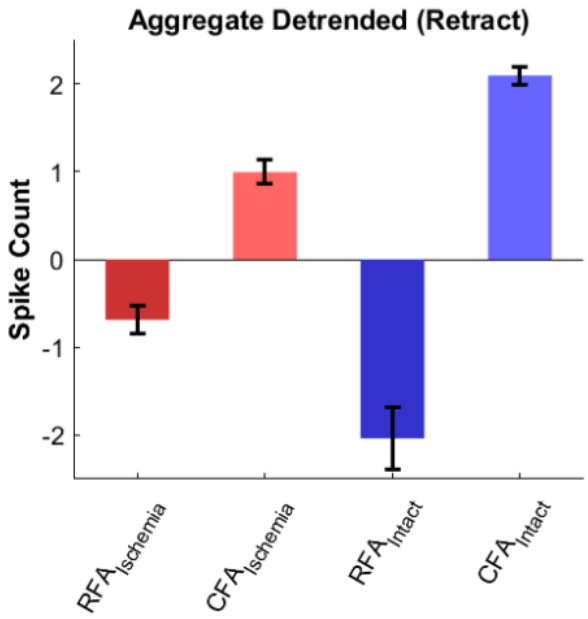

Trends in pellet retrieval trial duration

The pellet retrieval behavior was broken into discrete phases that were delimited by three behavioral events: **Reach Onset**, **Grasp**, and **Complete** (**Figure 5.2A**). Each event was required for further analytical consideration of a given pellet retrieval trial. These behavioral landmarks demarcate three phases of the movement: **Pre**, **Reach**, and **Retract** (**Figure 5.2A**; definitions in **Methods** section). The phasic delimitation of rat pellet retrieval movements in this manner has been suggested by the past work of other groups; in fact, it is likely that the behavior could be better-described with the addition of landmarks such as the “arpeggio” that occurs when the rat extends each digit just prior to the grasp (Whishaw & Pellis 1990, Whishaw et al. 1991). However, in consideration of the camera frame rate, rat group sizes, and the decision to intentionally limit the number of retrieval trials (in an attempt to mitigate the effects of behavioral rehabilitation), the two longest and most-clearly distinct phases of the movement were used in this study.

In general, the stricter criteria for trial inclusion eliminated trials when a behavioral event was missing: applying this restriction retained 4,294 total **Successful** and **Unsuccessful** unique

pellet retrieval trials for which **Reach Onset**, **Grasp**, and **Complete** events (as well as a pellet: in many instances, the rat attempted to retrieve a pellet despite its absence from the platform). The majority of these trials were included after application of thresholds determined for total duration (1.5-seconds, 98.9% of trials met criterion), **Reach** phase duration (0.65-seconds, 96.7% of trials met criterion), or **Retract** phase duration (0.75-seconds, 95.6% of trials met criterion). Of these duration-based exclusions, the majority corresponded to **Unsuccessful** trials in **Intact** rats (**Figure S5.1C**).

The length of phases observed during the behavior were consistent with past studies in the reaching rat (**Table 5.1**; Whishaw & Kolb 1988). A GLME that included fixed-effect terms for an intercept term, *Group, Day*, and a *Group* by *Day* interaction, as well as a random effect intercept and coefficients for *Day* grouped by rat was used to fit **Trial Duration** for all unique trials, without considering duration-based exclusions or outcome. A log link function was used in order to improve heteroskedasticity among longer trials (**Table S5.1**: *Model-5,* R^2 = 0.28). ANOVA indicated that none of the fixed-effect terms were statistically significant (**Figure S5.2A**). However, the model was substantially improved after reducing the dataset to 1,632 unique trials by removing **Unsuccessful** trials as well as the remaining outliers based on phase duration thresholds (**Table S5.1**: *Model-6,* R^2 = 0.42). The improvement in fit was not due to the fixed effect coefficients, with ANOVA indicating that only the fixed-effect intercept was statistically significant. Therefore, the improved fit reflected the heterogeneous longitudinal changes in **Total Duration** at the level of individual rats (**Figure S5.2B**), which most likely related qualitatively to the diversity of strategies adopted by the rats after surgical implant, as observed during video scoring.

GLME models for fitting the remaining movement timing metadata (**Table S5.1**: *Models 7-9*) focused exclusively on the reduced dataset of 1,632 **Successful** retrievals. In addition to the model terms used for regression of **Total Duration**, each of these models used **Total Duration**

as an additional random effect grouped by rat. Most rats (6 of 10; random effect coefficient for *Day* with $p > 0.05$) maintained a relatively constant **Reach Duration** over the course of the postacute period (**Table S5.1**: *Model-7,* R^2=0.46). One rat (RC-18) in the **Intact** group employed a comparatively interesting strategy in which he extended his paw much more slowly and deliberately to the point that it qualitatively seemed exploratory rather than a short and deliberate movement like the rest (**Figure S5.2C** random intercept effect grouped by rat estimates that this phase on average lasted 180-ms longer for this particular animal compared to all others; $p = 0.027$).

Retract Duration trends were also more strongly-associated with individual rats, with only the Intercept term estimated as a significant fixed effect (**Table S5.1**: *Model-8,* R^2=0.25). Again, changes were heterogeneous, with some rats increasing and some rats decreasing in a manner that did not necessarily depend upon cohort (**Figure S5.2D**). The ratio between the **Reach** and **Retract** phases tended to remain constant (**Figure S5.2E**), although rats in the **Ischemia** group trended towards a significantly shorter relative proportion of each trial spend in the **Reach** phase ($p = 0.060$, $t(1,628) = -1.88$; **Table S5.1**: *Model-9,* R^2=0.17).

Trends in spike counts during phases of movement

Multi-unit spikes were counted during each phase as a proxy for cortical excitability of cells near each recording channel (**Table 5.2**). Because there was no pre-movement cue in this task, a fixed 600-ms epoch (**Pre**) starting 1,350-ms prior to the **Grasp** was used to set a baseline estimate of premotor activity. Spike counts during the **Pre** epoch were regressed using a binomial GLME with a logistic link function to estimate the fraction of “pre-movement” spikes, given the combination of *Group* and *Area* (levels: **RFA** and **CFA**), and the total number of spikes predicted by weekly trends on a per-animal basis (**Table S5.1**: *Model-10,* R^2=0.38). There was a statistically significant effect of the interaction *Group* by *Area* ($p = 0.001$, $t(68) = -$

3.37), indicating a significant relative decrease in the likelihood of spikes occurring during this period in **RFA** of **Ischemia** rats (**Figure 5.2B**).

Models to detrend spike counts during **Reach** and **Retract** phases additionally contained the duration of those phases as a covariate, since unlike the **Pre** phase (which by definition was a fixed epoch), these two phases were demarcated by behavioral events (**Figure 5.2A**). During the **Reach** phase, values for each group and area combination were similar (**Figure 5.2C**; **Table S5.1**: *Model-11,* R^2=0.79). Perhaps most-interestingly, when spikes were counted during the **Retract** phase, there was a statistically significant interaction effect (p = 0.009, $t(68)$ = 2.68; **Table S5.1**: *Model-12*, R^2 = 0.86) indicating that the likelihood of spikes in **RFA** of **Ischemia** rats during this phase was relatively closer to the likelihood of spikes in **CFA** during the same phase, compared to the relative likelihoods of **RFA** and **CFA** spikes in **Intact** rats during the **Retract** phase (*log-odds* = 1.05; **Figure 5.2D**). While a model specified in this way suggests that the effect size (Cohen's d) is approximately 0.66, post-hoc comparison by week and area indicates that such estimates of effect size range from 0.23 and 1.53 (**Table 5.3**). When translating to estimated total spike counts, these differences ultimately yield expected differences on the order of 1 or 2 spikes above or below an average of roughly 20 spikes expected during the **Retract** phase across *Area, Group*, and *Week* differences (**Figure 5.2D**). The same effect was further diminished when data were examined on a per-*Day* as opposed to per-*Week* basis (**Figure S5.3**). It is unclear whether such changes reflect salient changes in a subset of responsive units; whether they reflect differences in **Retract** phase duration (**Figure S5.2D**); or if the relatively linear falloff in expected spike counts over time (**Figure 5.2D**, *top panel*) reflects other non-specific processes related to the general loss in sensitivity and ability to detect units, such as probably happens during gliosis (Chestek et al. 2007). Classification of **Support** forelimb movements (**Figure 5.2A**, *red box*) as belonging to a particular phase of the behavior suggests that the timing of movements in the non-reaching forelimb is better accounted for on a per-

Animal basis, as opposed to by *Day* and especially *Group*, which was the least-predictive feature in a trained ensemble classifier model (**Figure S5.5A**).

Prediction of trial outcomes using spike counts during phases of movement

The previous results suggest that if reoptimization occurs at the level of the cortical microcircuit, then it probably only occurs in a small subset of units whose changes are washed out when activity is averaged as a population. Qualitative observations of such changes agree with the model findings: there are clear longitudinal trends in spike rate surrounding the **Grasp** at the level of multi-unit activity on individual microwire array channels, beyond what would be expected due to loss of signal sensitivity due to apparent electrode impedance increases (e.g. **Figure S5.4F**, a channel in animal RC-05 that was associated to the lateral microwire array in distal forelimb ICMS motor territory in RFA shows a shift in timing of peak excitation). If the movement-coherent changes in these units contributes to *functional* reoptimization that correlates directly with changes in the motor phenotype, then the changed activity of such units should provide predictive power in classifying single trial outcomes[55]. Alternatively, changes, such as those observed by Ramanathan and colleagues, might be explained more simply by direct changes in motor phenotype, such as an increase in movement speed (Ramanathan et al. 2018).

[55] This is predicated upon the traditional model assumption that successful pellet retrievals are a useful covariate of motor reorganization such as occurs after focal cortical ischemia.

Figure 5.3A

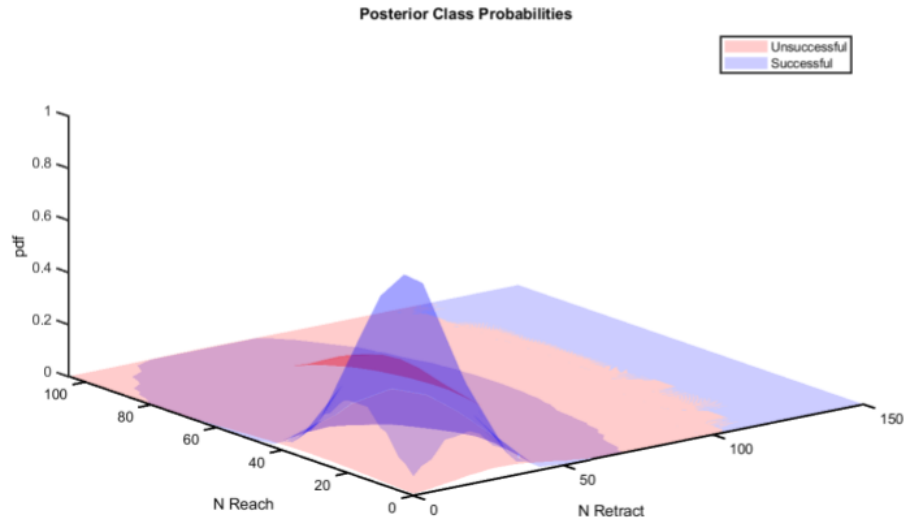

Figure 5.3B

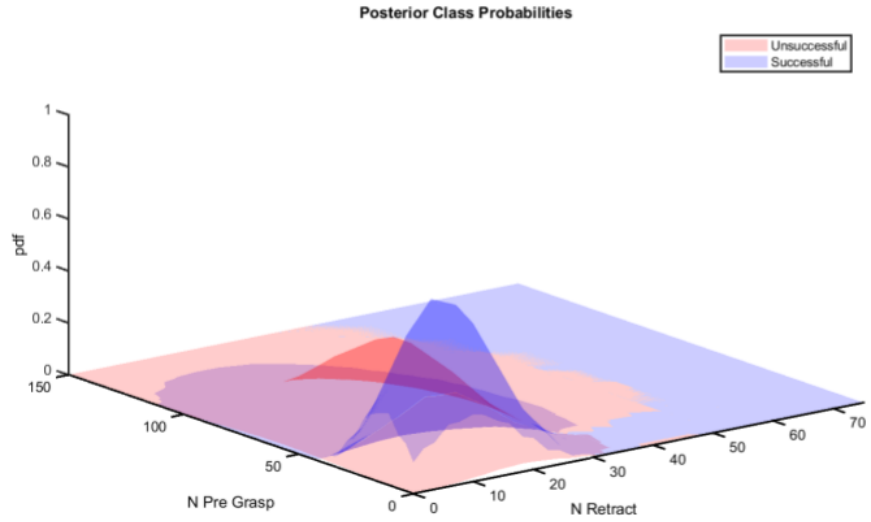

Figure 5.3C

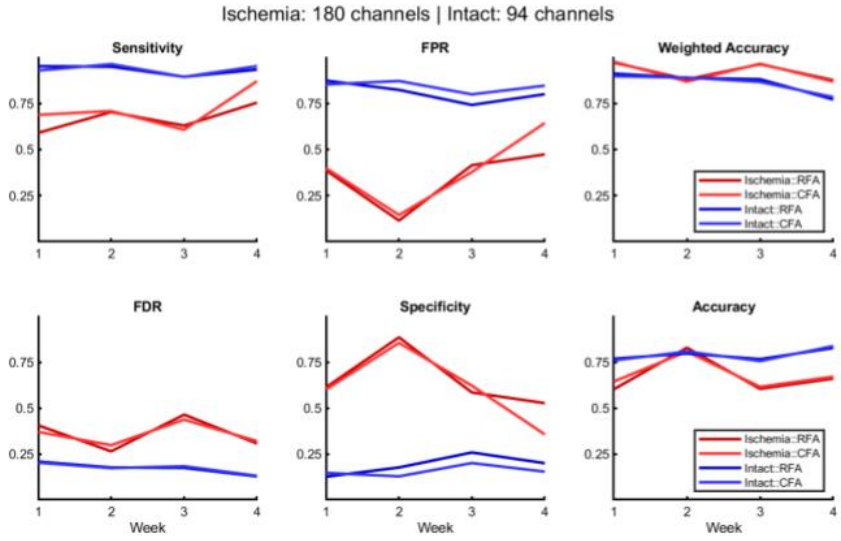

Figure 5.3D

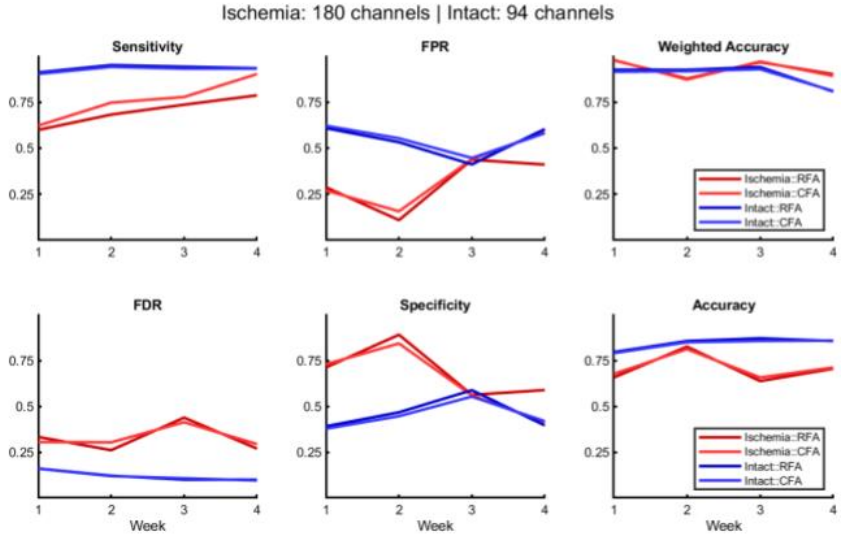

Figure 5.3: Using spike counts during specific phases of

movement to predict individual trial outcomes.
A) Predicting trial outcomes using individual channel activity is typically inaccurate. This joint-distribution shows two of the predictors: the number of spikes counted during the **Reach** phase and the number of spikes counted during the **Retract** phase. While the likelihood of a successful trial has a much sharper peak in the joint conditional posterior distribution estimated by the naive Bayes classifier ensemble, the distribution for likelihood of an unsuccessful trial overlaps considerably with it.
B) Example with better posterior joint distribution separation. This joint-distribution shows two of the predictors: the number of spikes counted during the **"Pre-Grasp"** phase and the number of spikes counted during the **Retract** phase. Because there are multiple predictors, the probability manifold is difficult to visualize in one image without dimensionality reduction or multiple joint conditional plots such as this one and the one shown in **Panel A**. In this case, the distribution peaks show slightly better separation, suggesting a stronger substrate for a decision-surface threshold in predicting successful or unsuccessful trials.
C) Ensemble prediction confusion metrics using only phase-specific spike counts. Phase-specific activity in Intact rats is sensitive to, but not specific for trial outcome success. Predictions are therefore most-influenced by the prior on overall success rate, as indicated by the relative false positive rate (FPR) between Intact and Ischemia rats.
D) Ensemble prediction confusion metrics using phase-specific spike counts supplemented with total trial duration and reach phase duration. Including a covariate for movement speed improves the specificity of Intact rat single-trial outcome predictions and lowers the FPR.

To test this, two classification models were estimated (**Table S5.1**: *Models 13-14*). Each model consisted of an ensemble of naive Bayesian classifiers estimated individually for each unique combination of micro-wire channel and postoperative *Week*. Both predicted individual trial *Outcome* (**Successful** or **Unsuccessful**) by recovering the joint posterior probability for each category given the spike counts during the **Pre**, **Reach**, and **Retract** phases (e.g. **Figure 5.3A,B** show cases with poor and moderate separability, respectively). The extended model additionally used the **Total Duration** and **Reach Phase Duration** of the trial to predict the categorical **Unsuccessful** or **Successful** outcome. General trends in classifier accuracy tended to relate most strongly to the average weekly performance by group rather than qualities of individual channels (**Figure 5.3C**). Inclusion of **Duration** variables as a covariate improved performance, but did not substantially differentiate predictive power on the basis of channel

differences by area (**Figure 5.3D**). In general, this strategy likely suffers from heterogeneity of the neural response during **Unsuccessful** pellet retrievals; therefore, during the population analyses, only **Successful** trials were considered. Similarly, applying principal components analysis (PCA) at the level of individual units to uncover longitudinal trends on the basis of spike counts during the **Reach** or **Retract** phases (**Figure S5.6A,B**) did not show a meaningful differentiation of units on the basis of *Area* or *Group* (**Figure S5.6C,D**).

Neural population dynamics

The largest portion of variance in the motor cortex neural state during pellet retrievals should relate to the largest portion of variance in the limb state. Movement implies the existence of a dynamical system describing the physics of the position of the limb. Therefore, an initial assumption was that dynamics in the neural population state that mirror some predictive model of the limb state were to be expected. Furthermore, if plasticity occurs diffusely throughout the network, then qualitative changes in neural population dynamics should be detected in the combined patterns of activity from units, even if they are not output or output-adjacent and therefore do not demonstrate clear changes in tuning (Michaels et al. 2016). Previous studies have suggested that system dynamics can be well-approximated using a first-order linearized system to fit the main population-level features of the neural population (Churchland et al. 2012). We decomposed the neural state of **Successful** pellet retrievals using multi-unit spike rates from individual microwire channels from epochs that spanned a fixed period from 660-ms prior to 330-ms after alignment relative to **Reach** or **Grasp** events. After subtracting the average expected spike rates on a per-channel basis using PCA. The top-12 principal components were retained and their scores were used as the neural state variable on a per-recording basis. Because a fundamental prerequisite in describing such dynamics is the criterion that the modeled system does in fact represent the observed data (Lebedev et al. 2019), we characterized the amount of the original rates that were explained by the retained principal components. For a 32-channel array, if each channel contributed independent white Gaussian noise,

then the top-12 components would be expected to explain 37.5% of the data. In only a few cases observed did the top-12 components explain less than 80% of the data (**Figure S5.7A**), indicating that the neural state variable did not over-reduce the population data.

Following the procedures of (Churchland et al. 2012), the first difference of the neural state variable was fit by MLS regression of the neural state to recover the linear transformation matrix $\mathbf{M}_{MLS}$ or $\mathbf{M}_{Skew}$, which were used to compute the associated values of R^2_{MLS} and R^2_{Skew}. To test the initial assumption--that dynamics in the neural state were present in a ubiquitous manner--we fit R^2_{MLS} using a GLME with fixed terms of intercept and the ordinal dummy variable of *Week*, as well as a random effect of *Day* and *Day-Cubed* grouped by *Animal* (**Table S5.1**: *Model-15;* $R^2 = 0.66$). While there was not a significant fixed effect for *Week* ($p = 0.403$, $F(4, 111) = 1.014$), linearized first-order dynamics were not always present as was evident from the longitudinal trends by *Animal* (4 of 6 rats had a significant random effect coefficient related to *Day;* **Figure 5.4A**). This was not due to the loss of units as might result due to electrode degradation: on the contrary, dynamics were typically not evident until the end of the second week, with the exception of one **Intact** rat in which dynamics were present as early as the first week and one **Ischemia** rat that did not show strong evidence of dynamics in general (**Figure 5.4A**). Due to the constraints on both number of channels and also total trial counts, these trends were only available in two rats from the **Intact** group (one of which only had values from the first two weeks) and four rats from the **Ischemia** group. Therefore, a random effects GLME model was fit to predict behavioral Performance using a fixed effect intercept and the factorial interaction of *Group* and *Day*, while specifying intercept, *Duration*, and R^2_{MLS} terms grouped by *Animal* for the random effects (**Table S5.1**: *Model-16*; $R^2 = 0.96$). Each of the four **Ischemia** rats demonstrated a significant random effect of R^2_{MLS}. Puzzlingly, in the three **Ischemia** rats for which R^2_{MLS} increased over time, there was a negative association of R^2_{MLS} with behavioral performance.

Figure 5.4A

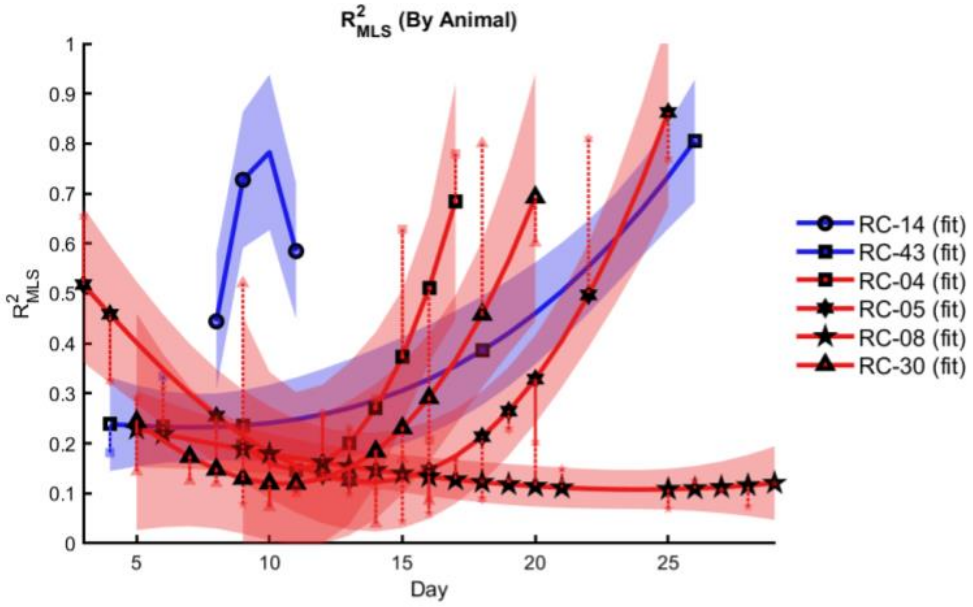

Figure 5.4B

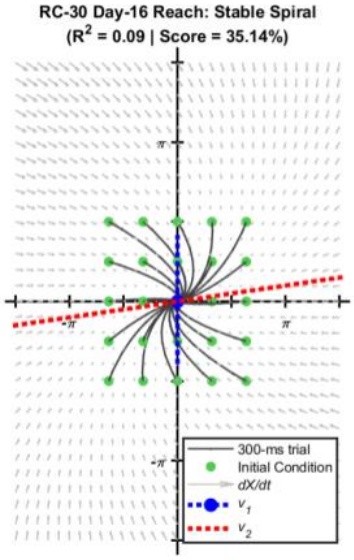

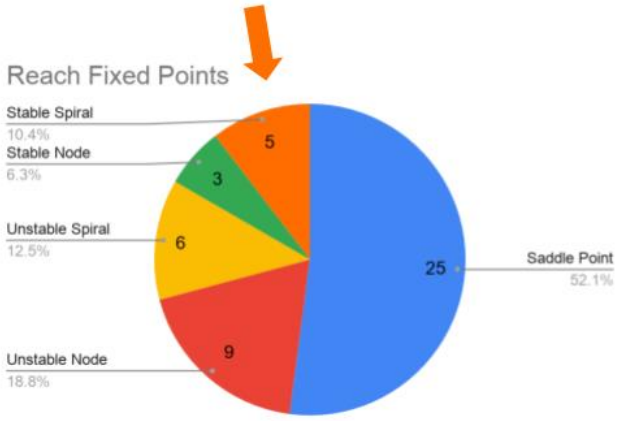

Figure 5.4C

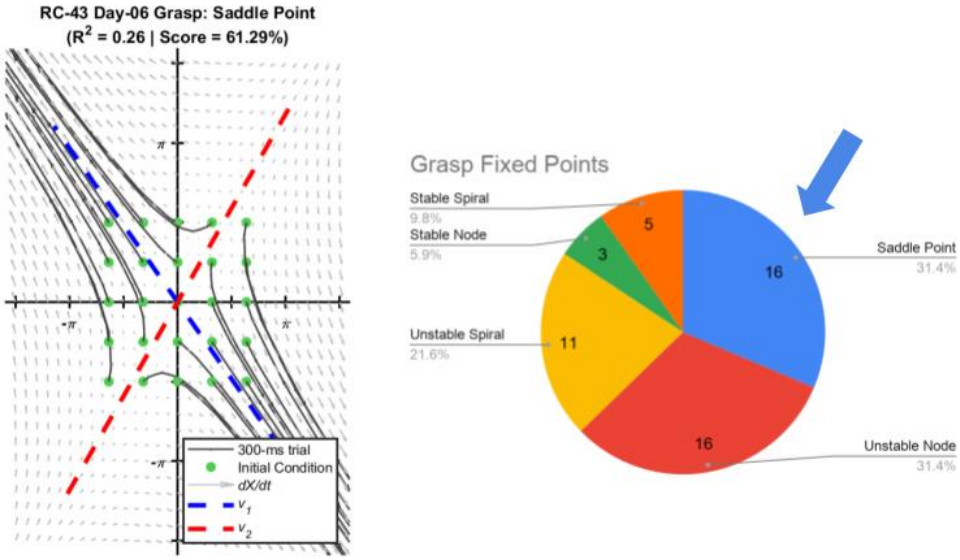

Figure 5.4D

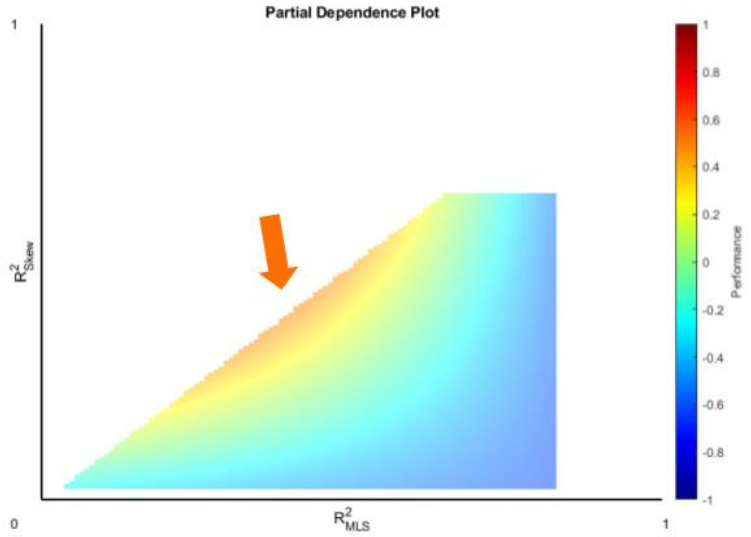

Figure 5.4: Population dynamics and motor performance.

A) Adjusted R^2_{MLS} by animal for first-order population dynamics as a function of postoperative day. If correlators of functional outcomes at the level of individual channel multi-unit were modest or better-explained by simple features of movement, such as the total overall duration of the pellet retrieval, then perhaps averaging single-channel trial activity across trials obscures neural signals related to the most-salient computations related to behavioral reorganization. While the lack of strong longitudinal trends by group that relate to aggregate unit activity at the level of individual channels is surprising, it is possible that very different mechanisms from motor learning are invoked. Using principal components analysis to define "neural state" variables comprised of scalar combinations of the spike rate estimate for each channel concurrently, we observed that a simple multiple-least-squares regression of the top-12 principal components onto their first difference yielded the most-striking trends in the neural data that were striking with respect to postoperative day. With the exception of RC-08 (***Ischemia***), rats tended to increase the ability to fit linearized dynamics as a function of postoperative day. The relative low percent of the data explained for RC-08 using the top-12 principal components suggests that the effect in this animal may simply be driven due by the loss of behaviorally-related signals.
B) Fixed points during *Reach* and example. This example is a stable spiral: such a population vector could form in relation to a steady-state calculation related to moving to a specific point in space, as may be necessary during reaching.
C) Fixed points during *Grasp* and example. This example is a saddle point. The bifurcation formed by points on either side of the dashed red line could relate to processes such as successfully or unsuccessfully realizing that the pellet has been contacted, which may lead to diverging state transitions with respect to the neural state space.
D) Partial Dependence of Performance on R^2_{MLS} & R^2_{Skew}. As R^2_{Skew} becomes an accurate approximation to the data, then the better that the population trends are fit by imposing constraints that impose rotatory fixed-point dynamics on the first-order planar dynamics, predicted outcomes improve (*orange arrow*). Because R^2_{skew} must be less-than or equal-to R^2_{MLS}, by definition, the impossible response region in the partial-dependence contour is removed. In this model, likelihood of pellet retrieval success on a given day (a proportion from 0 to 1) was scaled between -1 and 1 using a scaling of the hyperbolic arctangent transformation so that "majority-success" values were closer to 1 and "majority-failure" values were closer to -1. Note that for any value of R^2_{MLS}, as R^2_{skew} decreases, the predicted performance is worse (interaction effect is statistically significant; $F = 4.99$, $DF = 100$, $p = 0.028$).

This finding was unexpected: if neural dynamics were present, and only data from successful trials was used to estimate the neural dynamics, then why would a stronger indicator of a first-order dynamical system correlate with poorer behavioral outcomes? If such a dynamical system is intrinsically related to the generation of movement by the cerebral cortex, then the opposite is expected. There are some caveats about this statement: first, the assumption that first-order linearized dynamics provide a useful approximation to the nonlinear neural activity around the motor

behavior may not hold. While such an assumption is worth examining in its own right, because it is beyond the scope of the present study, we focused on a second possibility: not only the presence of first-order dynamics, but the specific kind of fixed point indicated by the dynamical system is a qualitatively important indicator of behavioral outcomes that relate to accurate generation of movement. For example, a non-isolated fixed point that forms a plane of fixed points with rotatory structure has been suggested previously as an intrinsic feature of motor cortical activity (Churchland et al. 2012).

In these data, during alignment to the **Reach**, when considering the primary plane formed by the two basis vectors recovered during the MLS regression which captured the largest percent of the variance in neural state, fixed point analysis seldom indicated the presence of stable spirals and never stable centers. Trajectories with rotatory structure were often only able to reconstruct the observed system poorly (**Figure 5.4B**). By comparison, a substantial portion of the fixed point dynamics during both the **Reach** and during the **Grasp** indicated the presence of a saddle point (**Figure 5.4C**). A random effects GLME was fit using only a fixed effect intercept term and two random effects groupings: an intercept term, as well as the factorial interactions of *Classification* and R^2_{MLS}, grouped by *Alignment* (**Reach** or **Grasp**), and a second random effect of intercept and *Day* grouped by *Animal* (**Table S5.1**: *Model-17*; $R^2 = 0.82$). Interestingly, the random effects model indicated that when a stable node was present during the **Reach**, there was a positive correlation between system reconstruction accuracy and the performance on a given day (**Table 5.4**; $p = 0.009$, $t(98) = 2.65$). Similarly, when a saddle point was detected during the **Grasp**, there was a positive correlation between system reconstruction accuracy and the performance on a given day (**Table 5.4**; $p = 0.005$, $t(98) = 2.89$). These results suggest the significance of different fixed points at distinct phases of the behavior, which may relate to the expected dynamics during a behavior: for example, as the forelimb moves toward a pellet of consistent size and shape that always resides at the same

location, then a transient and stable fixed point in the neural state may reflect the learned expectation about these properties which relate to the movement of the limb.

The lack of fixed points with rotatory structure suggests that the MLS linearization probably contains some amount of inaccuracy due to the selected timescale, which may not always reflect a stationary system with a single fixed point, as well as due to the general noise that is expected from stochastic point processes (spikes), which act as noisy signalers of the underlying system dynamics. Therefore, fixed point analysis of only the MLS regression transformation may not capture the full picture. In order to compare our results with others, we estimated a final GLME to fit the *Performance* response surface associated with the factorial fixed effect interactions of R^2_{MLS}, R^2_{Skew}, *Group*, and *Explained*[56] as well as random effect intercept, *Day*, and *Duration* terms grouped by *Animal* (**Table S5.1**: *Model-18*; $R^2 = 0.85$), since R^2_{Skew} may be a more robust descriptor of the presence of rotatory structure in the data compared to categorization of least-squares optimal fixed points. Interestingly, for **Ischemia** rats, there is a negative correlation between the interaction of R^2_{MLS} and R^2_{Skew} ($p = 0.028$, $t(100) = -2.23$), but a positive correlation for R^2_{Skew} ($p = 0.055$, $t(100) = 1.94$). When R^2_{Skew} is large, it indicates that the cortical dynamics are capable of forming a stable fixed point manifold, which relates to the evolution of the neural system state through time. While these data can only provide a sparse characterization of system states, the performance response surface that relates R^2_{MLS} and R^2_{Skew} suggests that during the accurate generation of movement by the cerebral cortex, the non-isolated fixed point must exhibit rotatory structure to indicate that the neural controller generates *optimal* movements (**Figure 5.4D**).

[56] The total amount of the original spike rate data explained by the included principal components.

Discussion

In this study, we examined neural unit and population signals from bilateral motor cortex in a rat model of ischemic stroke during a skillful forelimb movement sequence. A subset of units drove small but significant trends in spike rate that distinguished between **Intact** and **Ischemia** groups on the basis of motor cortical area. These units demonstrated changes in tuning, as evidenced by the timing of a clear peak in average excitation with respect to behavioral events, suggesting that motor-learning-like phenomena may account for changes observed during the reoptimization of movement such as occurs after stroke in a relatively small number of cells. However, it is unclear whether such changes reflect an abstract factor related to the functional execution of the task; if they relate to the recruitment of different muscles and/or nervous subsystems during compensatory task restitution; or if they simply reflect changes in overall movement speed as indicated by clear reductions in total time required to execute the pellet retrieval behavior.

By contrast, neural population signals were not expected to change substantially due to the constraints imposed by movement sequence similarities required to successfully perform the pellet retrieval behavior. Instead, the bilateral motor cortices typically did not exhibit signs of a dynamical system until the second week after the surgery. Furthermore, when a dynamical system did provide an adequate approximation of the neural population signals, the primary fixed point recovered in different animals and in alignment to different landmarks of the behavior was not consistent. This suggests that a diversity of population-level strategies emerge during network plasticity after injury, as might be expected intuitively. Interestingly, in sessions where a least-squares dynamical system reconstruction was reasonable, the accuracy of reconstructing the system dynamics with an imposed rotatory structure was positively correlated with the overall pellet retrieval success rate. This suggests that while shifted motor tunings of individual cells likely does play a role in reorganization after injury, it is plasticity that occurs throughout the bilateral cortical networks which allows the neural population to “explore” a vast response surface and ultimately converge upon strategy

enabling the generation of movement. When this process converges upon a strategy that causes the first-order system dynamics of the bilateral neural population signal to exhibit rotatory structure, it indicates successful reoptimization, which is sometimes called *recovery*.

Because there are many ways in which such a reoptimization could result in a system capable of generating a movement sequence resulting in the adequate completion of a motor goal, the optimal network state or capacity to converge to such a state is often not attained while plastic processes are most-active. Similarly, it does not require a large leap to imagine how network-level plasticity could serve as a basis for rehabilitation effects observed during behavioral therapies such as constraint-induced movement therapy (CIMT). The set of movements capable of generating the desired functional outcome is constrained (Wolf et al. 1989, Wolf et al. 2006, Wolf et al. 2010), which regularizes the network reoptimization and biasing it so that it is more capable of generating the relevant motor output in an efficient manner. When considered in this light: that the reoptimization reflects a stochastic process that can be biased toward a particular local minimum which becomes locked-in as the typical time-course of molecular cascades that are incurred after injury unfold, the apparent “paradox” that suggesting that it is surprising that small secondary injuries led to improved recovery can be understood as a second-chance, jump-starting reoptimization that had converged to a suboptimal state (Zeiler et al. 2016).

It should be noted that regardless of the constraints imposed on movements, reoptimization that results in the ability to execute any arbitrary task-specific motor function may result in the apparent change in tunings of cortical spiking to specific facets of the motor output in a way that arises from the nonlinear and probably non-monotonic relation between neural activity and motor output (Griffin & Strick 2015). This confound can be addressed in animal models through the collection of a suitable control covariate to aid interpretation, such as electromyographic recordings from the muscles of interest (Evarts 1968, Griffin & Strick 2020). Alternatively, causal evaluation of the system response to experimental changes, such as by perturbing cortical inputs using optogenetic manipulations

(Sauerbrei et al. 2020), might be used to ensure the utility of tunings taken from individual cells during behavior.

What does the relation of motor performance to the presence of rotatory structure in population activity tell us about rehabilitation? This requires a brief explanation of the neuroanatomical and neurophysiological reasons why rotatory dynamical structure, at least in the cerebral cortex during motor behavior, is interesting to begin with. First, both movement generation and suppression require activity due to the manner in which the nervous system encodes and decodes information (Stinear et al. 2009). Descending corticospinal cells not only synapse upon motoneuron pools that excite muscle fibers, but they also synapse onto interneurons capable of exerting an inhibitory influence on motoneuron output (Griffin & Strick 2020). Activity within the nervous system must perpetuate itself to continue to exist through time; the manner in which it perpetuates dictates function and likely reflects the intrinsic organizational arrangement of a given cortical area or even layer (Granger et al. 1989). For motor cortical cells to encode a target such as a pellet, this means that the relevant network structural elements must allow activity related to the pellet to propagate indefinitely while allowing for the trajectory's disruption at any instant as the system updates its own state (i.e. switches to a new target or goal). An efficient strategy would be to organize population activity so that only two components are required in order to perpetuate a target in the form of a fixed point. This places the population activity into a transient "orbit," until subtle alterations (such as contact or predicted contact with the pellet) perturb it from this target fixed point. Importantly, the manner in which this activity perpetuates itself is predicated upon the arrangement of neuroanatomical connections of the system motor outputs: the system must maintain balanced excitation and inhibition during "hold" periods, which would require a minimum of two independent components that could sum in order for the net output to balance to zero (Kaufman et al. 2014). Furthermore, this putative strategy is grounded in an empirical observation from neurophysiological recordings that has been observed by many groups: transient but salient multi-peaked excitations in

individual unit activity when synchronized with specific motor events (i.e. **Figure S5.4**; Churchland et al. 2012, Musall et al. 2019).

It would be unlikely that each unit demonstrating such tuning reflects a direct corticospinal motor neuron-related cortical output. The cortical engine probably isn't involved directly in controlling movement of the limb along the majority of the trajectory between the **Reach** and **Grasp**. Instead, it would be more efficient if the cortex kicked in at key times during the compound sequence of movements required for the digits to arrive at the stationary pellet. Selecting the appropriate onset times may involve supplementary motor areas of cortex (Tanji & Shima 1994), but in general probably requires the involvement of the basal ganglia and related subcortical circuits in order to ensure that efficient output combinations are selected while manipulating limb trajectory (DeLong et al. 1983). This offloads most of the work to some combination of the momentum and mechanical properties of the limb along with small online error corrections allowing maintenance of the trajectory and which occur via subcortical mechanisms (Shadmehr & Mussa-Ivaldi 1994, Tseng et al. 2007). An abundance of past research indicates that, particularly in the case of a learned skillful movement, this is probably the case (Rothwell et al. 1980, Shadmehr et al. 2010). Correlated activity in the cerebral cortex may reflect spatial attention related to visual information and its integration into the behavior (Lebedev & Wise, 2001), which allows the sparse corticospinal cells with motoneuron-related output projections to impose acceleration on the limb at the right moment to move the effector as desired. This suggests a secondary importance of ongoing cortical activity: prediction and representation of an internal coordinate transformation on the state of the limb, enabling the ability to adjust and integrate visual information during motor task execution (Georgopoulos et al. 1986, Georgopoulos et al. 1989). Indeed, sensorimotor cortical interactions may enable motor adaptation, such as occurs on the slower timescale of multiple trials (Mathis et al. 2017) rather than adaptation that occurs within single trials (Albert et al. 2020).

What does it mean if the system converges to fixed point dynamics that do not exhibit rotatory structure; specifically, why would this correlate with suboptimal functional outcomes? In general, this is not intuitively problematic, which is part of what makes the finding interesting. Could such a phenomenon relate to higher-order modulators of cortical activity that are known to change after injury (Mohajereni et al. 2011, Kokinovic & Medini 2018)? It is tempting to speculate that synaptic changes in terminals of the *de novo* sprouting axonal processes that emerge after ischemia (Dancause et al. 2005, Dancause 2006) may be involved, particularly given the correspondence between the timing of the system dynamics emerging and the expected timescale of weeks required for sprouting processes to connect with horizontal cortical targets. Future experiments, wherein simultaneous measurements from motor and sensory cortex would enable the reformulation of this speculation as a system identification problem. Does the sparse distribution of corticomotoneuronal cells mean that in some cases the damaged tissue disproportionately affects the “wrong” cells, the basis for rescaling network weightings loses full rank, and the network state can never recover? Or, does suboptimal convergence relate to instability that arises from sensory feedback during refinement of the cortical limb state representation, suggesting therapies targeting the specific role of cortical sensorimotor interactions during adaptive motor control contain hope for the future of behavioral interventions after stroke?

Methods

Animals used in study

Ten young-adult, male Long-Evans rats (weight = 312 – 353 grams, Harlan Laboratories[57], Inc., Indianapolis, IN) were acquired at three months of age. Rats were singly housed and provided with food and water. The room was kept on a 12-h:12-h light/dark cycle, and ambient temperature was maintained at 22 °C. Protocols for animal use were approved by the Kansas University Medical Center Institutional Animal Care and Use Committee and complied with the *Guide for the Care and Use of Laboratory Animals (Eighth Edition, The National Academies Press, 2011).* Rats (*n* = 10) were assigned randomly to either the **Intact** group (*n* = 4) or **Ischemia** group (*n* = 6).

Use of the rodent model

Although upper extremity tasks still often use monkeys, due to the typically terminal endpoints required in neuroanatomical or molecular experiments, rodent models played an essential role in evaluating cortical reorganization after injury: the rat neocortex contains both an M1 forelimb homologue (caudal forelimb area; CFA) and a second motor area in M2 that may function analogously to PM or SMA (rostral forelimb area; RFA). The rat motor cortex consists of two defined areas related to volitional motor control of the forelimb. The caudal forelimb area (CFA) is akin to primary motor cortex (M1) and has motor representations as shown via intracortical microstimulation (ICMS) (Donoghue & Wise 1982, Neafsey & Sievert 1982, Neafsey et al. 1986). The rostral forelimb area (RFA) functions somewhat analogously to the pre-motor (PM) and supplementary motor areas (SMA) of primates. RFA and CFA have similar, though not identical, efferent projections to subcortical regions such as the caudate, putamen, subthalamic nucleus, substantia nigra, red nucleus, pontine nuclei, and inferior olive and spinal cord (Rouiller et al. 1993). Even though rats lack

[57] There may be breeder-specific differences in learning rate and performance plateaus that reflect intrinsic differences in colony genetic distributions (O'Bryant et al. 2011).

fine individual digit control, they can execute complex forelimb movements such as a skilled reaching task (Whishaw & Coles 1996). After cortical injury, rats demonstrate deficits during the pellet retrieval task (Whishaw et al. 1993).

Behavioral training

Rats were trained on a reach-to-grasp pellet retrieval task for up to four weeks before surgery. Each rat was placed within a 30-cm x 30-cm x 53-cm Plexiglas box with a 1-cm-wide slot allowing access to a tray where food pellets were placed. Forelimb preference was determined at the beginning of the skilled reach task training. The task, which has been detailed extensively by multiple groups, requires the rat to reach through the slot, grasp a food pellet (45 mg; Bio-Serv. Flemington, NJ) from a fixed target location 2-cm away, and lift the food pellet to the mouth. Initially, the rats are trained using a retrieval slot in the middle of the box, with pellets placed at closer targets that are accessible by either the left or the right forelimb. The preferred forelimb was determined as the first forelimb that is used in an attempt to retrieve the pellet. Once forelimb preference was determined, rats were then trained using an opening on the side of the box from which it would only be possible to retrieve pellets using the preferred forelimb. Trials were recorded with a digital video camera (29.97 frames per second) for playback and analysis (**Supplementary Videos S1, S2**). Rats were required to obtain at least a 70% successful reach rate (60 trials per day) for three consecutive days (baseline behavior) before inclusion into the study. Throughout the duration of the study, food intake was monitored on a scheduled feeding regimen to encourage performance on the skilled reach task.

Scoring pellet retrievals

Two separate procedures were used for scoring pellet retrievals as successful or unsuccessful. The first method reflects the standard scoring procedure used in previous studies in reaching rats (Nishibe et al. 2010). It allows the rat to attempt to retrieve the pellet up to three times before a failure was marked. If the pellet was dislodged from the platform prior to the three

attempts, then it was automatically counted as a failure. This method is more forgiving toward rats that seem to be able to reach correctly out of the box but are either impatient or very slightly miss the pellet target. The second scoring procedure was more stringent: any movement of the forelimb out of the box and toward the pellet was counted as a failed retrieval attempt if the rat did not successfully bring the pellet back into the box. This did not apply to trials in which the rat attempted to retrieve the pellet, but no pellet was present on the pedestal.

Surgical procedures

Each rat was anesthetized initially with isoflurane (to effect) followed by ketamine (80-100 mg/kg, intraperitoneal (IP)) and xylazine (5-10 mg/kg, intramuscular (IM)). Anesthesia was maintained throughout the procedure with repeated bolus injections of ketamine (10-15 mg/kg/ IM) as needed. After the rat was secured in the stereotaxic frame, bupivacaine (0.5-1.0 mL) was delivered subcutaneously (SC) to the scalp/incision area and penicillin (0.15 mL; G benzathine and G procaine, 300 K/mL) was delivered SC under the skin of the back. A rectal probe attached to a homeothermic blanket (Harvard Apparatus, Holliston, MA) was used to maintain core body temperature at approximately 36.7ºC throughout the experiment. A craniectomy was made based on stereotaxic coordinates relative to bregma over the PM contralateral to the reaching forelimb (anterior-posterior (AP) +3.5 mm, medial-lateral (ML) +2.5 mm) and the M1 ipsilateral to the reaching forelimb (AP +0.5 mm, ML + 3.5 mm). To control brain edema after the craniectomy, the muscles of the neck overlying the cisterna magna were reflected and a small puncture was made in the spinal dura (foramen magnum) to allow for CSF drainage. Six holes (three on either side of the skull midline) were drilled caudal to the M1 craniectomies for placement of stainless steel screws used during the procedure to ground the electrodes and anchor them to the skull with dental acrylic. The dura was then removed over the exposed PM and M1. ICMS was used to identify the forelimb motor representations (Figure 1B). Following completion of the surgical procedure, the incision was closed with sterile 4.0 silk surgical suture

and treated topically with EMLA cream, and triple antibiotic ointment. The rat was removed from the stereotaxic device and the temperature probe removed and placed within the homeothermic blanket, upon which the animal was monitored for anesthetic recovery. Each rat received an additional injection of penicillin 0.15 mL SC (G benzathine and G procaine 45,000 IU), and then was moved to a recovery area until the rat was able to maintain an upright posture and locomote freely. Once stabilized, the rat was returned to its home cage. Post-surgery analgesics were given to the rat during the 72 hours after surgery [four SC injections of Buprenorphine (0.05-0.10 mg/kg every 12 hours; four doses of Acetaminophen (20-40 mg/kg, oral) every 12 hours].

ICMS motor mapping

Intracortical microstimulation (ICMS) procedures were used to identify the caudal and rostral forelimb areas (CFA and RFA). A digital image of the cortical surface was acquired and overlaid with a 250 µm grid in order to co-register insertion sites with their corresponding cortical target. Responses at the grid intersections (avoiding surface vasculature) were noted and used to inform microelectrode array placement. Pulse trains synchronized with an audio monitor were delivered at 1-Hz, and each train consisted of bursts of 13 bi-phasic pulses at a pulse frequency of 300-Hz and phase duration of 100-ms. During data analysis, responses were grouped categorically by the following scheme: "Distal Forelimb" (DF), which included wrist extension or flexion, or digit movements; "Proximal Forelimb" (PF), which included elbow flexion; "Distal-Proximal" (DF-PF), which was assigned when an interpolated electrode site was likely to be between a Distal or Proximal site; "No Response" (NR), when threshold stimulation (up to 80 µA) did not elicit any movement; or "Other" (O), when a trunk, shoulder, neck, mouth, face, or vibrissae response was elicited (**Figure 5.1B,** inset examples).

Ischemia model

After identification of CFA and RFA, rats assigned to the **Ischemia** group had six 0.7-mm diameter holes drilled over the CFA contralateral to the reaching forelimb. Relative to bregma and using a stereotaxic coordinate system in which anterior and lateral directions are positive, injection sites were distributed in two rows mediolaterally (+2.5-mm and +3.5-mm), along three anteroposterior locations (+1.5-mm, +0.5-mm, and -0.5-mm). A focal, ischemic infarct targeting CFA cortical territory was induced with the vasoconstrictor endothelin-1 (ET-1; 0.3 µg ET-1 dissolved in 1 µl sterile saline (~120 pmol)). Each hole was injected with 0.33 µL of ET-1 through a glass micropipette (160 µm o.d.) attached to a Hamilton syringe with the tip inserted to a depth of 1.5-mm below the cortical surface. Injections were made at a rate of 4-nl/sec by a programmable motorized micro-injector (Hamilton Company, Reno, NV). The injection pipette remained in place for an additional 5 minutes after injection to minimize backflow of ET-1 during pipette removal from the cortex.

Electrode implants

Following ICMS and ET-1 lesion procedures, skull screws (Pan Head Phillips head machine Screws, 0-80 thread, 1/8'' length, stainless steel, McMaster-Carr, Elmhurst, IL) were placed in the six screw holes to ground the electrodes and to act as an anchor for dental acrylic applied to the skull. Two 16-channel microwire arrays (Tucker-Davis Technologies; 16 shank, 2x8 electrode, 50 µm wire diameter, 45° tip angle, 250 µm electrode spacing, 500 µm row spacing) were implanted in the RFA contralateral to the reaching forelimb (i.e., ipsilesional RFA) and CFA ipsilateral to the reaching forelimb (i.e., contralesional CFA). Online recording of activity from the microelectrode arrays was used to determine a depth with high neuronal firing on the majority of channels as the array was lowered into place with a mechanical micro-drive (at a depth ~1,550 µm perpendicular to the cortical surface). A quick-curing polymer was used (Kwik-Cast, WPI, Sarasota, FL) to cover the cortex, fix the arrays in place, and seal the cranial opening. Dental acrylic was then used to add additional anchoring to the skull by adhering to the stainless steel

screws placed in the skull. The acrylic also served as a protective barrier over the sealing polymer.

Data acquisition

Each rat was tethered to the implanted arrays through a motorized commutator (TDT) that allowed free movement within the testing chamber. Neuronal activity was recorded using TDT hardware and a custom TDT OpenEx system circuit with a biquadratic bandpass filter designed to approximate cutoff frequencies of 300 and 5,000 Hz and a sampling rate of 25 kHz. The circuit was synchronized with an analog stream denoting the intact state of an infrared beam on the opposite side of the slot from the rat, which allowed the co-registration of pellet retrieval video trials with the neurophysiological data by providing landmarks in the data streams that could be correlated with video frames in which the rat broke the plane of the beam. A boolean stream denoting user-operated button presses corresponding to successful pellet retrievals was used to facilitate offline video scoring, and also served as a secondary verification that video and neurophysiological records were aligned correctly. Following the lesion and array implants, each rat was tested on the reach task on post-operative days 3-28 for a maximum of 20 minutes. On days where the rat was unmotivated to attempt pellet retrievals, the protocol was extended to allow the chance to observe pellet retrievals, since all analyses were predicated on the rat performing the behavior; in some cases, it was not possible to obtain a sufficient number of pellet retrieval observations to include the recording for further analysis.

Histological characterization of injury

Rats were perfused transcardially with normal saline followed by 3% paraformaldehyde. Brains were post-fixed in a 30% glycerol solution. Coronal sections were cut at 50 µm and stained with cresyl violet. Sections were mounted to slides, dehydrated, and cover slipped. Gliosis at the site of microwire arrays caused adherence of the tissue to the wire array during recovery of the perfused brain in some cases; therefore, a formal lesion volume analysis was not conducted. An

exemplar of coronal hemisections that correspond to CFA from an animal in each group is shown in **Figure 5.1B**.

Data Processing

All custom Matlab scripts used in data processing is freely and publicly available (initial filtering and spike detection used version R2017a: https://github.com/m053m716/CPLtools; video scoring and neural data analyses specific to this manuscript used version R2020b: https://github.com/m053m716/rc-proj).

Video alignment and behavioral metadata tagging

Detailed instructions for the specific video analysis procedure are available online (https://github.com/m053m716/rc-proj/tree/master/videoAnalyses#video-alignment). Briefly, videos were aligned using a procedure requiring the visual co-registration of the approximate timing of paw crossings with the analog signal obtained from an infrared beam break placed in front of the box opening. In some cases, a second pellet sensor was available that helped synchronize the videos. To verify that data were accurately synchronized, a trained network using DeepLabCut (Mathis et al. 2017), a method for markerless kinematic tracking that is specific to animal models of behavior (Nath et al. 2019), was trained and used to obtain time-series for the presence of the reaching forelimb. This time-series was then cross-correlated with the analog beam break signal so that the two could be aligned on average as accurately as possible, giving the best possible alignment. four behavioral events were defined: **Reach Onset**, **Support**, **Grasp**, and **Complete**. These events were associated with individual video frames in order to provide markers in the neural data for coherent alignment in subsequent analyses.

Processing applied to neural data

Only bandpass filtered data were saved (cascaded bi-quadratic bandpass filter 300 to 5,000 Hz; TDT); therefore, no analysis of the LFP was conducted beyond analyses focused on multi-unit

activity. A virtual common re-reference was applied to the filtered data, subtracting the mean signal of each microwire array from the individual channels on the respective probe. Threshold-crossings, as opposed to classified neural units, were used during spike detection in order to avoid bias and because they still contain information about behaviorally-relevant activity (Chestek et al. 2011). Previous work by our group indicates that multi-unit threshold crossings are stable indicators of neural activity during pellet retrievals over the timescale on which these recordings were conducted (Bundy et al. 2019).

Recovery of neural population dynamics

Only successful trials were used during population analyses; a mask was applied to remove any channels that were not present across each included recording for each rat. Spike rates were obtained using a 60-ms sliding window. A square-root transformation was applied to any spike rates (not spike counts) to reduce heteroskedasticity that occurs at higher values. Rates used in population analyses were z-scored on a per-channel basis using an epoch spanning 2,000-ms to 1,000-ms prior to each trial. The cross-trial average event-aligned spike rate was recovered for each channel and subtracted from the individual trial spike rate estimates in order to only consider the population variance (Churchland et al. 2011). To recover the population neural state, rates from all trials were concatenated and principal components analysis (Matlab `pca` function) was used to recover the principal component scores for the top-12 components. Multiple least-squares (MLS) regression was applied to obtain both the least-squares optimal and skew-symmetric transformation matrices onto the first time-difference of the neural state vector (the principal component scores) as described elsewhere (Churchland et al. 2012).

Statistical models

Generalized linear mixed-effects models (GLME) were estimated using the Matlab `fitglme` function (version R2020b) using restricted maximum pseudo-likelihood. Naive Bayesian classifier ensembles were estimated using the Matlab `fitcnb` function. Relevant model

parameters are described in the pertinent Results sections; the models used in all analyses are summarized in **Table S5.1**.

References

Alaverdashvili, Mariam, et al. ""Learned baduse" limits recovery of skilled reaching for food after forelimb motor cortex stroke in rats: a new analysis of the effect of gestures on success." *Behavioural brain research* 188.2 (2008a): 281-290.

Alaverdashvili, Mariam, and Ian Q. Whishaw. "Motor cortex stroke impairs individual digit movement in skilled reaching by the rat." *European Journal of Neuroscience* 28.2 (2008b): 311-322.

Albert, Scott T., et al. "Postural control of arm and fingers through integration of movement commands." *Elife* 9 (2020): e52507.

Allred, Rachel P., Colleen H. Cappellini, and Theresa A. Jones. "The "good" limb makes the "bad" limb worse: Experience-dependent interhemispheric disruption of functional outcome after cortical infarcts in rats." *Behavioral neuroscience* 124.1 (2010): 124.

Brown, Craig E., Charles Wong, and Timothy H. Murphy. "Rapid morphologic plasticity of peri-infarct dendritic spines after focal ischemic stroke." *Stroke* 39.4 (2008): 1286-1291.

Brown, Craig E., Jamie D. Boyd, and Timothy H. Murphy. "Longitudinal in vivo imaging reveals balanced and branch-specific remodeling of mature cortical pyramidal dendritic arbors after stroke." *Journal of Cerebral Blood Flow & Metabolism* 30.4 (2010): 783-791.

Bundy, David T., et al. "Chronic stability of single-channel neurophysiological correlates of gross and fine reaching movements in the rat." *PloS one* 14.10 (2019): e0219034.

Bury, Scott D., and Theresa A. Jones. "Unilateral sensorimotor cortex lesions in adult rats facilitate motor skill learning with the "unaffected" forelimb and training-induced dendritic structural plasticity in the motor cortex." *Journal of Neuroscience* 22.19 (2002): 8597-8606.

Carmichael, S. Thomas, et al. "New patterns of intracortical projections after focal cortical stroke." *Neurobiology of disease* 8.5 (2001): 910-922.

Carmichael, S. Thomas. "Cellular and molecular mechanisms of neural repair after stroke: making waves." *Annals of Neurology: Official Journal of the American Neurological Association and the Child Neurology Society* 59.5 (2006): 735-742.

Chestek, Cynthia A., et al. "Single-neuron stability during repeated reaching in macaque premotor cortex." *Journal of Neuroscience* 27.40 (2007): 10742-10750.

Chestek, Cynthia A., et al. "Long-term stability of neural prosthetic control signals from silicon cortical arrays in rhesus macaque motor cortex." *Journal of neural engineering* 8.4 (2011): 045005.

Churchland, Anne K., et al. "Variance as a signature of neural computations during decision making." *Neuron* 69.4 (2011): 818-831.

Churchland, Mark M., et al. "Neural population dynamics during reaching." *Nature* 487.7405 (2012): 51-56.

Dancause, Numa, et al. "Extensive cortical rewiring after brain injury." *Journal of Neuroscience* 25.44 (2005): 10167-10179.

Dancause, Numa. "Vicarious function of remote cortex following stroke: recent evidence from human and animal studies." *The Neuroscientist* 12.6 (2006): 489-499.

DeLong, M. R., A. P. Georgopoulos, and M. D. Crutcher. "Cortico-basal ganglia relations and coding of motor performance." *Experimental Brain Research* 49.Suppl. 7 (1983): 30-40.

Donoghue, John P., and Steven P. Wise. "The motor cortex of the rat: cytoarchitecture and microstimulation mapping." *Journal of Comparative Neurology* 212.1 (1982): 76-88.

Evarts, Edward V. "Relation of pyramidal tract activity to force exerted during voluntary movement." *Journal of neurophysiology* 31.1 (1968): 14-27.

Friel, Kathleen M., and Randolph J. Nudo. "Recovery of motor function after focal cortical injury in primates: compensatory movement patterns used during rehabilitative training." *Somatosensory & motor research* 15.3 (1998): 173-189.

Georgopoulos, Apostolos P., Andrew B. Schwartz, and Ronald E. Kettner. "Neuronal population coding of movement direction." *Science* 233.4771 (1986): 1416-1419.

Georgopoulos, Apostolos P., et al. "Mental rotation of the neuronal population vector." *Science* 243.4888 (1989): 234-236.

Granger, Richard, José Ambros-Ingerson, and Gary Lynch. "Derivation of encoding characteristics of layer II cerebral cortex." *Journal of Cognitive Neuroscience* 1.1 (1989): 61-87.

Griffin, Darcy M., Donna S. Hoffman, and Peter L. Strick. "Corticomotoneuronal cells are “functionally tuned”." *Science* 350.6261 (2015): 667-670.

Griffin, Darcy M., and Peter L. Strick. "The motor cortex uses active suppression to sculpt movement." *Science Advances* 6.34 (2020): eabb8395.

Jones, Theresa A., and Timothy Schallert. "Overgrowth and pruning of dendrites in adult rats recovering from neocortical damage." *Brain research* 581.1 (1992): 156-160.

Jones, Theresa A., and Timothy Schallert. "Use-dependent growth of pyramidal neurons after neocortical damage." *Journal of Neuroscience* 14.4 (1994): 2140-2152.

Jones, Theresa A., et al. "Motor skills training enhances lesion-induced structural plasticity in the motor cortex of adult rats." *Journal of Neuroscience* 19.22 (1999): 10153-10163.

Kirkland, Scott W., Lori K. Smith, and Gerlinde A. Metz. "Task-specific compensation and recovery following focal motor cortex lesion in stressed rats." *Journal of integrative neuroscience* 11.01 (2012): 33-59.

Kaufman, Matthew T., et al. "Cortical activity in the null space: permitting preparation without movement." *Nature neuroscience* 17.3 (2014): 440-448.

Kawamata, Takakazu, et al. "Intracisternal basic fibroblast growth factor enhances functional recovery and up-regulates the expression of a molecular marker of neuronal sprouting following focal cerebral infarction." *Proceedings of the National Academy of Sciences* 94.15 (1997): 8179-8184.

Krakauer, John W., et al. "Getting neurorehabilitation right: what can be learned from animal models?." *Neurorehabilitation and neural repair* 26.8 (2012): 923-931.

Krakauer, John W., and S. Thomas Carmichael. *Broken movement: the neurobiology of motor recovery after stroke*. MIT Press, 2017.

Kokinovic, Bojana, and Paolo Medini. "Loss of GABAB- mediated interhemispheric synaptic inhibition in stroke periphery." *The Journal of physiology* 596.10 (2018): 1949-1964.

Lebedev, Mikhail A., and Steven P. Wise. "Tuning for the orientation of spatial attention in dorsal premotor cortex." *European Journal of Neuroscience* 13.5 (2001): 1002-1008.

Lebedev, Mikhail A., et al. "Analysis of neuronal ensemble activity reveals the pitfalls and shortcomings of rotation dynamics." *Scientific Reports* 9.1 (2019): 1-14.

Levin, Mindy F., Jeffrey A. Kleim, and Steven L. Wolf. "What do motor “recovery” and “compensation” mean in patients following stroke?." *Neurorehabilitation and neural repair* 23.4 (2009): 313-319.

Li, Songlin, et al. "An age-related sprouting transcriptome provides molecular control of axonal sprouting after stroke." *Nature neuroscience* 13.12 (2010): 1496-1504.

Masamizu, Yoshito, et al. "Two distinct layer-specific dynamics of cortical ensembles during learning of a motor task." *Nature neuroscience* 17.7 (2014): 987-994.

Mathis, Mackenzie Weygandt, Alexander Mathis, and Naoshige Uchida. "Somatosensory cortex plays an essential role in forelimb motor adaptation in mice." *Neuron* 93.6 (2017): 1493-1503.

Mathis, Alexander, et al. "DeepLabCut: markerless pose estimation of user-defined body parts with deep learning." *Nature neuroscience* 21.9 (2018): 1281-1289.

Michaels, Jonathan A., Benjamin Dann, and Hansjörg Scherberger. "Neural population dynamics during reaching are better explained by a dynamical system than representational tuning." *PLoS computational biology* 12.11 (2016): e1005175.

Mitz, Andrew R., Moshe Godschalk, and Steven P. Wise. "Learning-dependent neuronal activity in the premotor cortex: activity during the acquisition of conditional motor associations." *Journal of Neuroscience* 11.6 (1991): 1855-1872.

Mohajerani, Majid H., Khatereh Aminoltejari, and Timothy H. Murphy. "Targeted mini-strokes produce changes in interhemispheric sensory signal processing that are indicative of disinhibition within minutes." *Proceedings of the National Academy of Sciences* 108.22 (2011): E183-E191.

Musall, Simon, et al. "Single-trial neural dynamics are dominated by richly varied movements." *Nature neuroscience* 22.10 (2019): 1677-1686.

Nath, Tanmay, et al. "Using DeepLabCut for 3D markerless pose estimation across species and behaviors." *Nature protocols* 14.7 (2019): 2152-2176.

Neafsey, E. J., and Carl Sievert. "A second forelimb motor area exists in rat frontal cortex." *Brain research* 232.1 (1982): 151-156.

Neafsey, E. J., et al. "The organization of the rat motor cortex: a microstimulation mapping study." *Brain research reviews* 11.1 (1986): 77-96.

Nishibe, Mariko, et al. "Rehabilitative training promotes rapid motor recovery but delayed motor map reorganization in a rat cortical ischemic infarct model." *Neurorehabilitation and neural repair* 29.5 (2015): 472-482.

Nudo, Randolph J., and Garret W. Milliken. "Reorganization of movement representations in primary motor cortex following focal ischemic infarcts in adult squirrel monkeys." *Journal of neurophysiology* 75.5 (1996): 2144-2149.

Nudo, Randolph J., Kathleen M. Friel, and Steven W. Delia. "Role of sensory deficits in motor impairments after injury to primary motor cortex." *Neuropharmacology* 39.5 (2000): 733-742.

O'Bryant, Amber J., et al. "Breeder and batch-dependent variability in the acquisition and performance of a motor skill in adult Long–Evans rats." *Behavioural brain research* 224.1 (2011): 112-120.

Pack, Andrea, et al. "Restoration of rodent cortical dynamics after stroke." *In Preparation* (2020).

Pack, Andrea, et al. "Task Related Neural Activity Following Primary Motor Cortical Ischemic Injury in Rats." *bioRxiv* (2020).

Papale, Andrew E., and Bryan M. Hooks. "Circuit changes in motor cortex during motor skill learning." *Neuroscience* 368 (2018): 283-297.

Peters, Andrew J., Haixin Liu, and Takaki Komiyama. "Learning in the rodent motor cortex." *Annual review of neuroscience* 40 (2017a): 77-97.

Peters, Andrew J., et al. "Reorganization of corticospinal output during motor learning." *Nature neuroscience* 20.8 (2017b): 1133.

Ramanathan, Dhakshin S., et al. "Low-frequency cortical activity is a neuromodulatory target that tracks recovery after stroke." *Nature medicine* 24.8 (2018): 1257-1267.

Rothwell, J. C., M. M. Traub, and C. D. Marsden. "Influence of voluntary intent on the human long-latency stretch reflex." *Nature* 286.5772 (1980): 496-498.

Rouiller, Eric M., Veronique Moret, and Fengyi Liang. "Comparison of the connectional properties of the two forelimb areas of the rat sensorimotor cortex: support for the presence of a premotor or supplementary motor cortical area." *Somatosensory & motor research* 10.3 (1993): 269-289.

Sauerbrei, Britton A., et al. "Cortical pattern generation during dexterous movement is input-driven." *Nature* 577.7790 (2020): 386-391.

Shadmehr, Reza, and Ferdinando A. Mussa-Ivaldi. "Adaptive representation of dynamics during learning of a motor task." *Journal of neuroscience* 14.5 (1994): 3208-3224.

Shadmehr, Reza, Maurice A. Smith, and John W. Krakauer. "Error correction, sensory prediction, and adaptation in motor control." *Annual review of neuroscience* 33 (2010): 89-108.

Stinear, Cathy M., James P. Coxon, and Winston D. Byblow. "Primary motor cortex and movement prevention: where Stop meets Go." *Neuroscience & Biobehavioral Reviews* 33.5 (2009): 662-673.

Stroemer, R. Paul, Thomas A. Kent, and Claire E. Hulsebosch. "Neocortical neural sprouting, synaptogenesis, and behavioral recovery after neocortical infarction in rats." *Stroke* 26.11 (1995): 2135-2144.

Tanji, Jun, and Keisetsu Shima. "Role for supplementary motor area cells in planning several movements ahead." *Nature* 371.6496 (1994): 413-416.

Tennant, Kelly A., et al. "The vermicelli and capellini handling tests: simple quantitative measures of dexterous forepaw function in rats and mice." *JoVE (Journal of Visualized Experiments)* 41 (2010): e2076.

Tseng, Ya-weng, et al. "Sensory prediction errors drive cerebellum-dependent adaptation of reaching." *Journal of neurophysiology* 98.1 (2007): 54-62.

Whishaw, Ian Q., O'Connor, William T., and Dunnett, Stephen B. "The contributions of motor cortex, nigrostriatal dopamine and caudate-putamen to skilled forelimb use in the rat." *Brain* 109.5 (1986): 805-843.

Whishaw, Ian Q., and Bryan Kolb. "Sparing of skilled forelimb reaching and corticospinal projections after neonatal motor cortex removal or hemidecortication in the rat: support for the Kennard doctrine." *Brain research* 451.1-2 (1988): 97-114.

Whishaw, Ian Q., Jo-Anne Tomie, and Ricki L. Ladowsky. "Red nucleus lesions do not affect limb preference or use, but exacerbate the effects of motor cortex lesions on grasping in the rat." *Behavioural brain research* 40.2 (1990): 131-144.

Whishaw, Ian Q., and Sergio M. Pellis. "The structure of skilled forelimb reaching in the rat: a proximally driven movement with a single distal rotatory component." *Behavioural brain research* 41.1 (1990): 49-59.

Whishaw, Ian Q., et al. "The impairments in reaching and the movements of compensation in rats with motor cortex lesions: an endpoint, video recording, and movement notation analysis." *Behavioural brain research* 42.1 (1991): 77-91.

Whishaw, Ian Q., Sergio M. Pellis, and Boguslaw P. Gorny. "Medial frontal cortex lesions impair the aiming component of rat reaching." *Behavioural Brain Research* 50.1-2 (1992): 93-104.

Whishaw, Ian Q., et al. "Proximal and distal impairments in rat forelimb use in reaching follow unilateral pyramidal tract lesions." *Behavioural brain research* 56.1 (1993): 59-76.

Whishaw, Ian Q., and Brenda LK Coles. "Varieties of paw and digit movement during spontaneous food handling in rats: postures, bimanual coordination, preferences, and the effect of forelimb cortex lesions." *Behavioural brain research* 77.1-2 (1996): 135-148.

Wise, S. P., et al. "Changes in motor cortical activity during visuomotor adaptation." *Experimental Brain Research* 121.3 (1998): 285-299.

Withers, Ginger S., and William T. Greenough. "Reach training selectively alters dendritic branching in subpopulations of layer II–III pyramids in rat motor-somatosensory forelimb cortex." *Neuropsychologia* 27.1 (1989): 61-69.

Wolf, Steven L., et al. "Forced use of hemiplegic upper extremities to reverse the effect of learned nonuse among chronic stroke and head-injured patients." *Experimental neurology* 104.2 (1989): 125-132.

Wolf, Steven L., et al. "Effect of constraint-induced movement therapy on upper extremity function 3 to 9 months after stroke: the EXCITE randomized clinical trial." *Jama* 296.17 (2006): 2095-2104.

Wolf, Steven L., et al. "The EXCITE stroke trial: comparing early and delayed constraint-induced movement therapy." *Stroke* 41.10 (2010): 2309-2315.

Zeiler, Steven R., et al. "Paradoxical motor recovery from a first stroke after induction of a second stroke: reopening a postischemic sensitive period." *Neurorehabilitation and neural repair* 30.8 (2016): 794-800.

Supplementary Materials

Supplementary Figures

Figure S5.1A

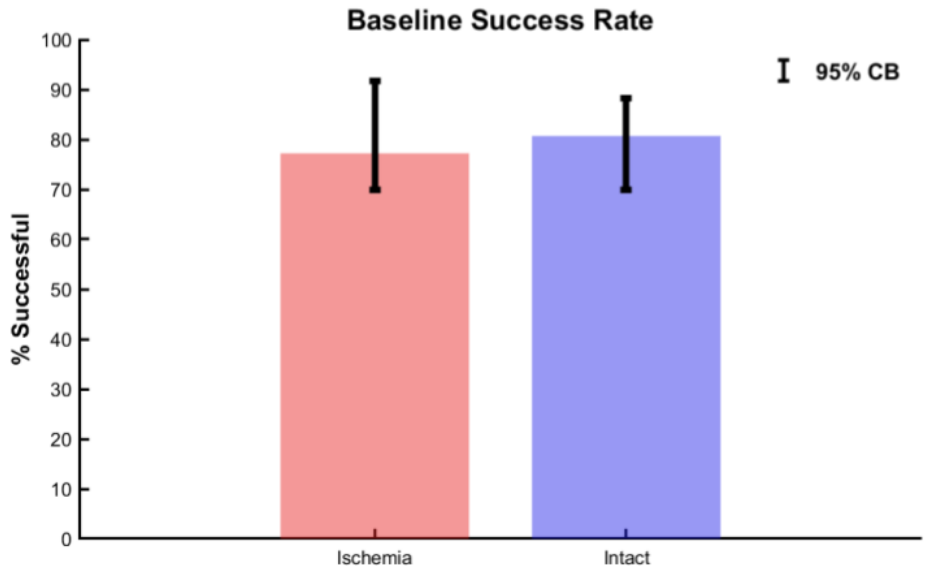

Figure S5.1B

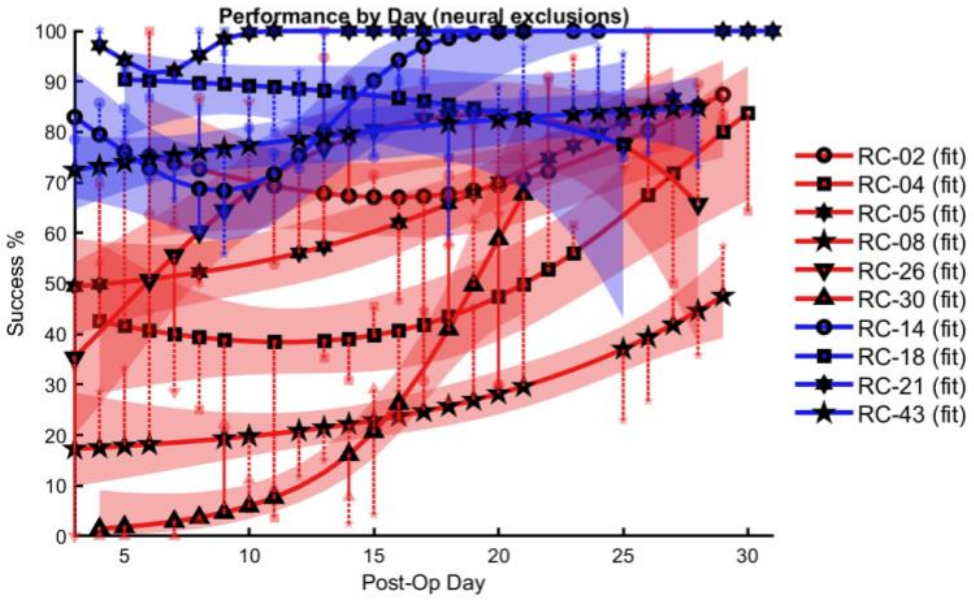

Figure S5.1C

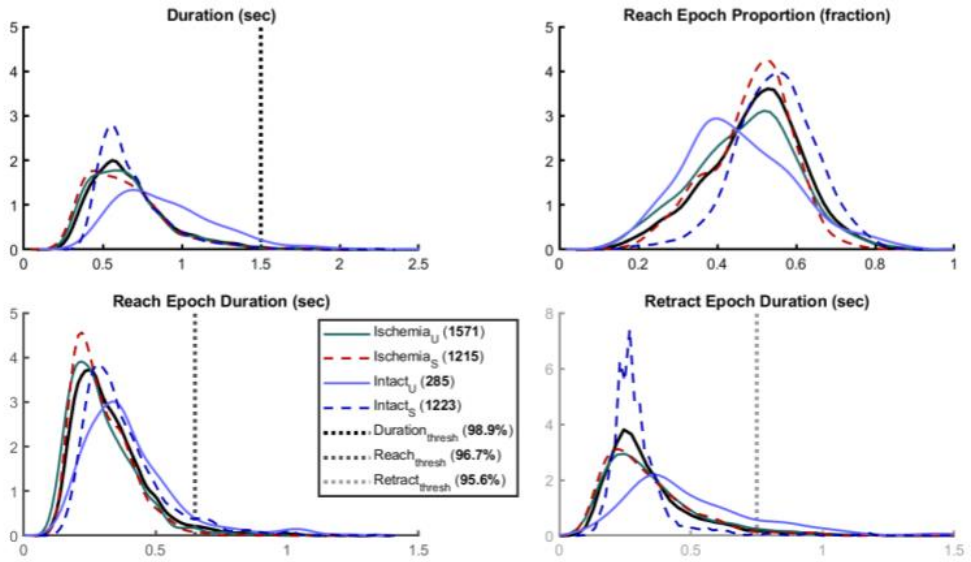

Figure S5.1: Supplementary characterization of pellet retrieval motor behavior.

A) There were no clear differences in baseline performance success rate by group. Rats included in the ***Ischemia*** cohort (n = 6) and ***Intact*** cohort (n = 4) demonstrated comparable levels of pellet retrieval proficiency prior to surgery. Rats were required to successfully retrieve 70% or more pellets over the course of 60 attempts, and maintain that accuracy for at least three baseline sessions prior to surgical implant. This process typically required training for 4-5 weeks, at which point rats were 3-4 months of age, meaning they were at a developmental stage intermediate to **young** and **adult** as defined elsewhere.

B) Performance by day using only trials included for neural analyses. While there was a statistically significant difference between behavioral scores when the rules for excluding trials to be used in neural analyses were enforced, the same general trends of deficit and recovery for the **Ischemia** group and overall better behavioral performance for the **Intact** group indicate that the exclusions did not alter the relation between neural dataset and overall daily performance substantially.

C) Distribution of movement phase durations and thresholds for inclusion or exclusion. One of the major phenotypic differences between groups manifested in the total duration of the pellet retrieval, which was reduced as a function of post-op day for rats in the ***Ischemia*** group. To identify salient changes in cortical movement control related to the injury, efforts were made to only compare phenotypically comparable elements of behavior. Therefore exclusion criteria (dotted lines) were used on the total (*top-left*), reach advance phase (*bottom-left*), and retract phase (*bottom-right*) of the reach. It was also noted that during successful retrievals, the reach/advance phase was relatively longer and tended to last longer than the retract phase.

Figure S5.2A

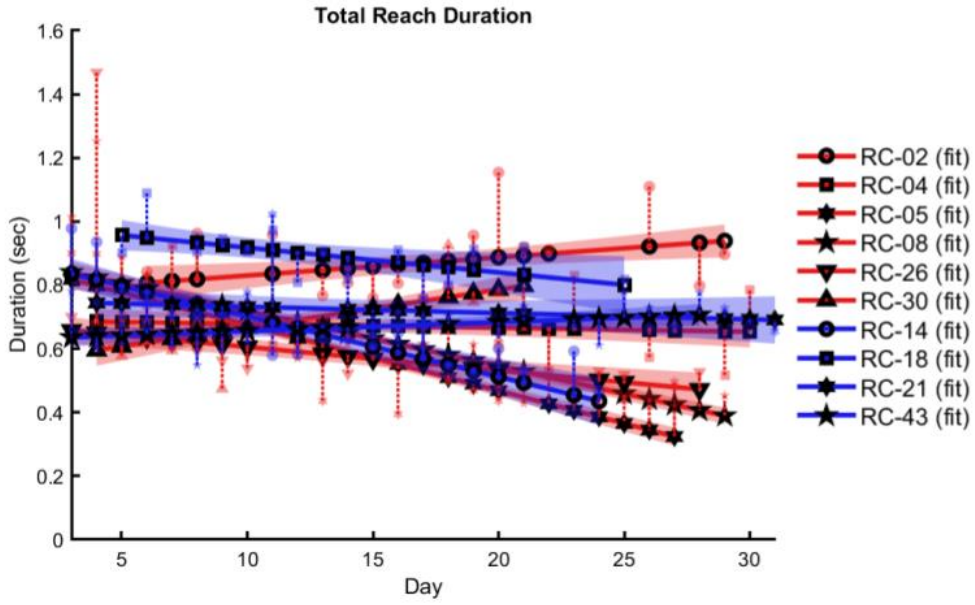

Figure S5.2B

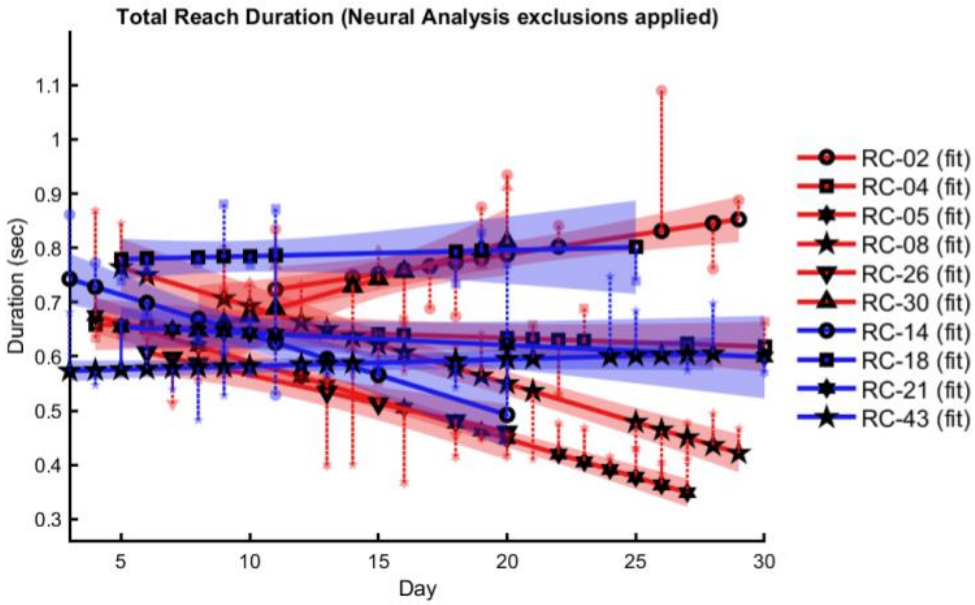

Figure S5.2C

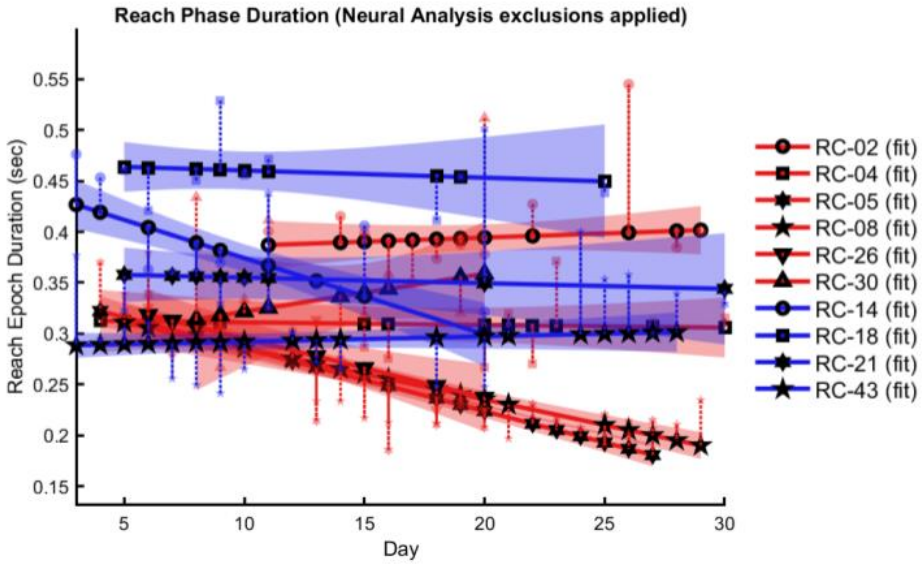

Figure S5.2D

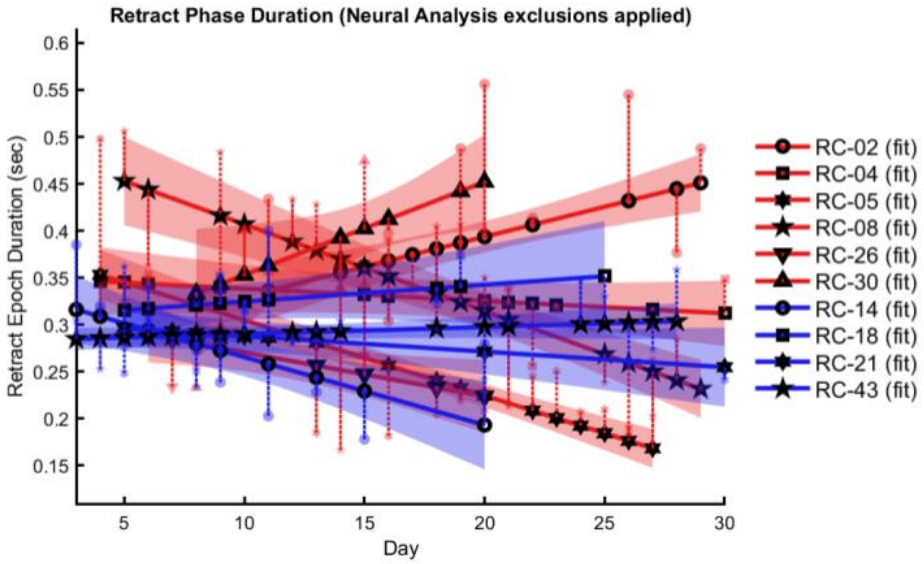

Figure S5.2E

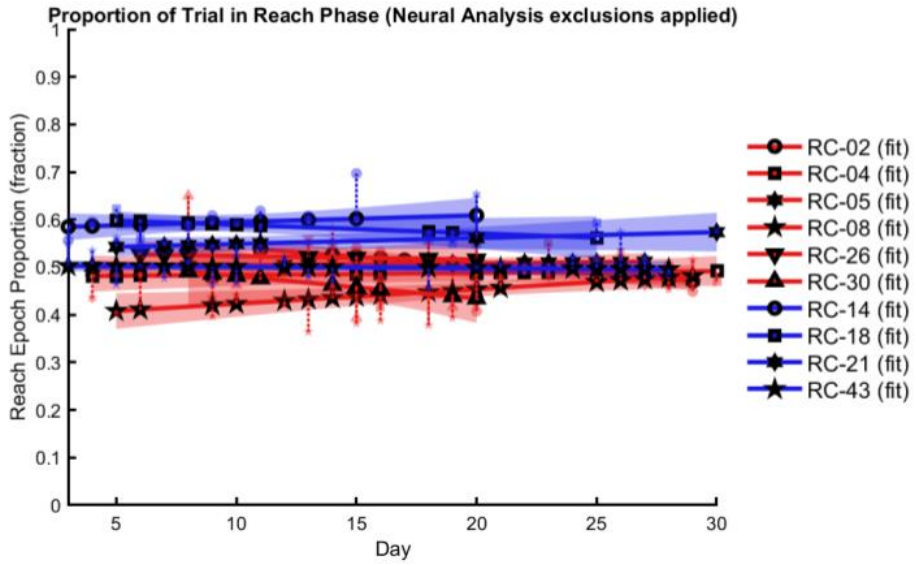

Figure S5.2: Characterizing timing parameters.

A) Total pellet retrieval duration (for all trials). In general, there was a trend in most animals toward an overall reduction in total reach duration, although two rats in the **Ischemia** group showed a tendency toward an increase in total reach duration as did a rat in the **Intact** group.

B) Total pellet retrieval duration (for only trials included in neural analyses). When only considering trials that were used in neural analyses, the trends seen in **panel S5.2A** are essentially magnified.

C) *Reach* phase duration is reduced in a subset of *Ischemia* rats that exhibit recovery. As in **panel S5.2B**, when only considering trials that were used in neural analyses and only measuring the duration of the **Reach** phase, the trends seen in **panel S5.2A** are essentially magnified.

D) *Retract* phase duration is extended in a subset of *Ischemia* rats. Interestingly, trends during the ***Retract*** phase are different. Most of the **Intact** rats maintain a relatively constant duration of this phase, while only the **Ischemia** rats that did not decrease the duration of the ***Reach*** phase exhibit *increases* during this phase. Notably, ***RC-08***, who exhibited a significant difference between behavioral performance using the standard scoring method (**Fig. 5.1A**) and behavioral performance using the rigorous criteria for inclusion in neural analyses (**Fig. S5.1B**), displayed decreases in both phases of the behavior. Incidentally, this same rat is the only rat that exhibited a clear decline in signatures of neural population dynamics during the course of experimental recordings (**Fig. 5.4A**).

This suggests that during apparent recovery, some of the **Ischemia** rats adopt one or more different compensatory strategies (as has been reported in past work by other groups). These strategies result in an apparent overall improvement in functional outcome when scored by

traditional methods, but when the movements are broken down carefully it is seen that the apparent improvements may actually be the result of a different movement strategy altogether. In this case, rats with an increased duration of the ***Retract*** phase.

E) The relative proportion of the reach spent in each phase remains deceptively similar when considered as a fraction of the total reach duration. This alternative way of looking at the reach duration strategy suggests another reason why standard scoring methods do not capture the trends observed when the reach is even broken up as crudely as by two phase components. As shown, the relative proportion spent in one part of the behavior or the other does not appear to change significantly, which may cause a typical scoring of the behavior to miss the otherwise striking trends in phase duration.

Why might this be important? Returning to the increased ***Retract*** phase durations discussed in **Panel S5.2D**, the causes the behavior to take longer during the ***Retract*** phase, which means that it may involve a slower closing of the digits about the pellet, or a more careful scraping of the pellet into the paw in order to ensure its collection. If sensory feedback from cutaneous contact with the pellet is involved in any way with the successful execution of this behavior, then this differentiation suggests that a subset of rats either cannot integrate this sensory feedback, or integrate it via a pathway that takes longer to compute; identification of such a thing is beyond the scope of this study.

Figure S5.3A

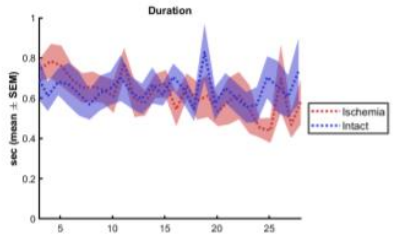

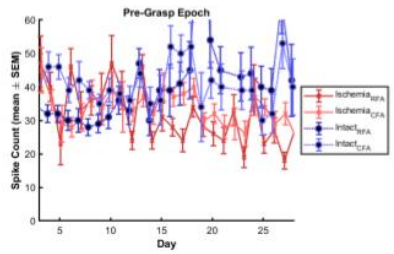

Figure S5.3B

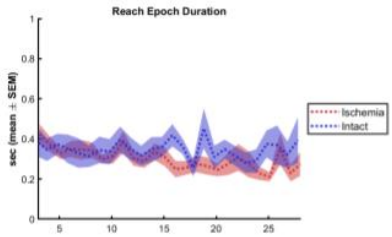

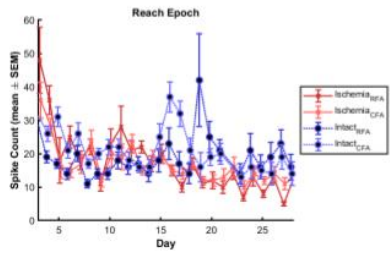

Figure S5.3C

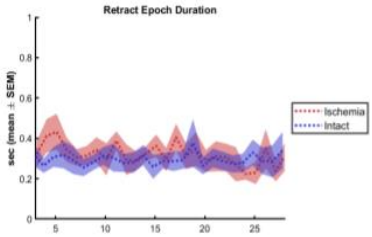

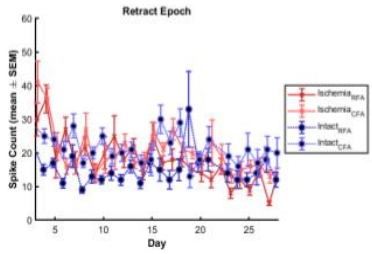

Figure S5.3: Mean spike **counts** by Day, Phase.

A) There is no significant interaction effect for detrended spike counts during the *Pre* **phase of pellet retrievals.** By day, the ***Intact*** group tends to have more spikes during this phase than the ***Ischemia*** group regardless of the level of ***Area*** (*bottom inset*). It should be noted that these relatively minor differences do correlate with differentiation observed in the total reach duration (*top inset*).

B) There is a significant interaction effect of *Ischemia* **and** *RFA* **levels for detrended spike counts during the** *Reach* **phase grouped by day.** However, when grouping is performed at the per-day level, the effect size is even smaller than when groupings are made at the weekly level. It is more-likely that the Matlab GLME function for estimating significance in this instance overestimates the number of degrees of freedom, resulting in a spuriously significant estimate. The correlation between the apparent increase of spike counts in ***Intact-CFA*** between postoperative days 16 to 19 (*bottom inset*) directly correlates with fluctuation in the estimated ***Reach*** phase duration for those same days (*top inset*).

C) There is a significant interaction effect of *Ischemia* **and** *RFA* **levels for detrended spike counts during the** *Retract* **phase by day.** Again, the correspondence to ***Retract*** phase duration should be noted, particularly for spikes in the daily trend line for **Intact** rats.

Individual data points and per-animal trends (black) are shown in Figure **S5.3D** and **S5.3E**.

Figure S5.3D

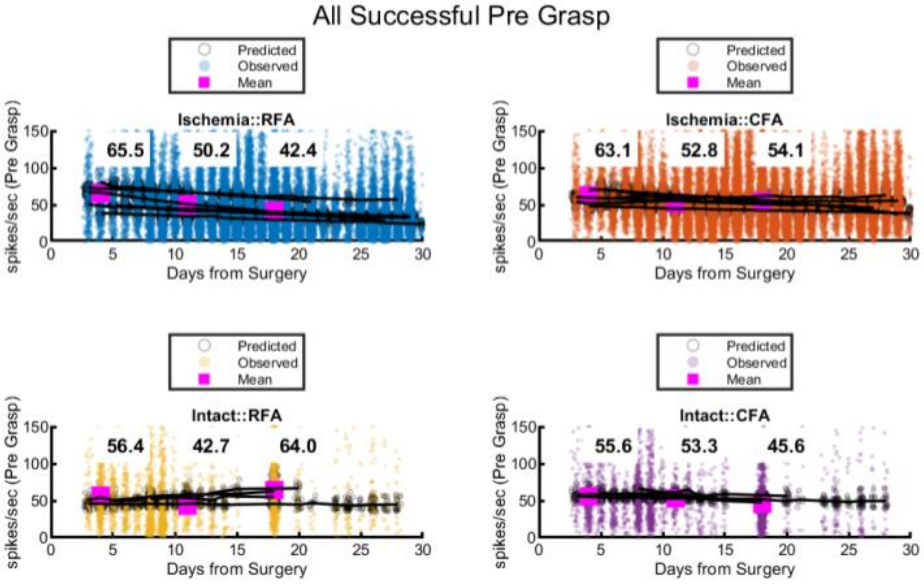

Figure S5.3E

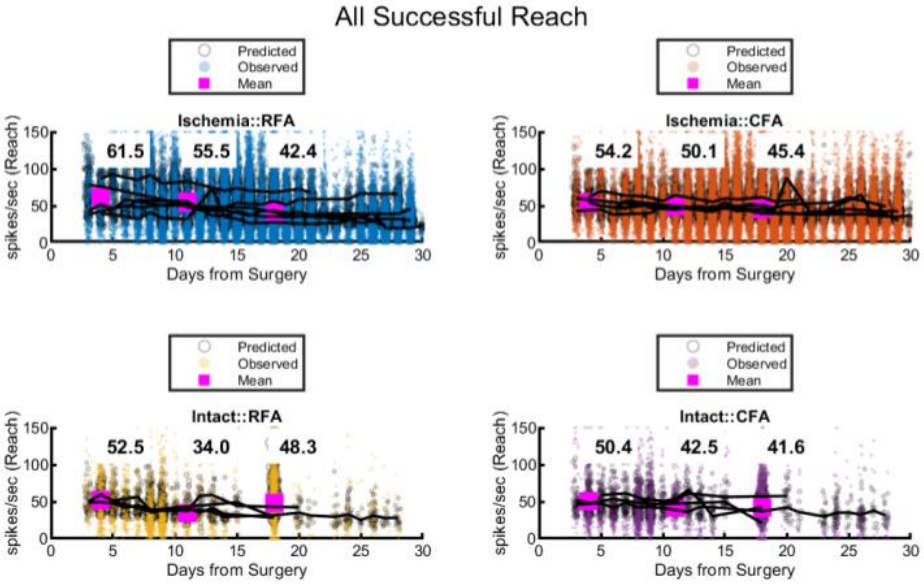

Figure S5.4A

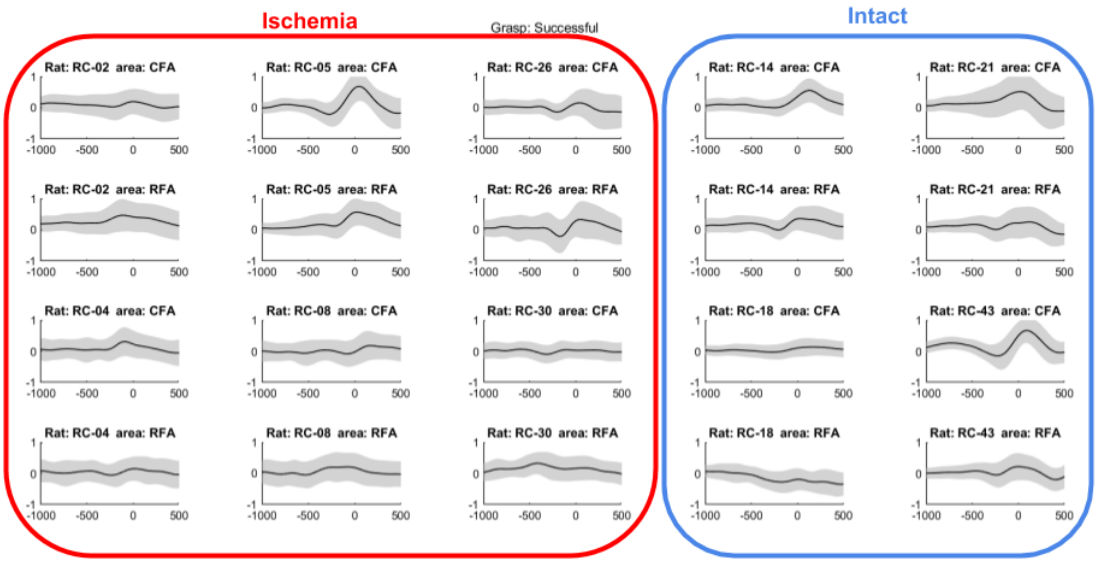

Figure S5.4B

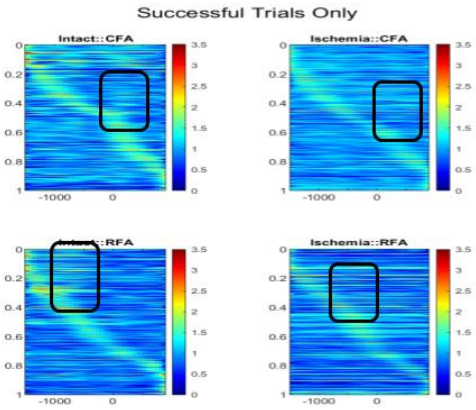

Figure S5.4C

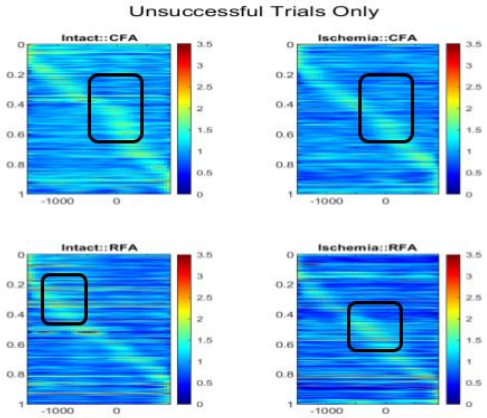

Figure S5.4: Mean spike rate by channel.

A) Mean channel normalized activation, from -1.5 to +0.5 with respect to successful grasp, averaged across all days and channels within an area. Bands represent +/- 1 standard error of the mean (SEM). **B)** and **C)** contain the same groupings for successful and unsuccessful *Grasp* trials respectively but channel rates are expressed as heat maps, where warmer colors represent a higher normalized activity level. Shifted RFA activations in Ischemia rats overall are a little closer to zero. Remaining panels are trends by rats, with earlier days shown in greener hues. The first 6 panels are Ischemia rats and the last 4 are Intact rats. Panels are ordered by RC-identifier number from smallest to largest, within each group.

Figure S5.4D

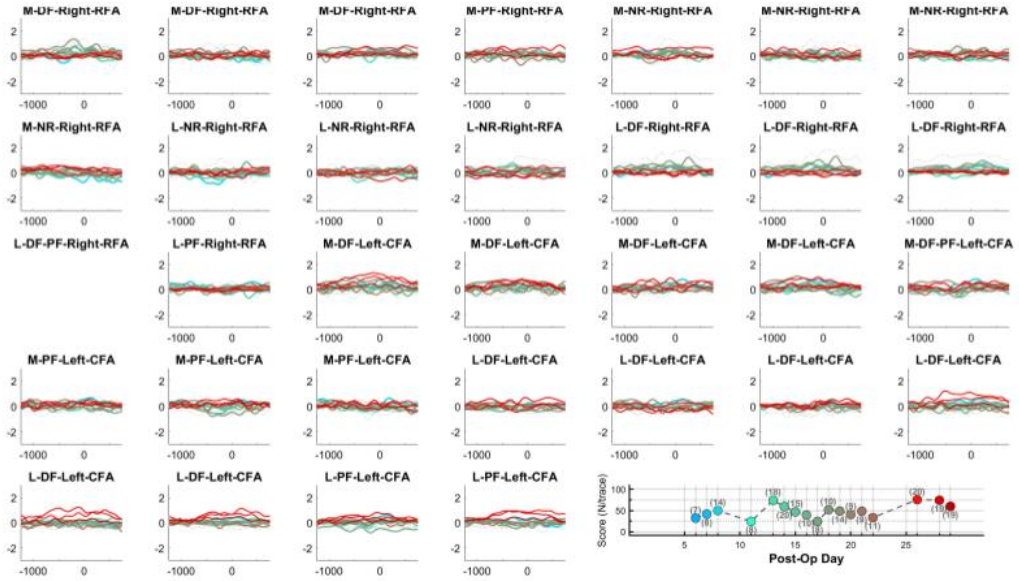

Figure S5.4E

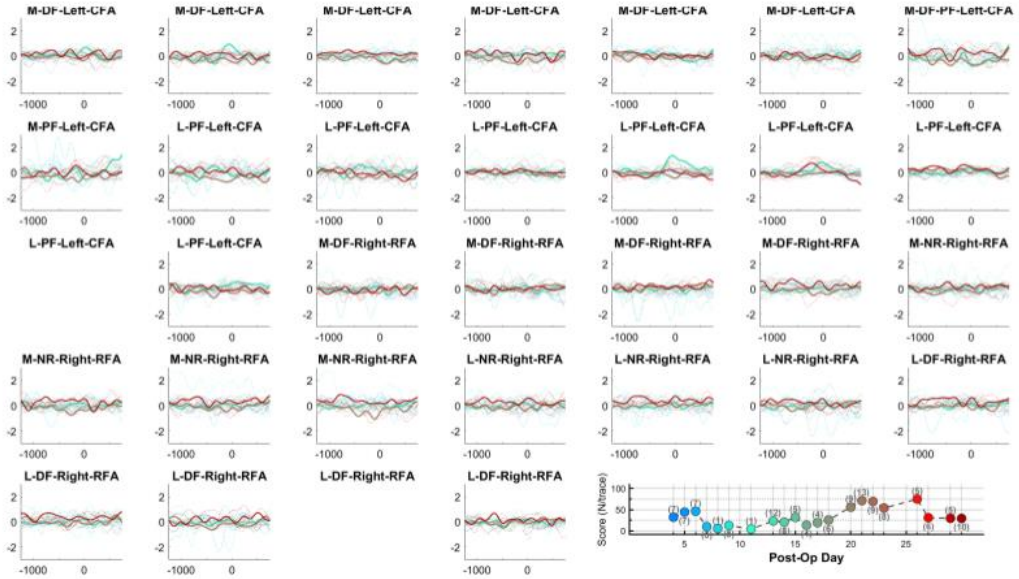

Figure S5.4F

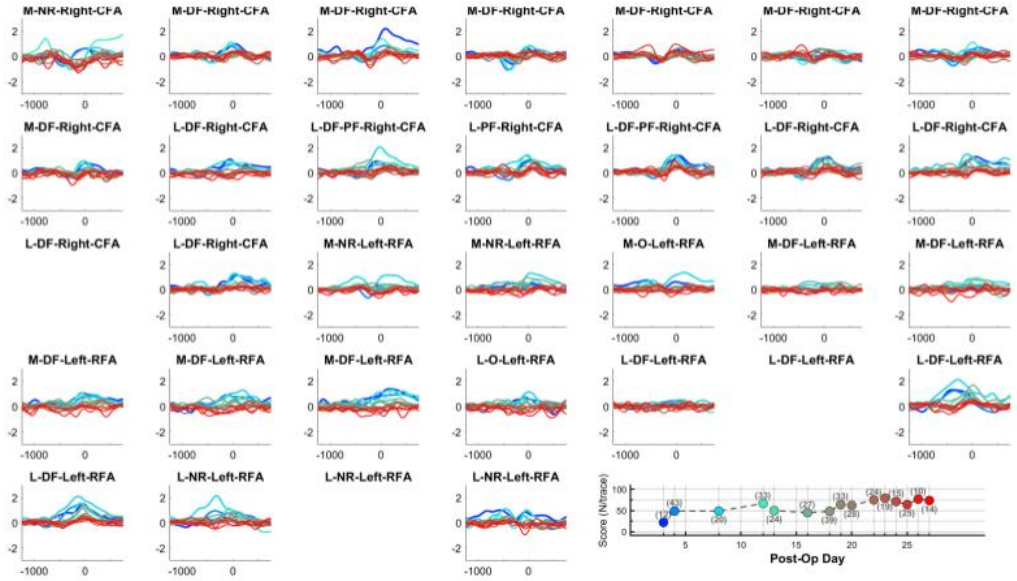

Figure S5.4G

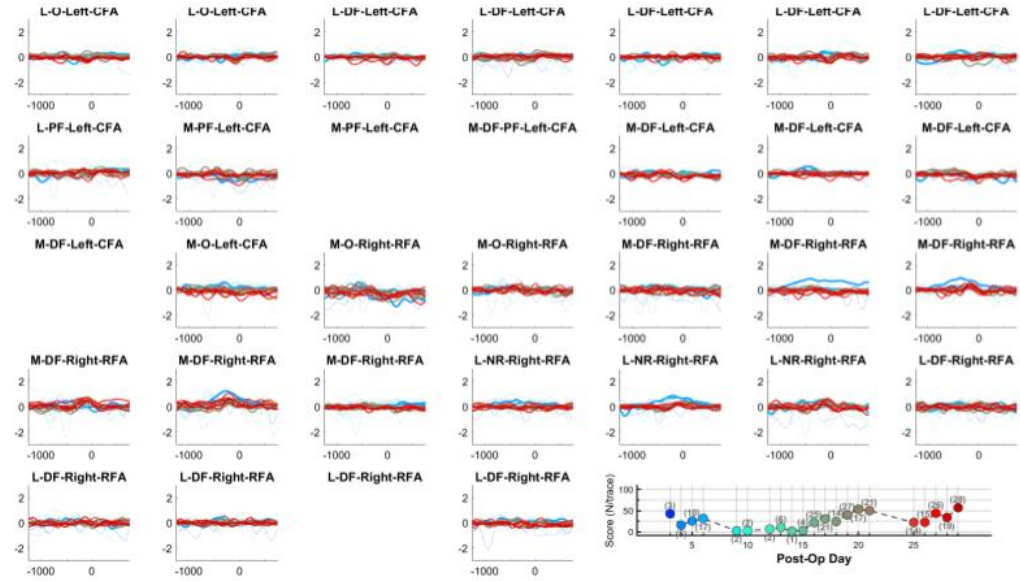

Figure S5.4H

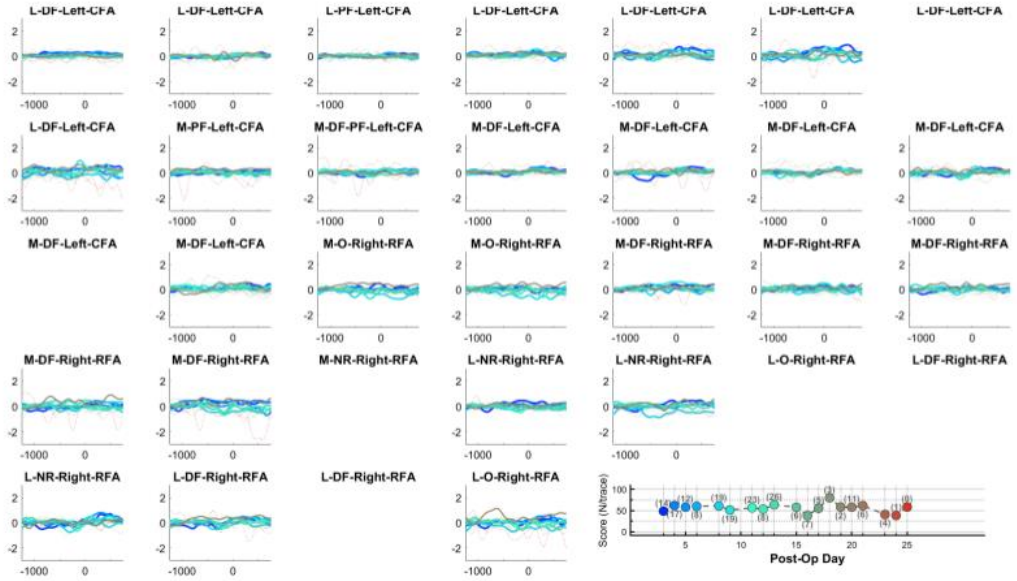

Figure S5.4I

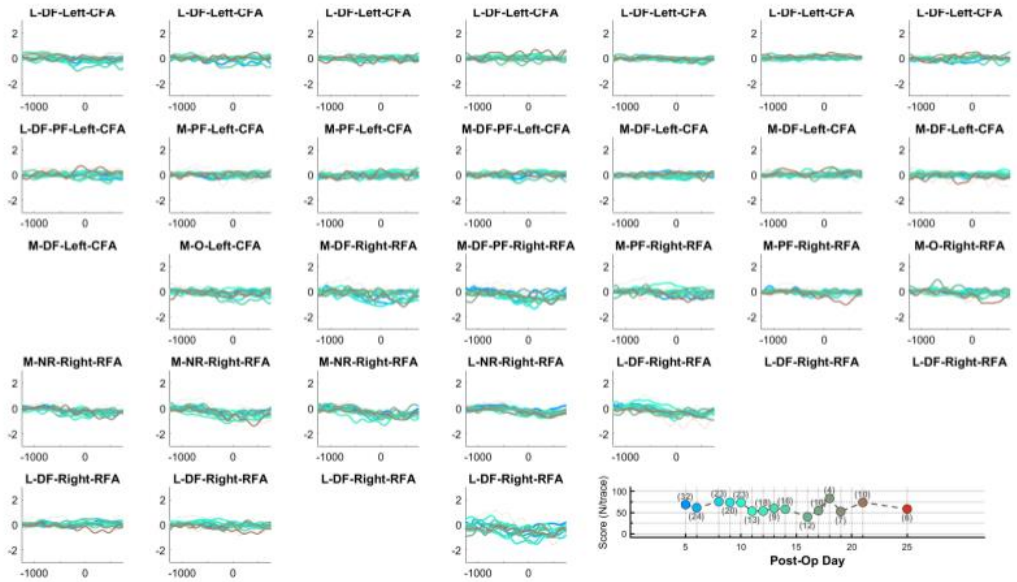

Figure S5.4J

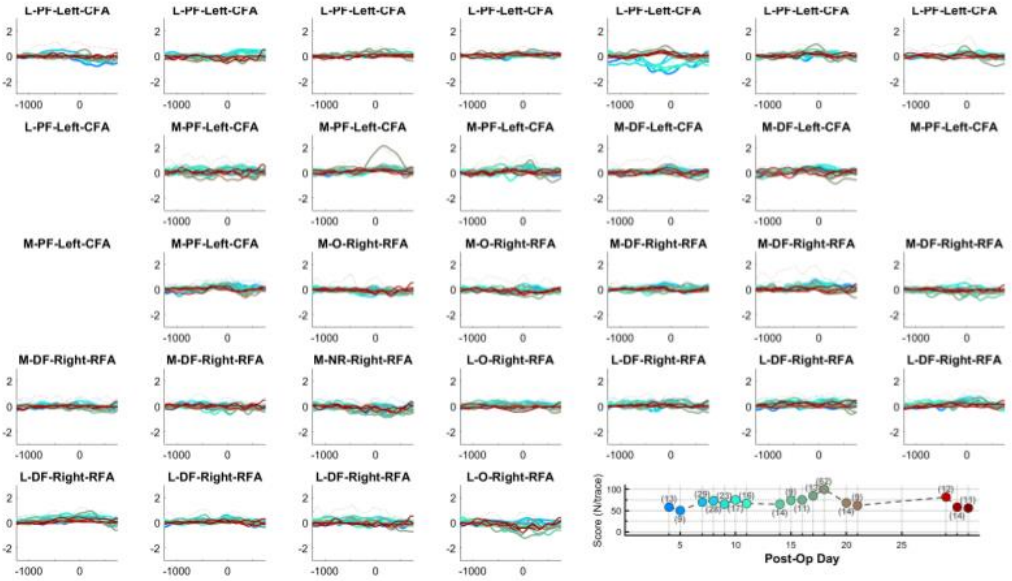

Figure S5.4K

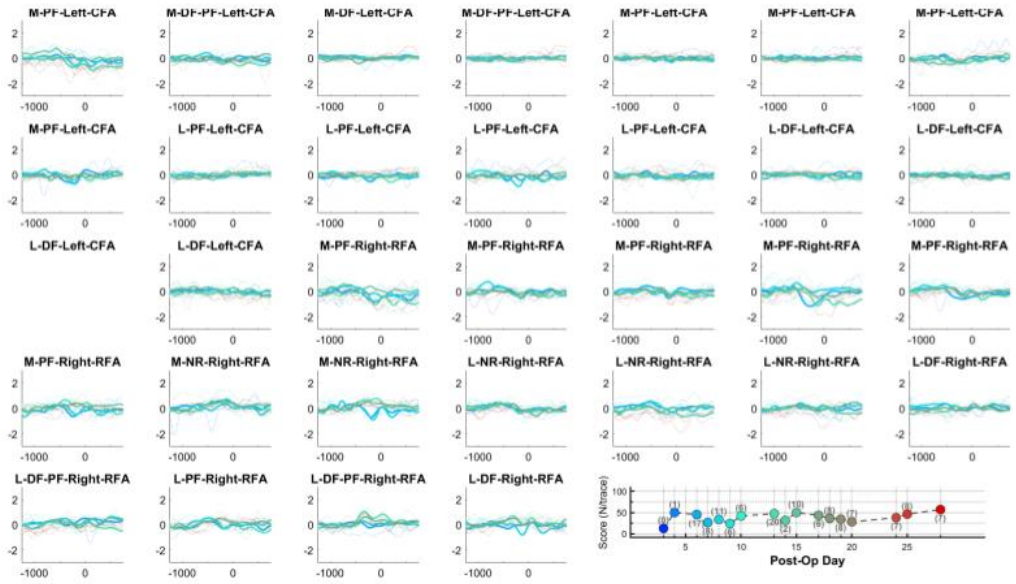

Figure S5.4L

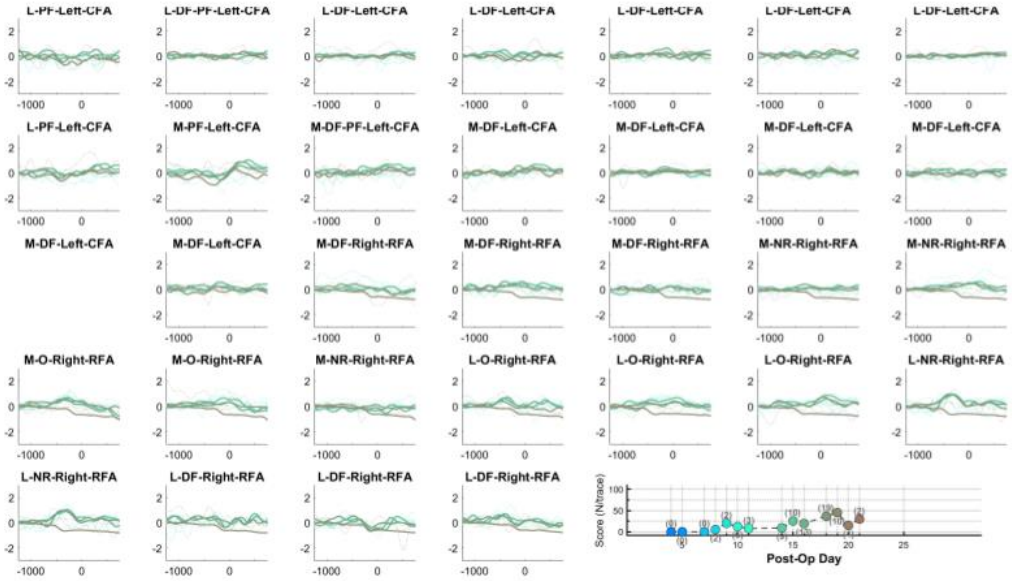

Figure S5.4M

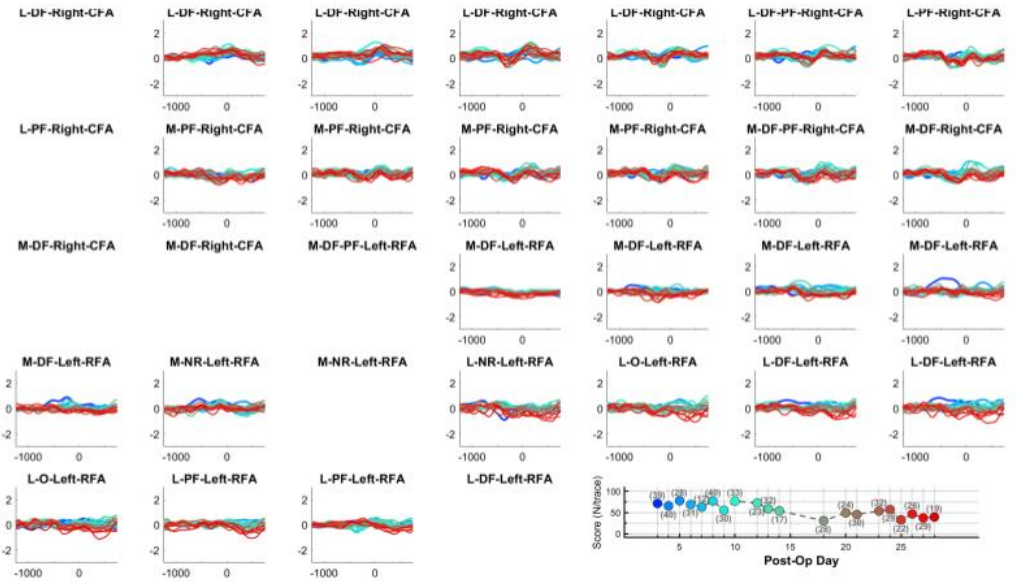

Figure S5.5A

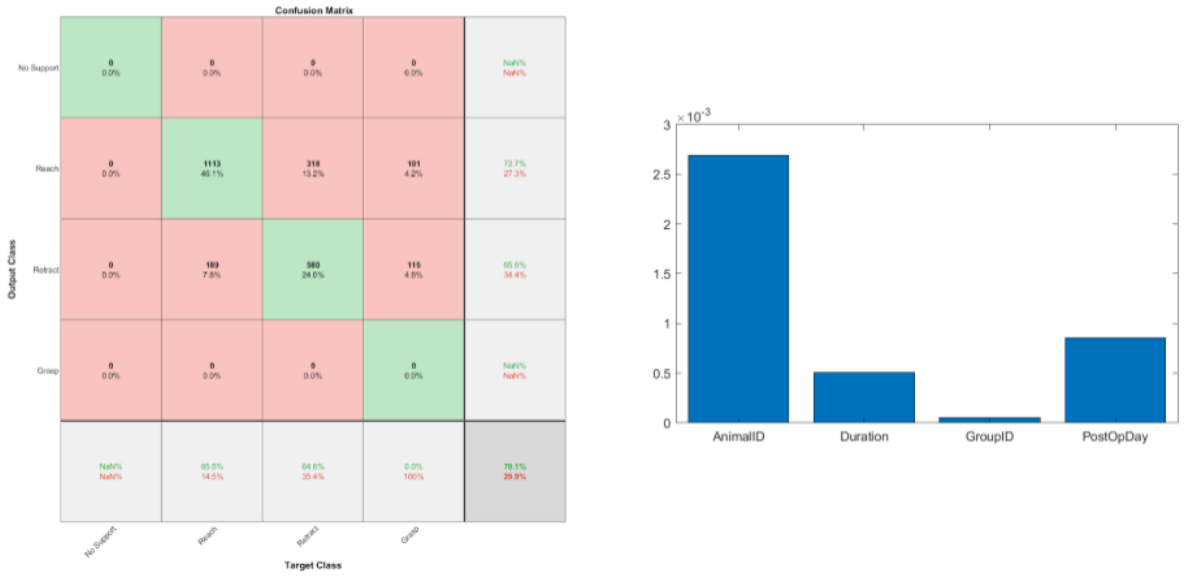

Figure S5.5B

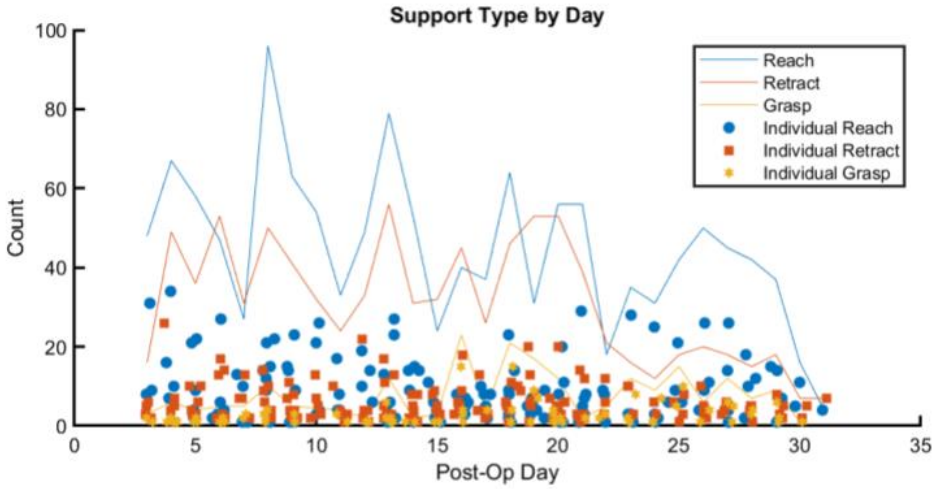

Figure S5.5: Support forelimb movements do not bias data

A) Movement of the support forelimb is not systematically associated with a particular phase of the behavior. One possible confounder, particularly since half of all channels were from microwires in CFA contralateral to the support forelimb, is that timing of movements in

the supporting forelimb were systematically biased in injured rats, such that observations (particularly in contralesional CFA) are more likely a reflection of output related to that limb than the reaching limb of interest. ***Support*** was tagged as the first frame in which movement of the supporting forelimb was observed. We found that this movement was ubiquitous across both groups (the ***"No Support"*** category never occurred across trials included for neural time-series analysis). Timing of the movement appeared to be related more idiosyncratically to individual rats than to group. A support vector machine model was trained to classify the ***Support*** movement as occurring during the ***reach/advance*** phase, synchronous with the ***Grasp***, or during the ***retract*** phase. The most-accurate model (70.1%, *top-left*) supports this conclusion, with *AnimalID* weighted as the most important classifier variable (*bottom-left*).

Figure S5.6A

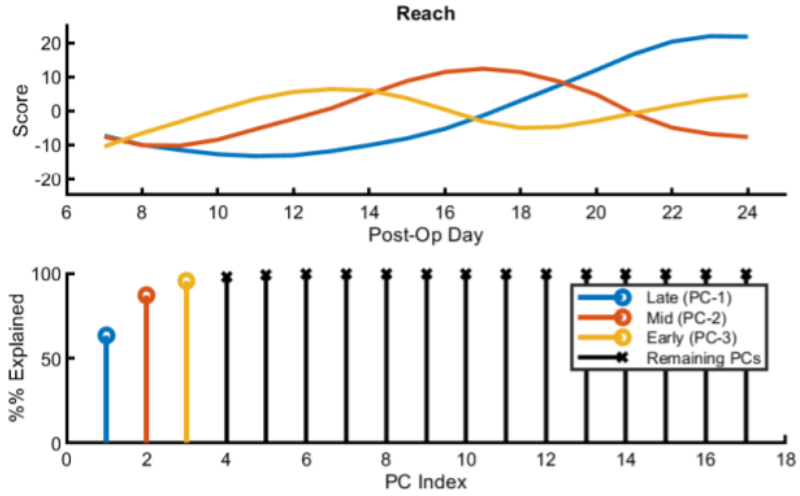

Figure S5.6B

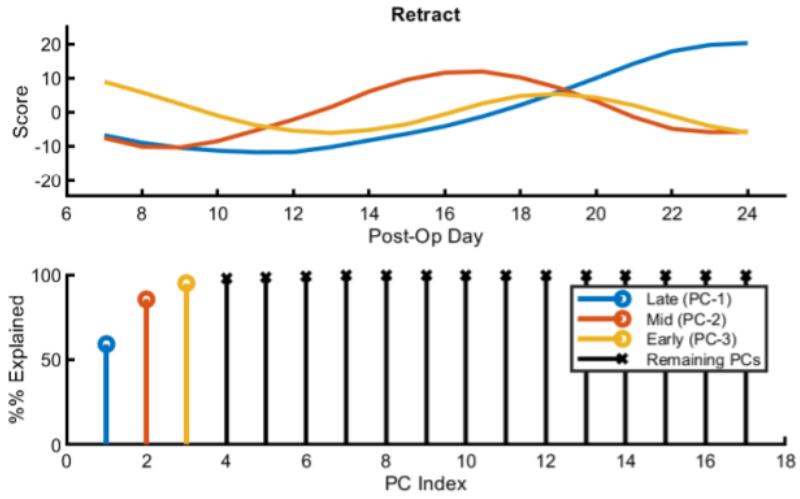

Figure S5.6C

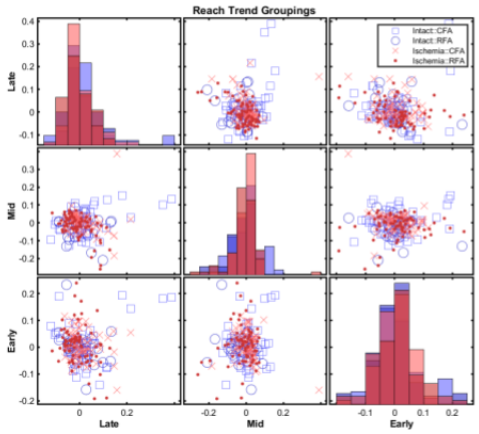

Figure S5.6D

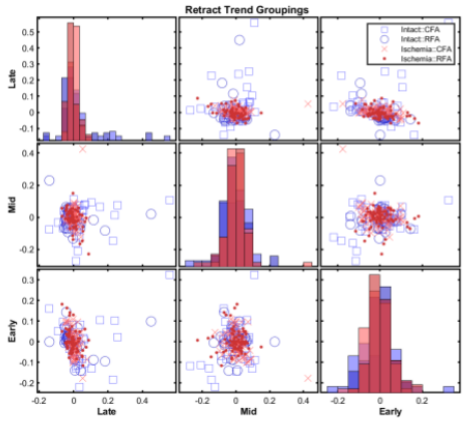

Figure S5.6: PCA Scores for trends in channel-phase association by postoperative day by phase.

A) Channel trends in peak activation by postoperative day for spike counts during the *Reach* phase. Principal components analysis (PCA) breaks down the trends in spike counts associated with a particular phase (here: ***Reach***) for each given channel over the course of all recordings. Some channels showed their peak spike counts during this period only in the latter sessions; if this type of trend were associated to units more frequently conditionally upon whether such channels were more frequently present in a particular area or experimental group, then this might also be an indicator of where plasticity is most-likely to occur.

B) Channel trends in peak activation by postoperative day for spike counts during the *Retract* phase. Principal components analysis (PCA) breaks down the trends in spike counts associated with a particular phase (here: ***Retract***) for each given channel over the course of all recordings. Some channels showed their peak spike counts during this period only in the latter sessions; if this type of trend were associated to units more frequently conditionally upon whether such channels were more frequently present in a particular area or experimental group, then this might also be an indicator of where plasticity is most-likely to occur.

C) Distribution "Early," "Mid," and "Late" component groupings by Area and experimental Group during the *Reach* phase. Cluster analysis reveals that there is no systematic trend in coefficient for a particular trend in longitudinal peak excitability, as demonstrated by spike counts during this phase of the movement, for any combination of Area and Group.

D) Distribution "Early," "Mid," and "Late" component groupings by Area and experimental Group during the *Retract* phase. Cluster analysis reveals that there is no systematic trend in coefficient for a particular trend in longitudinal peak excitability, as demonstrated by spike counts during this phase of the movement, for any combination of Area and Group.

Figure S5.7A

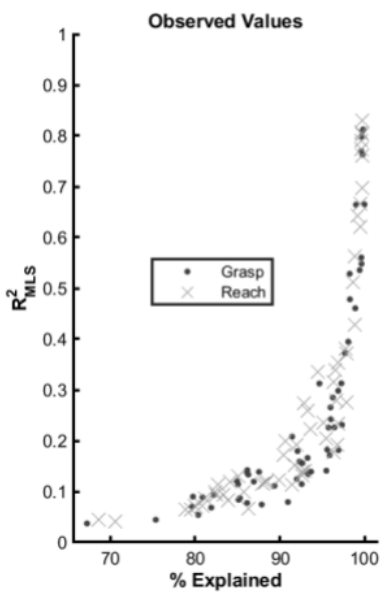

Figure S5.7B

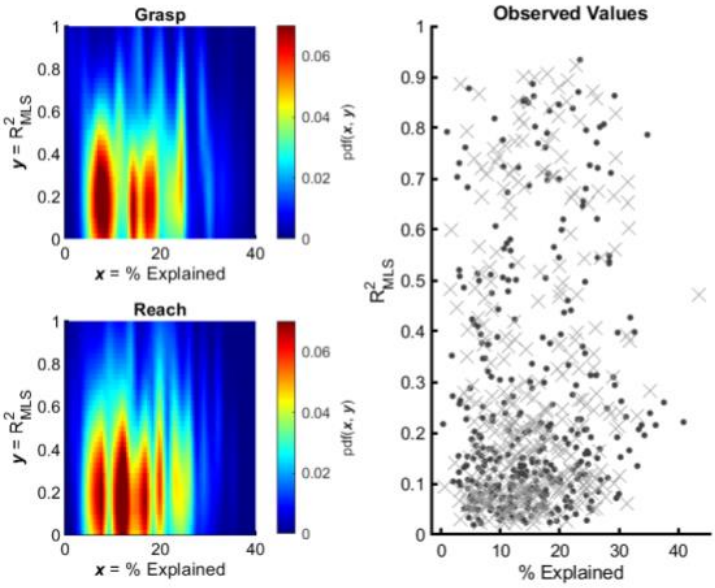

Figure S5.7: Do population features capture the data?

A) Adjusted R^2_{MLS} and percent of data explained. Excellently, there appears to be a pretty strong relationship between the amount of data that is explained by the top-12 principal components. *Note that if 12 principal components do not capture most of the data, then it is strongly suspected that much of the data is noise.*

B) Joint distributions of all planes percent data explained, when projection matrix is broken into pairs of vectors forming subspace planes (such as are used during fixed point analysis). There are many instances when the plane of interest capture a relatively large portion of the data and are still an accurate representation of the original data (*right; dots represent grasp-aligned analyses, crosses represent reach-aligned analyses).*

Figure S5.8A

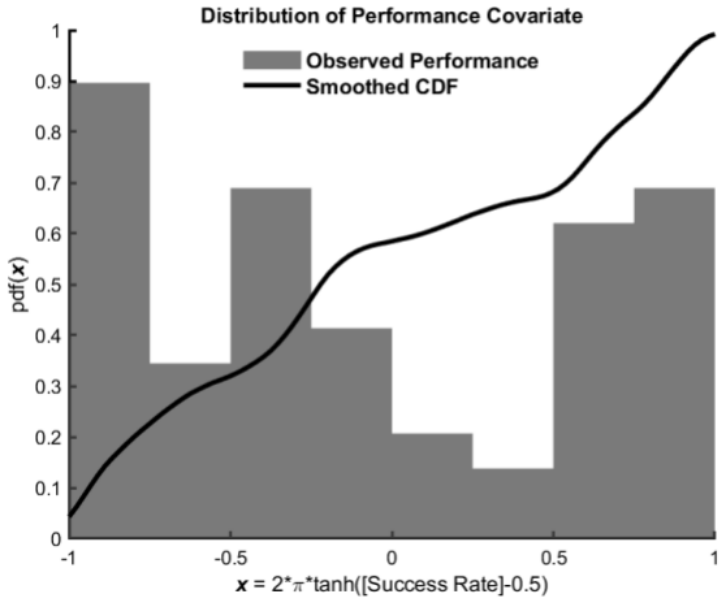

Figure S5.8B

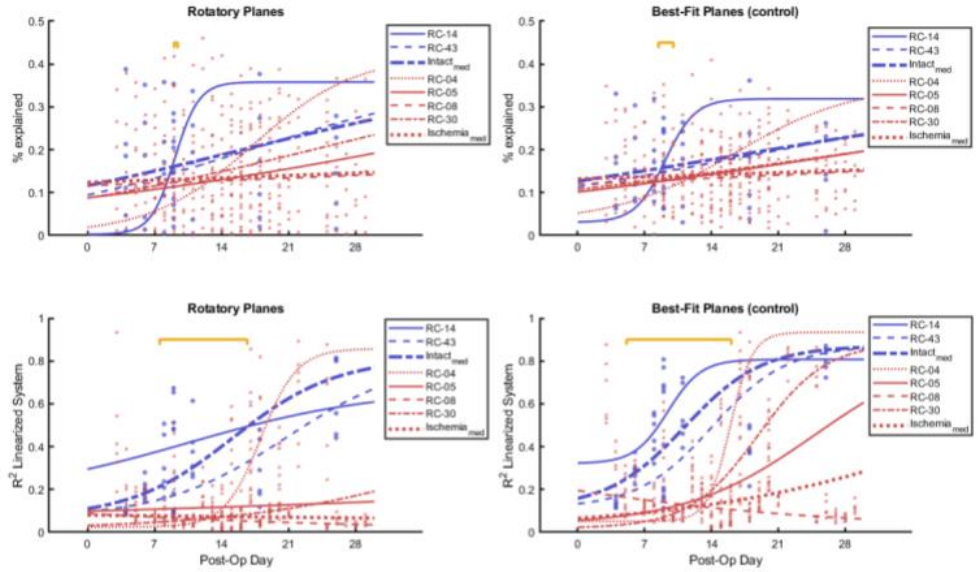

Figure S5.8C

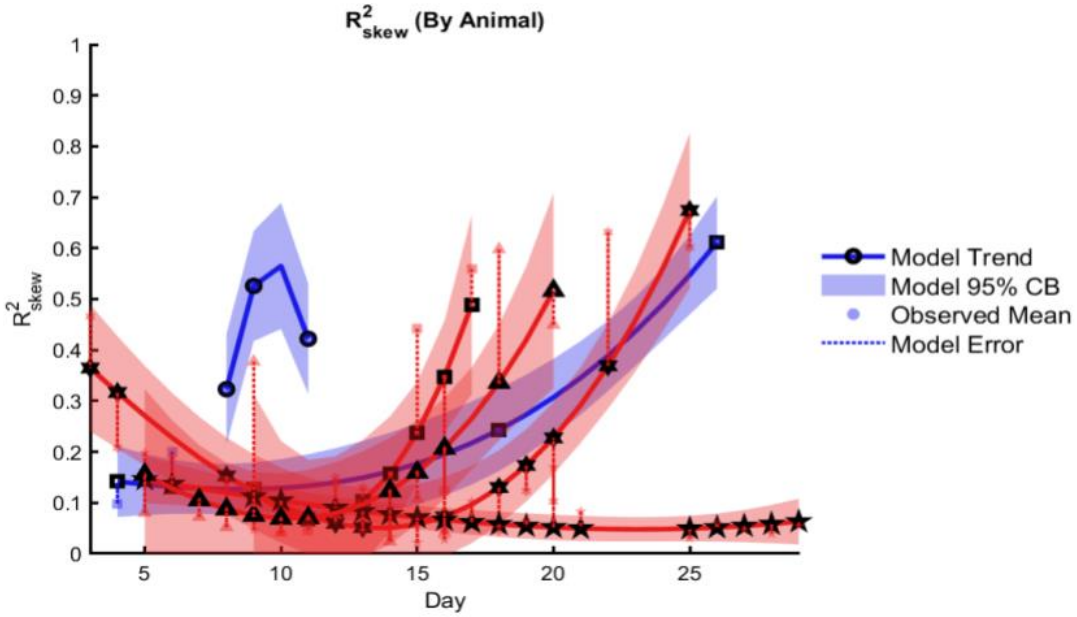

Figure S5.8D

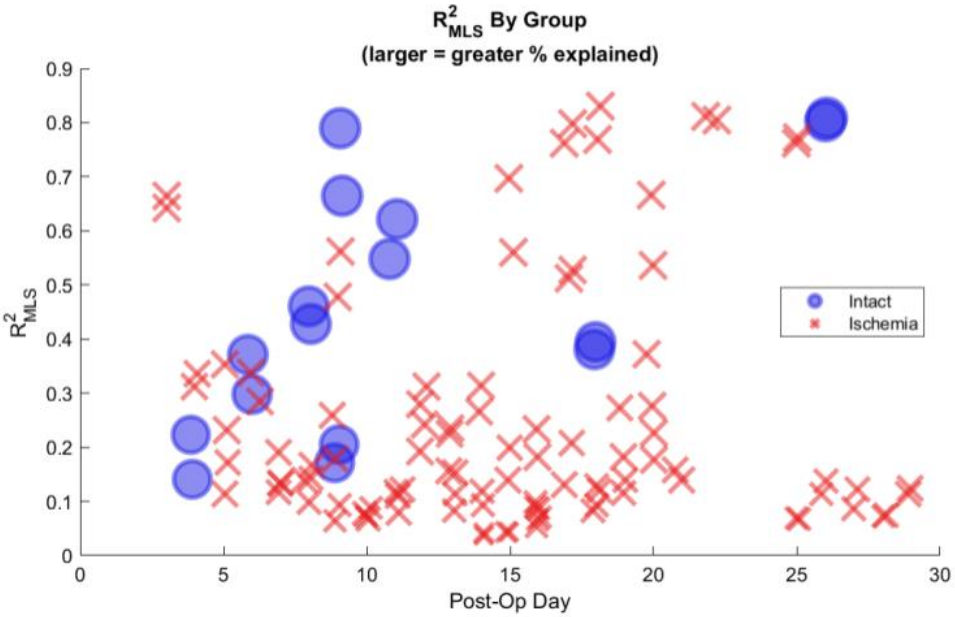

Figure S5.8: Supplementary information for population dynamics models.

A) Performance distribution (response variable in GLME) for statistical models. *A priori,* we know that this covariate is definitely "non-normal" (at least from the presently-observed data). Therefore, we should also look to see if there are "clusters" where the predicted output can be aggregated in a similar fashion. For example, if the predicted output is normally distributed, or only has two clusters, these suggest some nonlinearity between the performance covariate and the predicted output. Note that the ***Success Rate*** used here corresponds to trends shown in **Figure 5.1A** that represent the "Standard" scoring method. The distribution may be approximately tri-modal:

1. At the lower extreme (-1 is the lower bound on tanh output given input bounded by [-0.5, 0.5]), there are a bunch of days for different animals where they got no or very few pellets.
2. In the middle (slightly below "0" Performance score), there are days where there is average behavior.
3. At the upper end of the distribution, there is another cluster of days where the score is really good and hardly any pellets were reached.

B) Trends in rotatory dynamical structure by day. The animal with the largest increases in all categories is RC-04 (Ischemia); the animals with increases in behavioral performance as a function of time are RC-02 (Ischemia), RC-04 (Ischemia) and RC-30 (Ischemia). While RC-02 is not shown here due to losing too many trials in the exclusion process, RC-04 increases in accuracy of linearized system for the best-fit system precede increases in linearized system accuracy for the rotatory-constrained system. While increases for both kinds of systems are comparable for RC-04, the increases for RC-30 are substantially larger in the best-fit system by comparison to the rotatory-constrained system.

C) Adjusted R^2_{skew} by animal. While the data were rarely reconstructed as accurately as when the regression recovered the least-squares optimal regression of the linearized dynamics, regression constrained to impose skew-symmetry on the recovered regression matrix (i.e. jPCA) tended to fit the data with similar temporal trends as when the MLS regression was used. One interesting case on a per-animal basis is ***RC-04*** (***Ischemia; red squares***). This rat had a fairly large difference between R^2_{skew} and R^2_{MLS}, and also evidence of a discrepancy between ***functional*** improvement and ***motor*** improvement. Namely, there was a discrepancy in scoring when comparing results for this rat (particularly in the first and second weeks) between standard scoring on this behavioral task and the scoring required for inclusion in analyses. During the same longitudinal epoch, RC-04 tended to score higher using the ***functional*** rating, but was apparently worse at the task when rigid behavioral rejection criteria were applied. Eventually, the rat adopted a pellet retrieval strategy that allowed both scoring scales to indicate its proficiency was comparable to pre-surgical retrieval levels; however, the strategy typically required multiple "flail" attempts, with the first rapid, short attempts inevitably missing the pellet. In general, the principal components explain most of the data, which indicate that analysis using the top-12 PCs to decompose the data is okay. Panel **D** contains identical information, but scales the size of markers by percent of overall data that is explained by population components.

Table 5.1

Subset	GroupID	Outcome	Variable	Mean	LB_95	UB_95
Included	Intact	Successful	Duration	0.673 (sec)	0.434 (sec)	1.201 (sec)
Included	Intact	Successful	Reach Epoch Duration	0.373 (sec)	0.200 (sec)	0.767 (sec)
Included	Intact	Successful	Retract Epoch Duration	0.300 (sec)	0.167 (sec)	0.634 (sec)
Included	Intact	Successful	Reach Epoch Proportion	0.549 (fraction)	0.346 (fraction)	0.741 (fraction)
Included	Intact	Unsuccessful	Duration	0.850 (sec)	0.434 (sec)	1.368 (sec)
Included	Intact	Unsuccessful	Reach Epoch Duration	0.383 (sec)	0.200 (sec)	0.801 (sec)
Included	Intact	Unsuccessful	Retract Epoch Duration	0.467 (sec)	0.167 (sec)	0.968 (sec)
Included	Intact	Unsuccessful	Reach Epoch Proportion	0.457 (fraction)	0.235 (fraction)	0.756 (fraction)
Included	Intact	All	Duration	0.705 (sec)	0.434 (sec)	1.301 (sec)
Included	Intact	All	Reach Epoch Duration	0.375 (sec)	0.200 (sec)	0.767 (sec)
Included	Intact	All	Retract Epoch Duration	0.330 (sec)	0.167 (sec)	0.801 (sec)
Included	Intact	All	Reach Epoch Proportion	0.532 (fraction)	0.286 (fraction)	0.750 (fraction)
Included	Ischemia	Successful	Duration	0.626 (sec)	0.300 (sec)	1.201 (sec)
Included	Ischemia	Successful	Reach Epoch Duration	0.295 (sec)	0.167 (sec)	0.534 (sec)
Included	Ischemia	Successful	Retract Epoch Duration	0.331 (sec)	0.133 (sec)	0.801 (sec)
Included	Ischemia	Successful	Reach Epoch Proportion	0.485 (fraction)	0.256 (fraction)	0.667 (fraction)
Included	Ischemia	Unsuccessful	Duration	0.639 (sec)	0.300 (sec)	1.201 (sec)
Included	Ischemia	Unsuccessful	Reach Epoch Duration	0.294 (sec)	0.133 (sec)	0.601 (sec)
Included	Ischemia	Unsuccessful	Retract Epoch Duration	0.345 (sec)	0.133 (sec)	0.834 (sec)
Included	Ischemia	Unsuccessful	Reach Epoch Proportion	0.473 (fraction)	0.200 (fraction)	0.727 (fraction)
Included	Ischemia	All	Duration	0.633 (sec)	0.300 (sec)	1.201 (sec)
Included	Ischemia	All	Reach Epoch Duration	0.294 (sec)	0.133 (sec)	0.567 (sec)
Included	Ischemia	All	Retract Epoch Duration	0.339 (sec)	0.133 (sec)	0.801 (sec)
Included	Ischemia	All	Reach Epoch Proportion	0.478 (fraction)	0.226 (fraction)	0.700 (fraction)

Table 5.1: Descriptive statistics for **included** phase durations.

Each table row contains the total trial duration, as well as individual phase durations, for the phases of movement (*Reach*, *Retract*, or *Total Duration*) that describe the pellet retrieval behavior.

Table 5.2

Group	Area	Week	Trials	Channels	Recordings	Performance*	Reach Duration* (ms)	Retract Duration* (ms)	P(Baseline)	Mean Spikes Baseline	P(Reach)	Mean Rate Reach	P(Retract)	Mean Rate Retract
Ischemia	RFA	1	176	91	17	-0.42	317.5	291.0	0.335	49 ± 6.42	0.825	26 ± 4.39	0.089	49 ± 3.64
Ischemia	RFA	2	736	91	25	-0.43	310.0	285.6	0.641	39 ± 6.28	0.748	21 ± 3.26	0.834	39 ± 3.28
Ischemia	RFA	3	1296	91	32	-0.12	290.1	289.4	0.674	30 ± 4.65	0.839	13 ± 2.32	0.068	30 ± 2.69
Ischemia	RFA	4	781	59	17	0.37	255.9	254.3	0.338	23 ± 5.49	0.547	8 ± 2.47	0.670	23 ± 2.66
Ischemia	CFA	1	173	89	16	-0.38	317.4	290.0	0.335	42 ± 5.45	0.825	19 ± 3.22	0.089	42 ± 3.42
Ischemia	CFA	2	736	88	25	-0.39	310.0	285.5	0.641	36 ± 4.53	0.748	17 ± 2.47	0.834	36 ± 2.75
Ischemia	CFA	3	1310	89	33	-0.07	289.0	289.6	0.674	38 ± 4.48	0.839	13 ± 2.26	0.068	38 ± 2.67
Ischemia	CFA	4	781	57	17	0.41	255.4	254.6	0.338	39 ± 6.59	0.547	11 ± 2.91	0.670	39 ± 3.23
Intact	RFA	1	88	25	8	0.88	338.5	316.9	0.335	37 ± 8.92	0.825	18 ± 4.88	0.089	37 ± 5.37
Intact	RFA	2	133	38	17	0.90	351.8	288.0	0.641	33 ± 8.08	0.748	13 ± 3.86	0.834	33 ± 2.93
Intact	RFA	3	72	27	5	0.70	331.4	315.5	0.674	49 ± 14.73	0.839	30 ± 13.03	0.068	49 ± 4.44
Intact	RFA	4	19	13	6	0.74	280.1	353.3	0.338	58 ± 20.22	0.547	17 ± 7.86	0.670	58 ± 8.67
Intact	CFA	1	91	26	9	0.87	332.6	324.0	0.335	45 ± 9.32	0.825	21 ± 4.95	0.089	45 ± 6.45
Intact	CFA	2	133	41	17	0.89	350.6	292.2	0.641	40 ± 6.52	0.748	18 ± 3.42	0.834	40 ± 3.88
Intact	CFA	3	72	25	5	0.70	332.9	312.3	0.674	31 ± 12.52	0.839	20 ± 10.44	0.068	31 ± 7.09
Intact	CFA	4	19	12	6	0.74	278.8	354.1	0.338	46 ± 16.58	0.547	16 ± 7.86	0.670	46 ± 10.15

Table 5.2: Descriptive statistics for weekly spike data (by group).
Table shows mean spike counts, plus or minus one standard error of the mean, for different groupings by area, group, and postoperative week, during the different phases of the motor behavior.

Table 5.3

Area	Week	Effect Size (Cohen's D)	
CFA	1	0.78	
CFA	2	0.24	
CFA	3	0.82	Mean: CFA
CFA	4	1.16	0.75
RFA	1	0.23	
RFA	2	0.44	
RFA	3	0.88	Mean: RFA
RFA	4	1.53	0.77

Table 5.3: Effect size for weekly spike data by area and week.
Weekly effect size estimates are given using Cohen's D for comparisons between the **Ischemia** and **Intact** groups by area and postoperative week. Values range from week effect sizes to very strong effect sizes, when estimated in this way.

Table 5.4

Alignment	Term	Estimate	tStat	p
Grasp	(Intercept)	0.017	1.245	0.216
Grasp	FP_Classification_Unstable Node	0.092	1.006	0.317
Grasp	FP_Classification_Saddle Point	-0.084	-2.725	0.008
Grasp	FP_Classification_Unstable Spiral	0.435	2.872	0.005
Grasp	FP_Classification_Stable Node	-0.218	-1.716	0.089
Grasp	FP_VarCapt	-0.001	-0.985	0.327
Grasp	FP_Classification_Unstable Node:FP_VarCapt	-0.003	-2.150	0.034
Grasp	FP_Classification_Saddle Point:FP_VarCapt	0.003	2.889	0.005
Grasp	FP_Classification_Unstable Spiral:FP_VarCapt	-0.013	-2.541	0.013
Grasp	FP_Classification_Stable Node:FP_VarCapt	0.010	1.953	0.054
Reach	(Intercept)	-0.022	-1.348	0.181
Reach	FP_Classification_Unstable Node	0.208	2.533	0.013
Reach	FP_Classification_Saddle Point	-0.044	-1.654	0.101
Reach	FP_Classification_Unstable Spiral	0.149	1.029	0.306
Reach	FP_Classification_Stable Node	-0.276	-2.695	0.008
Reach	FP_VarCapt	0.001	1.501	0.137
Reach	FP_Classification_Unstable Node:FP_VarCapt	-0.003	-2.545	0.012
Reach	FP_Classification_Saddle Point:FP_VarCapt	0.001	0.822	0.413
Reach	FP_Classification_Unstable Spiral:FP_VarCapt	-0.009	-2.070	0.041
Reach	FP_Classification_Stable Node:FP_VarCapt	0.011	2.650	0.009

Table 5.4: Fixed point classification Random Effects

Table of statistically significant random effects for fixed point classification model that predicts behavioral performance.

Supplementary Table S5.1

Name	Reference	Purpose	Distribution	Link	Fit	Wilkinson Model Notation
Model-1	Figure 5.1a	Compare baseline performance of Ischemia and Intact groups.	binomial	logit	REMPL	nSuccess~1+GroupID+(1|AnimalID)
Model-2	Figure 5.1a	Compare Pre- vs. Post- Surgery performance.	binomial	logit	REMPL	nSuccess~1+GroupID*PrePost+(1|AnimalID)
Model-3	Figure 5.1a	Compare by-group recovery trends.	binomial	logit	REMPL	nSuccess~1+GroupID*Day_Cubed+(1+Day+ Day_Cubed|AnimalID)
Model-4	Figure S5.1b	Compare standard scoring with restrictive scoring used in neural analyses.	binomial	logit	REMPL	nSuccess~1+Method*GroupID*Day_Cubed+(1+Day+Day_Cubed|AnimalID)
Model-5	Figure S5.2a	Test for trends in total trial duration (all trials) by Post-Op Day and Group.	normal	log	REMPL	Duration~1+GroupID*(Day+Day_Cubed)+(1+Day+Day_Cubed|AnimalID)
Model-6	Figure S5.2b	Test for trends in total successful trial duration (only those included for neural analyses) by Post-Op Day and Group.	normal	log	REMPL	Duration~1+GroupID*(Day+Day_Cubed)+(1+Day+Day_Cubed|AnimalID)
Model-7	Figure S5.2c	Test for trends in reach phase duration by Post-Op Day and Group for successful trials used in neural analyses.	normal	log	REMPL	Reach_Duration~1+GroupID*(Day+Day_Cubed)+(1+Day+Day_Cubed+Duration|AnimalID)
Model-8	Figure S5.2d	Test for trends in retract phase duration by Post-Op Day and Group for successful trials used in neural analyses.	normal	log	REMPL	Retract_Duration~1+GroupID*(Day+Day_Cubed)+(1+Day+Day_Cubed+Duration|AnimalID)
Model-9	Figure S5.2e	Test for trends in reach phase proportion (relative to total trial duration) by Post-Op Day and Group for successful trials used in neural analyses.	normal	log	REMPL	Reach_Proportion~1+GroupID*(Day+Day_Cubed)+(1+Day+Day_Cubed+Duration|AnimalID)
Model-10	Figure 5.2b	Test for trends in individual spike count differences during pre-grasp epoch.	poisson	log	REMPL	n_Pre_mean ~ 1 + GroupID*Area + (1 + n_Pre_pred | AnimalID)
Model-11	Figure 5.2c	Test for trends in individual spike count differences during Reach epoch.	poisson	log	REMPL	n_Reach_mean ~ 1 + GroupID*Area + (1 + n_Reach_pred | AnimalID)
Model-12	Figure 5.2d	Test for trends in individual spike count differences during Retract epoch.	poisson	log	REMPL	n_Retract_mean ~ 1 + GroupID*Area + (1 + n_Retract_pred | AnimalID)
Model-13	Figure 5.3c	Do individual units allow the prediction of single-trial outcomes, differentiating between RFA and CFA on the distribution of such units with predictive power?	**Matlab (R2020b) fitcnb: Naive Bayes Classifier**			Labels ~ 1 + Performance_mu + (1 + N_Pre_Grasp + N_Reach + N_Retract | ChannelID)
Model-14	Figure 5.3d	Do individual units allow the prediction of single-trial outcomes, when accounting for the "speed" with which the trial is performed, differentiating between RFA and CFA on the distribution of such units with predictive power?	**Matlab (R2020b) fitcnb: Naive Bayes Classifier**			Labels ~ 1 + Performance_mu + (1 + N_Pre_Grasp + N_Reach + N_Retract + Reach_Duration + Duration | ChannelID)
Model-15	Figure 5.4a	Was there a trend in R2_MLS by Week, accounting for individual animal trends?	normal	identity	REMPL	R2_Best ~ 1 + Week + (1 + PostOpDay + PostOpDay3 | AnimalID)
Model-16	Figure 5.4a	Do individual animal trends in R2_MLS account for more of the variance beyond what is explained by interaction of Group*PostOpDay?	normal	identity	REMPL	Performance ~ 1 + GroupID*PostOpDay + (1 + Duration + R2_Best | AnimalID)
Model-17	Figure 5.4b,c	Does performance relate in some way to the presence of a particular fixed-point, regardless of experimental grouping?	normal	identity	REMPL	Performance~1+(1+FP_Classification*FP_VarCapt|Alignment)+(1+PostOpDay|AnimalID)
Model-18	Figure 5.4d	Is there a significant relation between Performance and the deviation between R2_Skew and R2_Best?	normal	identity	REMPL	Performance ~ 1+GroupID*R2_Best*R2_Skew*Explained+(1+PostOpDay+Duration|AnimalID)

Supplementary Table S5.1

Summary of Statistical Models

Summary of statistical models used in estimating different responses related to the pellet retrieval task and cortical dynamics. This table lists models by name as they are described in order in Chapter 5. A brief summary of the model's purpose, along with the distribution and link function (if the model was obtained using the Matlab `fitglme` function) are provided. All GLME fits made use of the restricted maximum pseudo-likelihood (REMPL) fit method. The final column defines the statistical model terms in Wilkinson notation; the key point about this notation is that a term defined as "A*B" includes both the individual main fixed-effects of A and B, as well as their interaction. Terms grouped using parenthesis are random effect coefficients that are grouped by the variable listed after the "|" operator.

CHAPTER 6

Cortical sensorimotor engagement in movement

Introduction

The results discussed in **Chapter 5** suggest that if *recovery* after stroke is possible, then intervention must be targeted in such a way that facilitates cortico-cortical sensorimotor interactions. This suggestion is primarily observational and attempts to account for key neuroanatomical (sprouting; Dancause et al. 2005, Dancause et al. 2006) and behavioral (increased sensory error rate; Nudo et al. 2000) made by our group in the past. This chapter will briefly describe other areas where reorganization could occur, arguing that such cases represent the suboptimal convergence of nervous system reorganization during post-stroke plasticity. A modified version of the pellet retrieval task as previously described is presented along with example data obtained from a behaving rat using this setup. Task data from a small cohort of rats is not presented in its entirety, but could be a rich source of information for future experiments or research proposals.

The example dataset is used to make concrete points illustrating the value of the technical model schema as they are presented. A critical contribution is simply to explain which parametric elements of such model schema act as “sliders,” corresponding to neurorehabilitation research designs that study interventions targeted to specific mechanisms of the nervous system in control of movement. Thinking about such problems in this way clarifies unknown parametric components that could introduce complications in experimental design later, or challenges that might introduce nonsignificant noise sources during the collection of experimental data in practice.

Any discussion of theoretical models is supplemented using examples from findings in either the behaving rat or from a second dataset collected in the acute rat preparation. In these latter experiments, anesthetized rats were subjected to a peripheral sensory mechanical solenoid stimulus while measuring field potentials in both motor and sensory cortex. Findings from the acute rat are currently in preparation to be submitted to *Frontiers in Human Neuroscience* for a special issue about the utility of brain stimulation mapping (Hayley et al. 2020); the full manuscript and total findings do not apply to this Chapter and therefore are not included in their entirety.

Background

The debate about recovery and restitution after stroke

The late 1980s and 1990s were an exciting time in the field of neurorehabilitation research. Beginning in the 1980s, strategies for physical therapy emerged suggesting more efficacious behavioral interventions that could augment existing techniques that made use of a combination of the Reflex and Hierarchical theories of movement (Bobath & Bobath 1984, Wolf et al. 1989). As understanding of the nervous control of movement evolved, the approach to physical therapy was modified to include the active suppression of abnormal movement sequences while simultaneously providing somatosensory or proprioceptive stimuli to the patient (Brock et al. 2002). Motor mapping experiments in monkeys with subtotal focal ischemia in the hand representation of motor cortex provided evidence for an association between functional reorganization of motor representation in the cerebral cortex and behavioral recovery of hand function (Nudo et al. 1996), suggesting that volitional use of the paretic limb during the postacute window may shape reorganization in nearby cortical territory.

With the notion that behavioral interventions *could* be associated with functional reorganization of nervous tissue, research during the subsequent decades sought to uncover specific mechanisms linking these things. The rat model helped to uncover molecular and transcriptional mechanisms that occur serially during the postacute window (Carmichael 2006, Carmichael et al. 2012). At the same time, research in rat models of injury showed that the rats became more proficient in performing behavioral tasks with the forelimb ipsilateral to the injury (Bury & Jones 2002, Linslee et al. 2004), and that overuse during the postacute period was associated with worse functional outcomes (Kozlowski et al. 1996, Bland et al. 2001). This transitioned to the study of the relative roles of the intact and paretic limbs in the rat injury model, particularly during pellet retrievals; findings suggested that the use of the non-paretic limb during this time could incur deficits on the use of the paretic limb (Allred et al. 2005, Allred & Jones 2008, Allred

et al. 2010). Instead, if rats performed a skilled motor behavior that involved the paretic limb, their pellet retrieval skill was improved, but only if the motor behavior required some element of dexterity (Maldonado et al. 2008). These results were supported by the findings that motor training using the impaired forelimb was associated with a reduction in forelimb representation in the uninjured hemisphere (Barbay et al. 2013) and that inactivating the contralesional hemisphere improved recovery after cortical injury (Mansoori et al. 2014). At the same time, other groups who had studied the reaching rat model for decades urged caution in interpreting such results due to the many possible feature-specific peculiarities of the reaching behavior that could relate to the observed changes (Whishaw 2000, Whishaw et al. 2008). Instead, they suggested that changes observed in the rat model and associated with molecular, cellular, or neuroanatomical correlates of plasticity after stroke might actually relate to compensatory mechanisms or could even indicate deleterious plasticity (Alaverdashvili & Whishaw 2008a, Alaverdashvili et al. 2008b, Alaverdashvili & Whishaw 2010).

These disagreements stem from a deeper issue: it was and remains extraordinarily difficult to determine the causal relationship between plasticity mechanisms and functional recovery when both the putative mechanism and the outcome are emergent processes of many underlying factors. Such arguments will continue to plague the rat (and likely any animal) model until specific features of movement are clearly related to filtering in the nervous tissue where plasticity occurs. Furthermore, as soon as an experimentally-specific indicator of reorganized dynamics is detected in relation to movement, the longitudinal experiment must be immediately terminated so that histological and molecular techniques might isolate underlying mechanisms at the time of emergence in such a filter feature. Of course, it is one thing to suggest these things: in practice, such an endeavor would be tremendously difficult and would probably require an inter-institutional collaborative effort in order to properly address personnel and budgetary constraints. At a technical level, the ability to detect such dynamics and relate them

to movement on the same timeline as the experiment is simply something that does not exist anywhere in the world (although it could) as of the time of this writing. Therefore, the following perspective and methodological illustrations are provided so that this effort, which will be required inevitably, might start sooner rather than later.

Simplified movement control perspective: nervous control as a black box

A more comprehensive review of motor control perspectives is introduced in **Chapter 3**. This Chapter assumes the Systems perspective when it comes to movement. The idea of treating the nervous system like a black box while observing movements is not new (Todorov & Jordan 2002, Stergio & Decker 2011). Neither is the idea that it is possible to study internal subsystems responsible for such dynamics by making specific experimental perturbations to the subject in the context of the motor behavior (Shadmehr & Mussa-Ivaldi 1994, Churchland et al. 2006). In general, these studies make use of some linear or nonlinear metric that serves as a heuristic to qualitatively describe some feature of the system that is to be approximated. For example, the apparently random movement of markers tracking the movement of the knees or waist can be broken down into regimes that indicate whether movements indicate the presence of underlying mechanisms suggestive of a specific type of pathology (Huisinga et al. 2018).

Most such studies do not have access to recording elements from the “black box” of the nervous system directly. While this chapter will not discuss perturbing the reaching dynamics of the rat (e.g. the behavior shown in **Videos 6.1**, **6.2**, and **6.3**), it aims to provide models at differing levels of complexity with concrete parametric suggestions.

Neural substrates for movement reoptimization after injury

Cortical activity in humans

Observations that motor learning effects on simple finger-tapping tasks could be observed using fMRI to co-register shifts in activation occurring over the course of 3 weeks upon learning a

trained sequence in a finger-opposition task (Karni et al. 1998, Ungerleider et al. 2002) suggested a possible assay for motor-related imaging of stroke survivors. This conclusion was supported by a clinical study that used both fMRI and transcranial magnetic stimulation (TMS) to test "laterality" of response time inhibition with respect to TMS pulses aimed at motor targets in each hemisphere and at different latencies relative to a finger tapping response task (Johansen-Berg et al. 2002). The study found that dorsal premotor cortex (PMd) of the intact hemisphere may be more-involved when deficits in stroke survivors were more severe, possibly subserving a compensatory role. Similarly, a prospective study of stroke survivors grouped by injured or intact premotor cortex (12 patients with intact PM, and 19 patients with injured PM territory) found that mobility outcomes were worse in the group with injured PM territory (Miyai et al. 1999). Cramer and colleagues found that reduced fMRI activations in the injured hemisphere may actually relate with improved functional outcomes, although it is noted that the signal could be confounded by biasing factors ubiquitous in T2*-weighted images, such as might occur during gliosis which likely occurs at the site of injury in stroke survivors (Cramer et al. 2006).

This type of rearrangement of responsibility for motor output may occur broadly and involve subcortical areas: a longitudinal fMRI study of stroke survivors found that task-related activations across many areas of the brain decreased as a function of session in stroke survivors, but not in intact controls (Ward et al. 2003).

Cortical activity in the rat model

Improvements in noninvasive imaging and stimulation techniques allowed more studies in the early 2000s to measure neurophysiological correlates of cortical reorganization. In rats, functional magnetic resonance imaging (fMRI) found that there was an initial increase in activity in the contralesional hemisphere (Dijkhuizen et al. 2001), and that by the second week

hemispheric imbalance is more normalized although inhibition of responses in the injured sensorimotor cortex persists (Dijkhuizen et al. 2003). In combination with the rat behavioral experiments previously described, this seems to suggest a maladaptive role of inhibition in the injured hemisphere that arises from the uninjured. More recently, activity measured directly from the rat perilesional cortex after photothrombotic ischemia has been shown to demonstrate quasi-oscillatory, low-frequency oscillations in the local field potential (LFP), which seem to cause phasic spiking entrainment coherently around the behavior, and which are associated with improvements in the ability of the rat in pellet retrievals (Ramanathan et al. 2018). This suggests that activity in the rat cerebral cortex is probably related, at least in some cases, to recovery after ischemic stroke.

More recently, there have been substantial improvements in the understanding of motor cortical activity in intact rats that should be considered when interpreting results obtained in injured rats. In mice, it was found that on the basis of layer (layer ⅔ vs. layer 5b), the response to learning a lever task was quite different, presumably reflecting differences in the shifting tunings of outputs, but not “horizontal” connections within the network (Masamizu et al. 2014). Calcium imaging in mice performing the same lever task indicates that a large number of neurons become active even when no movements are apparently being performed; furthermore, as the task is learned, dissimilar movements led to more decorrelated activity and demonstrated heterogeneous associations even with the same movement, suggesting their reduced involvement in the movement as learning progressed over the course of two weeks (Peters et al. 2017a, Peters et al. 2017b). This again leads to the idea that cortex takes an active role in movements particularly when movements are new or challenging, but as they become more practiced, their representation becomes fixed elsewhere (Papale & Hooks 2018). This makes sense: learning in the motor cortex must be different from plasticity processes such as those occurring during development; as individuals grow and change they must learn to use new and environment-

specific patterns of behavior, which would be impossible if every representation learned by cortex needed to remain static.

Known rat nervous system contributors during pellet retrievals

Movements made by the rat during pellet retrieval have long been known to associate with apparent tunings of unit spiking from extracellular recordings in both motor cortex contralateral to the reaching forelimb, as well as in the caudate nucleus (Dolbakyan et al. 1977). Both the rostral (RFA) and caudal (CFA) forelimb areas also contain units that demonstrate coherent increases in spiking activity when aligned to particular phases of the behavior, such as crossing the plane separating the inside of the box from its outside (Hyland 1998). The red nucleus, which has more influence on the fine movements of the digits in rats specifically, also shows evidence of coherent activity during pellet retrievals in the rat (Hermer-Vazquez et al. 2004).

Figure 6.1a: Complex Box for rodent behavior

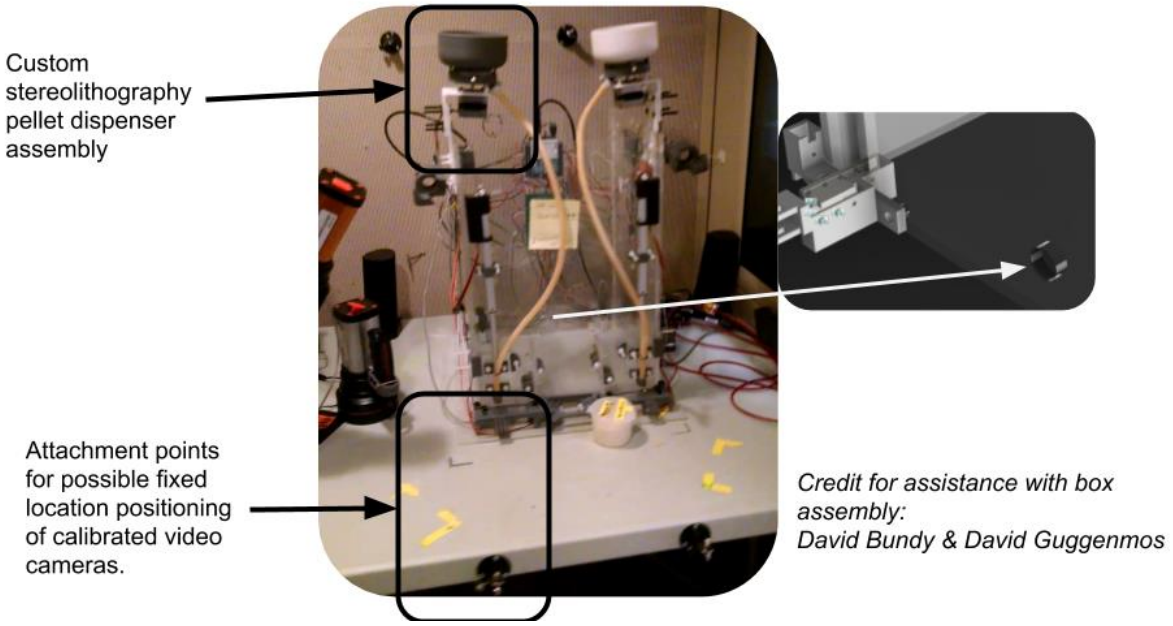

Figure 6.1: Complex Box for rodent behavior and 3D kinematics reconstruction

A) Complex box used for rodent behavior, with key components indicated. Example complex box that was used to train rats in both the Bilateral Pellet Retrieval task as well as the standard reaching task involved with the solenoid procedure described in this chapter. Boxes indicate notable components involved during practical operation of the boxes. The black box is the custom pellet dispenser assembly, which is displayed in greater detail in **Figure S6.1**. The red box indicates attachment points for possible placement locations of fixed cameras for use in calibrated video recordings. An additional attachment point anchored to the ceiling above the box is not shown. The *right inset* shows a rendering of the "nose-poke" hole that was added to boxes to provide a possible point of premotor alignment. *Credit for assistance with box assembly: David Bundy & David Guggenmos*

Figure 6.1B

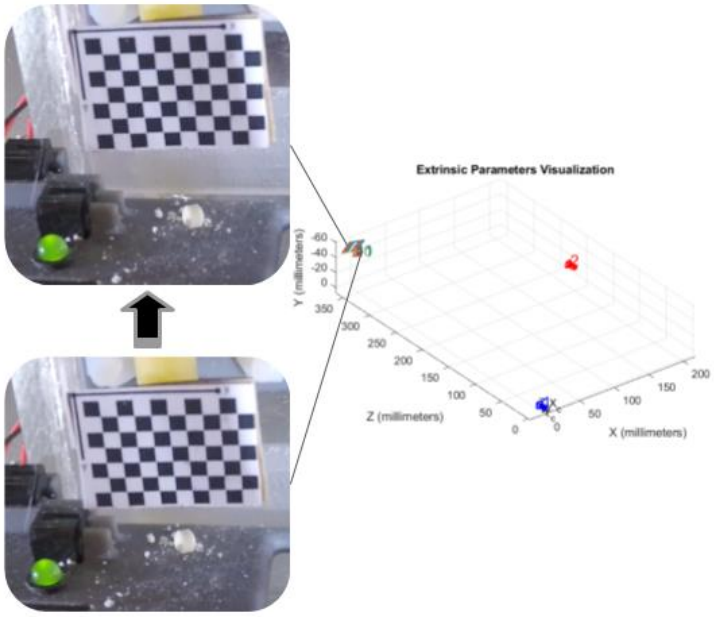

Figure 6.1C

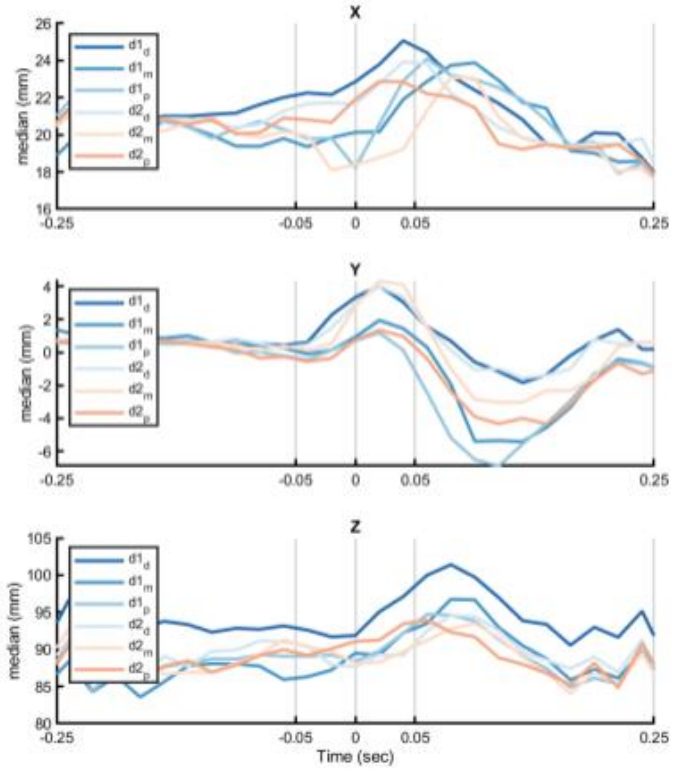

Figure 6.1 (continued)

B) Example of stereo-calibration for marker 3D-reconstruction. By mounting a checkerboard pattern adhered to a piece of cardboard so that it stays reasonably flat, it is possible to perform a stereo calibration on pairs of cameras that both have the checkerboard pattern in view as long as the angle between the cameras is not too steep. The checkerboard pictured here contains squares that were measured using calipers after printing and determined to be 2.79-mm on each side; using this information, the world points corresponding to the space that the checkerboard passes through can be triangulated by the detected points from each camera that correspond to one another. The known spacing between points is used to calculate the camera intrinsic matrix, which accounts for things like the lens distortion etc.
C) Smoothed, 3D-reconstructed trajectories. Cross-trial medians for individual marker coordinates, relative to trial onset. Dimensions are technically a combination of axes, but qualitatively a list of the primary components corresponding to each dimension is given below.
X-Dimension represents the "Right (negative) - Left (positive)" axis with respect to the aperture on the box. (Note that with respect to cameras facing the box, this becomes "Right (positive) - Left (negative)"). The distal marker on the first digit initially is the furthest-left, as we would expect given that it is a right-reach and digit-1 was the "index" finger digit. As the pellet is grasped and supination occurs, this digit moves to the "outside" and becomes the furthest-right.
Y-Dimension represents the "Down (positive) - Up (negative)" dimension. The initial trajectory is "forward" out of the box, as the tracker struggles to identify the paw prior to its appearance above the bottom transverse plane of the aperture. The delay and then "rise" represents the movement of the pellet towards the mouth.
Z-Dimension represents the "In (negative) - Out (positive)" dimension. Notice that the two most-distal markers have the furthest excursion from the box.

Results

Using an automated training box (**Figure 6.1A**), it was possible to train rats to perform a variety of tasks that isolate purposeful components of the cortical response during motor behavior, such as hemispheric specificity during a mirrored version of a lateralized behavior (**Video 6.2A**,**B**), or premotor activity in preparation for a motor task involving a decision (**Video 6.5**).

Dynamics of Limb Position

While the reach-to-grasp may seem like a fairly mundane behavior with respect to the difficult, complex movements such as those of a professional athlete, which may come to mind when "skillful movement" is mentioned, even this relatively simple behavior is a compound movement

that comprises several sub-movements that must be coordinated seamlessly in order to accomplish the functional goal of grasping the pellet (Whishaw et al. 1991, Whishaw & Coles 1996). Furthermore, even the basic sub-movements of this behavior form an effectively complicated dynamical system that at a high-level relates control signals from motor neurons in the spinal cord to the muscles that exert contractile forces on the agonist and antagonist

Figure 6.2A

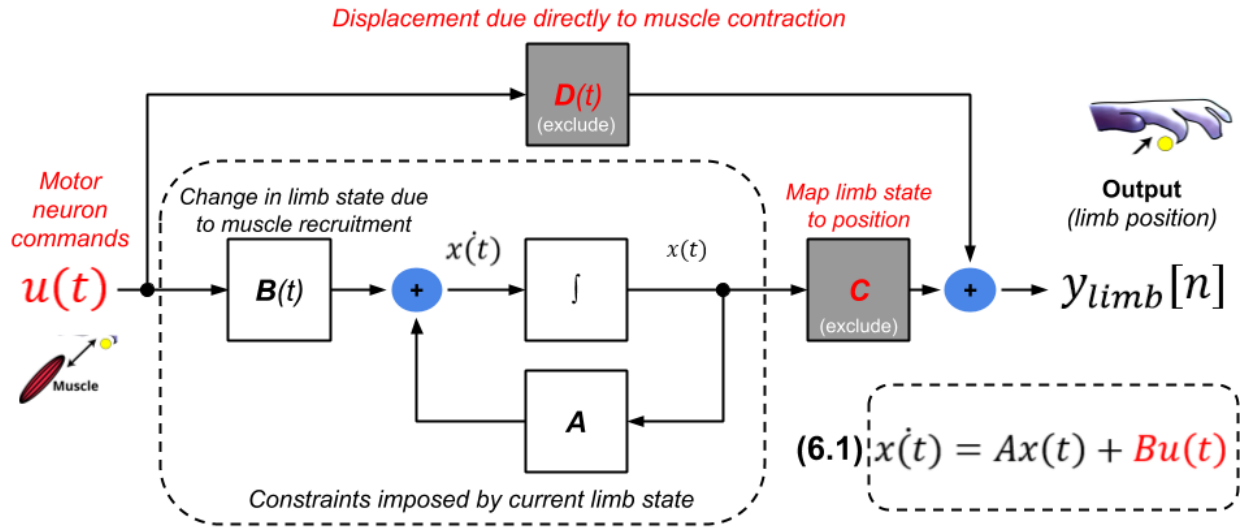

Figure 6.2B

(6.2) $y_{limb}[n] = \boldsymbol{h_{move}[n]} * \dot{\boldsymbol{x}}[\boldsymbol{n}]$ *Note: samples are discrete.*

(6.3) $y_{limb}[n] \overset{Z}{\Leftrightarrow} Y_{limb}(z) = H(z)\dot{X}(z)$

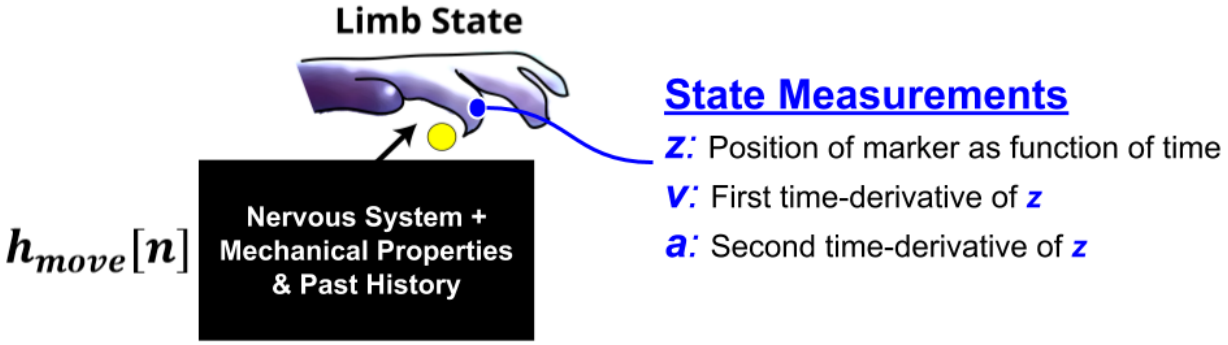

Figure 6.2C

(6.4) $y[n] = K_{state}\, w[n-1] - K_{movement}\, y[n-1]$

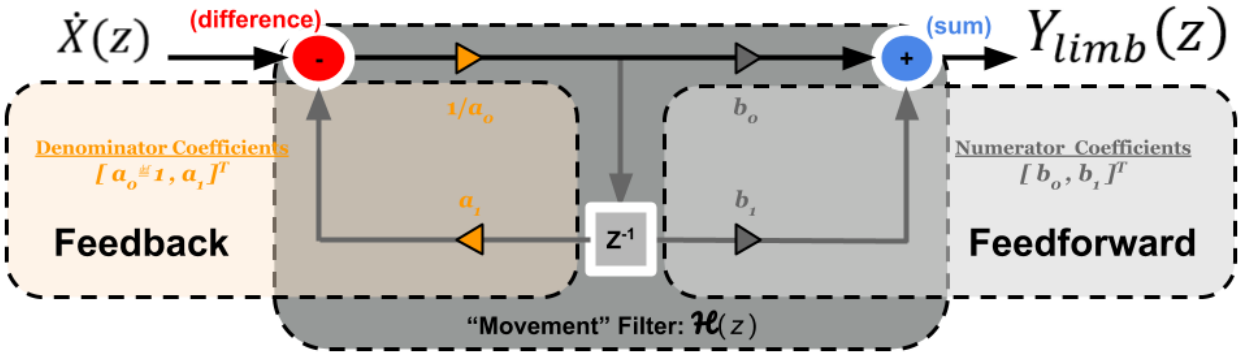

(6.4a) $w[n] \stackrel{?}{\Leftrightarrow} y_{cortex}[n]$ | "State" $\stackrel{?}{=}$ *Internal model*

(6.4b) $K_{state} = \dfrac{b_1 - a_1 b_0}{1 - b_0}$

(6.4c) $K_{movement} = \dfrac{b_0}{1 - b_0}$

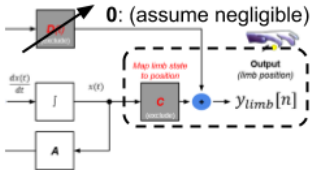

Figure 6.2D

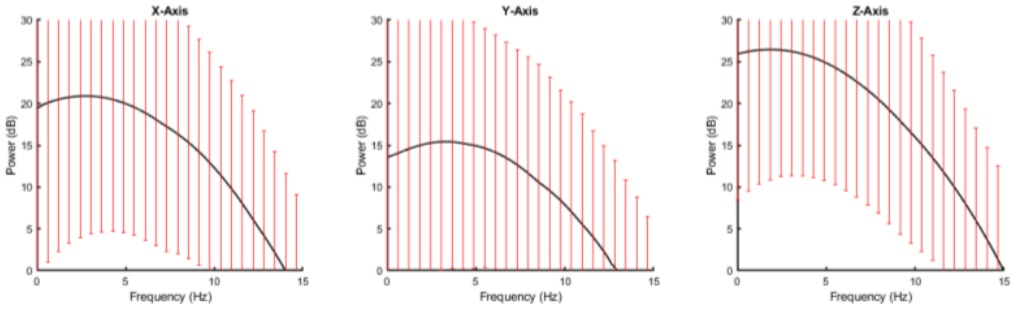

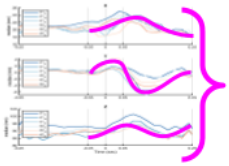

The movement itself is not complicated.

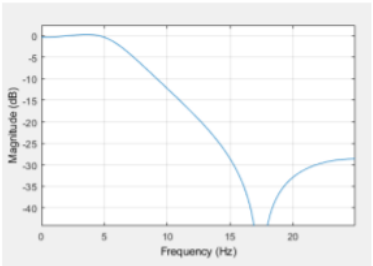

We can easily tune the coefficients to generate a range of acceptable pass bands.

- This could be used to constrain a more complicated model.

Figure 6.2: Forelimb state-space control model.

A) State-space model with output as limb position (discrete-time-domain). A schematic for a standard state-space model to describe the limb position as a function of sample [n]. The model indicates that while the motor neuron commands occur continuously (t) in the time-domain, we really only realize the limb measurements in the discrete sampled domain which is why there's a change of output argument to indicate this discretization. This model represents the very "front" of the dynamical system formed by the reaching limb.

B) Alternative formulation for limb position. If we consider the integration and transformation ***C*** as part of a time-varying system transfer function (***$h_{move}[n]$***), then the limb position would be described as the convolution of this transfer function with the rate of change of the limb state, which includes not only the limb position, but the rate of change of the position and possibly the rate of change of that rate of change (acceleration), depending on formulation. If we transform the output time-series to its discrete frequency domain representation using the Z-transform, then based on the convolution-multiplication duality we can see that the output becomes the product of these two things.

C) Simple transfer system model. We can re-express the system described by equations from **Figure 6.3** using a simple Direct Form II realization, where the $\mathbf{Z^{-1}}$ block essentially represents a sample-delay. When we write out the impulse response function for this system, we will have to use the "state" variable ***w[n]*** due to the system architecture (Equation 6.4a). Algebraic rearrangement of the coefficients in the difference equations describing this system allows us to create the formulation in **Equation 6.4**, which might give a little bit of intuition about what this state variable ***w[n]*** means. We know that b_0 must be less than 1 and that in general the system becomes less stable as this coefficient becomes closer to 1. This might represent something like a viscoelastic coefficient intrinsic to the muscle and tissue, which opposes the rate of change. Ultimately we do not empirically estimate these kind of properties of the tissue, but hopefully formulating it in this way shows how such things could be used in a model if desired.

D) Using forelimb position filter characteristics to sanity-check model formulations. Red bars are +/- one standard deviation, which includes each kind of marker. In general, there is more clear frequency content in the range of 2-5 Hz (which corresponds to the expected frequencies of the reach) on the X-Axis and Z-Axis. The Y-Axis does not demonstrate a clear trend, which makes sense.

muscles that generate the forces necessary to alter the movements of the limb (Figure 6.2A). While the state of the limb, as well as the command signals to the muscles issued by the motor neurons are continuous functions of time (Equation 6.1), the measurements of the limb kinematics reflecting such things are discrete samples indicated by the discrete function $y_{limb}[n]$. In order to simplify the system, components that probably do relate to the behavior of the system in some way, but which are not measured directly and will not be inferred from

experimental manipulation, are assumed to contain a negligible influence and lumped together into error covariance noise terms. These things include the displacement of the limb that is directly due to the muscle fiber contraction (***D(t)***), as well as the map of the limb state to its position (***C***). Furthermore, the constraints imposed by the limb state (its past history of movement, which may include its velocity and acceleration depending on model order) due to mechanical properties of the tissue, such as the viscoelasticity of tendons and muscle, as well as the mass of the limb segment under consideration, are not measured directly, but should contribute to the interpretation of any regression to estimate a linear matrix (***A***) relating the state of the limb to the rate at which the state changes (**Equation 6.1**).

If we consider the state of the limb as immediately preceding some filter that is applied to the state of the limb and which realizes the position of the limb, we could also theoretically measure the filter characteristic of such a system from its impulse response to a very slight perturbation ($\boldsymbol{h_{move}[n]}$; **Figure 6.2B**, **Equation 6.2**). To get some intuition about the limb state filter, we can change the basis for how the data is expressed. In the state-space formulation, the limb state and position signals exist in the time-domain. Applying the Z-transform to the system described by **Equation 6.2** changes the basis to a discrete frequency-domain representation (**Equation 6.3**), which enables an alternative realization of the filter using a Discrete Form II diagram (**Figure 6.2C**).

When posed as a Discrete Form II system with a single delay, which represents the dependence of the system on its past state under the assumption that the limb state is only described by its past position[58], solving the system difference equations[59] and rearranging them algebraically yields **Equation 6.4**. This format gives us two interesting pieces of intuition about

[58] Approximately, the value $dx[n]/dt \propto y[n] - y[n-1]$ approximates the change in limb position when the limb state function $x[n]$ only represents the past and current values of the limb position $y[n]$.
[59] That is, $y[n] = b_0w[n] + b_1w[n-1]$, where the system state variable $w[n] = x'[n]/a_0 - a_1w[n-1]$.

the limb movement system. The first is that such a system description, which represents the simplest discrete realization of a system with a feedback and feedforward delay term, necessitates the use of a “hidden” state variable; could this state variable contain a representation in the nervous system (**Equation 6.4A**)? Second, when the equations are rearranged to relate the past “hidden” state value to the past movement value, we see that at any instant, the current position of the limb is some weighted difference between the “hidden” state and the past position, indicating that the “hidden” state correlates with the velocity of the limb in some way, while the weightings between the two terms may represent a combination of intrinsic tissue properties and time-varying command signals from the nervous system. As a final point about the value of the Direct Form II realization in this context, it can be used as a model validation to check the final coefficients for a more granular model: once the filter coefficients for the system are recovered, the frequency content passband can indicate whether the filter allows movements in the physiological plausible range of frequencies (e.g. **Figure 6.2D**), as well as if the filter poles and zeros exhibit bounded-input, bounded-output (BIBO) stability.

Dynamics of cortical sensorimotor signals

The standard state-space diagram can also be used to describe the cortical extracellular field potentials which are the real subject of interest when evaluating cortico-cortical sensorimotor integration in the rodent stroke model (**Figure 6.3A**). In this format, the output *g(t)* becomes the rate of action potentials specifically in corticospinal units that innervate the motoneuron pools influencing the output limb effector muscles. In the chronically implanted rat, it is impossible to directly target recordings to such a specific sub-population of cells, so it is not known if units with this kind of a relation are present in every recording (i.e. cells of this type are typically about 1.5-mm below the surface of the exposed cortex, as shown in **Figure S6.4** prior to the electrode implantation; rostrocaudal and mediolateral location of the microwire array bundles is

approximated with respect to the patterns of the vasculature and the movements of the stereotaxic arm).

Figure 6.3A

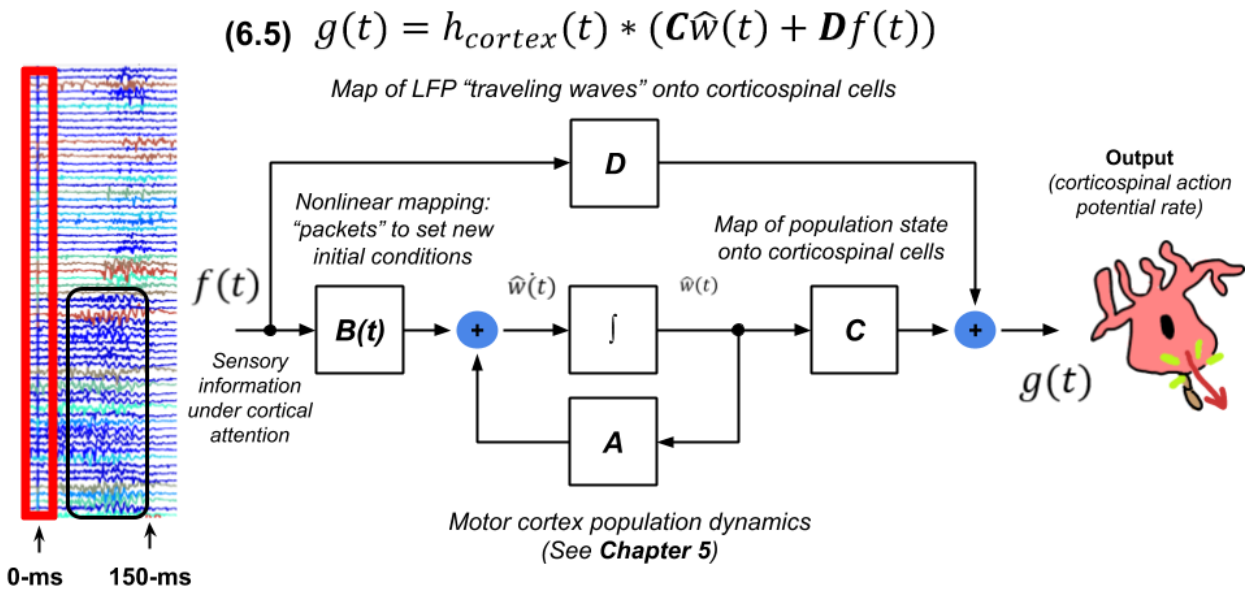

Figure 6.3B

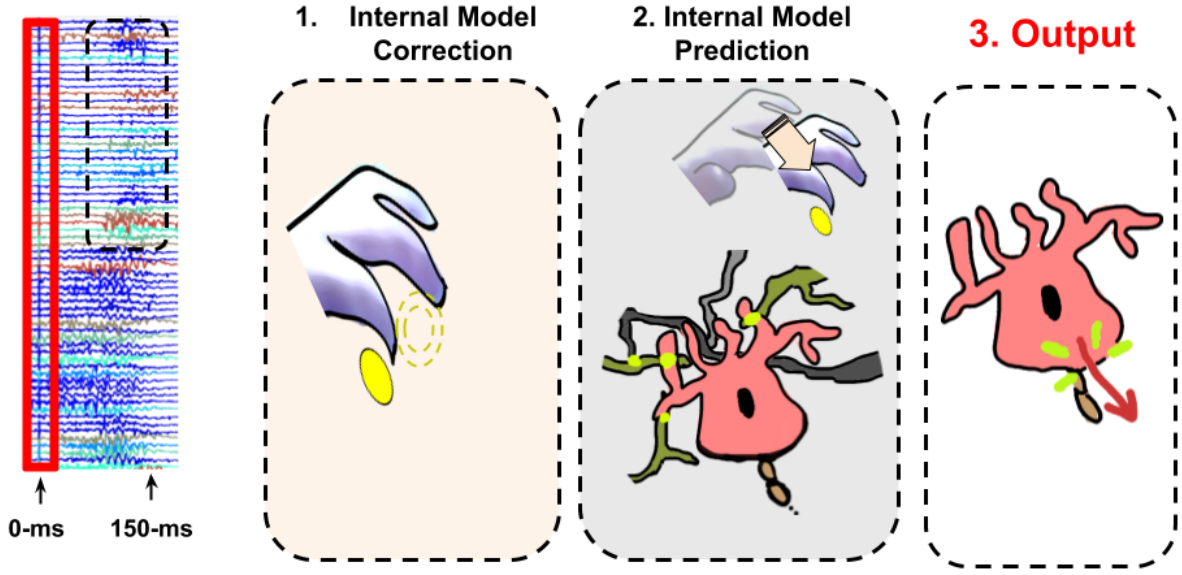

Figure 6.3: Standard cortical output state-space control model.

A) State-space model with output as corticospinal action potential rate. This panel suggests the core problem facing the neurorehabilitation engineer who is interested in understanding how sensory and motor cortices "reconnect" after injury by virtue of signaling observed in one or both locations. The activity on the left represents channels obtained from a real recording in a rat with channels in both sensory and motor regions. The boxed region shows an evoked response to a stimulus (red), which will be described in the next panels. There appears to be a large population-level response that is evident in the LFP and possibly also in the spiking that occurs approximately 100-ms after the stimulus. Given that cortex is probably involved in regulating several kinds of processes, which must necessarily be mediated via the signaling of its neural constituents, is there a way to delimit whether the apparent "response" observed later (non-boxed channels) relates to the observed one?
B) Which parts of the neural signal are which? Generically, these terms could be thought of analogously to the feedback, feedforward, and state components in the Direct Form II block schematic, although there is no guarantee that the neural architecture implements these things in the same way. This is simply to illustrate that there are some core components of the system that may be difficult to distinguish given that they are probably all "meshed together" somehow within the information contained by the network.

1. **Internal Model Adaptation**. Cerebral cortex is not implicated in online feedback and error correction, with the exception of responding to visual stimuli. Instead, in this context, cerebral cortex may be more likely to be involved in motor adaptation that occurs over the course of multiple trials (and which resembles changes observed during motor learning, with respect to "shifts" in tunings of unit activity).
2. **Prediction**. Cerebral cortex probably does implement some sort of internal model that allows it to predict the limb state over the course of the behavior in order to issue subsequent commands accurately. **Chapter 5** provides empirical evidence that it is often possible to fit a first-order linear recursion to the system in order to capture it fairly adequately.
3. **Output**. Corticospinal cells in the cerebral cortex in some (rare) cases project directly to the motoneuron pools of interest with respect to the target limb effectors. These pools contain cells that innervate individual muscle fibers; their contractions exert force on the limb segments via contractions that act on points of attachment to the skeleton. Therefore, such output likely does not form a directly linear relation due to the nonlinearities introduced by things like the mechanical properties of the connective tissue and the summation of movement in a multi-segment model with multiple degrees of freedom.

More recent work that makes use of optical signals in the mouse model has fortunately addressed this to some extent (Masamizu et al. 2014). Specifically, there appears to be a distinct task-related response differentiation between the horizontally-connected cells of Layer ⅔ and the cells with descending corticospinal output in Layer 5b when learning to pull a lever. Interestingly, this may relate to the putative consolidation of the motor behavior, which could subserve the decrease in apparent tuning of Layer 5b cells with respect to active involvement during movements (Peters et al. 2017a, Peters et al. 2017b). Taken together, in the context of the **Chapter 5** results, these studies suggest that cortical dynamics that are robustly present and related to movement may relate more strongly to ongoing patterns of activity in the horizontal, presumptively cortico-cortical unit activity (here, represented by $w^*(t)$)[60]. Note that this cortical population state is intentionally denoted $w^*(t)$, suggesting that it may relate intrinsically to the "hidden" filter state describing the limb movements in the Direct Form II realization ($w[n]$). We will return to this point shortly, but first the rest of the system diagram presented in **Figure 6.3A** should be addressed.

Again, we are interested in the relation between putative sensory-related information and putative motor-related output during behavior, since this would provide an indicator of the functional relevance to the cortical circuit of axonal sprouting suggested in the works of Dancause and colleagues (2005). The left inset of **Figure 6.3A** shows unfiltered field potentials recorded from two electrode arrays in different regions of the rat cortex. The red box indicates a stimulus, while the black box indicates robust deviations from standard activity that are evident across most channels in one of the arrays approximately 100-ms after the stimulus. Even within the array, we see that there is somewhat of a gradient in the distribution of onset times of the large oscillatory activity that may relate to the stimulus; it is tempting to relate such activity directly to the network state (e.g. the mapping $\boldsymbol{D}$), for example in the oscillations observed later

[60] For formatting reasons, *w "hat"* is referred to as *w** in the text; it is shown correctly in **Figure 6.3a**.

on the channels of the other probe in the array (Figure 6.3B). More immediately, could there be a potentially nonlinear mapping of such activity to the cortical state (***B****(t)*)? For example, if the amplitude of such oscillations sets a criterion for phase-entrainment of unit activity that resets "initial conditions" of a cortical dynamical system, it's one way that information could transfer via such a mechanism.

In fact, each of the probe groupings (Figure 6.3A,B) represents activity recorded from forelimb sensory cortex, with the top channels located on the same side as a mechanical solenoid stimulus delivered to the paw while the bottom channels are from the sensory representation opposite the solenoid stimulus. Therefore, we see that the representation even of a sensory response that is isolated from behavior becomes more complicated: the "traveling" LFP waves are likely intrinsically related to some combination of model correction, prediction, and (during behavior) corticospinal output that occurs across both hemispheres during behavior (Figure 6.3B). Because of this complication, it means that some experiments in the anesthetized animal which model the sensory response to cutaneous stimuli (i.e. as occurs during contact between the skin and pellet during the retrieval) in isolation from motor output can help greatly in calibrating and simplifying models attempting to capture information transfer related to the sensory and motor signals.

Figure 6.4A

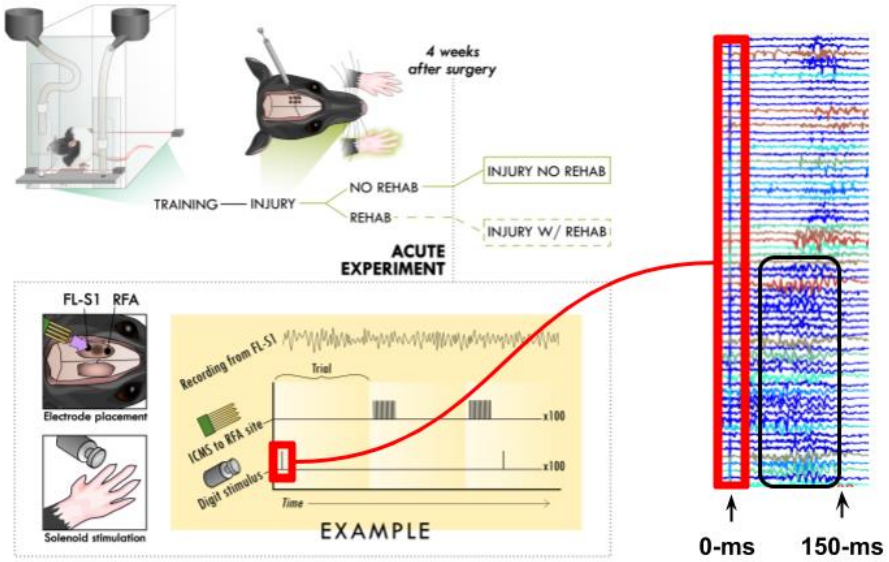

Art credit: ***Page Hayley*** (manuscript in preparation)

Figure 6.4B

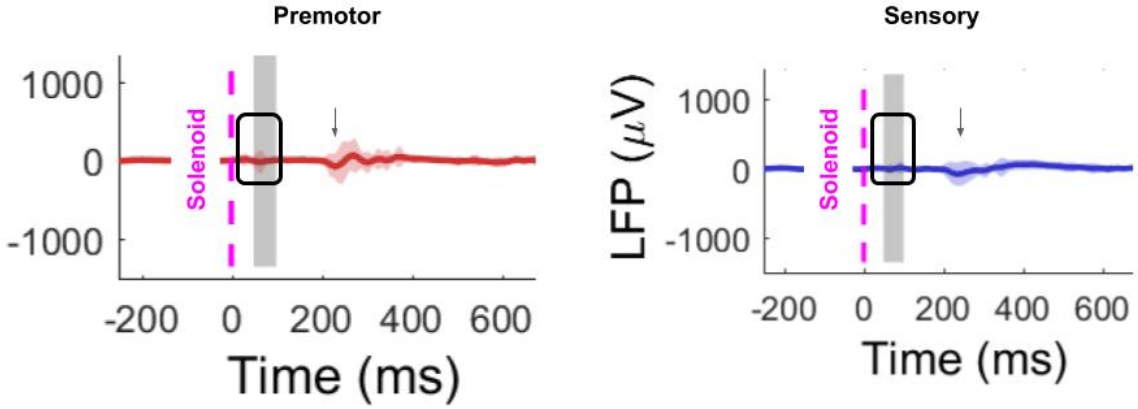

Figure 6.4C

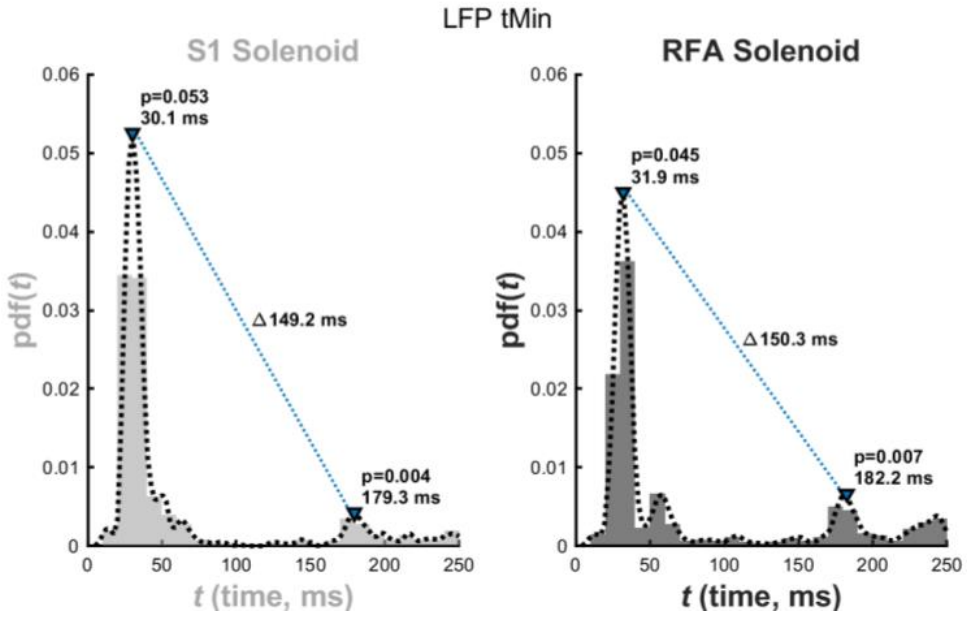

Figure 6.4D

(6.5a) $g(t) = h_{cortex}(t) * (\boldsymbol{C}\hat{w}(t))$ for $\boldsymbol{D}f(t) = 0$

(6.5b) $g(t) = h_{cortex}(t) * (\boldsymbol{D}f(t))$ for $\hat{w}(t) = 0$

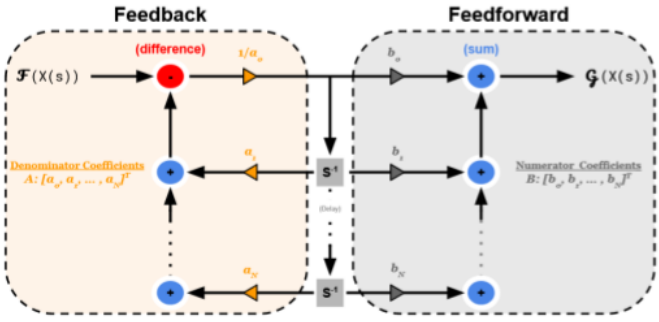

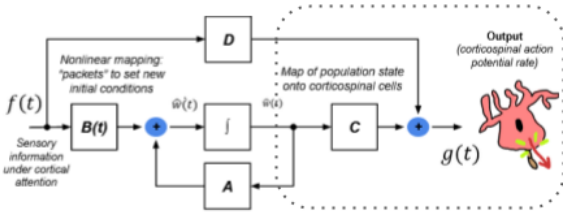

Figure 6.4: Signal substrates for cortical sensorimotor information transfer.

A) Acute solenoid experiment overview. In this case, the recording was actually taken from bilateral sensory areas; the "early" activity corresponds to the contralateral hemisphere and the "late" activity corresponds to the ipsilateral hemisphere.
B) Possible role of LFP in sensory transfer. This holds for sensory and motor areas when we use the solenoid paradigm as well. Here, we can see that the LFP "bump" that occurs approximately 250-ms after trial onset (in this case, subtracting the latency for the solenoid strike suggests that it is closer to 200-ms after the strike or 150-ms after the retraction of the solenoid). The LFP appears to robustly reflect some kind of mechanism that either directly mediates information transmission between these areas, or at the very least is epiphenomenologically related to it. While the latter case is somewhat dissatisfying, if all we are interested in is using this as an assay of recovery related to the motor performance on a task, this at least provides a starting point.
C) LFP minima may indicate "packets" for information transfer. Returning to the solenoid stimuli, if the LFP seems to robustly show us some response to the solenoid stimulus, it seems like a key might be either the negative-going or positive-going peak of the LFP, which is probably caused by some sort of synaptic sink or source that is ubiquitous in the region of the recording electrode. The time to the peak of the negative-going deflection that follows the solenoid strike in this rat indicates that both S1 and RFA experience peaks that are much more closely "linked" temporally than we would expect on the basis of synaptic delays, which is interesting. The RFA peaks do occur after the S1 peaks, which intuitively does make sense. So this indicates that there might be some sort of nonlinearity that also "binds" the sensory and motor activity in an extraordinarily tightly-coupled manner.
D) Modeling considerations for population-level motor cortex feedback and feedforward activity. There are two components in the sum that produces *g(t)*: one mapping from the population state (***w_hat(t)***) and one mapping from the gross population events mediated by the LFP. While in the case of the moving rat it is impossible to accurately assign either term to zero definitively without creating an extremely large parameter-space, in the anesthetized preparation it should be safe to assume that ***w_hat(t)*** is zero: there is not some movement target in mind, there is only the response to the solenoid stimuli.

Isolating sensory-specific signals

Unilateral recordings in the unilateral forelimb sensory and premotor cortex of the anesthetized rat in response to mechanical solenoid stimuli allowed us to test for sensory-specific signals (**Figure 6.4A**). Coherent averaging of the LFP in response to solenoid-only stimuli indicate the presence of both a short- and long-latency response that may be more salient in the increased variance of the LFP in both the short- (approximately 30-ms) and long- (approximately 150-to-

180-ms) latency responses (**Figure 6.4B**,**C**). A manuscript quantifying these responses, as well as their modulation by intracortical microstimulation (ICMS) in the premotor cortex, is in preparation (Hayley et al. 2020). Given that there is an LFP response present in both sensory and premotor cortices contralateral to the stimulus at both a short- and long-latency relative to the stimulus, it suggests that the direct mapping of the LFP response onto the corticospinal output could be achieved in such a preparation, provided that there actually is a corticospinal output (**Figure 6.4D**; in the anesthetized rat not performing a motor behavior, there is an expectation that $w^*(t) = 0$). During ICMS, $g(t)$ is non-zero in the anesthetized preparation, suggesting that such a mapping could be recovered. Since ICMS induces large signal artifacts that would preclude the ability to tie the LFP response to corticospinal output directly without some calibration of the relative timing of the combined ICMS and peripheral stimulus, it may be advantageous to utilize other known neurophysiological substrates for studying such a response.

The H-reflex, which is typically used as an electrical analog of the stretch reflex in order to measure reflexive sensorimotor integration, is known to be potentiated via cortically-mediated pathways (Wolpaw & Chen 2001, Chen et al. 2006). However, as far as the author is aware[61], the H-reflex response has been surprisingly unstudied at the cortical level. An anesthetized rat preparation using EMG to measure the response in the stimulated muscle while simultaneously recording from the cerebral cortex would then allow the indirect measurement of putative corticospinal output by virtue of the amplitude of the H-wave that follows the initial M-wave that is due to the immediate recruitment of corticospinal axons during muscle stimulation. It is interesting to note that the expected onset of the H-wave is in the approximate 30-ms time window that may relate to the early response observed in cortical LFP. One possibility is that

[61] Studies of reflex pathways are not the author's area of familiarity and so this is an important qualifier that such studies may exist but the author could not find them from a review of the literature regarding the H-reflex.

this component of the LFP response represents some sort of intrinsic tracking of limb position or limb sensory response that is intrinsic to the cerebral cortex, which is all the more fascinating given that the response is observed under anesthesia. Could this response also relate to the modulation of ICMS somatotopic territory that occurs when the position of the limb of interest is manipulated (Sanes et al. 1992)?

Neural signaling substrate for sensorimotor information transfer

While the ability to isolate some components of the sensory response is afforded by the anesthetized model, open questions remain regarding the transfer of this information to the motor cortex. For example, if the LFP represents some sort of information transfer mechanism to the motor cortex, it might be expected that this signature would show up in the average LFP signal of the cortical population, perhaps indicating some sensory-related calculation during this time (**Figure 6.5**). While coherent LFP oscillations do occur in motor areas, the relative alignment of these things when averaged across trials (at least in the example rat of **Figure 6.5B**) indicates that there is probably some nonlinear relation between the coherent LFP deflections in sensory areas and the population code in motor cortical areas during behavior.

Figure 6.5A

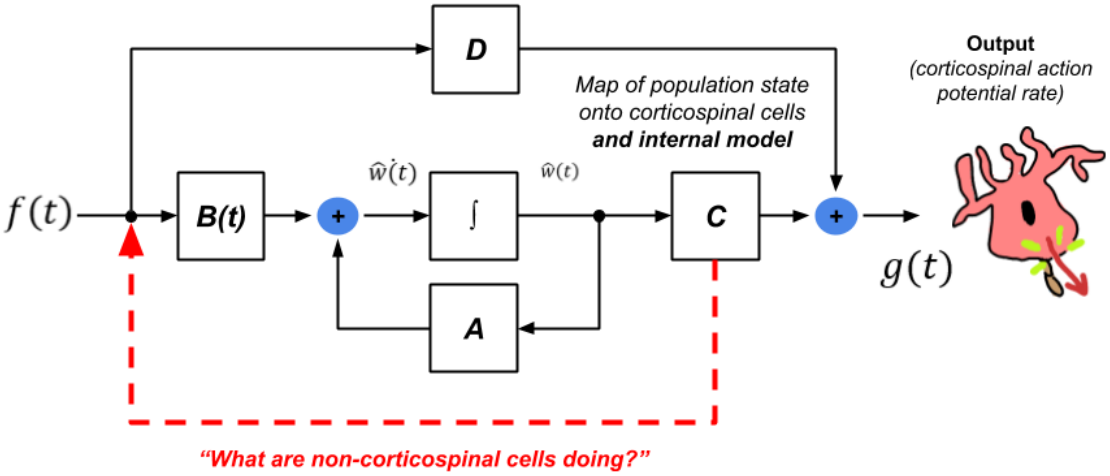

Figure 6.5B

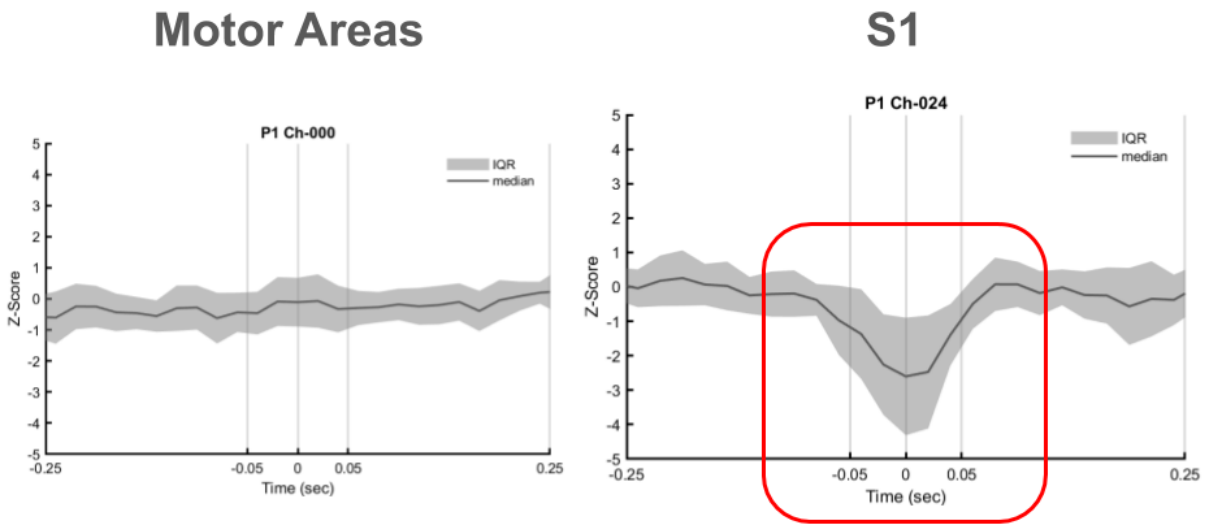

Figure 6.5: Where to look for indication of sensory

prediction in motor cortical signals?

A) Modeling considerations for the rest of the population activity in the motor cortices. Another helpful illustration that is realized by putting the system in this state-space formulation is that the mapping to the corticospinal action potential rate is actually constrained by the corticospinal cells being the output; therefore, if it were possible to directly identify the corticospinal units, while simultaneously recording from the other cells, a more accurate model that defines what filtering is occuring in the rest of the population could be refined by connecting more pathways (signaled abstractly by the dashed red line). In this case, since ***g(t)*** is technically a subset of ***w_hat(t)*** itself, there is a recurrence relation there which would need to be included in the block diagram to accurately capture those relations in a model.

B) Cross-trial comparisons of motor and sensory LFP during Grasp alignment. Further suggesting the significance of the LFP, here we see that the cross-trial average of the LFP in alignment to **Grasp** shows a substantial negative-going peak across trials. The **Grasp** should coincide quite tightly with physical contact to the pellet.

Motor signal indicator of sensorimotor information transfer

Returning to the anesthetized data, we see that after a subtotal cortical ischemia in primary motor cortex of the same hemisphere from which premotor and sensory unit activity are recorded, there is a difference at the level of individual rats in terms of the evoked unit responses in premotor cortex with respect to the solenoid stimulus (**Figure 6.6A-D**). Interestingly, the second rat in this comparison sustained the worst deficits in behavioral performance following the injury, which may have been larger than any of the other rats (*lesion volume analysis in progress;* Hayley et al. 2020). Also of interest is the fact that the combination of ICMS and solenoid stimulus (**Figure 6.6D**) leads to a suppression of activity in the temporal region surrounding the ICMS response, with the end result that the solenoid-evoked unit activity is apparently more salient in premotor cortex. The ability of ICMS to induce a “rebound” response at a long latency during stimulation of RFA to the secondary peaks observed in S1 in some cases after solenoid stimuli (e.g. **Figure 6.6E**) may relate in some manner to therapeutic effects of closed-loop ICMS protocols in fostering behavioral recovery (i.e. Guggenmos et al. 2013), although such a thing is purely speculative.

Kalman filter state models

The anesthetized model provides some indications that the LFP may be involved somehow in relating sensory and motor information between sensory and motor cortical regions. It suggests that this may somehow relate to the spiking response of units in motor territory that is further removed from sensory territory, and this relation may be highly nonlinear. However, the issue of how the sensory, motor, and kinematic signals are all tied together has still been left unaddressed; it cannot be answered in the anesthetized model. Instead, it requires the reconstruction of markers on the relevant limb segments in three-dimensional space during the pellet retrieval (Methods).

Figure 6.6A

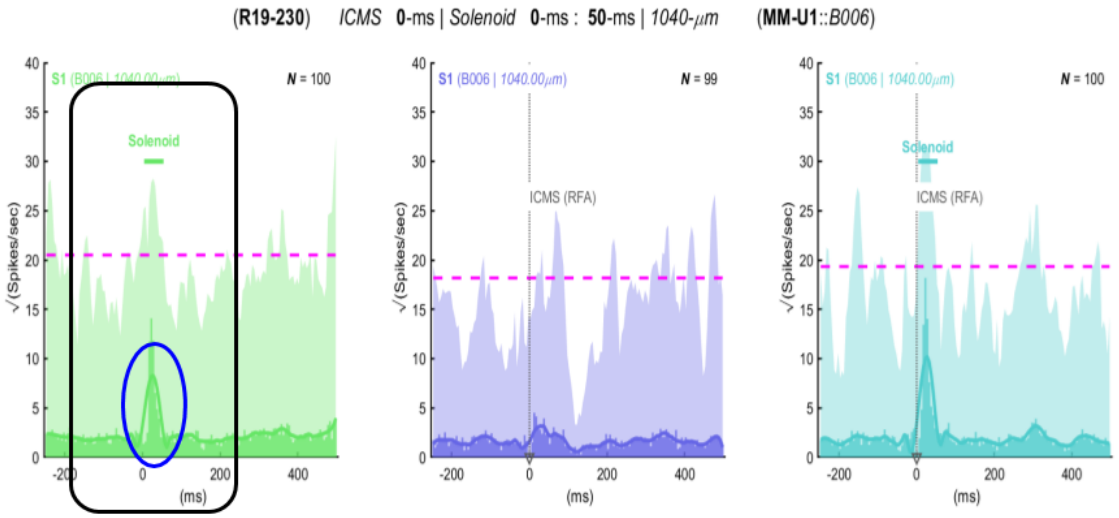

Figure 6.6B

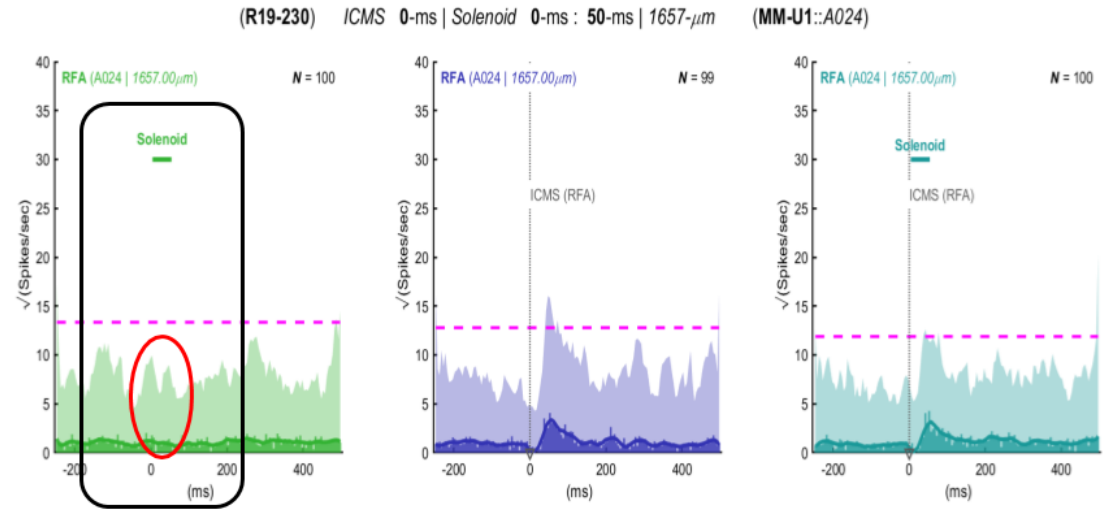

Figure 6.6C

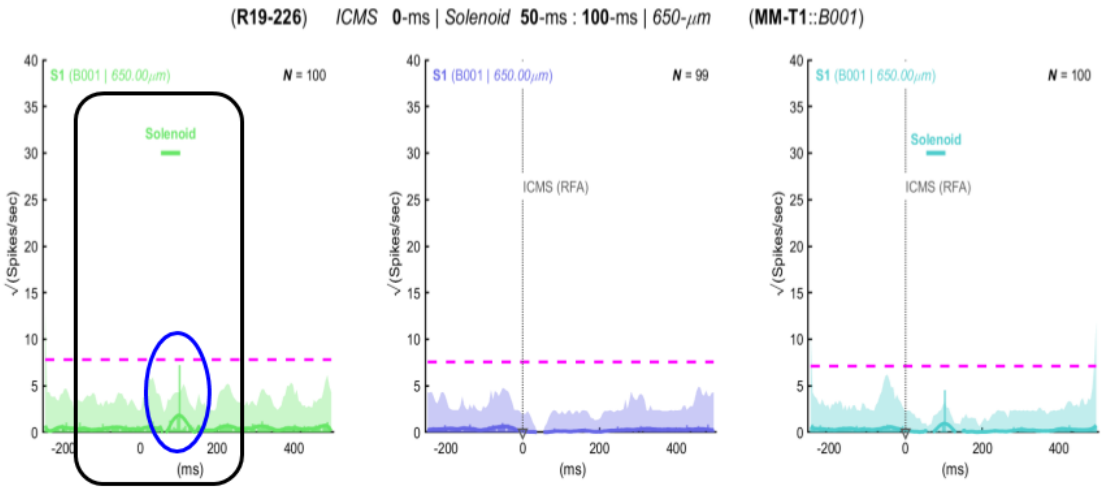

Figure 6.6D

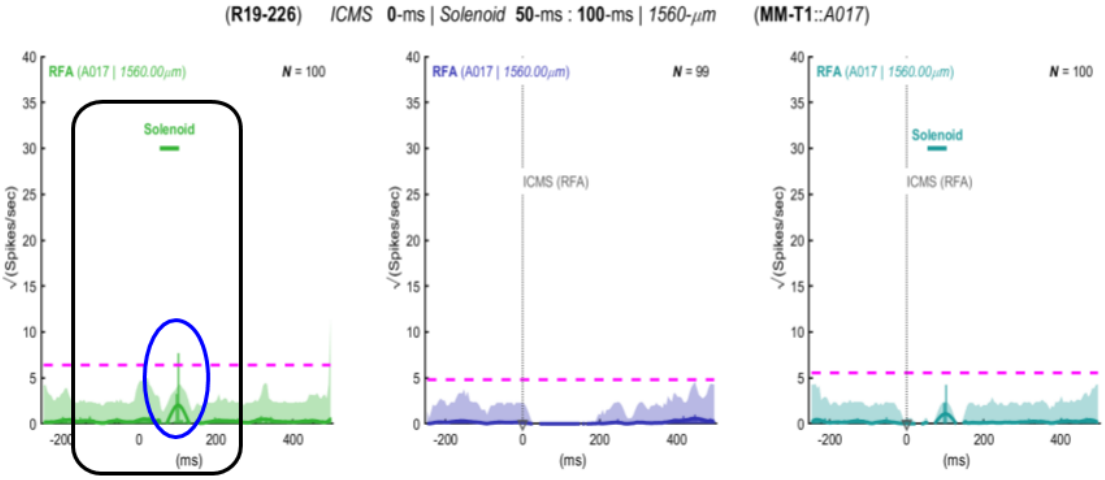

Figure 6.6E

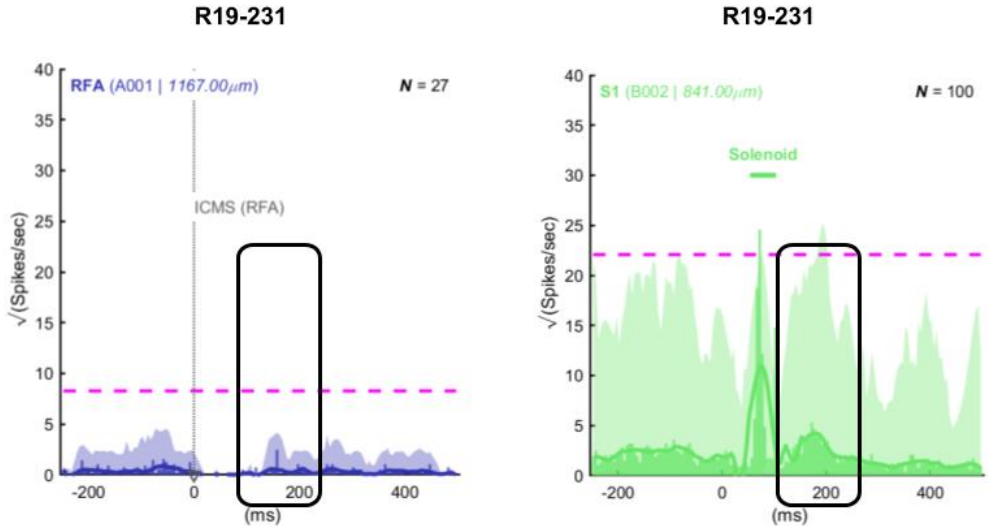

Figure 6.6: Where to look for indication of sensory feedback in motor cortical signals?

A) and **B) Example of short-latency evoked unit responses in FL-S1 only. Sensory response shown in A, Premotor response shown in B.** Also interesting is the apparent nonlinear response between evoked spiking activity in premotor areas and in sensory cortex. In this case, the solenoid strike elicits activity in sensory cortex, but not in premotor cortex.

C) and **D) Example of short-latency evoked unit responses in both the rat S1 and RFA. Sensory response shown in C, Premotor response shown in D.** However, in a different rat (which, incidentally, had the largest ischemic lesion volume of any rat in the solenoid study), evoked unit activity is present in both Sensory and Premotor cortices in response to the solenoid stimulus. Interestingly, in this case, when ICMS in RFA precedes the solenoid strike, it appears to make the evoked activity more salient.

E) Examples of long-latency "rebound" responses. These longer latency responses could be potentially explained on the basis of rebound from a hyperpolarized membrane potential "state." The time until the observed evoked spikes is "long" (hundreds of milliseconds); this suggests a possible relation to the known duration of inhibitory postsynaptic potentials (IPSP) caused by $GABA_b$, which could last up to 200-ms or 250-ms.

Figure 6.7A

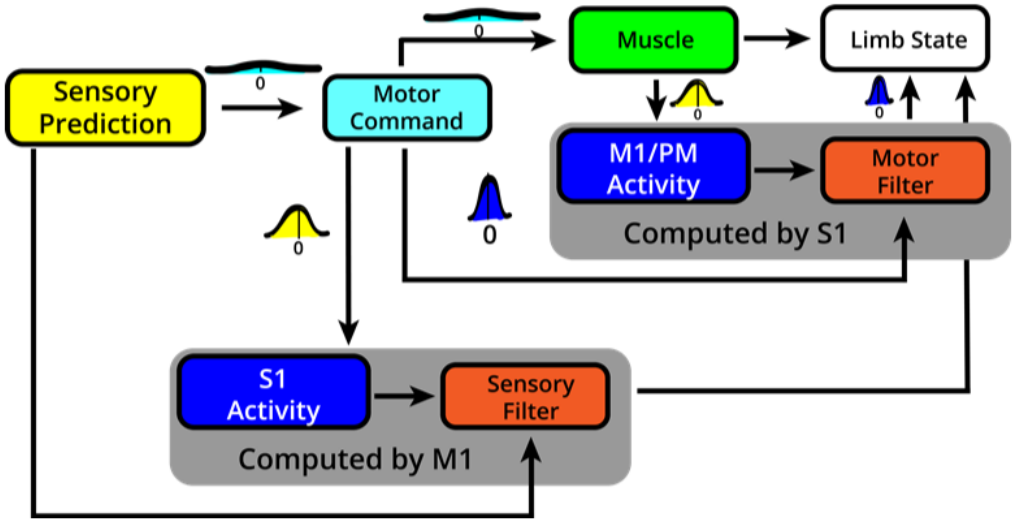

Figure 6.7B

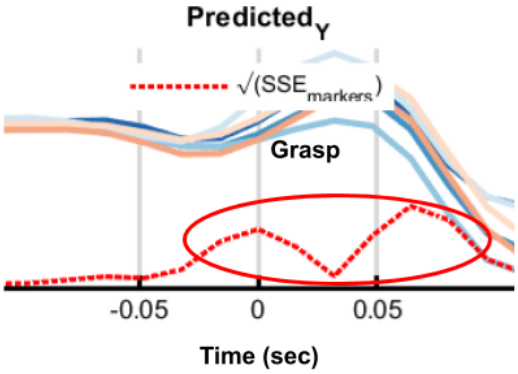

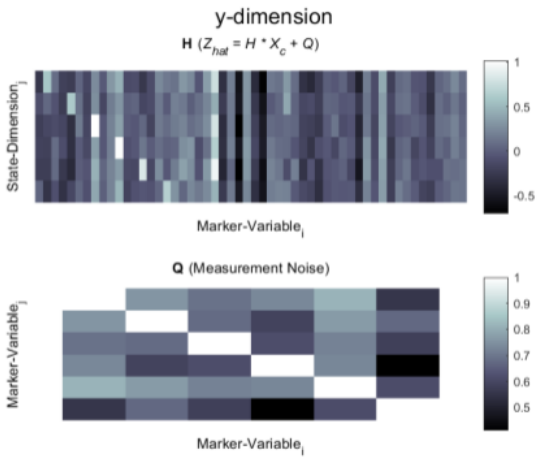

Figure 6.7C

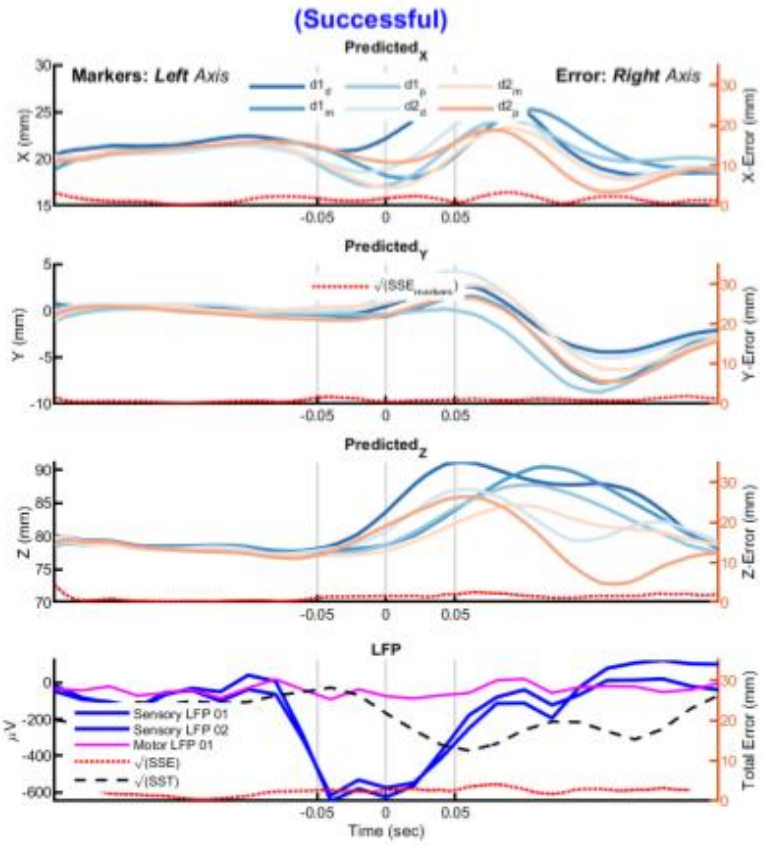

Figure 6.7: Kalman state filter model

A) Kalman state filter model overview in sensorimotor cortex. Another way that we could think about the state-space model is by using the Kalman filter. The model provides a solution to optimally combine the error covariance matrices of some *prior* on the data with *posterior* observations (measurements) so that the error terms due to both kinds of information about the output process (which is to be estimated) is combined in a statistically optimal way that makes the predictions (hopefully) more accurate. In this case, the output is the "Limb State."

B) Example of "cleaning" markers by predicting limb state using past limb state. The Kalman filter can be applied to limb markers on their own, setting acceptable bounds for post-hoc recovered measurements in order to denoise the recovered trajectories.

C) Example of estimating limb state using all data in state vector and allowing matrices to exhibit adaptation on a short timescale. This further improves the estimated limb trajectory, but is this strategy informative with respect to recovering the encoding of movements and sensory information in the neural state space?

Figure 6.7A provides a diagram of possible calculations and considerations involved in the Kalman formulation of a state filter that includes some of the computational mechanisms discussed previously. Permutations of this filter are possible by rearranging the system measurement and system state variables. For example, a simple “cleaning” filter for the noisy marker position data returned by a deep learning network that was used to label individual digit and forelimb markers (DeepLabCut, Mathis et al. 2018) can be created by using the limb position as the Kalman output and using the limb position in combination with its past history as the Kalman filter state. The probability of observing the estimated marker can be computed given the updated Kalman gain matrix combines the prediction covariance matrix that is based on the *prior* of the Newtonian equations governing an object in motion with the *posterior* observation and associated covariance from the AI markers. If this probability is lower than a desired threshold, it could be interpreted that the observation is an outlier and should be discarded, such as the intentionally mislabeled point in **Video 6.3**. In such a case, the data can either be interpolated via some other method, or the *prior* prediction value can be used directly (e.g. **Figure 6.7B**).

Using this formulation we can also go to the other extreme: we predict the marker position data using all the available data, including the past limb state, the LFP time-series and cross-correlations, and the unit activity from both cortical areas, while allowing our time-series estimates of the covariance to change as a function of the relative time within a given trial. The result is quite accurate (by comparison to the expected error if only the average movement trajectory is used; **Figure 6.7C**), but it does not really tell us anything that we are interested to learn about the state of the network.

If we consider the biological arrangement of a Kalman scheme, we might drastically rearrange the model (**Figure 6.8A**). In this case, the output is not actually the limb state; instead, the output is the activity of the motor population (and technically more specifically the corticospinal cells with descending outputs, **Figure 6.3A**). This formulation is more akin to what the brain might experience: it has no other "sensor" for building the limb state other than the propagation of nervous activity, presumably as reflected by activity in the sensory cortex. An extremely simplified representation that predicts spike rates using the "hidden" state could then be compared for accuracy by seeing what the deviation of the network estimated "hidden" state of the limb is from the actual measurement of the limb (recalling that the Kalman is statistically optimal with respect to prediction of the output in combining the *prior* and *posterior* covariances; therefore, the state variable could even exceed the total sum of squares if there is not a very strong relation between the state and the output variables). When covariance matrices are linear and time-invariant (LTI), this formulation is not very good at tracking the limb state (**Figure 6.8A**) as might be expected.

Retaining a similar arrangement of outputs and inputs makes sense and gives us a biological comparison that helps ground the model in reality. However, the previous inaccurate model did not attempt to add any interactions between sensory and motor signals that might be indicative of information transfer between the two. What if the limb state predicts the arrival of an incoming "sensory packet" (e.g. the large deflections in LFP present in FL-S1 but not consistent for motor channels)? Furthermore, what if the predicted output was not just spikes, but the average LFP signal in the motor areas? We can realize this arrangement quite easily, and introduce the *prior* expected model state that was obtained in the anesthetized experiments by suggesting that the transfer function for sensorimotor information is in the cross-correlation between the motor and sensory signals (**Figure 6.8B**). Note that this is a major model assumption (and as we will see, probably an area in which the model could be improved upon). When we use this formulation

and then recover the error in the forelimb state, we see that it represents an improvement on the model that uses only unit activity, but there is still a substantially poor relation between the model hidden state and the actual limb state (Figure 6.8A).

Figure 6.8

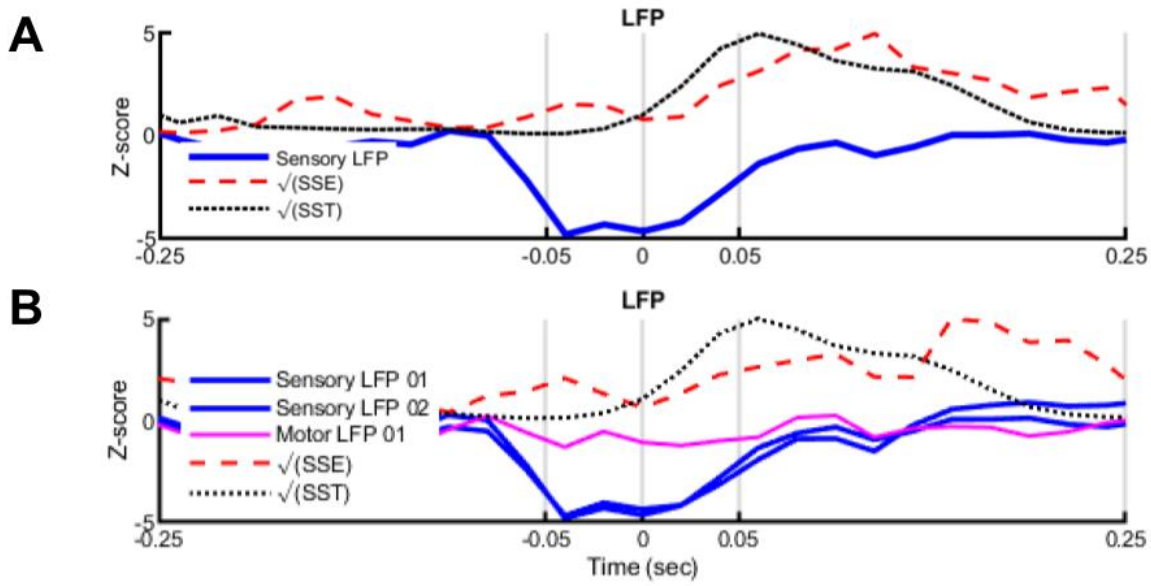

Figure 6.8: Neural state encoding

The Kalman equations are reformulated to predict the neural state using a combination of the limb state (kinematics) and LFP-derived features. Particularly in the sensory cortex, large event-related deviations may represent discrete events that give additional information and confidence in recovering the neural state encoding. Blue lines indicate the average LFP from sensory channels. The predicted update of the state vector $\boldsymbol{x}$ at each step yields values of the kinematic signal that can be compared to the measured values to estimate error in those signals as they relate to the encoding. The Kalman filter is not designed to be optimal with respect to error in the noisy sensor measurements with respect to updating the hidden state $\boldsymbol{x}$, but rather, with respect to estimating the output $\boldsymbol{z}$. Therefore, if our optimal regression of the neural state gains very little information or is even made worse by the observed kinematic estimates, we would expect for the sum of squares error (SSE; red dashed line) in the recovered state approximation used at each update step to potentially have a higher amount of error than occurs when taking error with respect to the mean value across all trials for that same kinematic information (black dotted line; total sum of squares (SST)).

A) Stationary Kalman formulation to recover population spike features using kinematics and only a single average sensory LFP is not very accurate. When lumping all of the LFP into one average signal from any channel in sensory territory, we get very little information from the kinematics in predicting the neural state, as indicated by the close relation between SSE and SST, especially when SSE exceeds SST.
B) Error is improved when breaking the LFP into multiple components based on spatial coverage, and augmenting with spike rate information. Here, the sensory LFP is used on two channels that have large event-related modulations in LFP signal (blue lines), alongside the average LFP signal from channels that were co-registered to motor territory (magenta line). The state variable that is given is actually the correlation time-series between each of the sensory LFP signals and the motor LFP signal. The yellow box emphasizes the improved utilization of kinematic information from the noisy sensor measurements, while the orange box emphasizes that assumptions on stationarity of these signals may change timescale at a time-point roughly corresponding to the time it takes for the rat to bring the pellet back to his mouth.

This mismatch might occur for several reasons. As alluded to in the first “accurate” model, it could relate to the requirement for model components to be LTI when in reality they are probably time-varying. Related to this, some of the model components might simply retain a nonlinear transfer function, which precludes the use of the standard Kalman filter where predictions and measurements are incorporated via matrix multiplication. Alternatively, future experiments that make use of empirical tissue property measurements to recover an estimate of the “hidden state” (*w[n],* **Figure 6.2C**) as it relates to the cortical population state (*w*[n]*, **Figure 6.3A**).

Methods

Complex rodent behavior box

An automated training box for the rat pellet retrieval task was developed as a modified version to one that was previously described by our group (Bundy et al. 2019). In this study, the box additionally features an approximately 1-inch diameter hole (**Figure 6.1A**), through which the rat can sniff the external environment. The box has an additional infrared collector-emitter pair that forms a beam across the exit of the hole, which is used by a microcontroller circuit to trigger other events during the behavioral task as described below. Custom box parts were printed using a stereolithography printer (FormLabs; **Figure S6.2**). Some of the notable features are described below. A general list of printable parts that are required for box assembly is provided in **Table 6.1**.

Table 6.1: List of parts for stereolithographic fabrication of rat behavioral box assembly

Part	Quantity
Pellet Platforms	
Left Platform	1/box
Right Platform	1/box
Midpoint Attachment	1/box
Button	
Left Button Holder	1/box
Right Button Holder	1/box
Button Paddle	2/box
Door	
Actuator Square Bracket	2/box
Tube Circle Bracket	2/box
Left Door Tube Alignment	1/box (6 alignments)
Right Door Tube Alignment	1/box (6 alignments)
Actuator Spacer	2/box
Dispenser	
Extender	2/box
Bracket	2/box
Nozzle	2/box
Hopper	2/box
Nozzle clamp	2/box
Rotor	2/box
Lid	2/box
Approach Blocker	
Top Attachment	2/box
Left Bottom Attachment	1/box
Right Bottom Attachment	1/box

Table 6.1: List of parts for stereolithographic fabrication of rat behavioral box assembly

Custom complex task components are broken down into several modules, and can be printed in batches. The rat behavioral box is broken down into 5 different modules that require 3D-printed parts: the **Pellet Platform** assembly, the **Button** assembly, the **Door** assembly, the **Dispenser** assembly, and the **Approach Blocker** assembly. Other parts are printed on an *ad hoc* basis; some experimenters prefer not to use the **Approach Blocker** assembly. It was found to be useful in these experiments in order to impose a greater stereotypy on the manner in which the rat approached the door, which has a tremendous effect on the production of associated neural activity that relates to the behavior.

Pellet Dispensers

The pellet dispensers are a major cost-saving component. They only require a relatively inexpensive stepper motor and motor driver, with total cost of parts per dispenser of less than $50 whereas a comparable commercial assembly costs anywhere from $800 to over $1,000 (**Figure 6.1A**); each box contains two dispensers, so to create an array of training boxes to scale up training of rats would quickly add up. Upon initial construction, such dispensers could reliably be expected to deliver between 48 to 50 of 50 test pellets; however, performance tends to degrade over time, typically due to accumulation of pellet fragments and dust along the grooves of the rotor and in the nozzle. With this in mind, two wing screws lock the bowl in place above the rotor; these screws are detachable and if the rotor or nozzle funnel gets jammed, the assembly can be detached, cleaned, and reassembled (**Figure S6.1**). Aside from the 3D-printed L-brackets (which could probably be replaced by comparable standard commercial components), we found that the standard grey photopolymer resin (FormLabs Grey Resin Pro v4) was suitable for each part, although some dispensers have versions printed using a fiber-glass impregnated resin (FormLabs Rigid Resin), which only seemed to be harder to remove from the stereolithography platform. A final note is that the accurate placement of the pellet at the target location is an important consideration in this behavioral task; incorrect delivery leads

to things like build-up of mounds of pellets that can have a deleterious effect on the manner in which the rat learns the behavior. To mitigate this, manual calibration of the dispenser once the full box is assembled is an important step. Using a custom dispense-guide to slightly alter the output location of the pellet dispense tubing helps greatly in ensuring the consistent delivery of the pellet to the target (**Figure S6.3**); such calibrations are necessary on a box-by-box basis because the expected tolerance in fabrication of the larger box components (such as the Plexiglas doors and walls that must be cut using larger machinery) is expected to result in jitter of part alignment that causes the slight deviation of the assembled door/pellet delivery system in this manner.

Selectable array of Behavioral Routines

The complex box contains an array of different routines (typically ranging between 9 and 11 routines depending on the box and which experimenters use it; on that note, the addition of a sign-in sheet to any location with a behavioral box is noted as an important component in ensuring the adequate maintenance of the box when used by multiple experimenters). In general, the tasks range from the simplest variety, which allow the experimenter to simply open one or both doors by pressing the corresponding button at the back of the box as the rat would typically learn to do, up through different degrees of difficulty. For example, in the lever-press task, an intermediate paradigm is to create a positive association with the button by automatically dispensing a pellet any time it is pressed, while also raising the door. In this way, the rat does not become startled by the opening of the door when he presses the lever. Each of these tasks may have specific components that can be programmed from the LCD on the side of the box without needing to reprogram the microcontroller directly; for example, after a button press or nose poke, the door should only remain open for a certain period of time before automatically shutting.

Alternating door task

During training, it was observed that rats could become reasonably proficient with both forelimbs during pellet retrievals. Since a major expense in each rat is the fixed cost associated with each electrode array that is embedded in the rat once it has learned a desired behavior, a prudent strategy for the investigator on a budget is to create an experimental design in which the rat might produce several different interesting behaviors, each of which serves as an interesting experimental endpoint in its own regard. While this requires a greater investment of time for both the individual investigator and the rat in terms of training the rat to proficiency, and poses greater risks on a per-rat basis, it is the only way to acquire sufficient data that it might be possible to get funding for the next round of experiments, hopefully allowing for more electrode arrays and therefore more rats.

The bilateral task is interesting for a number of reasons, and has several variants. In the initial training stage, the rat is required to learn to move back and forth from one door to the other, while a tone cue associated with the specific door is issued as it opens. The rat therefore is learning to associate a tone (and probably the sound of the door) with the reward pellet during this period, in addition to learning how to execute the motor behavior with both forelimbs. Once the motor task is learned with both limbs, it presents an interesting opportunity to compare the roles of each hemisphere during movement, and especially so after injury: it allows a within-animal comparison of activity, presuming that comparable cortical targets are recorded, for the behavior when it is mirrored to reflect the intact versus the paretic effector limb.

Nose Poke task and Audio Cues

Furthermore, the bilateral pellet retrieval task represents an opportunity for a decision task, where a binary outcome for classification can be used in information theoretic analyses to characterize premotor activity. Since the nose poke requires the rat to hold still for a short period of time, activity in premotor cortex that is aligned to it is more likely to be related to actual premotor processes as they might typically be observed in behaving macaques, as opposed to

in the standard reaching paradigm, where the approximate premotor alignment must be guessed and the relation of tuned cells with activations prior to a particular movement alignment is difficult to classify as premotor- or motor-related. For example, selection of the correct motor task and its execution are quite different processes (Diedrichsen et al. 2015). In the nose poke task, the rat is required to poke its nose through hole at the back of the box for some programmable period of time, at which point it will hear one of the two tones associated with each door. The idea is that the tone precedes the door opening slightly, giving the rat a better chance of running to the correct door in time. Notably, it cannot precede the door opening too much, or the rat will cheat and quickly run to both doors (some rats attempt to do this regardless, and the only way to mitigate such a strategy is to make the total allowable trial duration quite short). A final point about the nose poke task is that there is some preliminary data that has not been analyzed for this thesis, but wherein the tone cue was altered to an unlearned tone to determine the response of the rat. The idea is that if the rat demonstrates a comparable performance to when either of the other two tones is issued, the tone isn't really being used at all in the behavior and therefore it serves as a control to indicate whether it is even useful to perform neural analyses in relation to the tone to begin with.

Synchronization LEDs and Checkerboard Calibration Patterns

In the new version of the box, an LED is embedded in the platform next to each door on the front, as well as next to each lever (button press) on the back of the box. The LED corresponding to the opening door lights up as soon as the motor driver to its door begins to raise the door, so that a region of interest for any camera can be trained on this light source and a simple channel threshold can be invoked to create a digital synchronization signal; a digital output corresponding to this trial signal is synchronized with the neural signal as well, which allows the two to be related for each trial.

The checkerboard is attached to the door, and so it always moves up and down in approximately the region of interest for reconstructing three-dimensional reach markers any time that a trial begins. There are many automated algorithms that work with checkerboards; in all subsequent descriptions, Matlab (R2017a) was used. In order to detect such a checkerboard on a per-frame basis, the function `detectCheckerboardPoints` was applied to between ten and fifteen frames for which the checkerboard spans as much of the camera frame as possible. The checkerboard squares have a fixed square width of 2.79-mm; using this information, it is possible to triangulate the points identified with pairs of cameras in order to recover the tangential distortion and intrinsic matrices for stereo-calibrated camera pairs (`estimateCameraParameters`). Since this will change (non-trivially) if cameras are bumped between trials, the presence of the checkerboard in each trial guarantees that calibration can be performed as needed to reliably reconstruct the points.

Bilateral pellet retrieval task

Training procedures

Adult male Long-Evans rats (325g – 335g; 10 weeks on arrival; Charles River) were shaped over the course of 12 – 13 weeks until they began to associate audio stimuli with mirrored versions of a single food pellet retrieval task as follows.

Week-1: Handling and acclimation phase

Rats arrived pair-housed and were quarantined for the first three days upon arrival. The remainder of the first week was spent acclimating the rats to handling by the technician and at the end of the first week the rats were split into single housing with environmental enrichment to substitute for the presence of their littermate. After single housing, rats were placed on a food schedule receiving an average of 15-g of standard rodent chow biscuits per day.

Week-2: Initial reaching phase

In the first week after single-housing, rats were acclimated to the behavioral boxes. Any time the rats were placed into the box during the acclimation and subsequent sessions, they received a

few (2 – 4) food pellets (45-mg Dustless Precision Rodent Pellets; Bio-Serv). After an initial 15-minute session in which rats were acclimated to the box by periodic addition of food pellets directly to the box, rats were introduced to a modified version of the pellet retrieval task in which trays designed to hold 16 of the food pellets were placed in front of both doors. The trays removed the gap between the normal pellet platform and the reaching apertures milled out of the front panel of the box, making it easier for rats to initiate the reaching phase. Once a rat retrieved all pellets from one of the two trays using his forelimb, the tray was removed, and the door closed on that side to train rats as evenly as possible on both forelimbs. From this point on, to acclimate rats to the sounds of the door and pellet dispenser motors, retrievals with either forelimb were associated with the opening and closing of the door. By the end of the second week, most rats were able to retrieve the pellet from the well on the normal platform with either forelimb.

Week-3: Bilateral audio cue phase

When allowed to sit in front of either pellet retrieval aperture for an extended duration (on the order of minutes at a time), rats become very accurate in retrieving the pellet. During the third week, several rats exhibited the ability to retrieve pellets with both forelimbs with such proficiency. At this point of training, rats within the cohort began to diverge in level of proficiency, and so the exact stage of training for each rat was not identical. Rats proficient with either forelimb were moved to a task in which a preparatory tone cue (10 kHz, 500 ms) immediately preceded a left (8 kHz, 500 ms) or right (12 kHz, 500 ms) tone cue. During this phase, the left or right door corresponding to the tone cue opened with a starting duration of 1.5 seconds. The tone pattern alternated between the two doors conditionally upon the pellet needing to be replaced. If the pellet was undisturbed, indicating that a reach had not been attempted, the tone for that door was replayed for the subsequent trial, and the door stayed open for 0.5 seconds longer. If the pellet was successfully disturbed, indicating that the rat had gone to the correct door, the door opening was reduced by 0.25 seconds, to a minimum of 1.5

seconds for each trial, which was limited by the speed of the door motors and the minimum distance the door needed to travel. After any successful pellet disturbance, a conditioning tone identical to the door cue tone was played to reinforce pairing of moving to the correct door with the door's cue frequency. We found that this additional conditioning cue improved the rats' ability to learn the association of the audio cues with the correct door. This phase took considerably longer for the rats to both acclimate to the tone cues as well as become accurate at retrieving pellets, sometimes taking several weeks to complete.

Week-4: Initial nose poke phase

A few of the fastest-learning rats were able to learn the bilateral audio cued pellet retrieval by this point. These rats were introduced to the nose poke component of the behavior. During the initial phase associating the nose poke with a reward, any time the rat stuck his nose through the nose poke hole and crossed the plane of the infrared beam, a pellet was dispensed directly into the behavioral box. A variable lockout time, which ranged between 0.25 and 1.25 seconds, was enforced as a lockout to discourage the rat from sitting stationary with his nose through the hole. Custom blockers were printed to barricade the apertures typically used for the lever press, and these were secured in place during any of the subsequent training and behavioral stages involving the nose poke so that the beam could only be crossed by pressing the nose through the nose poke hole. During this phase of training, it was helpful to place a pile of 10-20 pellets directly below the nose poke hole, which attracted the rat to sniff through the hole. Typically, rats became motivated to do many nose pokes within one or two training sessions in this phase.

Rats that could not perform reaches with both forelimbs were discontinued from the study at this point; such rats were typically fixated on retrieving pellets using their tongue were discontinued from the study at this point.

Week-5 onward: Full-task phase

As early as the fifth week from arrival, rats that learned the nose poke were initiated on the full task involving a combination of the nose poke, audio cue indicating which door is opening, and

pellet retrieval on that side. Upon crossing the plane of the infrared beam break, a 500-ms audio tone played immediately preceding the opening of the left (8-kHz tone) or right (12-kHz tone) door.

As soon as the door began to open, the timer for the trial began running, such that a specified trial duration corresponded to the duration from the beginning of door opening to the onset of door closing. Initially, the trial duration was fixed to 10 seconds, as the rat typically did not immediately run directly to the door after performing the nose poke. Once the rat showed that it could reliably retrieve the pellet within the 10-second trial window, the duration of trials were set to 5 seconds, with the duration lengthening by 0.5 seconds on trials in which the pellet was not dislodged from the well, and shortening by 0.25 seconds to a minimum of 1.5 seconds on trials in which the pellet was dislodged from the well.

During training, at the technician's discretion, the relative proportion of openings for the left or right door could be programmed using an interactive LCD (LCD Shield Kit ID 772; Adafruit) attached to the microcontroller circuit running the box. In the initial phase, it was beneficial to pick one door that remained at 100% opening likelihood until the rat did several nose-poke-to-door trials successfully in a row. After this pattern had been established, the proportion of door openings was catered individually between and within sessions depending on the progression of the rat's training, with specific emphasis on extinguishing the behaviors described below.

Rats would try to cheat on the task by selecting only one door and preferentially running to that door regardless of which stimulus was played. To eliminate this behavior, the proportion was adjusted so that only the "non-selected" door was opened until the rat showed hesitation during the audio cue. Although 1.5 seconds was a short enough period that the majority of rats could not make it to the correct door if they chose the incorrect door first, a few very fast rats could quickly run to one door and then check the second door with enough time to retrieve the pellet as the door was closing. To extinguish this behavior, the same procedure was used for setting

the “non-selected” door to 100% likelihood, and additionally the technician was tasked with quickly removing the pellet if the rat ran to the wrong door first.

In some cases, the difficulty of this task caused the rats to become apprehensive and stop doing nose pokes. For these rats, it was helpful to switch to purely deterministic regimes for prolonged trial epochs (25-50 trials) in which the same door opened for 100% of the trials. Once the rat was encouraged to begin doing the nose pokes again and started to get into a rhythm of successful trial completion, the behavior was then transferrable to the opposite door. Qualitatively, rats that became initially discouraged in this way were typically more cautious about selecting the door overall, and rarely displayed the “cheating” behavior described previously.

Although rats never reached 100% selection of the correct door, they showed clear signs of associating the door cue with one door or the other, such as twitching the corresponding ear as the tone was played or showing hesitation when they initially ran the wrong direction and then switching to the correct direction.

While all steps prior to those with audio cues allowed the rats to be trained in parallel using multiple automated boxes, even the use of a foam sound chamber to isolate the audio cue of one box from its neighbors seemed to produce confusion in training rats. Therefore, during this period, rats were trained serially using the same box. As a result, rats at this stage could expect one-to-two training sessions per week.

Expert phase: ready for implant

By 12 – 13 weeks, rats included in the study were ready for implant. Prior to the implantation, baseline recordings, consisting of 100 trials with a 50% probability of either door opening, were recorded using a digital camera (GoPro Hero 5). No inclusion criteria for learning the audio cue was required, as the behavioral schedule in the subsequent section is designed to account for the degree to which the rat makes use of the audio cue.

Surgical implantation and electrode array targets

The implantation of electrodes, built as described in **Chapter 3**, primarily follows the surgical procedure described in **Chapter 5**. However, a larger bilateral craniectomy was made in order to expose the sensorimotor cortex in both hemispheres of the rat (e.g. **Figure S6.4**). Depending on the area of exposed skull rostral to the opening, either one or two steel skull screws (00-80, McMaster-Carr) were inserted rostral to both openings, while four more skull screws were situated caudal to the openings. In general, the skull screws form an important bonding point for the dental acrylic that encapsulates the opening and fixates the recording electrodes in place; there is a tradeoff between the total number of skull screws that can be fit onto the rat's head and the overall integrity of the skull, which is an important consideration when a relatively large array with respect to the overall size of the rat's skull is to be mounted. **Figure S6.5** provides a generic overview of the implant process; however, the practical realization of this process typically varies considerably from rat to rat, and it is made more variable if custom non-commercial electrodes are introduced. The caudal-most two screws were used as common reference points for each electrode microwire array.

Data collection

While not all of the data that was collected from these rats is presented in this Chapter, because these data may be used in future studies or research proposals, a description of the overall collection methods is provided. Recording cameras were mounted from several points around the behavioral box (**Figure 6.1A**); in general, camera frame rates were 240 frames-per-second (GoPro Hero Black v5). A 33-Ω resistor connected in series to a standard green 5-mm LED (Adafruit) produces an 18-mA forward current when attached to the voltage divider circuit for the trial-related digital synchronization circuit; the brightness of the LED when powered in this way was enough so that even with only 1/1920 second exposure, the lit and unlit state of the LED could be distinguished readily. For recordings in which the rat performed the nose poke task, an additional video camera was mounted on the ceiling above the entire box, providing a view of

the transverse plane of the box floor. The sampling rate of this camera was only 60 frames-per-second, which was sufficient to capture the general location of the rat traversing the behavioral box in order to generate a reconstruction of the path traveled from the nose hole location to the target door. Depending on the behavior under consideration, between two and six other cameras were trained on the two doors at the front of the box.

Two of the rats (R19-51 and R19-54) only performed bilateral reaching tasks in which they either randomly alternated in moving between doors, deterministically alternated between the doors, or sat in front of one door and then the other door on a fixed retrieval schedule. Four of the rats (R19-162, R19-163, R19-165, and R19-166) performed variants of the nose-poke task: a scheduled version that set a fixed number of nose pokes for which only the left door would open, followed by the same number of nose pokes for which only the right door would open (**Task-L**; the left-door trials preceded the right-door trials); a reversed scheduled task (**Task-R**; the right-door trials preceded the left-door trials); and a “hard” version of the task in which there was a 50% chance of either door opening for all trials (**Task-P**). Each design allowed for a minimum of 100 pellet retrieval trials, but if the rat would perform more behavioral trials in a reasonable time (approximately 45-minutes), then as much data as possible was collected. Two additional rats were to be used in collecting data for this latter set of trials (R19-161, and R19-164); unfortunately, in R19-161 torque on one of the microwire bundles caused it to become dislodged during the implantation process and this caused behavioral problems as well as poor recordings so the rat was discontinued; R19-164 succumbed to anesthesia following the buprenorphine injection that was administered per protocol during recovery from the implantation surgery, although it appeared that he was recovering well prior to this injection.

System models

All system models as described in the **Results** section were obtained using Matlab (R2020b, Prerelease version). Data processing in terms of filtering and spike detection were performed using the methods described in **Chapter 3** and **Chapter 5**.

Acute sensory solenoid preparations

Training procedures

Rats that did not meet inclusion criteria for the audio-cued bilateral pellet retrieval task (e.g. they spent more than 1-2 weeks learning any one part of the full behavior) were used in acute experiments designed to measure the influence exerted by ICMS upon evoked sensory responses to mechanical stimulation of the forelimb.

Initial Surgery and Injury

Rats were anesthetized using an initial dose of isoflurane followed by bolus injections of ketamine and xylazine as described previously in the protocol. The animal's anesthetic state was monitored and maintained using bolus injections of ketamine, supplemented by xylazine or isoflurane as appropriate. The first surgical procedure followed the description in **Chapter 5**, except that no craniectomy was performed and instead only the burr holes (#00-71 bit) were drilled in order to administer bolus injections of the vasoconstrictor Endothelin-1 (ET-1; **Figure S6.7**).

Postoperative care, training, and testing

Rats were administered postoperative analgesia and monitored as described in **Chapter 5**. In general, rats appeared to recover well from ET1 and performed better than expected on the pellet retrieval task. It is not clear if the use of the complex behavioral box, which includes a door that restricts the rats from attempting to repeatedly flail at the pellet unsuccessfully, causes the rats to become more accurate on this task in a way that enables them to perform the behavior more successfully after injury by comparison to previous works (e.g. Nishibe et al. 2015; **Figure S6.8**). Rats were semi-randomly (stratified to try and split initial proficiency equally

between groups) divided into two groups: ET1- and ET1+. All rats received focal vasoconstrictive injections of ET1 targeted stereotaxically to the caudal forelimb area (CFA) contralateral to the preferred reaching forelimb. Rats from both groups were tested on pellet retrieval accuracy over as many retrieval attempts as they could achieve within 20-minutes starting on postoperative day 8 (PO-8) and continuing every fourth day thereafter through PO-24. Rats in the “active” ET1+ group were additionally allowed to repeat this process daily as opposed to only on testing days. On PO-26, rats underwent a terminal procedure to test the ability to evoke sensory activity in the forelimb sensory cortex (FL-S1) and rostral forelimb area (RFA). After the acute recording, rats were perfused in order to perform a lesion volume estimation on the ischemic injury.

Secondary Surgery and Data Collection

In the second, acute procedure, a laminectomy, designed to prevent edema during the procedure, was made to allow drainage of cerebro-spinal fluid at the base of the skull. A bilateral craniectomy, exposing the sensorimotor cortex of both hemispheres, was performed using a dental burr bit to target stereotaxic coordinates for the forelimb sensory cortex. A sparse ICMS map was used if possible in order to verify the forelimb representation and boundary of the rostral forelimb area (RFA), although movement representation or a clear boundary between RFA and CFA was not always possible to determine definitively (**Figure S6.9**). High-density recording electrodes were inserted bilaterally into putative sensory cortex, which was confirmed by manually palpating the contralateral paw, and refined using Von Frey microfilaments once audible spiking responses were evident. Isoflurane became critical during the secondary acute procedure, in order to ensure that large deflections in the LFP that appeared to be related to whisking were mitigated and did not contaminate the forelimb response to the mechanical stimulus.

A miniature 5V solenoid (ID 2776; Adafruit) was then clamped to the stereotaxic apparatus and positioned above the forelimb. 1-Hz stimulus trains consisting of mechanical stimuli were delivered using this device in a setup resembling the one described in (Foffani et al. 2004, Moxon et al. 2008; **Figure 6.4A**). The solenoid could not hurt the rat: it weighed 12.6g and was capable of delivering a maximum impact capable of displacing a load up to 80g. In conjunction with the mechanical stimulation of the solenoid, pulses of intracortical microstimulation (ICMS) were delivered to the premotor cortex either ipsilateral or contralateral to the solenoid, at various offset latencies coupled to the delivery of each solenoid stimulus. Response properties of neural units were recorded using polymeric microelectrode arrays (NeuroNexus 4x8 acute array: shank spacing of 125-μm and site spacing of 100-μm), during three different types of trials: only-solenoid stimulation, solenoid and ICMS, or ICMS-only. Data processing in terms of filtering and spike detection were performed using the methods described in **Chapter 3** and **Chapter 5**.

Histological Preparation

A saline, heparin, and lidocaine solution was transcardially perfused to fixate the brain using a 3.5% paraformaldehyde solution, and 30%-glycerol post-fixation. 50-μm coronal sections were stained with cresyl violet. An example of coronal hemisections corresponding to CFA are shown with examples of the small, subtotal lesions generated in these experiments is shown in **Figure S6.7**.

References

Alaverdashvili, Mariam, and Ian Q. Whishaw. "Motor cortex stroke impairs individual digit movement in skilled reaching by the rat." *European Journal of Neuroscience* 28.2 (2008a): 311-322.

Alaverdashvili, Mariam, et al. ""Learned baduse" limits recovery of skilled reaching for food after forelimb motor cortex stroke in rats: a new analysis of the effect of gestures on success." *Behavioural brain research* 188.2 (2008b): 281-290.

Alaverdashvili, M., and I. Q. Whishaw. "Compensation aids skilled reaching in aging and in recovery from forelimb motor cortex stroke in the rat." *Neuroscience* 167.1 (2010): 21-30.

Allred, R. P., M. A. Maldonado, and T. A. Jones. "Training the "less-affected" forelimb after unilateral cortical infarcts interferes with functional recovery of the impaired forelimb in rats." *Restorative neurology and neuroscience* 23.5, 6 (2005): 297-302.

Allred, Rachel P., and Theresa A. Jones. "Maladaptive effects of learning with the less-affected forelimb after focal cortical infarcts in rats." *Experimental neurology* 210.1 (2008): 172-181.

Allred, Rachel P., Colleen H. Cappellini, and Theresa A. Jones. "The “good” limb makes the “bad” limb worse: Experience-dependent interhemispheric disruption of functional outcome after cortical infarcts in rats." *Behavioral neuroscience* 124.1 (2010): 124.

Barbay, Scott, et al. "Motor representations in the intact hemisphere of the rat are reduced after repetitive training of the impaired forelimb." *Neurorehabilitation and neural repair* 27.4 (2013): 381-384.

Bhatt, Tanvi, Shamali Dusane, and Prakruti Patel. "Does severity of motor impairment affect reactive adaptation and fall-risk in chronic stroke survivors?." *Journal of neuroengineering and rehabilitation* 16.1 (2019): 1-13.

Bland, Sondra T., et al. "Early overuse and disuse of the affected forelimb after moderately severe intraluminal suture occlusion of the middle cerebral artery in rats." *Behavioural brain research* 126.1-2 (2001): 33-41.

Bobath, K., and Bobath, B. (1984). “The neuro-developmental treatment.” In: Scrutton D, editor. *Management of the Motor Disorders of Children with Cerebral Palsy.* Clinics in Developmental Medicine No. 90. London: Spastics International Medical Publications.

Brock, Kim, et al. "The Bobath Concept has changed.(comment on critically appraised paper, australian journal of physiotherapy 48: 59.)." *Australian Journal of Physiotherapy* 48.2 (2002): 156-157.

Bury, Scott D., and Theresa A. Jones. "Unilateral sensorimotor cortex lesions in adult rats facilitate motor skill learning with the “unaffected” forelimb and training-induced

dendritic structural plasticity in the motor cortex." *Journal of Neuroscience* 22.19 (2002): 8597-8606.

Bundy, David T., et al. "Chronic stability of single-channel neurophysiological correlates of gross and fine reaching movements in the rat." *PloS one* 14.10 (2019): e0219034.

Carey, James R., et al. "Analysis of fMRI and finger tracking training in subjects with chronic stroke." *Brain* 125.4 (2002): 773-788.

Carmichael, S. Thomas. "Cellular and molecular mechanisms of neural repair after stroke: making waves." *Annals of Neurology: Official Journal of the American Neurological Association and the Child Neurology Society* 59.5 (2006): 735-742.

Carmichael, S. Thomas. "Brain excitability in stroke: the yin and yang of stroke progression." *Archives of neurology* 69.2 (2012): 161-167.

Chen, Xiang Yang, et al. "Corticospinal tract transection permanently abolishes H-reflex down-conditioning in rats." *Journal of neurotrauma* 23.11 (2006): 1705-1712.

Churchland, Mark M., Afsheen Afshar, and Krishna V. Shenoy. "A central source of movement variability." *Neuron* 52.6 (2006): 1085-1096.

Cramer, Steven C., et al. "Activity in the peri-infarct rim in relation to recovery from stroke." *Stroke* 37.1 (2006): 111-115.

Dancause, Numa, et al. "Extensive cortical rewiring after brain injury." *Journal of Neuroscience* 25.44 (2005): 10167-10179.

Dancause, Numa, et al. "Topographically divergent and convergent connectivity between premotor and primary motor cortex." *Cerebral cortex* 16.8 (2006): 1057-1068.

Diedrichsen, Jörn, and Katja Kornysheva. "Motor skill learning between selection and execution." *Trends in cognitive sciences* 19.4 (2015): 227-233.

Dijkhuizen, Rick M., et al. "Functional magnetic resonance imaging of reorganization in rat brain after stroke." *Proceedings of the National Academy of Sciences* 98.22 (2001): 12766-12771.

Dijkhuizen, Rick M., et al. "Correlation between brain reorganization, ischemic damage, and neurologic status after transient focal cerebral ischemia in rats: a functional magnetic resonance imaging study." *Journal of Neuroscience* 23.2 (2003): 510-517.

Dolbakyan, E., N. Hernandez-Mesa, and J. Bures. "Skilled forelimb movements and unit activity in motor cortex and caudate nucleus in rats." *Neuroscience* 2.1 (1977): 73-80.

Duque, Julie, et al. "Kinematically specific interhemispheric inhibition operating in the process of generation of a voluntary movement." *Cerebral Cortex* 15.5 (2005): 588-593.

Fridman, Esteban A., et al. "Reorganization of the human ipsilesional premotor cortex after stroke." *Brain* 127.4 (2004): 747-758.

Foffani, Guglielmo, Banu Tutunculer, and Karen A. Moxon. "Role of spike timing in the forelimb somatosensory cortex of the rat." *Journal of Neuroscience* 24.33 (2004): 7266-7271.

Guggenmos, David J., et al. "Restoration of function after brain damage using a neural prosthesis." *Proceedings of the National Academy of Sciences* 110.52 (2013): 21177-21182.

Hayley, Page, et al. “Modulation and representation of sensory responses in the premotor cortex of the rat following ischemic injury.” *Frontiers in Human Neuroscience*. (In Preparation)

Hermer-Vazquez, L., et al. "Distinct temporal activity patterns in the rat M1 and red nucleus during skilled versus unskilled limb movement." *Behavioural brain research* 150.1-2 (2004): 93-107.

Hughes, P. C., J. M. Tanner, and J. P. Williams. "A longitudinal radiographic study of the growth of the rat skull." *Journal of anatomy* 127.Pt 1 (1978): 83.

Huisinga, Jessie, et al. "Coherence analysis of trunk and leg acceleration reveals altered postural sway strategy during standing in persons with multiple sclerosis." *Human movement science* 58 (2018): 330-336.

Hyland, B. "Neural activity related to reaching and grasping in rostral and caudal regions of rat motor cortex." *Behavioural brain research* 94.2 (1998): 255-269.

Johansen-Berg, Heidi, et al. "The role of ipsilateral premotor cortex in hand movement after stroke." *Proceedings of the National Academy of Sciences* 99.22 (2002): 14518-14523.

Karni, Avi, et al. "The acquisition of skilled motor performance: fast and slow experience-driven changes in primary motor cortex." *Proceedings of the National Academy of Sciences* 95.3 (1998): 861-868.

Kawai, Risa, et al. "Motor cortex is required for learning but not for executing a motor skill." *Neuron* 86.3 (2015): 800-812.

Kozlowski, Dorothy A., Debra C. James, and Timothy Schallert. "Use-dependent exaggeration of neuronal injury after unilateral sensorimotor cortex lesions." *Journal of Neuroscience* 16.15 (1996): 4776-4786.

Linslee, Luke M., Allred, Rachel P., and Jones, Theresa A. "Unilateral ischemic sensorimotor cortical damage induces contralesional synaptogenesis and enhances skilled reaching with the ipsilateral forelimb in adult male rats." *Synapse* 54.4 (2004): 187-199.

Maldonado, Monica A., et al. "Motor skill training, but not voluntary exercise, improves skilled reaching after unilateral ischemic lesions of the sensorimotor cortex in rats." *Neurorehabilitation and neural repair* 22.3 (2008): 250-261.

Mansoori, Babak K., et al. "Acute inactivation of the contralesional hemisphere for longer durations improves recovery after cortical injury." *Experimental neurology* 254 (2014): 18-28.

Masamizu, Yoshito, et al. "Two distinct layer-specific dynamics of cortical ensembles during learning of a motor task." *Nature neuroscience* 17.7 (2014): 987-994.

Mathis, Alexander, et al. "DeepLabCut: markerless pose estimation of user-defined body parts with deep learning." *Nature neuroscience* 21.9 (2018): 1281-1289.

Miyai, Ichiro, et al. "Middle cerebral artery stroke that includes the premotor cortex reduces mobility outcome." *Stroke* 30.7 (1999): 1380-1383.

Moxon, K. A., et al. "Responses of infragranular neurons in the rat primary somatosensory cortex to forepaw and hindpaw tactile stimuli." *Neuroscience* 156.4 (2008): 1083-1092.

Nishibe, Mariko, et al. "Rehabilitative training promotes rapid motor recovery but delayed motor map reorganization in a rat cortical ischemic infarct model." *Neurorehabilitation and neural repair* 29.5 (2015): 472-482.

Nudo, Randolph J., et al. "Neural substrates for the effects of rehabilitative training on motor recovery after ischemic infarct." *Science* 272.5269 (1996): 1791-1794.

Papale, Andrew E., and Bryan M. Hooks. "Circuit changes in motor cortex during motor skill learning." *Neuroscience* 368 (2018): 283-297.

Peters, Andrew J., Haixin Liu, and Takaki Komiyama. "Learning in the rodent motor cortex." *Annual review of neuroscience* 40 (2017a): 77-97.

Peters, Andrew J., et al. "Reorganization of corticospinal output during motor learning." *Nature neuroscience* 20.8 (2017b): 1133.

Ramanathan, Dhakshin S., et al. "Low-frequency cortical activity is a neuromodulatory target that tracks recovery after stroke." *Nature medicine* 24.8 (2018): 1257-1267.

Sanes, Jerome N., Jing Wang, and John P. Donoghue. "Immediate and delayed changes of rat motor cortical output representation with new forelimb configurations." *Cerebral Cortex* 2.2 (1992): 141-152.

Savin, Douglas N., et al. "Poststroke hemiparesis impairs the rate but not magnitude of adaptation of spatial and temporal locomotor features." *Neurorehabilitation and neural repair* 27.1 (2013): 24-34.

Scheidt, Robert A., and Tina Stoeckmann. "Reach adaptation and final position control amid environmental uncertainty after stroke." *Journal of neurophysiology* 97.4 (2007): 2824-2836.

Shadmehr, Reza, and Ferdinando A. Mussa-Ivaldi. "Adaptive representation of dynamics during learning of a motor task." *Journal of neuroscience* 14.5 (1994): 3208-3224.

Stergiou, Nicholas, and Leslie M. Decker. "Human movement variability, nonlinear dynamics, and pathology: is there a connection?." *Human movement science* 30.5 (2011): 869-888.

Takahashi, Craig D., and David J. Reinkensmeyer. "Hemiparetic stroke impairs anticipatory control of arm movement." *Experimental brain research* 149.2 (2003): 131-140.

Todorov, Emanuel, and Michael I. Jordan. "Optimal feedback control as a theory of motor coordination." *Nature neuroscience* 5.11 (2002): 1226-1235.

Ungerleider, Leslie G., Julien Doyon, and Avi Karni. "Imaging brain plasticity during motor skill learning." *Neurobiology of learning and memory* 78.3 (2002): 553-564.

Ward, N. S., et al. "Neural correlates of motor recovery after stroke: a longitudinal fMRI study." *Brain* 126.11 (2003): 2476-2496.

Whishaw, Ian Q., et al. "The impairments in reaching and the movements of compensation in rats with motor cortex lesions: an endpoint, video recording, and movement notation analysis." *Behavioural brain research* 42.1 (1991): 77-91.

Whishaw, Ian Q., and Brenda LK Coles. "Varieties of paw and digit movement during spontaneous food handling in rats: postures, bimanual coordination, preferences, and the effect of forelimb cortex lesions." *Behavioural brain research* 77.1-2 (1996): 135-148.

Whishaw, Ian Q. "Loss of the innate cortical engram for action patterns used in skilled reaching and the development of behavioral compensation following motor cortex lesions in the rat." *Neuropharmacology* 39.5 (2000): 788-805.

Whishaw, Ian Q., Mariam Alaverdashvili, and Bryan Kolb. "The problem of relating plasticity and skilled reaching after motor cortex stroke in the rat." *Behavioural brain research* 192.1 (2008): 124-136.

Wolf, Steven L., et al. "Forced use of hemiplegic upper extremities to reverse the effect of learned nonuse among chronic stroke and head-injured patients." *Experimental neurology* 104.2 (1989): 125-132.

Wolpaw, Jonathan R., and Xiang Yang Chen. "Operant conditioning of rat H-reflex: effects on mean latency and duration." *Experimental brain research* 136.2 (2001): 274-279.

Supplementary Materials

Supplementary Figures

Figure S6.1: Pellet dispenser assembly 3D-render

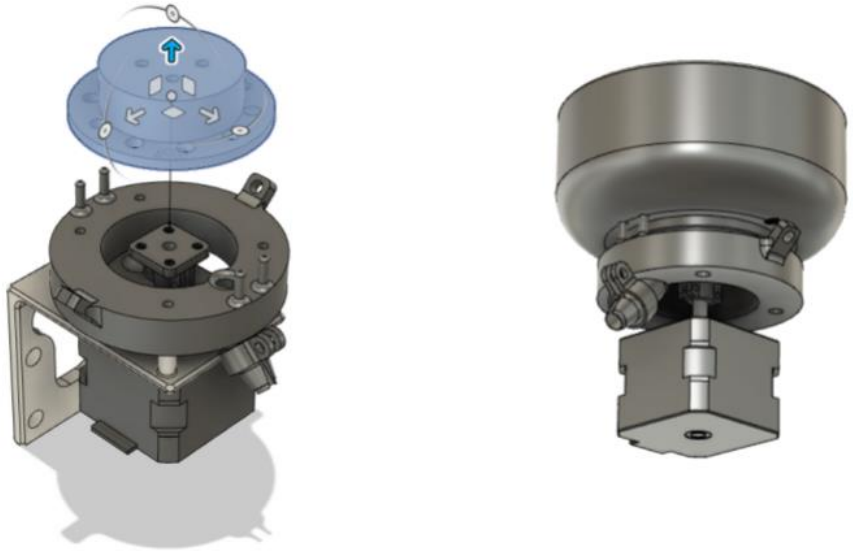

Figure S6.2: Pellet platform assembly 3D-render

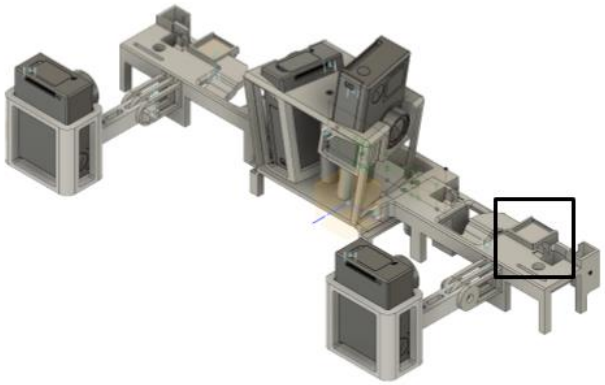

Figure S6.3: Box-specific tuning of pellet dispense location

Pellet Dispense Guide *L1* **Pellet Dispense Guide *C2*** **Pellet Dispense Guide *P3***

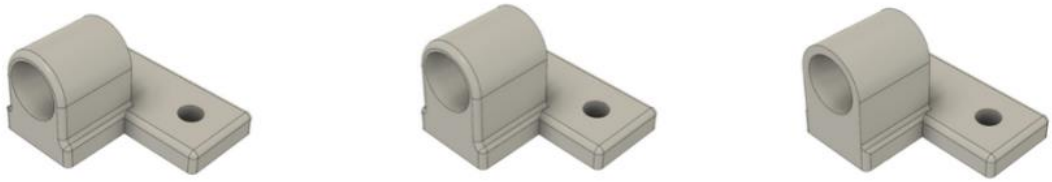

Credit for idea of specifically calibrated dispense target guides: David Bundy

Figure S6.4: Example electrode implantation

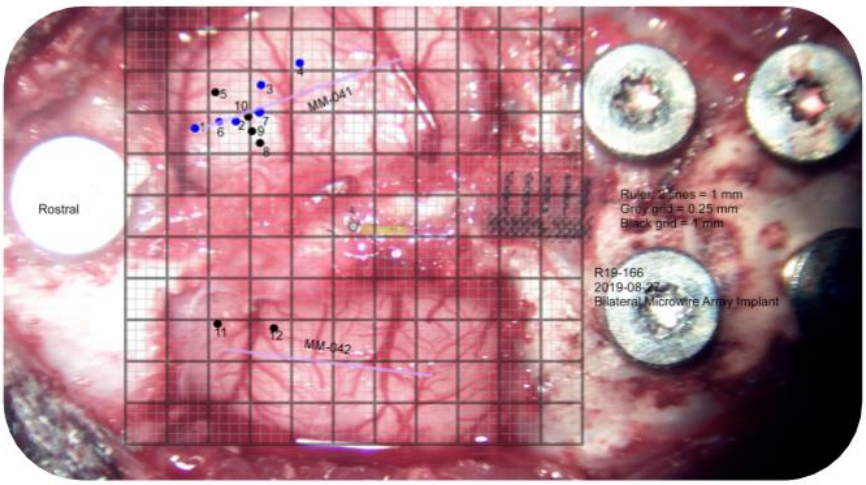

Credit for surgical assistance: Chad Tuchek

Figure S6.5a: Implantation overview - drilling skull screw holes

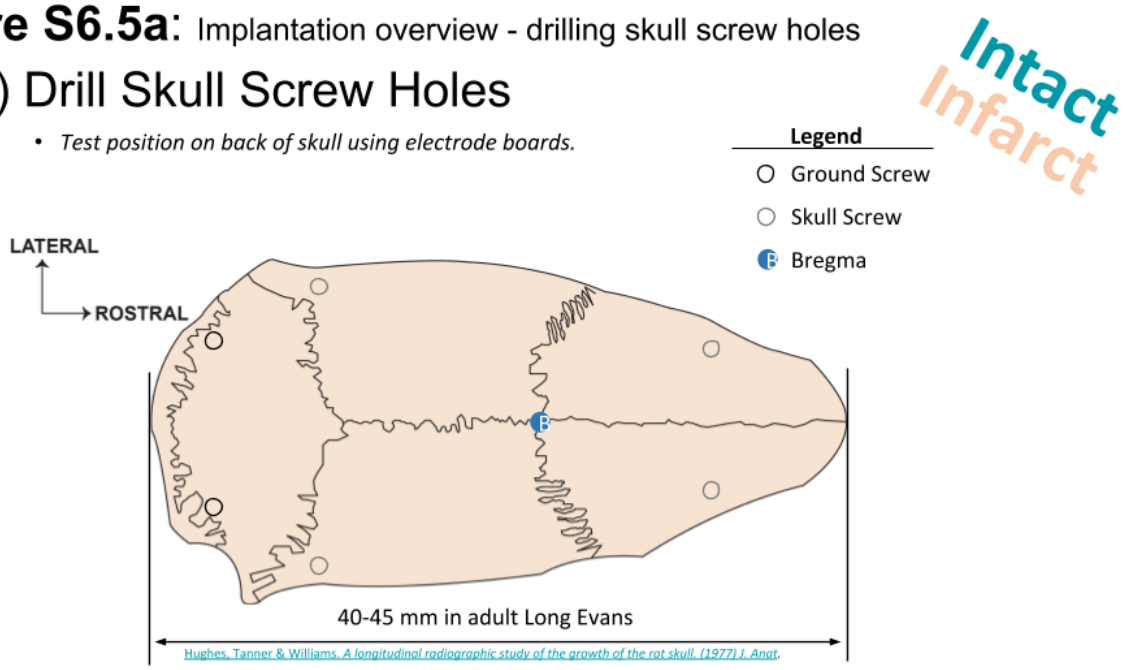

Figure S6.5b: Implantation overview - inserting caudal skull screws

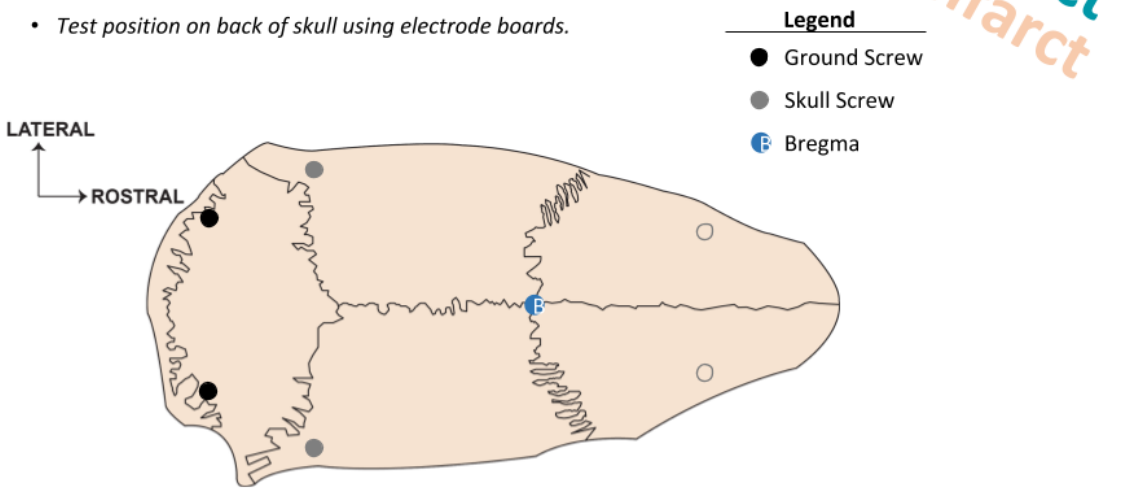

Figure S6.5c: Implantation overview - injecting Endothelin-1 (ET-1)

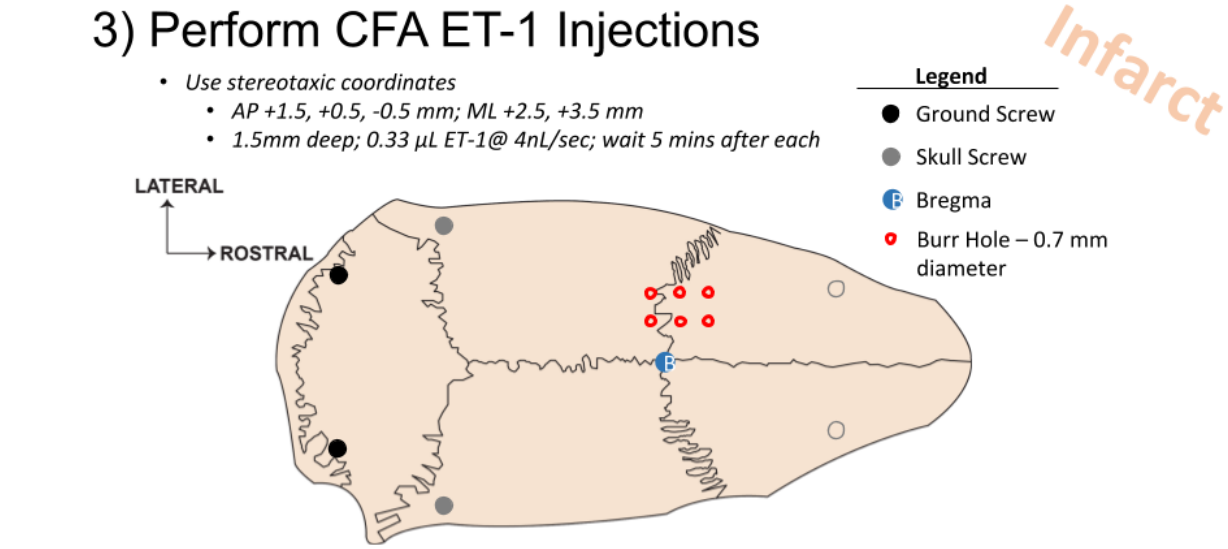

Figure S6.5d: Implantation overview - exposing cortical targets

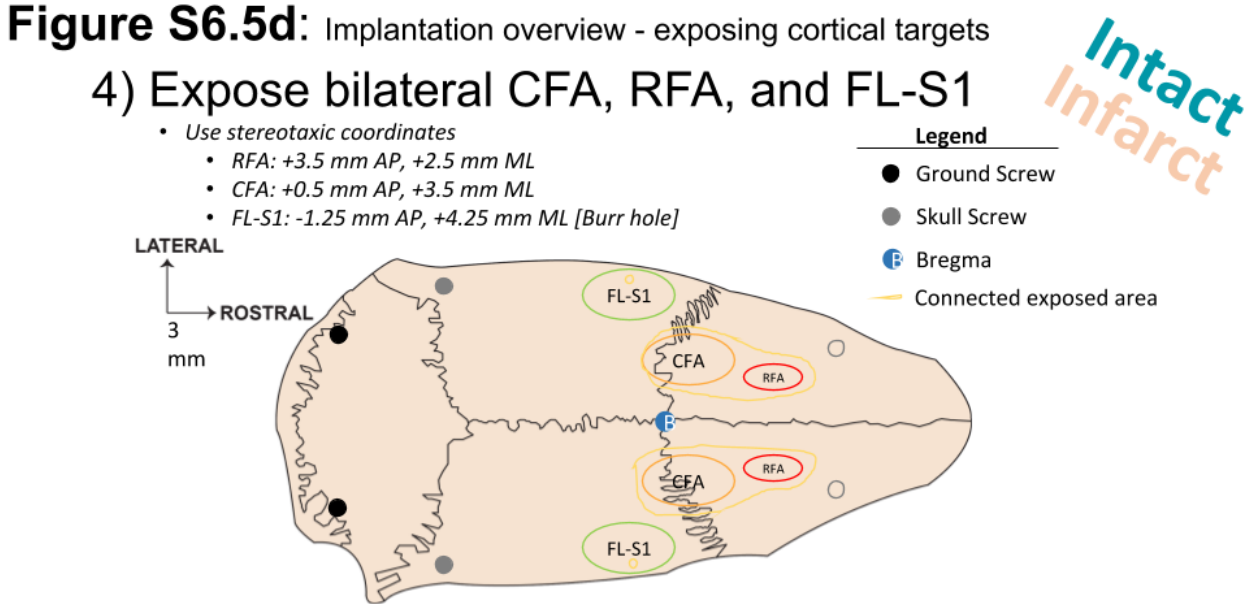

Figure S6.5e: Implantation overview - inserting LFP recording leads

Intact
Infarct

5) Insert "LFP" wires to FL-S1

- *Boards in back with stereotaxic arm A*
- *Arm B secures position 1, then position 2.*
- *Tack in place with polymer + dental acrylic?*

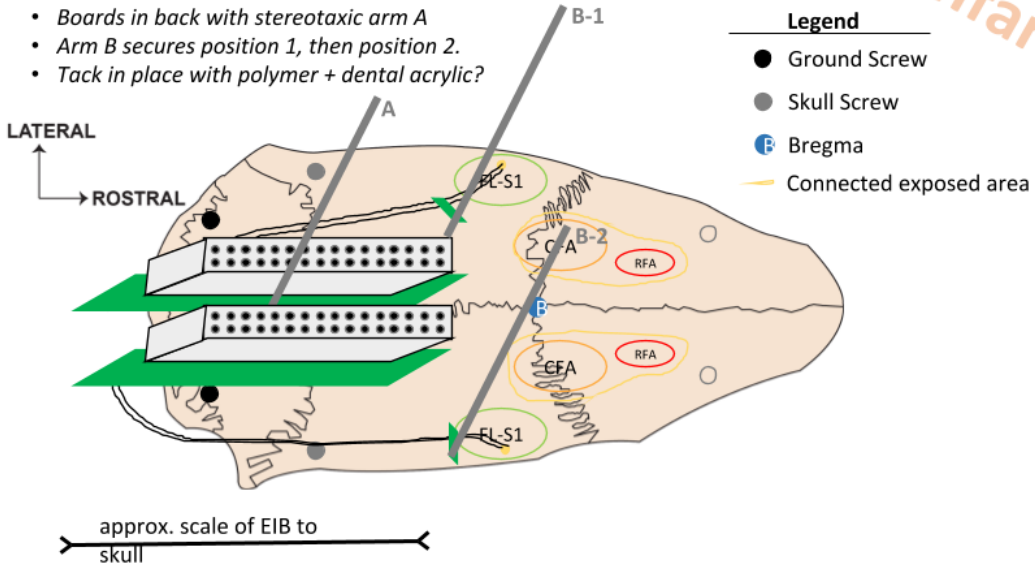

Figure S6.5f: Implantation overview - inserting wire array bundles

Intact
Infarct

6) Insert rigid wire arrays to CFA/RFA

- *Boards in back with stereotaxic arm A*
- *Tack in place with polymer + dental acrylic?*

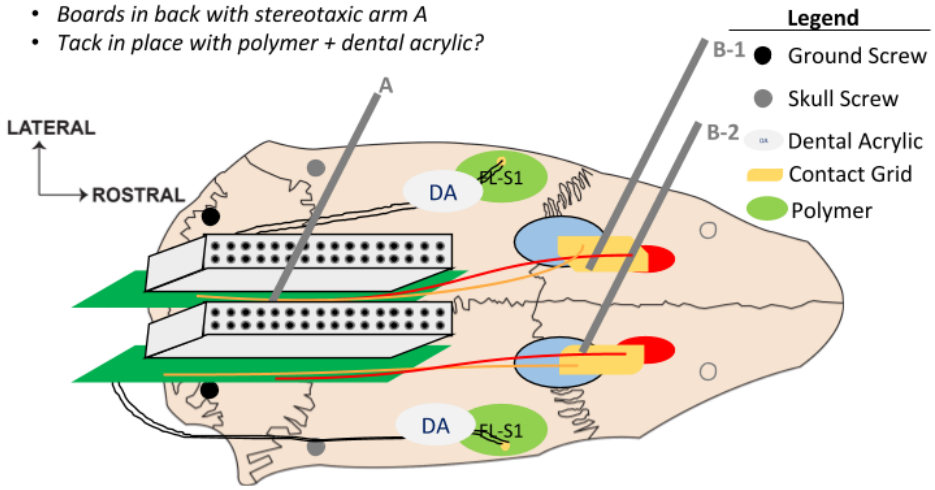

Figure S6.5g: Implantation overview - securing initial insertion

Intact
Infarct

7) Secure front with dental acrylic

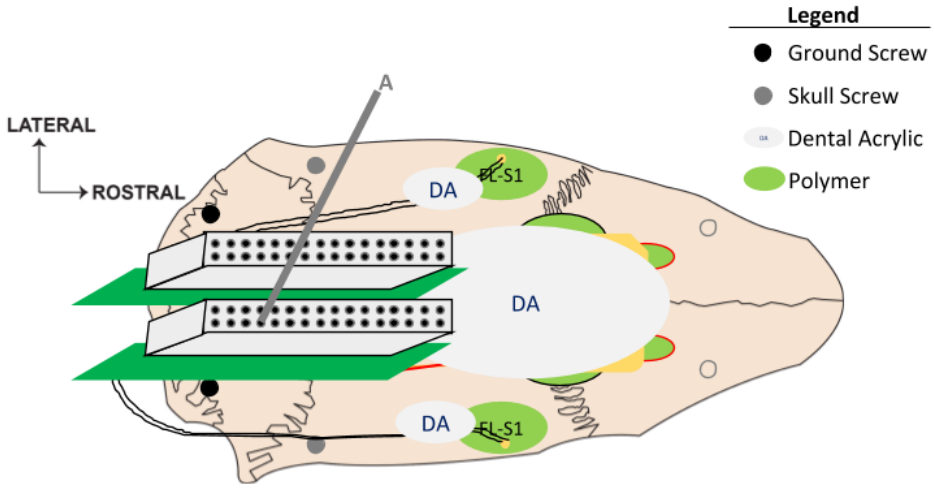

Figure S6.5h: Implantation overview - secure rostral attachments

Intact
Infarct

8) Attach rostral screws and grounds

- *Continue to fill in dental acrylic*

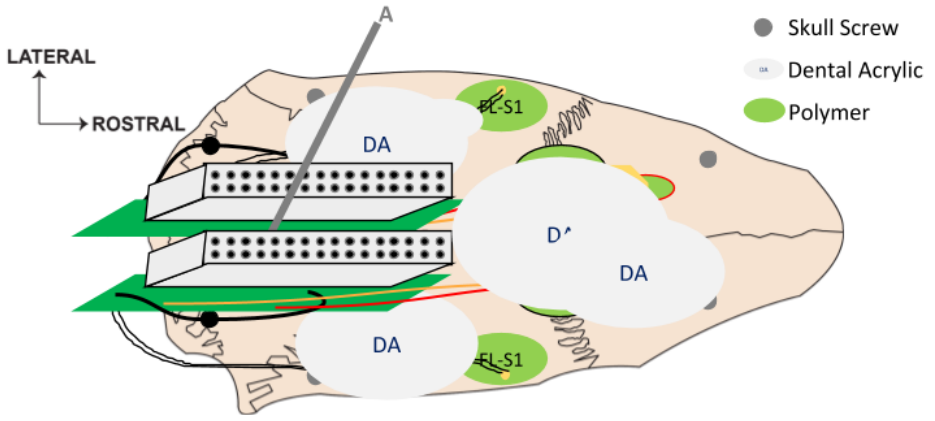

Figure S6.6: Example of spiking rasters in alignment to **Grasp**

Credit for collection of neurophysiological data during behavior: Andrea Pack

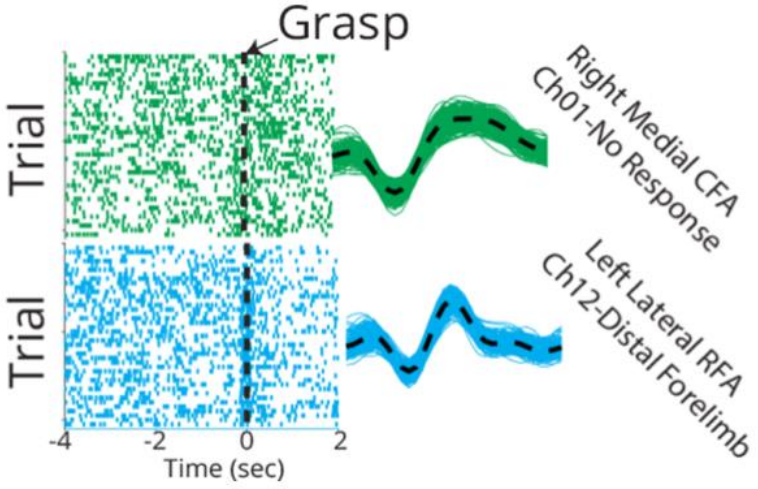

Figure S6.7: Example of ICMS and probe layout in solenoid recordings

*Credit for histological preparation and imaging (**right**): Jasmine Deng, Page Hayley, & Shiv Dalla. Credit for surgical assistance (**left**): Jordan Borrell, Page Hayley, Chad Tuchek*

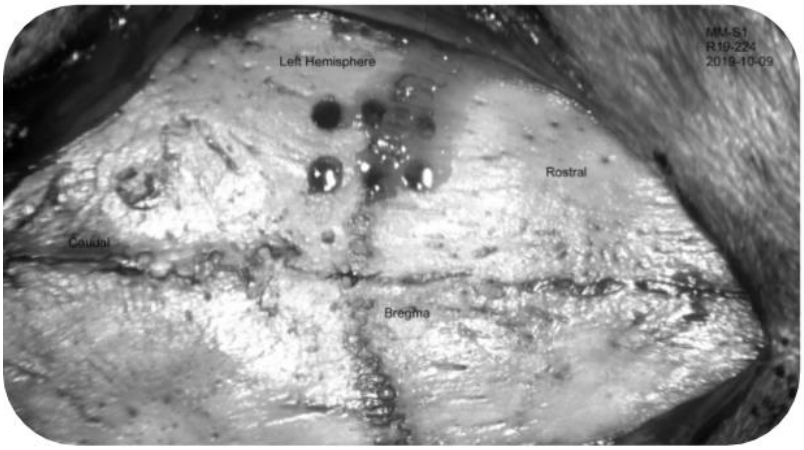

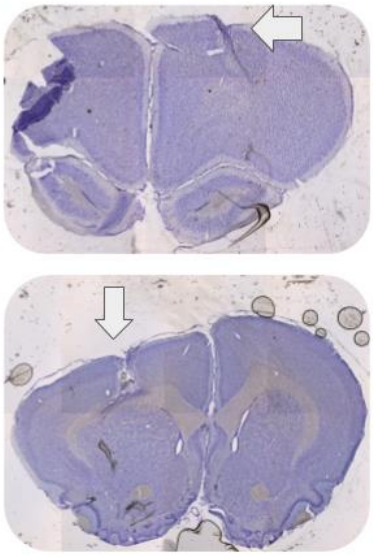

Figure S6.8: Recovery timeline for active and inactive rats after ET-1 injections

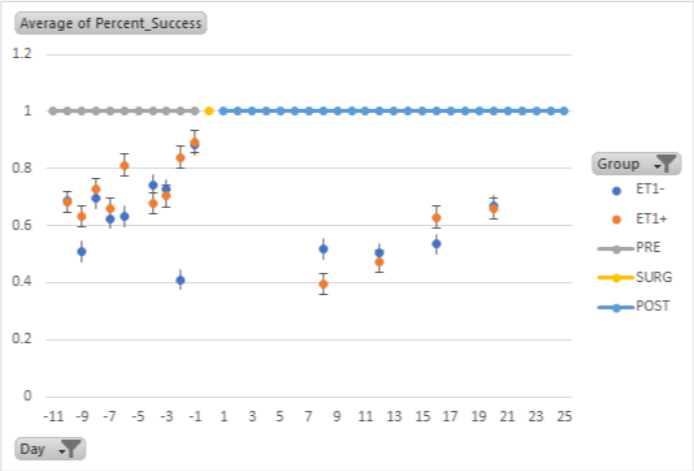

Figure S6.9: Example of ICMS and probe layout in solenoid recordings

Credit for surgical assistance: Jordan Borrell, Page Hayley, Chad Tuchek

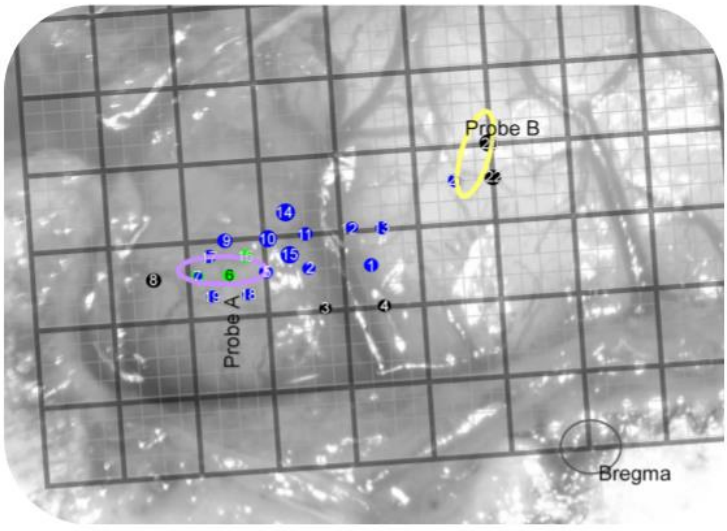

Conclusion

After stroke, changes in functional outcomes depend on reorganization of the spared nervous tissue and associated plasticity in the filtering that it performs in control of volitional movement. This reorganization may occur at many levels of the nervous system. Engineering strategies for rehabilitation and specifically the restoration of movement after brain injury are abundant, but may not realize their full therapeutic potential until better strategies emerge to evaluate their efficacy in modulating specific circuit elements (**Chapter 2**). Understanding the appropriate circuit elements requires a Systems Theoretic approach that incorporates Reflex Theory and Hierarchical Theory, while making use of the diverse array of technical tools required to perform such experiments in a preclinical model (**Chapter 3**). In most cases, such tools will necessarily be highly application-specific, but once they have been created they can be put to use in a variety of experiments that will benefit related preclinical models of rehabilitation at large (**Chapter 4**). It is proposed that *optimal* reorganization (i.e. *recovery*) only occurs when there is evidence of a cortical movement filter with specific fixed point dynamics (**Chapter 5**). Ultimately, relation of these dynamics to sensorimotor reintegration such as may occur following the termination of sprouting cortical axonal processes upon sensory or motor targets will require the formulation of a system model capable of separating sensorimotor integration from internal model prediction, internal model error correction, and generation of motor output (**Chapter 6**).